DECIPHERING MANTLE SOURCE COMPONENTS IN BASALTS FROM HOTSPOT TRACKS AND OCEANIC ISLANDS

by

Inês Garcia Nobre Silva

A THESIS SUBMITTED IN PARTIAL FULFILLMENT OF
THE REQUIREMENTS FOR THE DEGREE OF

DOCTOR OF PHILOSOPHY

in

The Faculty of Graduate Studies
(Geological Sciences)

THE UNIVERSITY OF BRITISH COLUMBIA
(Vancouver)

April 2011

ABSTRACT

The isotopic compositions of oceanic island basalts erupted at the Earth's surface can be used to directly constrain the isotopic signatures of their deep mantle sources. Basaltic rocks are highly susceptible to seawater alteration, which can significantly modify elemental contents and potentially hinder the use of radiogenic isotopes as geochemical tracers. In this study, multi-isotopic (e.g., Pb-Hf-Sr-Nd) analyses on the same acid-leached sample aliquot are shown to produce reliable results for use in the discrimination of mantle source components of oceanic basalts. Application to basalts from the Ninetyeast Ridge in the Indian Ocean and from Mauna Kea volcano on Hawaii in the Pacific Ocean allows for an enhanced resolution of their source components and distribution in the deep mantle. Isotopic geochemistry of the Ninetyeast Ridge sampled during Ocean Drilling Project Leg 121 reveals a Kerguelen and Amsterdam-St. Paul mantle plume origin with the presence of at least three source components and no contribution from an Indian mid-ocean ridge basalt source. The isotopic characteristics of the Ninetyeast Ridge basalts are typical of the Dupal isotopic domain and consistent with recycling of altered oceanic crust and a mixture of pelagic sediments and lower continental crust into their mantle source. This supports a deep origin for the enriched mantle "EM-1"-like Dupal signatures encountered in Indian Ocean island basalts. In the Pacific Ocean, isotopic heterogeneity in basalts from the deepest parts of the Hawai'i Scientific Drilling Project (HSDP2) core on Mauna Kea, combined with prior results from overlying flows, indicate that shield basalts can be explained by mixing of variable proportions of four isotopically distinct components intrinsic to the Hawaiian mantle plume. The "Kea" component is the prevailing composition in Mauna Kea basalts and

throughout volcanic activity of the Hawaiian hotspot. The relatively depleted isotopic compositions of this "Kea" component are shared by other Pacific oceanic island basalt groups and are very similar to those of the common mantle component "C". This suggests that "Kea" may be a common and widespread composition within the deep mantle beneath the Pacific Ocean basin.

PREFACE

This dissertation encompasses four chapters (2 to 5) that were prepared in manuscript format appropriate for submission to international scientific journals. I am the leading author of the four chapters and all are co-authored by my supervisors Dr. Dominique Weis and Dr. James S. Scoates. Dr. Jane Barling, member of my supervisory committee, is also a co-author of Chapters 2 and 4.

All samples used for this dissertation were part of the working sample collection of Dr. Dominique Weis, as a participant of major international scientific projects (IODP and HSDP). All research, analytical work (except as indicated below), and manuscript preparation was carried out by me. For each chapter, my supervisors and co-authors contributions included exchange of ideas, advice, insightful comments, careful reviewing, as well as financial support.

CHAPTER 2
Leaching Systematics and Matrix Elimination for the Determination of High-Precision Pb Isotope Compositions of Ocean Island Basalts — a version of this chapter has been published in the electronic journal *Geochemistry Geophysics Geosystems* from the American Geophysical Union.

Nobre Silva, I. G., D. Weis, J. Barling, and J. S. Scoates (2009), Leaching systematics and matrix elimination for the determination of high-precision Pb isotope compositions of ocean island basalts, *Geochem. Geophys. Geosyst.*, *10*. Q08012, doi:10.1029/2009GC002537.

CHAPTER 3
The Effects of Acid Leaching on the Sr-Nd-Hf Isotopic Compositions of Ocean Island Basalts — a version of this chapter has been published in the electronic journal *Geochemistry Geophysics Geosystems* from the American Geophysical Union.

Nobre Silva, I. G., D. Weis, and J. S. Scoates (2010), Effects of acid leaching on the Sr-Nd-Hf isotopic compositions of ocean island basalts, *Geochem. Geophys. Geosyst.*, 11, Q09011, doi:10.1029/2010GC003176.

The Sr isotopic compositions presented in this chapter were analyzed by Dr. Bruno Kieffer.

CHAPTER 4
The Ninetyeast Ridge and its Relation to the Kerguelen, Amsterdam and St. Paul Hotspots in the Indian Ocean — is intended for publication.
Authors: Inês G. Nobre Silva, Dominique Weis, James S. Scoates and Jane Barling

Dr. Bruno Kieffer and Claude Maerschalk analyzed the Sr isotopic compositions and some of the Nd isotopic compositions presented in this chapter.

CHAPTER 5
Pb-Sr-Nd Systematics of the Early Mauna Kea Shield Phase and Insight Into the Deep Mantle Beneath the Pacific Ocean — is intended for publication.
Authors: Inês G. Nobre Silva, Dominique Weis and James S. Scoates

APPENDIX B
Ninetyeast Ridge Supplementary Samples
Pb-Sr-Nd-Hf Isotope Systematics of the Ninetyeast Ridge from Dredged Samples – Implications for its Mantle Sources
This appendix includes a preliminary study on 32 samples that were collected during a scientific expedition to the Ninetyeast Ridge, in the summer of 2007, on which I participated. Dr. Frederick A. Frey was one of the Principal Investigators and provided the major and trace element XRF and ICP-MS analyses on the selected Ninetyeast Ridge samples. I was responsible for acquiring Pb-Sr-Nd-Hf isotopic compositions on all 32 samples. After further analyses of additional samples, this work is intended for publication.

TABLE OF CONTENTS

CHAPTER 1

CHAPTER 2

CHAPTER 3

The Effects of Acid Leaching on the Sr-Nd-Hf Isotopic Compositions of Ocean Island Basalts

CHAPTER 4

The Ninetyeast Ridge and its Relation to the Kerguelen, Amsterdam and St. Paul Hotspots in the Indian Ocean

CHAPTER 5

Pb-Sr-Nd Systematics of the Early Mauna Kea Shield Phase and Insight Into the Deep Mantle Beneath the Pacific Ocean..139

LIST OF TABLES

CHAPTER 4

CHAPTER 5

LIST OF FIGURES

CHAPTER 2

CHAPTER 5

APPENDICES

APPENDIX A

APPENDIX B

Acknowledgments

My PhD research could be metaphorically described as a "Journey to the interior of the Earth". It was a great personal journey and, as such, there have been many people who, in their own way, contributed throughout the years to the completion of this long adventure. Whether by providing guidance and help at the academic and technical level, or by simply being present at certain stages of my life here in Vancouver, they made this a fuller, character-building, and worthwhile experience. For all that, I thank:

Firstly, my supervisors Dominique Weis and James S. Scoates, for their mentorship, patience, and support throughout the years. For their constant availability to their students, for encouraging me to keep going in the right direction, and for allowing me to learn and grow with my research. To Dominique ("*Zee Boss*") I am especially grateful for her patience and all the chocolate comfort *made in Belgium* that she provided to us all when our brains were in need of a sugar high.

Jane Barling ("*Aunty Jane*"), for the long hours of training on the MC-ICP-MS, for her patience and friendly ear when I needed one, either regarding my analytical work and my writing, and for the enumerable trips to IKEA.

Bruno Kieffer and Claude Maerschalk, for introducing me to the clean lab work at the PCIGR, for their help with the chemical separation and for running Sr and some Nd on the TRITON TIMS. I also thank Claude for mailing extra chocolate whenever our supply in Vancouver was running low. To Bruno, special thanks for always being available to help and for all the funny translation moments between Portuguese, French and English.

Bert Mueller and Vivian Lai, for their invaluable assistance during HR-ICP-MS work; and to Richard Friedman, for always providing whatever was needed in the lab and for his friendly smile at all times.

Mike O. Garcia and Fred. A. Frey for giving me the opportunity to be part of the scientific party of the "*Underwater Volcanoes of the Northern Hawaiian Islands*" and

CHAPTER 1

Introduction

1.1 Motivation and Rationale of the Research Project

Geochemical studies on ocean island basalts related to mantle plumes provide essential information about the composition and evolution of the Earth's deep mantle. This research focuses on the acquisition of high-precision radiogenic isotopic compositions on stratigraphically controlled samples of basalt related to two major mantle plume systems, Kerguelen in the Indian Ocean and Hawaii in the Pacific Ocean. Specifically, this study focuses on two of the longest hotspot tracks on Earth, the ~5000 km-long Ninetyeast Ridge and the ~6000 km-long Hawaii-Emperor Seamount chain. They were chosen because they formed in different settings and overlie different mantle domains as expressed, for example, by the lead (Pb) isotopic differences between basalts from the Pacific and Indian ocean basins [*Dupré and Allègre*, 1983]. Hawaii corresponds to the simplest geodynamic case, being the archetype example of intra-plate volcanism, formed by interaction of a hotspot with an over-riding plate [*Morgan*, 1971]. The Ninetyeast Ridge formed in a more complex geodynamic case, where the associated Kerguelen mantle plume has also interacted with a spreading centre [*Luyendyk*, 1977; *Royer et al.*, 1991]. The primary goal of this study is to identify the composition and relative proportions of different mantle components sampled during melting of these long-lived mantle plumes and to use this information to assess the nature of their deep mantle domains.

In the following sections, a brief overview of the relevant background information related to the major topics covered in this dissertation are provided.

1.2. Mantle Heterogeneity, Components and End-member Compositions

Over the past four decades, studies of mantle-derived rocks have established that the mantle is chemically and isotopically heterogeneous at different scales, from centimeters to thousands of kilometers [e.g., *Gast,* 1969*; Tatsumoto,* 1978*; Zindler and Hart*, 1986*; Sun and McDonough*, 1989; *Hofmann*, 2003]. Such heterogeneities are the result of differentiation and recycling processes throughout Earth history that continuously generate

continental crust, and trace element enriched and depleted mantle domains [e.g., *Zindler and Hart* 1986*; Hart*, 1988; *Weaver*, 1991]. These mantle domains are commonly referred to as reservoirs [e.g., *Sun and McDonough*, 1989; *Willbold and Stracke*, 2006]. The distinctive isotopic compositions of a specific reservoir in the mantle are referred to as components, which have no physical implications, and upon mixing are better described by their end-member compositions [e.g., *Zindler and Hart*, 1986*; Stracke et al.*, 2005*; Albarède,* 1995; *Hofmann,* 2003].

The isotopic variability observed among oceanic basalts and the recognition of specific isotopic characteristics within certain ocean island groups are interpreted as resulting from mixing between these isotopically distinct mantle components (Figure 1.1). These components are considered to derive from separate mantle sources characterized by different histories of parent and daughter elemental fractionation [e.g., *Zindler et al.*, 1982; *White*, 1985; *Zindler and Hart*, 1986]. *Zindler and Hart* [1986] identified four components, which they defined as: DMM (depleted mid-ocean ridge basalt (MORB mantle), HIMU (high U/Pb mantle), EM-1 and EM-2 (enriched mantle 1 and 2). In addition, the observation that most oceanic basalts, both OIB and MORB, converge towards a common area in multi-isotope space, led to the recognition of an additional common mantle component, which *Zindler and Hart* [1986] termed PREMA for prevalent mantle component. In subsequent isotopic studies, other common components, differing from each other only in minor details, were defined and termed FOZO (focal zone) [*Hart et al.,* 1992; *Stracke et al.*, 2005], "C" [*Hanan and Graham*, 1996], or PHEM (primitive helium mantle) [*Farley et al.*, 1992]. The presence of specific and traceable components in the mantle source of oceanic basalts provides a framework for discussing the origins of these basalts as well as the dynamics of mantle cycling.

1.3. Large Igneous Provinces and Mantle Plumes

Large igneous provinces (LIP) are the largest magmatic events known to occur on Earth and encompass a wide range of geological structures in both continental and oceanic
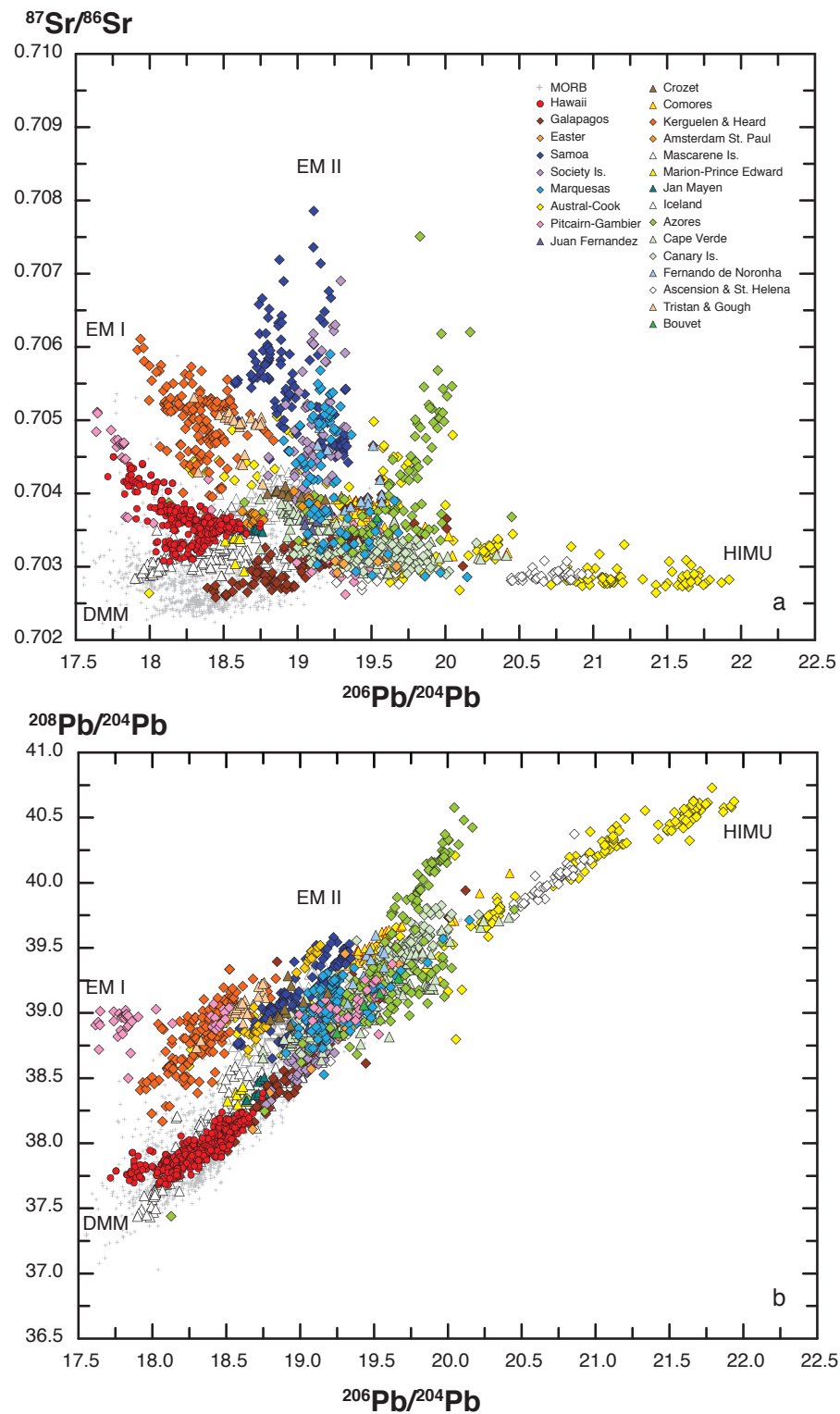
Figure 1.1. Diagrams of $^{87}Sr/^{86}Sr$ versus $^{206}Pb/^{204}Pb$ and $^{208}Pb/^{204}Pb$ versus $^{206}Pb/^{204}Pb$ for ocean island basalts worldwide. End-member compositions (DMM = depleted MORB mantle; EM-1 = enriched mantle 1; EM-2 = Enriched mantle 2; HIMU = high μ) are from *Zindler and Hart* [1986]. Data from the compilation of *White* [2010]; GEOROC database (http://www.georoc.mpch-mainz.gwdg.de).

environments (Figure 1.2). These include continental flood basalt provinces, volcanic passive margins and aseismic ridges, oceanic plateaus, submarine ridges, and seamounts and oceanic islands, which are the focus of this study. Large igneous provinces represent massive and rapid emplacements of predominantly mafic extrusive and intrusive rock at the Earth's surface. The processes responsible for their formation involve large amounts of thermal energy and are independent from "normal" seafloor spreading [*Coffin and Eldholm*, 1994]. LIP volumes can be up to 10^6 km^3 in a continental setting (e.g., Siberian traps) and up to 40×10^6 km^3 in an ocean setting (e.g., Ontong Java Plateau). They are typically emplaced within a geologically short period of time (<10 Myr), with the bulk of the magmatism commonly occurring within <1 Myr. In some cases, the magmatic activity may persist at a much-reduced rate for significantly longer time intervals (up to 100 Myr) and generate hotspot tracks or seamount chains [*Ernst et al.*, 2005; *Coffin et al.*, 2006] (e.g., Ninetyeast Ridge, Emperor-Hawaii Louisville, Chagos-Laccadive). The voluminous volcanism associated with LIP is assumed to account for ~10% of the heat released from the mantle [*Davies*, 1988; *Sleep*, 1992] and to have significant environmental impacts [e.g., *Larson*, 1991; *Kerr*, 2005; *Saunders*, 2005].

The origin of LIP was first explained by *Morgan* [1971] to be related to mantle plumes. These are buoyant upwellings of hot mantle that are chemically distinct from the upper mantle MORB source. Subsequently, numerous models of mantle plumes [e.g., *Richards et al.*, 1989; *White and McKenzie*, 1989; *Campbell and Griffiths*, 1990; *Gonnerman et al.*, 2004; *Jellinek and Manga*, 2004] and alternative theories have been developed and proposed (back arc processes, mantle "edge" convection, delamination, and bolide impact [*Saunders*, 2005; references therein]), to explain the origin of large igneous provinces. Despite the differences between the models, most agree that large amounts of thermal energy are required to produce the large volumes of magma over a geologically short period of time [*Saunders*, 2005].

Numerical and laboratory models for mantle plumes typically predict high melt production rates and high temperatures. The large volumes of magma erupted within short
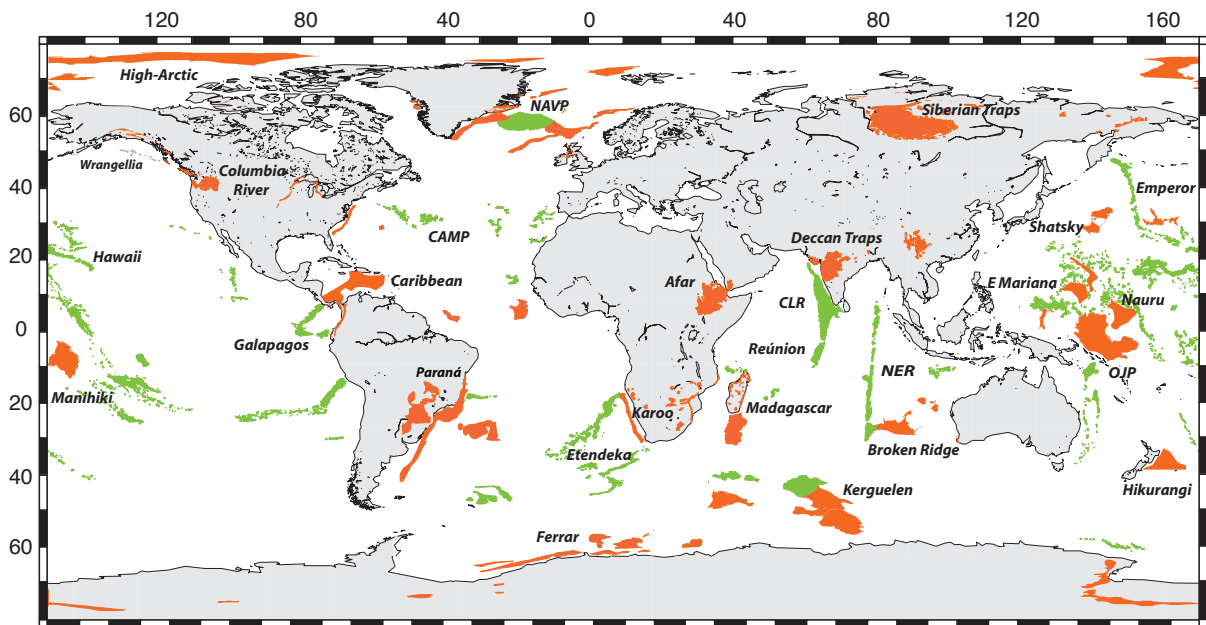
Figure 1.2. World map showing the global distribution of Phanerozoic Large Igneous Provinces (LIP). Short-lived or transient ("plume head") LIP are identified in orange and long-lived or persistent ("plume tail") LIP are identified in green, including the Ninetyeast Ridge and Hawaii hotspot tracks. Large Igneous Provinces are better preserved in the oceans where they are not subjected to terrestrial erosional processes and thus offer a prime target for scientific ocean drilling. Abbreviations: NAVP = North Atlantic Volcanic Province; CAMP = Central Atlantic Magmatic Province; CLR = Chagos-Laccadive Ridge; NER = Nintetyeast Ridge; OJP = Ontong Java Plateau. Map modified from Jules Verne Voyager maps (http://jules.unavco.org) and adapted from *Coffin et al.* [2006].

time intervals indicate that melt production rates for LIP must be at least 2 km^3/yr, when including the lower crustal intrusives, and require the involvement of deep mantle plumes [*White and McKenzie*, 1995]. Normal-temperature mantle is incapable of producing such large volumes of melt, even where it decompresses close to the Earth's surface, as it does beneath mid-ocean ridge spreading centers. This argument is supported by the petrology and geochemistry of the igneous rocks preserved in LIP, which suggests that plume temperatures are typically 150-300ºC higher than normal asthenospheric mantle [e.g., *Putirka*, 2005; *Herzberg et al.*, 2007]. These temperatures are also consistent with theoretical models of mantle plumes [e.g., *Campbell and Griffith*, 1991; *White and McKenzie*, 1995; *Davies* 1999; *Campbell*, 2005; *Herzberg et al.*, 2007].

The mantle plume model is the most widely accepted hypothesis for the origin of LIP, which are considered to result from decompression melting within the head of deep mantle plumes rising through the mantle from a hot boundary layer, most probably the core-mantle boundary (CMB) [e.g., *Campbell and Griffith*, 1990; *Coffin and Eldholm*, 1994; *Montelli et al.*, 2004; *Jellinek et al.*, 2003; *Jellinek and Manga*, 2004; *Campbell*, 2005; *Coffin et al.*, 2006]. Several theoretical studies [e.g., *Lenardic and Kaula*, 1994; *Farnetani*, 1997; *Kellogg et al.*, 1999] have focused on the composition, structure and geophysical properties of the D'' region, to gain a better understanding of the source of mantle plumes. Assuming that the D'' (the lowermost 200 km of the mantle) is the source region of most mantle plumes, the study of plume-related volcanic rocks is the best way geoscientists have to assess the geochemical variability of the deepest mantle [*DePaolo and Weis,* 2007]. Hence, study of the trace element and isotopic geochemistry of volcanic rocks associated with LIP provides a means to investigate the compositions and processes that occur in regions of the mantle other than the asthenospheric upper-mantle, which is the source of mid-ocean ridge basalts.

1.4 Hawaiian Mantle Plume – The Hawaiian-Emperor Seamount Chain

Located in the northern Pacific Ocean, the ~6000 km long Hawaiian-Emperor Seamount Chain (HESC) is one of the most remarkable features in the Pacific Ocean basin

(Figure 1.3). It comprises at least 129 volcanoes [*Regelous et al.,* 2003; *Sharp and Clague,* 2006] and is thought to result from a relatively simple geodynamic setting of the northward motion of the Pacific Plate over a long-lived, relatively fixed hotspot – *the Hawaiian mantle plume* [e.g., Morgan, 1971; *Clague and Dalrymple,* 1987]. The distinctive 60º bend at 32ºN separates the northward-trending Emperor seamounts and the westward-trending Hawaiian islands, and is interpreted to have resulted from a change of the Pacific Plate motion around 50 Ma [*Keller et al.,* 2000; *Tarduno et al.,* 2003; *Sharp and Clague,* 2006]. These two segments constitute an age-progressive chain of seamounts and islands, the oldest being Meiji seamount (85 Ma) located at 53ºN 165ºE and the youngest being Loihi seamount at 19ºN 155ºE (35 km southeast of the Big Island) and which is still in its pre-shield stage of volcanic activity [*Keller et al.,* 2000; *Regelous et al.,* 2003; *Dixon and Clague,* 2001]. Combined, the total volume of volcanic material erupted for the entire chain (7.08 x 10^6 km^3) [*Vidal and Bonneville,* 2004] is comparable to that of other large igneous provinces.

Of all the seamounts and islands, the Big Island of Hawai'i is the best studied. It is formed by the coalescence of five different shield volcanoes: Kohala, Mauna Kea, Hualalai, Mauna Loa and Kilauea, of which the last three are still historically active [e.g., *Clague and Dalrymple,* 1987]. As the different volcanoes grow, their lavas overlap and inter-layer, causing older volcanoes to become partially covered by lavas from younger volcanoes. From studies of lavas accessible at the surface of Hawaiian volcanoes, an ideal volcano growth model has been developed [e.g., *Clague,* 1987; *Moore and Clague,* 1992; *Chen and Frey,* 1983; *Wolfe and Morris,* 1996] to explain the change in different lava types, eruption rates and magma volumes encountered at each volcano as the Pacific Plate moves over the Hawaiian hotspot. In a thermally and compositionally concentric model for the Hawaiian plume [*Griffith and Campbell,* 1990; *Frey and Rhodes,* 1993; *Lassiter et al.,* 1996, *DePaolo et al.,* 2001], melt production is low at the cool periphery of the melt zone, initiating volcanism on the ocean floor with low eruption rates of alkalic and transitional tholeiitic basalts during the pre-shield phase. As the volcano migrates over the hotter central part of the plume, melt production increases, and high eruption rates of tholeiites and picrites are observed during the shield-building phase. During this phase, which accounts for ~95% of
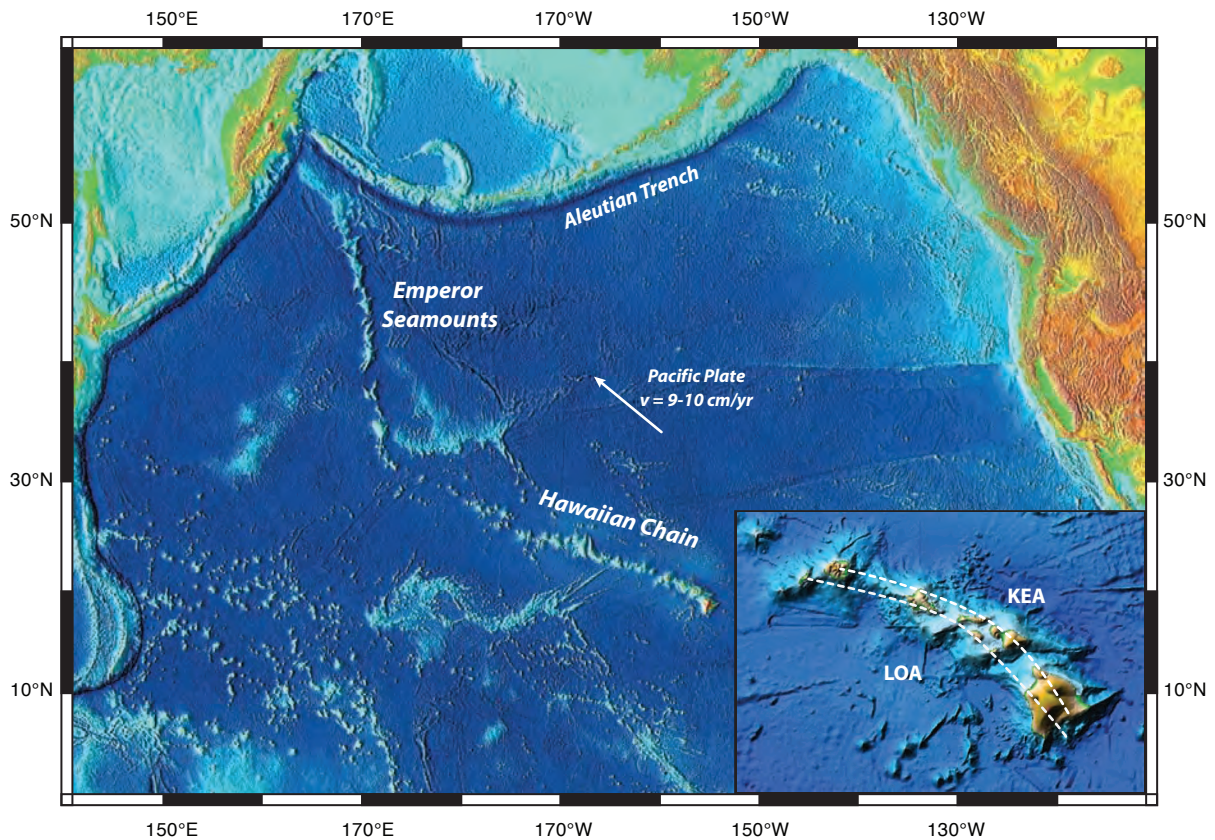
Figure 1.3. Bathymetric map of the Northern Pacific Ocean showing the Hawaiian-Emperor Seamount chain and its distinctive 60° bend. Inset shows the Hawaiian Islands and the distinctitve double chain of volcanoes including the southwestern Loa chain and the northeastern Kea chain. Adapted from the NOAA Surface of the Earth poster (http://www.ngdc.noaa.gov/mgg/fliers/00mgg05.html; http://www.ngdc.noaa.gov/mgg/global/global.html).

the volcano's volume, the volcano reaches subaerial heights (up to 4000-5000 m above sea level). As the volcano moves away from the melting zone, the melt production and eruption rates decline, giving way to the post-shield phase, characterized by inter-bedded eruptions of tholeiites, transitional tholeiites and alkalic basalts. As the volcano continues to move away, a period of quiescence (<0.4 to 2.5 Myr) follows, after which the volcano can undergo infrequent small-volume eruptions of strongly alkalic basalts from vents not associated with pre-existing structures [e.g., *Clague and Dalrymple*, 1987].

1.4.1. Hawai'i Scientifc Drilling Project (HSDP)

Drilling of ocean island volcanoes provides unique access to a continuous sequence of samples that can be studied and interpreted in the context of shallow-level magmatic processes and deeper mantle evolution with time. With the recovery of ~3500 m long continuous stratigraphic sequence of predominantly Mauna Kea lavas during the Hawaii Scientific Drilling Project (Figures 1.4 and 1.5), major advances have been made in terms of understanding the geochemical and petrological structure of an Hawaiian volcano [e.g., *DePaolo et al.*, 1996; *Stolper et al.*, 2009]. The HSDP provided a remarkable opportunity to quantify and characterize the geochemical evolution of a single volcano (in this case, Mauna Kea) as it moves with the Pacific Plate across a mantle plume and samples different zones of the melting region.

During the second phase of HSDP, a large amount of high-precision geochemical data was acquired [e.g., *Blichert-Toft et al.,* 2003*; Eisele et al.*, 2003*; Kurz et al.*, 2004*; Bryce et al.*, 2005], leading to a better understanding of the chemical structure of the Hawaiian mantle plume, involving different scales of heterogeneity within the plume. "Large scale" heterogeneities relates to the overall geochemical structure of the Hawaiian mantle plume and is best discriminated when comparing the several volcanoes that make up the Hawaiian Islands. The correspondence of the two geographically parallel chains (Loa and Kea, [*Dana,* 1849*; Jackson et al.*, 1972]) to two geochemically distinct trends is a reflection of this large-scale structure [*Tatsumoto,*1978]. "Small scale" heterogeneities relates to
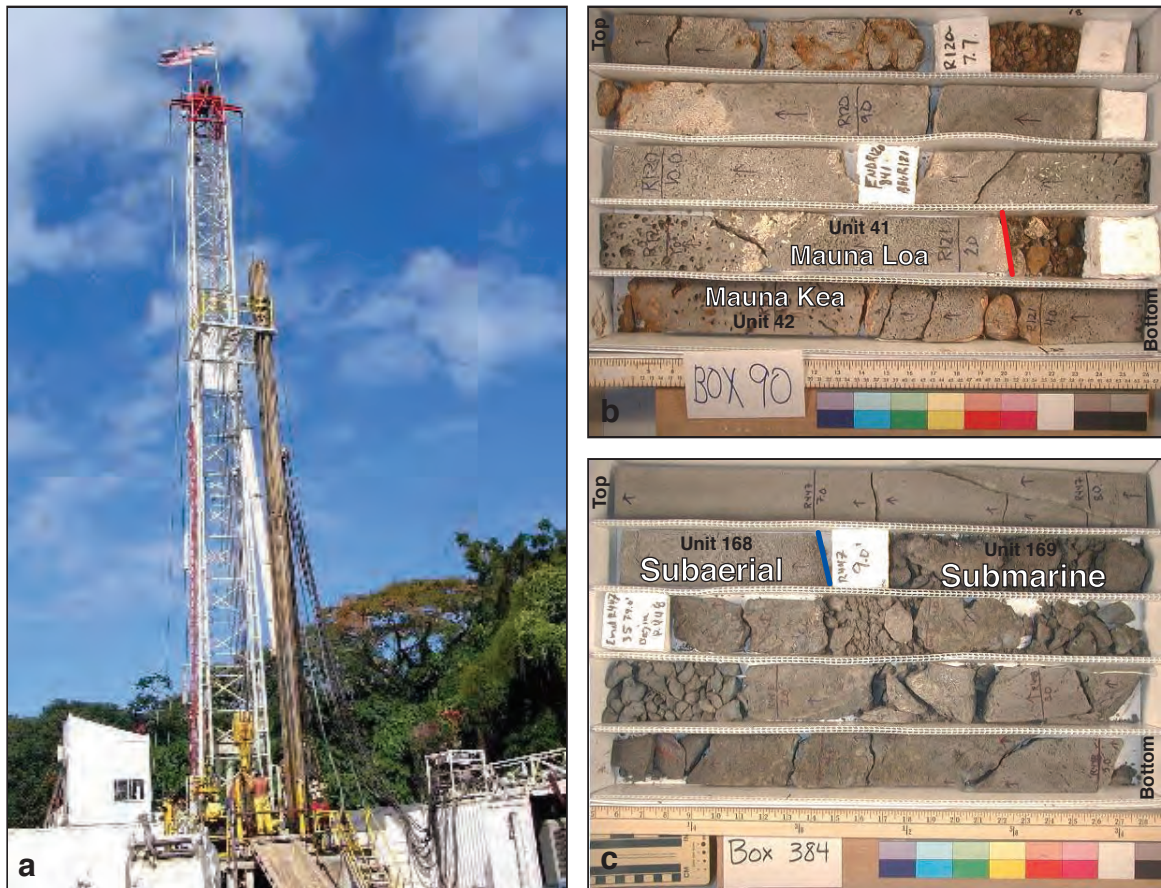
Figure 1.4. Photographs from the main drilling phase 2 of the Hawaii Scientifc Drilling Pproject at Hilo. (a) The HSDP2 drill rig (owned by the Drilling, Observation and Sampling of the Earth's Continental Crust Corporation, DOSECC). (b) Working half of core where the stratigraphic contact between subaerial basalts from Mauna Loa and Mauna Kea can be observed; (c) Working half of core where the stratigraphic contact between Mauna Kea subaerial and submarine lavas was encountered. Photographs from the HSDP public data at http://www.icdp-online.org.
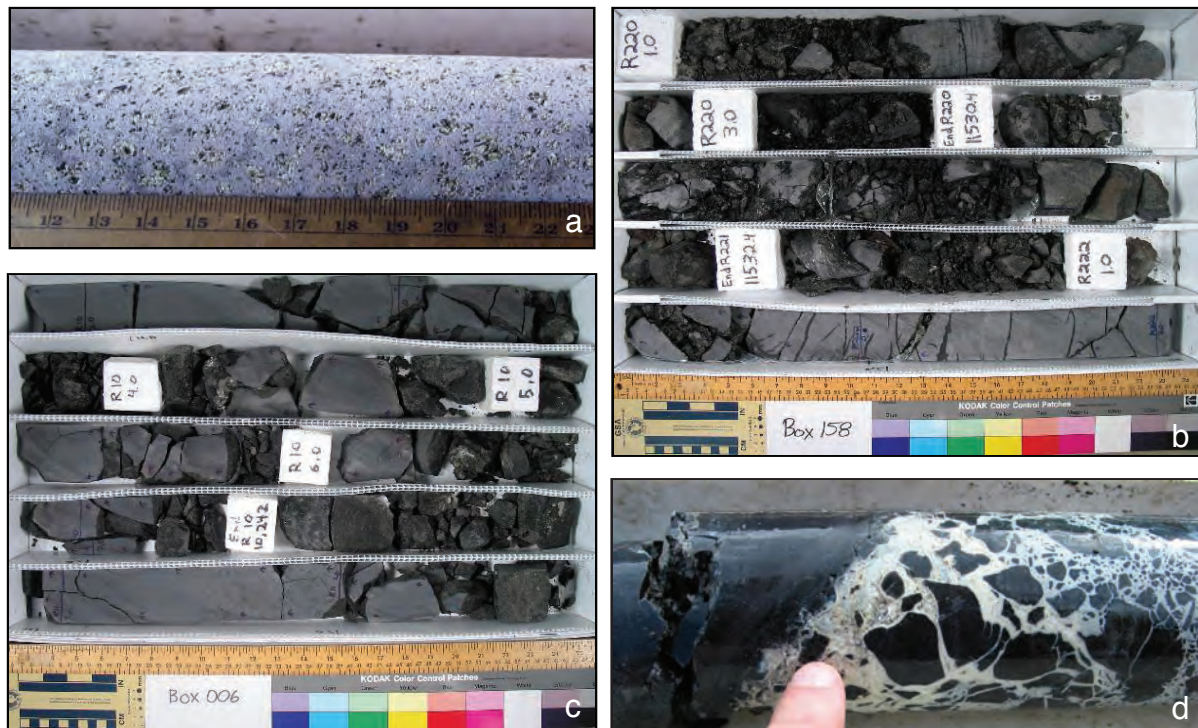
Figure 1.5. Photographs of representative core recovered during the HSDP2–B and HSDP2–C. (a) Intrusion with abundant olivine clasts. (b) Working box of core containing moderately plagioclase-clinopyroxene-olivine-phyric basalt, recovered at ~3098 mbsl. (c) Working box of core containing massive aphyric basalt, recovered at ~3348 metres below sea level (mbsl). (d) Pillow breccia – team scientist points to the clay of a pillow breccia (normally green) that was baked to a white color by an overlying intrusion. Photographs taken from HSDP public data at http://www.icdp-online.org.

smaller and more common geochemical variations within the mantle plume and is best distinguished when looking at the isotopic variations within a single volcano.

Elemental and isotopic distinctions observed between basalts from the Loa and Kea trend volcanoes have been interpreted as reflecting sampling of two different areas of the Hawaiian mantle plume. Some authors [e.g., *Lassiter et al.*, 1996; *DePaolo et al.*, 2001; *Kurz et al.*, 2004; *Bryce et al.*, 2005] have interpreted these two areas to be more central and peripheral zones, respectively, within a concentrically zoned mantle plume. At a broader scale, the elemental and isotopic differences between basalts from the Loa and Kea trends might reflect concentric zonation of the plume. However, this zonation model does not account for the variations observed in Pb isotopic space, nor of the other isotopic systems when combined with Pb for both the Loa and Kea trend volcanoes. Based on the Pb isotopic compositions of several Hawaiian volcanoes, *Abouchami et al.* [2005] interpreted the systematic differences between the two trends as reflecting a bilateral compositional difference between the southwest and northeast sides of the plume.

Pb isotopes are extremely useful in identifying different mantle components [e.g., *Tastumoto,* 1978*; Sun*, 1980]. Pb isotope systematics of Mauna Kea samples collected during HSDP-2 allowed for the identification of three distinct Pb linear arrays, which were inferred to represent at least four mantle components involved in the origin of Mauna Kea lavas [*Eisele et al., 2003*]. These Pb trends were interpreted as reflecting small-scale vertical heterogeneities within the plume stem. Whereas Sr, Nd, Hf and He isotopic compositions analyzed to date appear to mimic the concentric temperature distribution within the hotspot [*Blichert-Toft et al*., 2003*; Kurz et al*., 2004*; Bryce et al*., 2005], Pb isotopes are not as affected and are more sensitive to the superposition of vertical and lateral heterogeneities within the plume source.

1.5. Kerguelen Mantle Plume System

The Indian Ocean basin is dominated by volcanic features related to activity of the Kerguelen mantle plume, including the *Kerguelen Plateau, Kerguelen Archipelago, Broken Ridge* and the *Ninetyeast Ridge* (Figure 1.6). Together with their continental counterparts (Bunbury basalts, southwestern Australia; Rajmahal Traps, northeast India; lamprophyres in conjugate margins of India and Antarctica), they represent ~130 Myr of magmatic activity and ~2.5 x 10^7 km^3 of magma output by the Kerguelen mantle plume [*Coffin et al.*, 2002; *Frey et al.*, 2002]. The formation of these features involves a considerably more complex geodynamic setting than that of Hawaii and is intimately related to the break-up of Gondwana and evolution of the Indian Ocean during the Cretaceous and Cenozoic by the interaction of the deep-seated Kerguelen mantle plume with the newly forming spreading centre.

Based on new radiometric ^{40}Ar/^{39}Ar ages [*Coffin et al.*, 2002; *Duncan*, 2002], the Bunbury basalts represent the first clear manifestation of the Kerguelen plume, from ~132 to ~123 Ma. This period was characterized by low output rates (<0.1 km^3/yr), and coincides with the continental breakup between Australia/Greater India and Australia/Antarctica [*Frey et al.*, 2003]. Subsequently, the Naturaliste Plateau formed at ~124 Ma [*Davies et al.*, 1989]. Between ~123 and ~110 Ma, as spreading between India and Antarctica proceeded, magma output rates increased substantially (to ~0.9 km^3/yr) and the emplacement of the Southern Kerguelen Plateau, Rajmahal Traps and lamprophyres on the Indian and Antarctic continental margins took place.

From ~110 to ~105 Ma, low rates of volcanism gave rise to volcanic rocks found at Elan Bank [*Coffin et al.*, 2002], a western salient with different orientation than that of the Kerguelen Plateau, that has been interpreted as a fragment of continental crust isolated within oceanic lithosphere as pieces of East India broke off [e.g. *Coffin et al.*, 2002; *Frey et al.*, 2002a]. Another peak of volcanism resulted in the formation of the Central Kerguelen Plateau, between ~105 and ~100 Ma, and Broken Ridge between ~100 and ~95 Ma. For the period between ~95 and ~82 Ma, no record of volcanic activity by the Kerguelen plume has
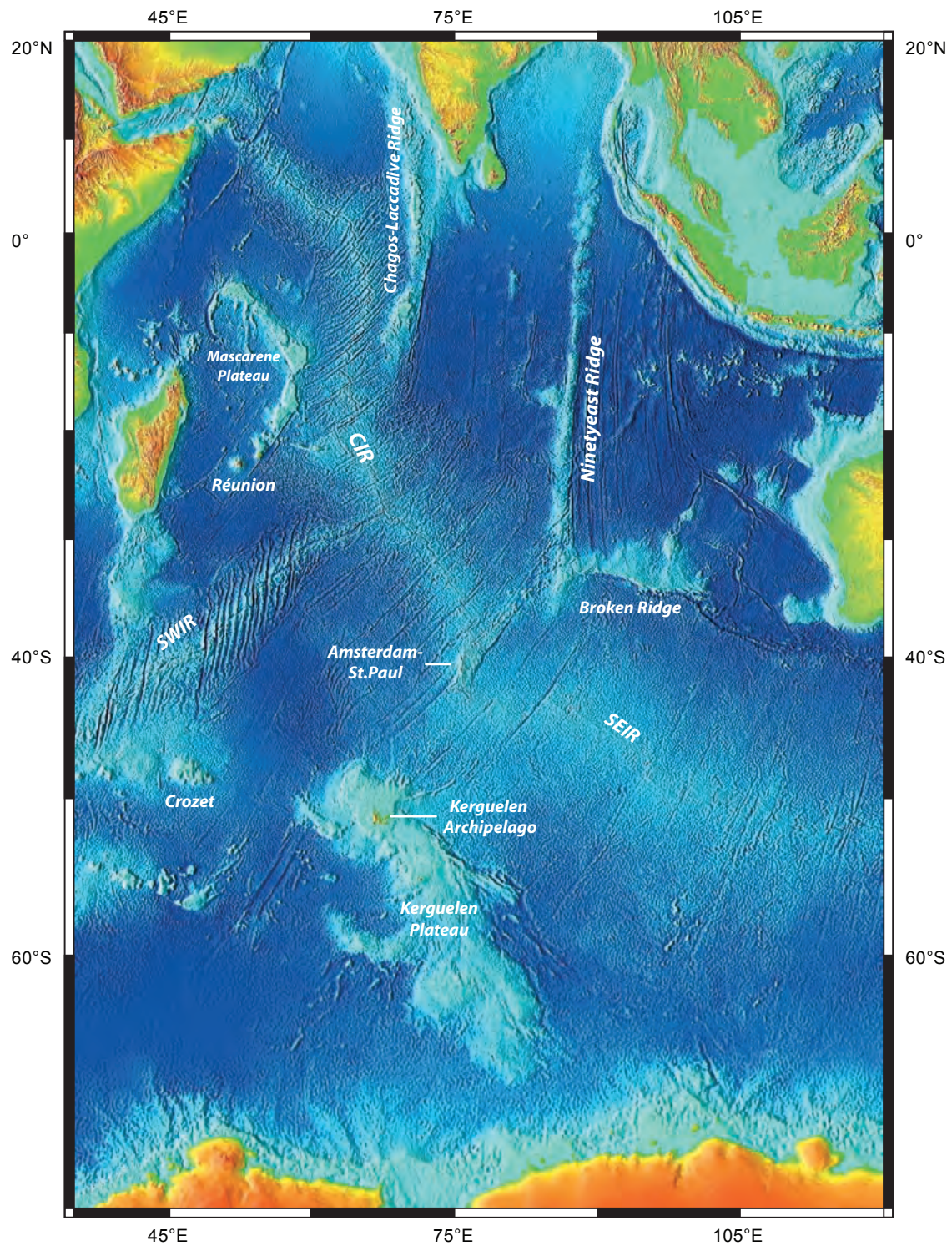
Figure 1.6. Bathymetric map of the Indian Ocean showing its major topographic features, including those related to the Kerguelen hotspot. Abbreviations: CIR = Central Indian Ridge; SWIR = Southwest Indian Ridge; SEIR = Southeast Indian Ridge. Adapted from the NOAA Surface of the Earth poster. (http://www.ngdc.noaa.gov/mgg/fliers/00mgg05.html).

yet been found, but may correspond to the oldest part of the Ninetyeast Ridge now buried beneath the Bengal Fan [*Frey et al.*, 2003]. A subsequent magmatic phase characterized by lower output rates (~0.1 km^3/yr) [*Coffin et al.*, 2002] gave rise to Skiff Bank (~68 Ma) and to the Ninetyeast Ridge from ~82 to ~38 Ma [*Duncan*, 1991], as the Indian Plate moved rapidly northward over the hotspot [*Frey et al.*, 2002].

Around 40 Ma, the recently formed Southeast Indian Ridge (SEIR) jumped northeastward intersecting the hotspot and leading to the breakup between the Central Kerguelen Plateau and Broken Ridge [*Coffin et al.*, 2002; *Frey et al.*, 2003]. Consequently, plume-related magmatism became confined to the Antarctic plate and the Northern Kerguelen Plateau formed on relatively old oceanic lithosphere. From ~30 Ma to ~24 Ma [*Nicolaysen et al.*, 2000], the Kerguelen Archipelago flood basalts formed on top of the Northern Kerguelen Plateau, at variable output rates, and significantly less voluminous alkalic volcanism continued until <1 Ma [*Weis and Giret*, 1994; *Weis et al.*, 1998]. Since ~21 Ma, magmatism related to the Kerguelen plume has created Heard and McDonald Islands [*Barling et al.*, 1990; 1994], as well as a northwest-southeast trending chain of submarine volcanoes (Kerimis seamounts) between these islands [*Weis et al.*, 2002], on the central sector of the Kerguelen Plateau. As Heard and McDonald Islands are currently volcanically active, they represent the most likely present-day position of the Kerguelen hotspot and underlying mantle plume [*Weis et al.*, 2002].

1.5.1. Ninetyeast Ridge: Longest Linear Feature on Earth

With a length of ~5000 km, the Ninetyeast Ridge (NER), an aseismic volcanic ridge, is the longest linear feature on earth. Located in the eastern Indian Ocean along the 90ºE meridian (Figure 1.4), it extends from 34ºS at its intersection with Broken Ridge to ~17ºN where it is buried beneath sediments of the Bengal Fan [*Royer et al.*, 1991; *Mukhopadhyay and Krishna*, 1995; *Krishna et al.*, 2001]. The ridge varies in width from 100 to 200 km [*Royer et al.*, 1991] and it is elevated to ~3.5 km above the Central Indian Basin to the west and the Warton Basin to the east [*Krishna et al.*, 2001].

The Ninetyeast Ridge was the scientific destination of several oceanographic cruises, among which two were from the Deep Sea Drilling Project (DSDP) and one from the Ocean Drilling Program (ODP). The basement of the NER was sampled in 1972 by DSDP drilling at four sites (Leg 22, Sites 214 and 216; and Leg 26, Sites 253 and 254) and in 1988 by ODP drilling at three sites (Leg 121, Sites 756, 757 and 758), where ~180 m of tholeiitic basalt, affected by variable degrees of post-magmatic low temperature alteration, were recovered from a total penetration of ~310 m [*Shipboard Scientific Party,* 1989; *Weis et al.*, 1991]. Paleontological, paleomagnetic and radiometric studies on samples recovered during these cruises indicate that basement rocks were erupted subaerially or in shallow water depths [*Shipboard Scientific Party,* 1989; *Saunders et al*., 1991] and that ages become systematically older in a northward direction, from ~38 Ma at DSDP Site 254 to ~82 Ma at ODP Site 758 [*Duncan*, 1978, 1991; *Royer et al.* 1991].

The origin of the Ninetyeast Ridge has been debated for decades [*Whitford and Duncan*, 1979; *Royer et al.*, 1991] with many tectonic models (e.g., horst structure, overthrusted plate boundary, interaction between a spreading center and transform fault, hotspot track) being proposed for its formation. After drilling results from the Ninetyeast produced during DSDP and ODP, the general consensus for its formation was that the ridge formed from enhanced volcanism generated by a fixed hotspot at the edge of the Indian Plate as it moved rapidly northward [*Whitford and Duncan*, 1979; *Royer et al.*, 1991; *Duncan*, 1991; *Frey et al.*, 1991; *Weis & Frey*, 1991]. However, the identity and number of mantle plumes (Kerguelen, Amsterdam-St. Paul) involved in the generation of the ridge [*Saunders et al.*, 1991; *Royer et al.*, 1991; *Weis and Frey*, 1991] remained open questions.

Basement paleolatitudes measured at drill sites 757 to 217 are mostly consistent with a volcanic source that remained at a constant paleolatitude near 50ºS. This was interpreted as the present-day latitude of the Kerguelen plume [*Royer et al.*, 1991], under the westernmost extremity of the Kerguelen Plateau. Given that no recent activity or seismicity has been reported from this area [*Royer et al.*, 1991] and that recent radiometric (^{40}Ar/^{39}Ar) dating from ODP Leg 183 at Site 1139 (Skiff Bank) give ages of ~68 Ma [*Duncan*, 2002], this

cannot be the present location of the Kerguelen mantle plume. According to *Steinberg* (2000), a present-day positioning of the plume under the Kerguelen Archipelago improves the fit of the Ninetyeast Ridge and Rajmahal Traps in a fixed hot-spot reference frame. However, the most recent volcanic activity is encountered at Heard and McDonald Islands ~400 km to the southeast of the archipelago [*Barling et al.*, 1994; *Weis et al.*, 2002]. As suggested by *Royer et al.* (1991) and others, the mismatch of the model tracks for the Ninetyeast Ridge assuming the Kerguelen hotspot is underneath Heard and McDonald Islands might imply a southern migration of the plume. This is coherent with the general trend of recent volcanism occurring in a southeasterly direction from the Northern Kerguelen Plateau to the Kerguelen Archipelago to Heard and McDonald Islands [*Weis et al.*, 2002]. However, some paleolatitudes (~43ºS) measured at Site 757 at Site 756 [*Klootwijk et al.*, 1991] do not agree with the latitude of Kerguelen, and may be related to the interaction of Amsterdam-St. Paul hotspot (which at present is at latitudes of ~40ºS) in the formation of the Ninetyeast Ridge [*Saunders et al.*, 1991; *Royer et al.*, 1991].

The uncertainty of the mantle source, or sources, for basalts of the Ninetyeast Ridge is also reflected in the different interpretations based on isotopic compositions. Ninetyeast Ridge basement lavas show incompatible element abundances and radiogenic isotope signatures (Sr-Nd-Pb) intermediate between those of Indian MORB and very enriched ocean island basalt compositions, with more similarities to the latter [*Frey et al.*, 1991; *Saunders et al.*, 1991; *Weis and Frey*, 1991; *Weis et al.*, 1991]. *Weis and Frey* [1991] and *Saunders et al.* [1991] interpreted the Ninetyeast Ridge isotopic compositions as indicating mixing between at least three mantle components: a depleted MORB-like component, an enriched Kerguelen hotspot-type component, and a component comparable to the one sampled by basalts from Amsterdam-St. Paul Islands along the Southeast Indian Ridge. Differences in the isotopic compositions between sites thus reflect differing relative proportions of each component due to the change in the tectonic setting, from hotspot centred volcanism at Site 758 to hotspot-ridge interaction volcanism at Site 756. *Class et al.* [1993] interpreted increasing Pb isotope trends with decreasing eruption age from Site 758 (~82 Ma) to Site 757 (~58 Ma) to Site 756 (~43 Ma) as reflecting the compositional evolution of a single young homogeneous plume by

secular changes in isotopic ratios resulting from radioactive decay in the source. This compositional trend with age, however, is not observed in the Sr and Nd isotopic systems [*Weis and Frey*, 1991; *Saunders et al.,* 1991].

Finally, numerous recent studies (especially those resulting from ODP Leg 183) on other parts of the Kerguelen LIP have significantly increased the trace element and isotopic dataset for the overall Kerguelen plume system. With this new dataset, new interpretations of the Kerguelen plume end-member compositions have been developed [e.g., *Mattielli et al.,* 2002; *Ingle et al.*, 2003; *Doucet et al.*, 2005]. *Ingle et al.* [2003] proposed the existence of two distinct parts of the Kerguelen plume system, the "plume head" and the "plume tail", to explain the isotopic differences between the Kerguelen Plateau-Broken Ridge and Kerguelen Archipelago lavas. The significantly expanded isotopic dataset for components of the Kerguelen plume system, combined with these new interpretations, offers the opportunity to re-examine the origin of the Ninetyeast Ridge and deep mantle composition beneath the Indian Ocean basin.

1.6. Analytical Challenges

The combination of analyses of different isotopic systems (e.g., Sr-Nd-Hf-Pb) on samples of oceanic basalts constitutes a powerful tool for the determination and characterization of their mantle sources and components [e.g., *Gast et al.*, 1964; *Tatsumoto*, 1966, 1978; *White and Hofmann*, 1982; *Dupré and Allègre*, 1983; *Hart*, 1984; *White*, 1985; *Hamelin et al.*, 1986; *Zindler and Hart*, 1986; *Weaver*, 1991; *Hofmann*, 1997; 2003; *Stracke et al.*, 2005]. Inherent to their emplacement in an oceanic environment, oceanic basalts are susceptible to seawater alteration (Figure 1.7), and the effects of this alteration on Rb-Sr and U-Pb isotope systematics have long been recognized [e.g., *Hart et al.*, 1974; *Hawkesworth and Morrison*, 1978; *Cohen and O'Nions*, 1982; *Verma*, 1992; *Staudigel et al.*, 1995; *Krolikowska-Ciaglo et al.*, 2005]. Another well-known cause of disturbance of the isotopic compositions of basalts, especially for Pb isotopes, is contamination during crushing and

a — J2-020-23 (ML, Hawaii)

Opx.

Plag.

Ol.

Ol.

1 mm

J2-020-23 (ML, Hawaii)
Submarine Tholeiitic basalt
~450 ka
MgO (wt%) = 14.3
A.I. =-0.87
LOI (wt%) = 0.99

c — OB93-165 (Mt. Crozier, KA)

Plag.

Ol.

Plag.

0.5 mm

OB93-165 (Mt. Crozier, KA)
Subaerial Alkalic basalt
~24 Ma
MgO (wt%) =3.5%
A.I. = 0.67

b — SR0954-8.00 (MK, Hawaii)

Ol.

Plag.

Ol.

Idding.

1 mm

SR0954-8.00 (MK, Hawaii)
Submarine Tholeiitic basalt
~550 ka
MgO (wt%) = 18.2%
A.I. = -1.31
LOI (wt%) = 0.86

d — ODP Leg183, 1140A-31R-1, 57-61 (NKP)

Ol.

Ol.

Plag

Plag.

1 mm

ODP Leg183, 1140A-31R-1, 57-61 (NKP)
Submarine Tholeiitic basalt
~34 Ma
MgO (wt%) = 5.7
A.I. = -0.81
LOI (wt%) = 1.65
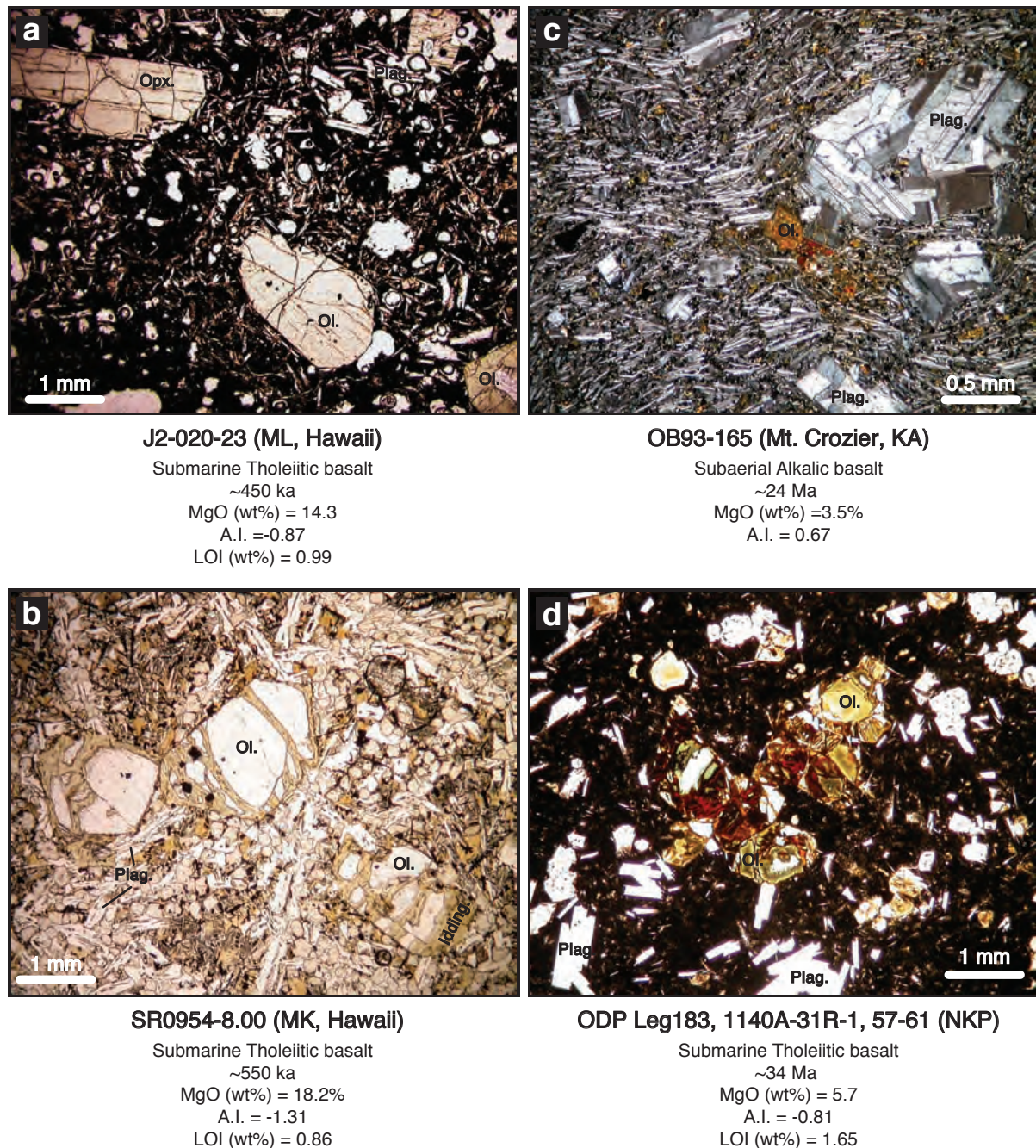
Figure 1.7. Photomicrographs in plane-polarized light of typical ocean island basalts analyzed in this study from Hawaii and Kerguelen. Abbreviations: ol. = olivine; plag. = plagioclase; Idding. = iddingsite. (a) Hawaiian basalt from Mauna Loa (sample J2-020-23), characterized by large unaltered olivine phenocrysts in a fine-grained groundmass with trace alteration. (b) Hawaiian basalt from Mauna Kea (sample SR0954-8.00), showing minor alteration of the olivine phenocrysts and moderate alteration of the groundmass (yellow-green patches). (c) Basalt from Mont Crozier on the Kerguelen Archipelago (sample OB93-165), characterized by unaltered, zoned euhedral plagioclase phenocrysts and minor olivine phenocryst partially to completely iddingsitized, set in a medium-grained groundmass, moderately altered. (d) Basalt from the northern Kerguelen Plateau (sample ODP Leg183, 1140A-31R-1, 57-61), showing plagioclase and olivine phenocrysts set in a fine-grained groundmass. Olivine phenocrysts are completely altered. Photomicrographs taken by M.O. Garcia and D. Hanano.

grinding [e.g., *Woodhead and Hergt*, 2000; *McDonough and Chauvel*, 1991; *Weis et al*., 2005].

Over the last decade, advances in analytical techniques, particularly the development of the multiple collector inductively coupled plasma mass spectrometry (MC-ICP-MS), have allowed the isotope ratios of numerous elements to be determined with significantly improved precision [e.g., *Albarède et al*., 2004] compared to that obtained by conventional TIMS. With the increase in precision afforded by the triple spike thermal ionization mass spectrometry (TS-TIMS) and MC-ICP-MS, the differences between unleached and leached samples is now resolved for Pb isotope compositions, with the unleached showing generally a more radiogenic character than the leached samples [*McDonough and Chauvel*, 1991*; Abouchami et al., 2000; Eisele et al., 2003; Baker et al., 2004; Weis et al.,* 2005]. To overcome the chemical disturbance caused by alteration, plus possible contamination during sample handling, careful acid leaching of samples prior to dissolution and analysis (Figure 1.8) has proven to be an effective and essential step in sample processing for mantle geochemistry studies [e.g., *Manhès et al*., 1978; *Dupré and Allègre*, 1980; *McDonough and Chauvel*, 1991; *Eisele et al*., 2003; *Stracke et al*., 2003; *Weis et al*., 2005; *Thompson et al*., 2008; *Hanano et al*., 2009; *Nobre Silva et al*., 2009].

1.7 Overview of this Dissertation

The contents of this dissertation focus on identification and interpretation of mantle source components in oceanic basalts whose variations in isotopic compositions reflect the presence of geochemical heterogeneities within the Earth's mantle [e.g., *White et al*., 1985; *Zindler and Hart*, 1986; *Hanan and Graham*, 1996]. Before one can confidently attribute a certain correlation of isotopic compositions observed in a suite of oceanic basalts to a specific mantle source component, one must be confident that the measured isotopic compositions are indeed primary or magmatic. Inherent to their emplacement in the oceanic environment, oceanic basalts (both MORB and OIB) are highly susceptible to the effects of seawater alteration that can vary from moderate to extensive depending on how long the

a) Sample collection

b) Sequential Acid Leaching

1st step

Last acid step (>15x)

Intermediate steps

c) Chemical Separation

d) High-Precision
   Isotopic Analyses

MC-ICP-MS   TIMS
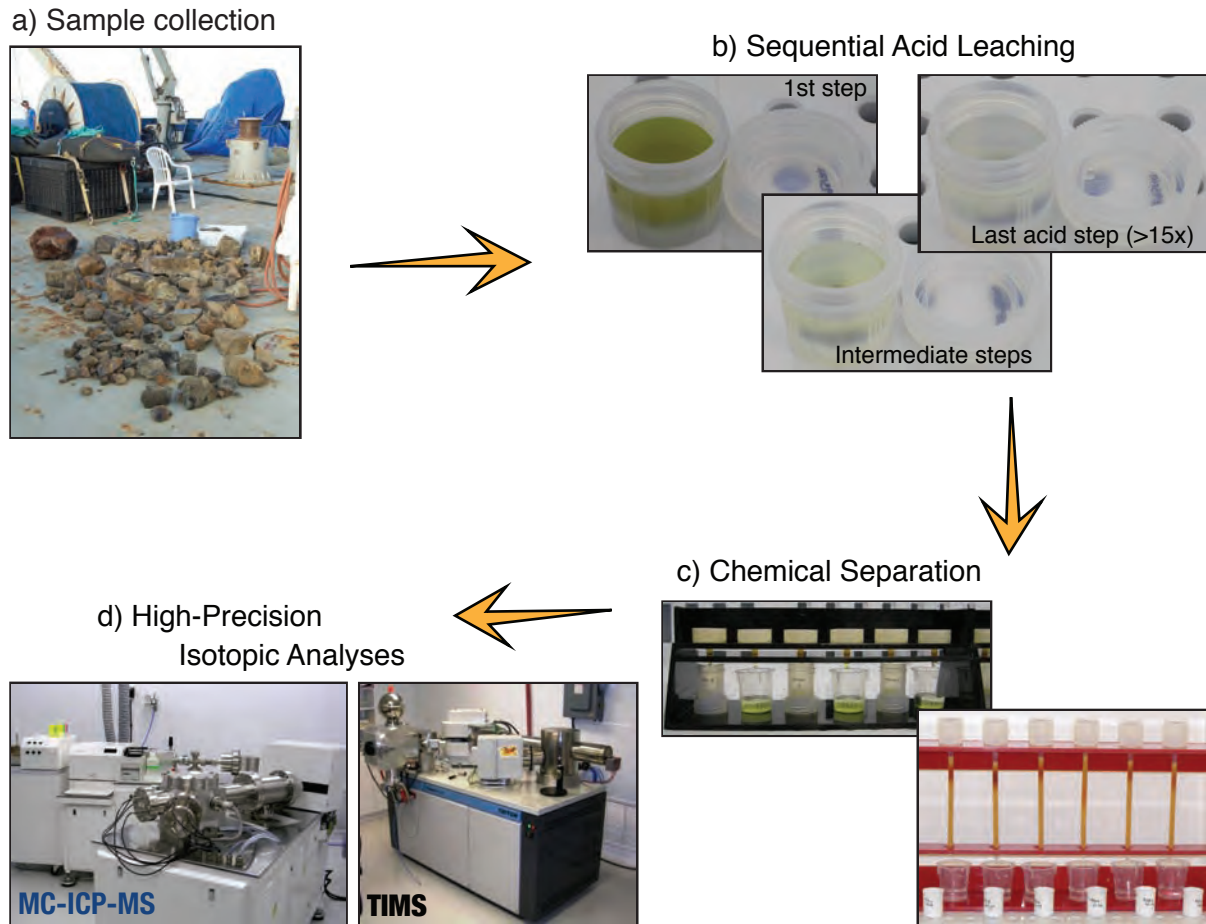
Figure 1.8. Photographs showing the analytical approach used in this study for the isotopic analysis of ocean island basalts, from sample collection to laboratory and chemical treatment to data acquirement. (a) Submarine basalts recovered by dredging. (b) Some of the acid leaching steps. Note the change in colour of the supernatant from green to pale yello and translucid. (c) Chromatographic columns used in the separation of the elements of interest for isotopic analysis. (d) Mass spectrometers used for the acquisision of the isotopic compositions.

basalts have interacted with the seawater and at what temperature [e.g., *Hart et al.*, 1974; *Staudigel et al.*, 1995; *Thompson et al.*, 2008]. Interaction with seawater can change the original elemental contents of the fresh basalts, which in turn can affect their isotopic systematics, especially with respect to the Rb-Sr and U-Pb isotopic systems. Additional disturbances to the isotopic compositions of basalts, especially for Pb isotopes, can be introduced by contamination during sample collection, crushing and grinding [e.g., *Weis et al.*, 2005]. To obtain the most accurate and precise isotopic compositions measured on basalts required to decipher mantle source components, one must then overcome the chemical disturbances produced by alteration and/or possible contamination during sample handling. An assessment of the effect of alteration on the Pb-Sr-Nd-Hf isotopic compositions of oceanic island basalts and its efficient removal by acid-leaching was a major part and contribution of this study, and is the subject of Chapters 2 and 3 of this dissertation.

Chapter 2 focuses specifically on the effects of acid-leaching and matrix elimination on the Pb isotopic compositions of ocean island basalts. The preliminary results were presented at the 2005 AGU Fall meeting and at the 2006 GAC-MAC Joint Annual Meeting (Appendix C: Nobre Silva et al., 2005; 2006a) and a version of this chapter was published in *Geochemistry Geophysics Geosystems* [*Nobre Silva et al.*, 2009]. This study documents the results of a systematic investigation of how the Pb elemental and isotopic compositions of two Hawaiian and two Kerguelen basalts are affected during multi-step (up to 14 steps) acid-leaching treatment prior to isotopic analysis (Figure1.8). Following these results, the Pb isotopic compositions of unleached and leached sets, of three sample aliquots each, from seven and eight different basalts from Hawaii and Kerguelen, respectively, are compared after being subjected to one and two passes through the purification process, to assess the importance of the removal of residual elemental matrix in the Pb fraction after anion-exchange chromatography. With a total of 174 isotopic analyses, the major conclusion of this study is that accurate and reproducible high-precision Pb isotopic compositions of oceanic basalts can be achieved by careful sample treatment, comprising both thorough acid leaching and two passes through the purification process.

Chapter 3 constitutes a complementary study to the previous chapter. The preliminary results were presented at the 2009 AGU Fall Meeting (Appendix C: Nobre Silva et al., 2009) and a version of this chapter was published in *Geochemistry Geophysics Geosystems* [*Nobre Silva et al.*, 2010]. In this study, the effects of multi-step acid leaching on the Sr, Nd, and Hf elemental contents and isotopic compositions of two Hawaiian and two Kerguelen basalts are assessed through a comprehensive study of elemental and isotopic analyses of unleached and leached aliquots of the same samples. The effects of acid leaching on the trace element abundances are also addressed. Integration of the results of this study with those from Chapter 2 leads to the conclusion that the Sr and Pb isotope compositions of oceanic basalts are highly susceptible to low temperature seawater alteration, as well as to interaction with external contaminants such as Fe-Mn oxides, deep-sea sediments, or loess. In contrast, Nd and Hf isotope compositions are not significantly affected by alteration, nor by the acid leaching treatment, despite the significant elemental losses during acid leaching. Although accurate and precise Pb, Sr, Nd, and Hf isotopic compositions representative of the magma source can be obtained on the same aliquot of acid-leached sample, the same cannot be concluded for elemental abundances. Therefore, in studies that require calculation of initial isotopic ratios at the time of crystallization, parent/daughter ratios should be determined from elemental concentrations measured on unleached sample powders.

The results achieved in Chapters 2 and 3 provide assurance that by following a careful sample treatment prior to isotopic analysis one can confidently assign the isotopic compositions measured on acid-leached oceanic basalts to their mantle source components. In the following two chapters of this dissertation (Chapters 4 and 5), this same sample treatment was applied to basalts from two of the major hotspot tracks on Earth – the Ninetyeast Ridge and Hawaii – in two major ocean basins (Indian and Pacific oceans, respectively) to discriminate their source components and relative proportions, and to provide insight into the origin of their distinct compositional mantle domains.

Chapter 4 details a high-precision Pb-Sr-Hf-Nd isotopic study of 38 Ninetyeast Ridge basalts recovered from Sites 758 (82 Ma), 757 (58 Ma), and 756 (43 Ma) during ODP

Leg 121 campaign in the late 1980s. The isotopic variations reported here, with significantly better precision and reproducibility than 20 years ago, are inconsistent with the hypothesis of an aging mantle plume for the Ninetyeast Ridge [*Class et al.*, 1993]. They support instead the involvement of three, possibly four, distinct components intrinsic to the mantle source of the ridge. Indian asthenospheric depleted mantle is not the "depleted" component within the Ninetyeast Ridge lavas. A Kerguelen and Amsterdam-St. Paul mantle plume origin for the ridge implies that the plume sources are compositionally more heterogeneous in time and space than previously assumed. The Ninetyeast Ridge, together with other Indian Ocean island basalts, has isotopic characteristics typical of the Dupal isotopic domain [*e.g., Weis et al.*, 1992]. Whereas the Dupal–like characteristic of Indian MORB and OIB that formed at the onset of continental rifting (e.g., Cretaceous Kerguelen Plateau) can be attributed to shallow level contamination by lower crust and/or subcontinental lithospheric mantle, the Ninetyeast Ridge basalts and other OIB formed in intraplate setting show no evidence for such shallow contamination. The EM-1-like compositions of the Ninetyeast Ridge basalts are best explained by a contribution of a mixture of pelagic sediments and lower continental crust recycled together with altered oceanic crust in their deep mantle source. The preliminary results from this study were presented at the 16th and 17th Annual Goldschmidt Conference (Appendix C: Nobre Silva et al., 2006b; 2007).

Chapter 5 presents a high-precision Pb-Sr-Nd isotopic study of 40 basalts from the last 408 metres of core recovered during the final drilling phase of the Hawai'i Scientific Drilling Project (HSDP2-B and -C) on Mauna Kea. The isotopic compositions of these deeper and older basalts show compositional continuity with the overlying younger basalts, making the ~3500 metre-long HSDP2 core the longest record of the magmatic output of a single volcano. These older basalts extend the isotopic compositions of Mauna Kea to both significantly more and less radiogenic values, similar to those of "ancestral" Kilauea lavas, and those of late shield and post-shield lavas (<400 kyr) from Mauna Kea and Kohala, respectively. The Pb isotopic compositions of the HSDP2 basalts are consistent with the presence of four source components during the growth of Mauna Kea. The "Kea" component is the prevailing component throughout the evolution of Mauna Kea, whereas the remaining

three components ("Loihi", Enriched Makapuu [EMK] and Depleted Makapuu [DMK]) were involved in different stages of volcano development and contributed to the short-term isotopic variability of Mauna Kea basalts. At a broader, regional scale, the isotopic compositions of the "Kea" component are shared by other Pacific OIB. In Pb-Sr-Nd binary isotope diagrams, "Kea" occupies an intermediate position towards which the main trends formed by other Pacific Ocean island groups (from EM-I, EM-II and HIMU) converge. This indicates that the "Kea" component is not only the common composition within the Hawaiian mantle plume, but also that it is a common composition within the deep Pacific mantle. The preliminary results from this study were presented at the 2006 AGU Fall Meeting and at the 18th Annual Goldschmidt Conference (Appendix C: *Nobre Silva et al.*, 2006c; 2008a).

A summary of the significant findings during the course of this dissertation is presented in the concluding Chapter 6, as well as ideas of additional future research that could be undertaken related to the topics focused on this dissertation. Additional material to this study is presented in appendices A and B. Appendix A reports the analytical precision and accuracy of the isotopic analyses on basalts from the HSDP2-B and –C. Appendix B reports a summary of the preliminary geochemical results obtained on the Ninetyeast Ridge basalts recovered by dredging during the IODP site survey cruise in the summer of 2007.

1.8. Contributions to this Research Project

Within the framework of this research project I had the remarkable opportunity to participate in two scientific research expeditions over the summer of 2007 and interact with scientists and graduate and undergraduate students in the field of marine geology, geochemistry and geophysics. The first expedition was a 48.6-day (departed Phuket on June 18th, 2007 and arrived at Singapore on August 6th, 2007) NSF – IODP funded site survey cruise to the Ninetyeast Ridge in the Indian Ocean – KNOX06RR, on board the R/V Roger Revelle (Figure 1.9). The expedition was led by *Dr. Wiliam Sager* (Texas A&M University; geophysics) and *Dr. Frederick A. Frey* (Massachusetts Institute of Technology;
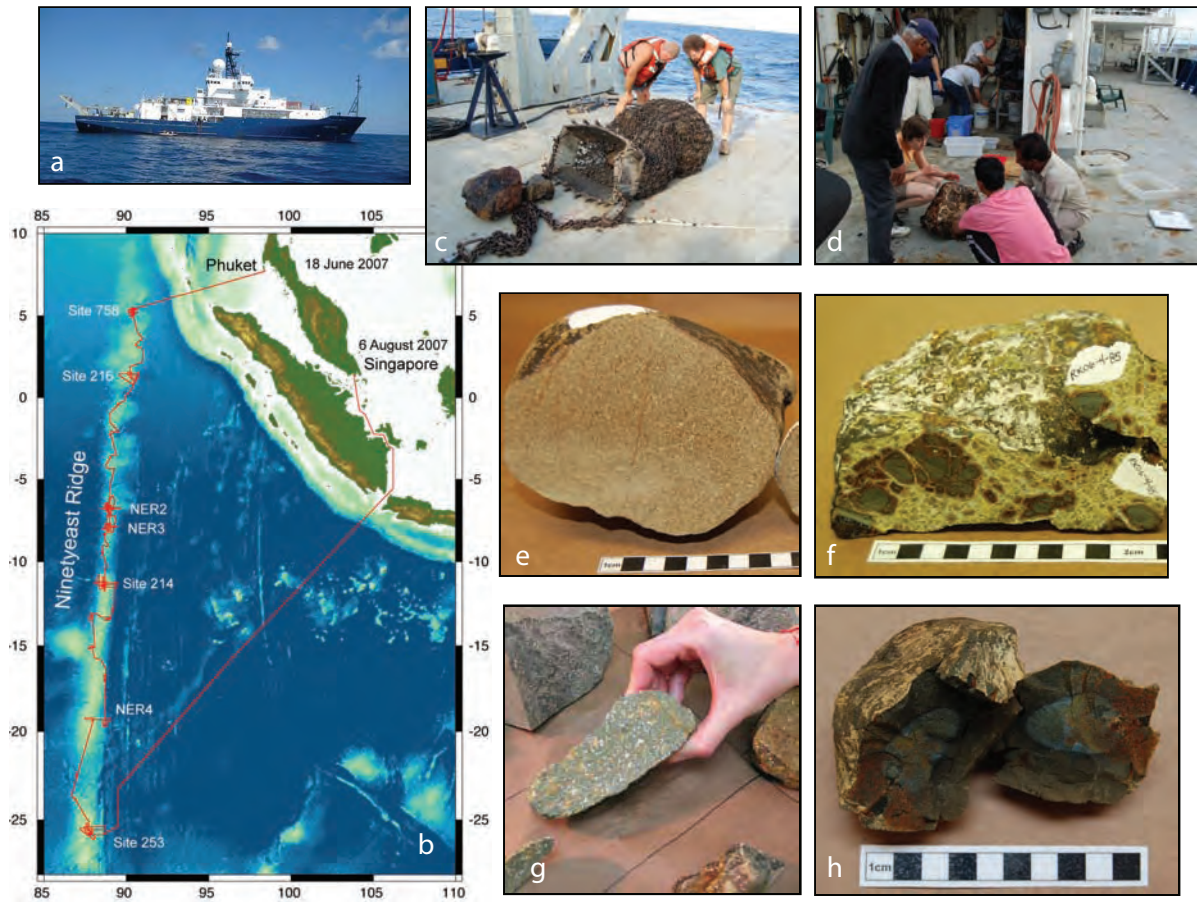
Figure 1.9. Photographs showing some of the geological highlights and typical rocks recovered during the two-month KNOX06RR expedition to the Ninetyeast Ridge in the summer of 2007. (a) The research vessel Roger Revelle. (b) Bathymetric map produced during the cruise, showing the course of the expedition. (c) Dredge basket with samples on deck. (d) Samples on board and scientists washing and cutting rocks. (e) Aphyric massive basalt. (f) Palagonite breccia. (g) Altered vesicular olivine-phyric basalt. (h) Altered aphyric massive basalt. Scale in centimetres.

geochemistry) and included the participation of included 29 members in the scientific party. The aim of the expedition was to collect geophysical data (bathymetry, magnetic, and seismic) and sample the igneous basement by dredging at several sites along the ~5000 km long ridge, for a proposed drilling program and to test the hotspot hypothesis for the Ninetyeast Ridge. As a PhD graduate student within the "petrology team", I worked under the supervision of Dr. Fred Frey and Dr. Malcolm Pringle, helping throughout the process of sample collection and preparation (washing and cutting samples as soon as they were on deck), as well as being in charge of the description and grouping of the numerous samples collected during each of the 33 dredges. As part of my research and contribution to this international project, I was responsible for the acquisition of Pb-Sr-Nd-Hf isotopic compositions on 55 selected samples. The preliminary results (on 31 samples) were presented at the 2008 AGU Fall Meeting (Appendix C: *Nobre Silva et al.*, 2008b) and are reported in the Appendix B of this dissertation. The full set of isotopic results on the 55 dredged samples is intended for future submission for publication.

The second expedition "*Underwater Volcanoes of the Northern Hawaiian Islands*" was a 28-day (from September 8th to October 8th, 2007) NSF funded cruise to the Northern Hawaiian Islands, on board the R/V Kilo Moana (Figure 1.10). The expedition was led by *Dr. M.O. Garcia* (University of Hawaii at Manoa; petrology and geochemistry) and *Dr. G. Ito* (University of Hawaii at Manoa; geophysics) and included the participation of 3 UBC scientists among 15 altogether plus the JASON crew (Woods Hole Oceanographic Institution). This expedition aimed at mapping the Kaua'i and Ni'ihau submarine volcanic fields (by multibeam bathymetry and acoustic imagery) and sampling many of its volcanoes formed by secondary volcanism using the JASON2 ROV to characterize the petrology, geochemistry and ages of these lavas. My participation in this international expedition included helping in the collection of geophysical (gravity, magnetics, multibeam and side-scan sonar) data, navigation and data logging, still imagery, and rock sampling during JASON2 dives, and subsequent sample preparation and description. Preliminary results from this expedition were published in the *Eos Transactions* of the American Geophysical Union [*Garcia et al.*, 2008; Appendix C].
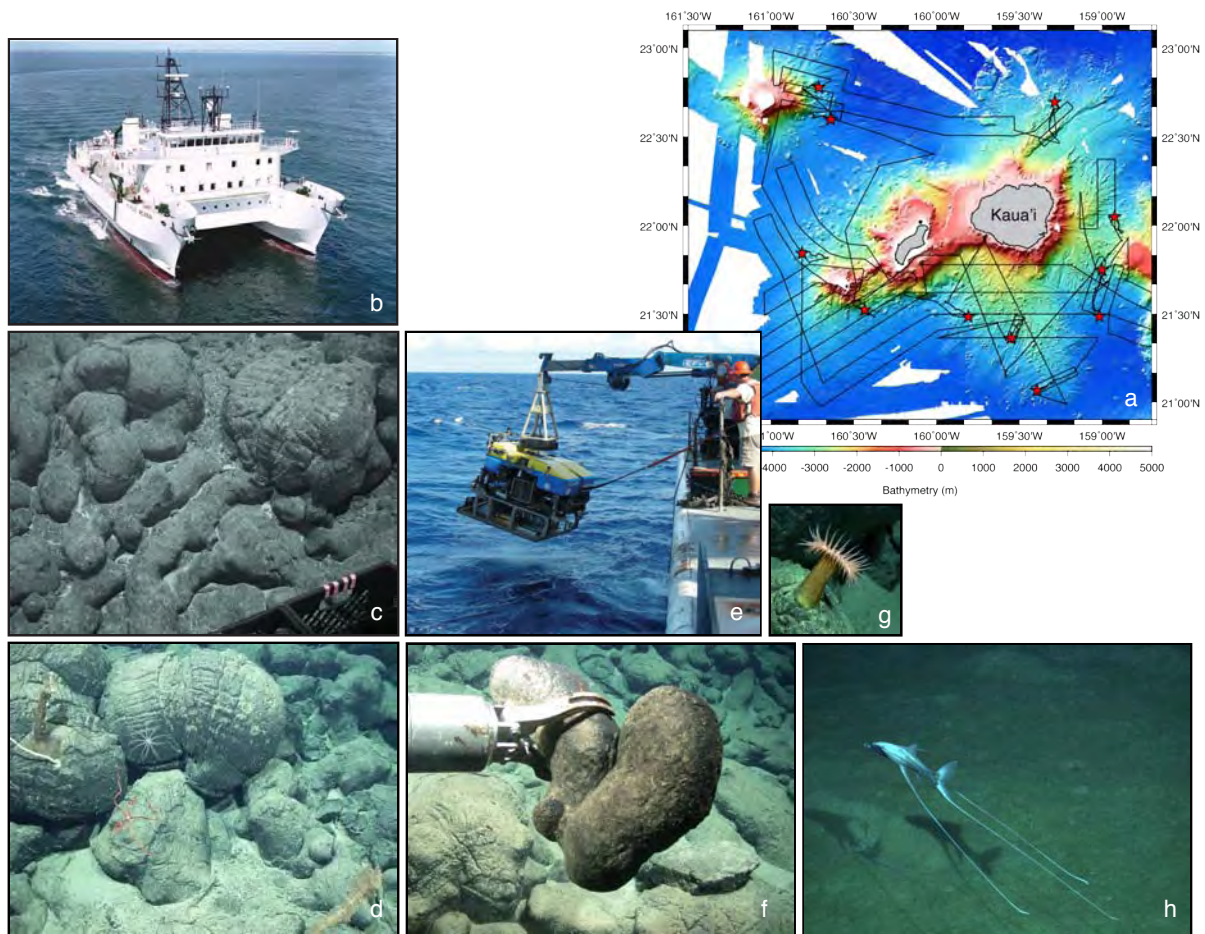
Figure 1.10. Photographs showing some of the natural and geological highlights during the 4-week *"Underwater volcanoes of the Northern Hawaiian Islands"* expedition to the Northern Hawaiian Islands. (a) Bathymetric map of the Northern Hawaiian Islands produced during the cruise, showing the cruise track and the location of the Jason2 dives [*Garcia et al.*, 2008; http://www.soest.hawaii.edu/expeditions/Kauai/]. (b) The research vessel Kilo Moana. (c) and (d) Submarine pillow lavas. (e) The remotely operated vehicle Jason 2. (f) Sampling with the robotic arm of Jason 2. (g) and (h) Marine wildlife. Submarine photographs were taken with the camera coupled to Jason2 (Jason Midnight-4 AM team, D. Weis (UBC) team leader and photographer, Kilo-Moana September 2007, University of Hawaii).

As part of my early training in the clean laboratory, I was involved in a study carried out at the Pacific Centre for Isotopic and Geochemical Research regarding the Hf isotopic characterization of United States Geologic Survey reference materials. I was responsible for determining the trace element concentrations and Sr, Nd and Hf isotopic compositions of different labware materials including borosilicate glass, glass frit material and quartz from the columns. The preliminary results of this study were presented at the 2005 AGU Fall Meeting (Appendix C: Weis et al., 2005), and the completed study was published in the electronic journal *Geochemistry Geophysics Geosystems* [*Weis et al.*, 2007; Appendix C].

CHAPTER 2

Leaching Systematics and Matrix Elimination for the Determination of High-Precision Pb Isotope Compositions of Ocean Island Basalts[1]

2.1. Synopsis

Ocean island basalts from Hawaii and Kerguelen were analyzed for their Pb isotopic compositions to assess the effect of acid-leaching and matrix elimination by Pb anion-exchange columns on reproducibility and accuracy. Unleached samples consistently yield Pb isotopic ratios that reflect the incorporation of foreign material. Leaching removes up to 70-80% of the total Pb content of the samples with corresponding weight losses between 35-60%. The older and more altered Kerguelen basalts show better external reproducibility than the Hawaiian basalts, which appears to be due to the presence in the Hawaiian samples of more radiogenic contaminants (e.g., seawater Pb, drilling mud and related alteration phases). All leached samples purified twice on anion-exchange columns show more radiogenic Pb isotopic ratios than those processed once. The difference is larger for tholeiitic basalts (Hawaiian and Kerguelen Plateau) than for transitional to alkalic basalts (Kerguelen Archipelago). The small differences in measured ratios of total procedural triplicates reflect differential elimination of residual alteration via leaching and matrix effects. The effectiveness of matrix elimination depends on the specific basalt composition and tholeiitic basalts (i.e., low-Pb concentrations) require two passes on anion-exchange columns. This study shows that all steps in sample processing are critical for achieving accurate high-precision Pb isotopic compositions of ocean island basalts.

2.2. Introduction

The Pb isotopic compositions of oceanic basalts are extremely useful for evaluating and characterizing the mantle sources and components of both ocean island basalts (OIB) and mid-ocean ridge basalts (MORB) [e.g., *Gast et al.*, 1964; *Tatsumoto*, 1966; 1978; *Abouchami et al.*, 2000; 2005; *Eisele et al.*, 2003; *Blichert-Toft et al.*, 2003; *Marske et al.*, 2007]. In order for the measured Pb isotopic compositions of basalts to be representative of their mantle source, any foreign elemental contribution introduced by post-magmatic processes, including secondary phases produced during seawater alteration and weathering or any surficial contamination from sample crushing, must be eliminated. Acid-leaching of

samples prior to dissolution and isotopic analysis has long been recognized as a means of removing such secondary material [e.g., *Manhès et al.*, 1978; *Dupré and Allègre*, 1980; *Hamelin et al.*, 1986; *McDonough and Chauvel*, 1991; *Weis et al.*, 2005] and a wide variety of leaching protocols are used by different laboratories [e.g., *Mahoney*, 1987; *McDonough and Chauvel*, 1991; *Weis and Frey*, 1991; *Stracke and Hegner*, 1998; *Abouchami et al.*, 2000; *Thirlwall*, 2000; *Eisele et al.*, 2003; *Stracke et al.*, 2003; *Baker et al.*, 2004; *Weis et al.*, 2005].

In the past, the reproducibility of leached samples was within the analytical precision of Pb isotope ratio measurements (per mil range). However, with the increase in precision (e.g., <200 ppm range on $^{208}Pb/^{204}Pb$) achieved by recent analytical developments, such as triple spike thermal ionization mass spectrometry (TS-TIMS) [e.g., *Galer*, 1999; *Woodhead and Hergt*, 2000] and double spike or Tl-corrected multiple collector inductively coupled plasma mass spectrometry (MC-ICP-MS) [e.g., *Longerich et al.*, 1987*; Walder and Furuta*, 1993; *Belshaw et al.,* 1998; *Rehkämper and Halliday*, 1998; *Thirlwall*, 2000; *White et al.*, 2000; *Weis et al.*, 2005], it has become clear that not all leaching techniques provide reproducible results. Reproducibility problems have been reported for Pb isotopic compositions in several studies of oceanic basalts, such as those from the Hawaii Scientific Drilling Project (HSDP) [*Abouchami et al.*, 2000; *Eisele et al.*, 2003] and some Icelandic basalts [*Stracke et al.*, 2003; *Baker et al.*, 2004; 2005; *Albarède et al.*, 2005]. The poor reproducibility in some of these studies was attributed to variable degrees of sample contamination, sample heterogeneity, and/or the inability of the leaching procedures to consistently eliminate various contaminants. Recently, it has also been documented that the accuracy of radiogenic isotope ratio measurements determined by MC-ICP-MS can be affected by non-spectral interferences (matrix effects that affect the ionization and transmission of the analyte, as well as instrumental mass bias) due to residual sample matrix [e.g., *Thirlwall*, 2002; *Woodhead*, 2002; *Barling and Weis,* 2008].

In this contribution, we report Pb isotopic analyses of basalts from two major hotspot systems, Hawaii (Pacific Ocean) and Kerguelen (Indian Ocean), by MC-ICP-MS to assess

the efficiency of multi-step acid-leaching in obtaining reproducible Pb isotopic compositions of OIB. This is a companion paper to that of *Hanano et al.* [2009], which documented different alteration assemblages in Hawaiian and Kerguelen basalts and their behavior during acid-leaching based on scanning electron microscopy (SEM) of thin sections and X-ray diffraction (XRD) characterization of sample powders (unleached and leached). To investigate how Pb isotopic ratios are affected by acid-leaching process, two Hawaiian and two Kerguelen samples were chosen from the sample set, where both the Pb contents and isotopic compositions were measured in the acid solutions (leachates) of each leaching step and in the bulk leachates (all leaching step solutions combined), as well as for unleached and leached powders (residues). We then compared the isotopic compositions of unleached and leached powders for other samples from the same hotspot systems. To assess the importance of the residual elemental matrix in the Pb fraction after anion-exchange chromatography, we also compared the isotopic compositions of two sets of full procedural triplicates of leached powder splits of samples that were passed once (1x) and twice (2x) through the purification process.

2.3. Samples

Fifteen basalts from the Hawaiian and Kerguelen oceanic islands were selected for this leaching investigation (see Table 2.1 for brief sample characterization). These samples are representative of basalts typically analyzed for radiogenic isotopic compositions from these two islands and span a wide range of MgO (3.5–18.0 wt%) with weak to moderate alteration (e.g. 0.40–2.8 wt% LOI) (Table 2.1). Four samples from this study were examined in detail for alteration mineralogy by *Hanano et al.* [2009]. For the Hawaiian hotspot system, we chose seven tholeiitic samples from the Mauna Loa and Mauna Kea volcanoes; the Mauna Kea samples were all collected from the HSDP-2 drill core. All of the Hawaiian basalts have ages less than 500 ka [*Sharp and Renne*, 2005] and, with the exception of one sample from Mauna Loa (SW-70), all are submarine in origin. For the Kerguelen hotspot system, seven samples from the Kerguelen Archipelago were chosen, varying from transitional tholeiites to alkalic basalts with ages ranging from 29 to 24 Ma [*Nicolaysen et*

Table 2.1. Summary of Sample Geochemical Characteristics: Hawaii and Kerguelen

Sample	Eruption Environment	Depth [a] (mbsl/masl)	Rock Type	SiO_2 (wt%)	MgO (wt%)	Na_2O (wt%)	K_2O (wt%)	Pb (ppm)	A.I.[b]	LOI [c] (wt%)	Age (Ma) [d]	References
Hawaiian Volcanoes												
Mauna Loa												
SW-70	subaerial	–	tholeiitic basalt	51.52	9.33	2.35	0.41	2.50	-1.87	–	0.140	Rhodes, J. M. (unpublished data, 2003)
J2-020-23	submarine	489	tholeiitic basalt	50.14	6.50	2.72	0.52	2.00	-0.87	0.99	–	Rhodes, J. M. (unpublished data, 2003)
J2-019-04	submarine	1986	tholeiitic basalt	49.86	14.19	1.62	0.27	1.00	-2.28	0.42	0.450	Rhodes, J. M. (unpublished data, 2003)
Mauna Kea (HSDP-2 [e])												
SR0705-0.15	submarine	1823.2	hyaloclastite	49.16	11.69	1.81	0.17	0.73	-1.76	2.32	0.488	*Rhodes and Vollinger* [2004]
SR0768-11.20	submarine	2157.4	hyaloclastite	50.39	6.76	2.26	0.37	1.09	-0.95	0.40	0.506	*Rhodes and Vollinger* [2004]
SR0954-8.00	submarine	3009.2	tholeiitic basalt	47.67	18.03	1.65	0.23	0.66	-1.31	0.85	0.550	*Rhodes and Vollinger* [2004]
SR0956-18.35	submarine	3019.0	tholeiitic basalt	49.70	7.01	2.25	0.35	1.08	-1.34	0.61	0.550	*Rhodes and Vollinger* [2004]
Kerguelen Basalts												
Mont Crozier												
OB93-165	subaerial	515	alkalic basalt	50.91	3.54	3.52	1.45	6.34	0.67	–	24.5	Weis, D. (unpublished data, 2005)
OB93-177	subaerial	380	alkalic basalt	48.75	3.89	3.54	1.86	-	1.90	–	24.5	Weis, D. (unpublished data, 2005)
OB93-202	subaerial	78	alkalic basalt	48.93	4.05	3.19	1.65	5.58	1.28	–	24.5	Weis, D. (unpublished data, 2005)
Mont des Ruches												
BY96-27	subaerial	455	transitional basalt	46.90	10.65	2.16	0.72	0.96	-0.04	2.01	28.0	*Doucet et al.* [2002]
BY96-31	subaerial	408	transitional basalt	49.91	4.31	2.84	1.21	1.69	0.01	1.82	28.0	*Doucet et al.* [2002]
Mont Fontaine												
BY96-86	subaerial	300	transitional basalt	45.87	11.50	1.94	0.77	1.71	0.17	2.80	28.0	*Doucet et al.* [2002]
Mont Bureau												
GM92-48	subaerial	250	transitional basalt	47.09	8.71	2.50	0.43	0.27	0.05	–	29.5	*Yang et al.* [1998]
Northern Kerguelen Plateau												
ODP Leg 183, 1140A-31R-1, 57-61	submarine	270.07	tholeiitic basalt	49.64	5.54	2.64	0.49	1.52	-0.81	1.65	34.3	*Weis and Frey* [2002]

[a]For submarine basalts, mbsl means meters below sea level; for subaerial basalts, masl means meters above sea level.
[b]A.I., alkalinity index (AI = total alkalis – (SiO_2 × 0.37 – 14.43)) [*Rhodes*, 1996].
[c]LOI, weight loss on ignition after 30 min at 1020ºC.
[d]Ages from Mauna Loa, B. Singer (unpublished data, 2007); Mauna Kea samples, *Sharp and Renne* [2005]; Mont Crozier and Mont Bureau, *Nicolaysen et al.* [2000]; Mont des Ruches and Mont Fontaine, *Doucet et al.* [2002]; Site 1140, *Duncan* [2002].
[e]HSDP-2, Hawaii Scientific Drilling Project, phase 2.

al., 2000], and all were erupted in a subaerial environment. In addition, to evaluate if compositional differences between samples would influence Pb isotopic compositions during leaching, a submarine tholeiitic basalt from the 34 Ma Northern Kerguelen Plateau (NKP) recovered during ODP Leg 183 [*Weis and Frey*, 2002] was also analyzed. All Hawaiian sample powders were prepared from chips that were repeatedly rinsed in deionized water and pulverized following the crushing and washing procedures described in *Rhodes* [1996] and *Rhodes and Vollinger* [2004]. For the Kerguelen samples, the powders were prepared following the method described in *Doucet et al.* [2002].

2.4. Analytical Techniques

All leaching and chemical separation were carried out in Class 1000 clean labs and the mass spectrometric analyses were performed in Class 10,000 labs at the Pacific Centre for Isotopic and Geochemical Research (PCIGR) at the University of British Columbia. Sample handling in all labs was carried out in Class 100 laminar flow hoods. All reagents used for leaching, dissolution and separation were sub-boiled, all dilutions were made using ≥18.2 MΩ·cm deionized water, and all labware was acid-washed prior to use. Whenever sample size permitted, the complete analytical procedure (separate leaching, dissolution and chemistry) was carried out in triplicate (i.e., three separate aliquots or splits of the same starting sample powder).

2.4.1. Leaching Procedure

The sequential acid-leaching procedure used in this study follows that of *Weis et al.* [2005], which was slightly modified after *Mahoney* [1987]. Approximately 0.2–0.4 g of sample powder (grain size <100 μm) were acid-leached with 10 mL of 6M HCl in a 15 mL screw-top Savillex® beaker in an ultrasonic bath (frequency of 40 kHz) for 20 minutes. This process brought the temperature up to ~50ºC. The supernatant (leachate solution) was immediately decanted before the fines had time to settle. This procedure was repeated until a transparent (i.e., free of fine-size particles), pale-yellow to colorless solution was obtained.

The same procedure was repeated two more times using ≥18.2 MΩ·cm water to eliminate any trace of acid. The leached rock powders were then dried to completion on a hot plate at ~120°C and weighed after cooling. A minimum of six acid-leaching steps was required for the least altered samples and up to 14 steps for the most altered ones. In addition, for four samples (Hawaii: J2-020-23 [Mauna Loa], SR0954-8.00 [Mauna Kea]; Kerguelen: OB93-165 [Mont Crozier, Kerguelen Archipelago], ODP leg 183, 1140A-31-R1, 57-61 [Northern Kerguelen Plateau]), the leachate solutions were collected at each step, as well as accumulated for bulk leachate analysis, and were measured for both their Pb contents and Pb isotopic compositions.

2.4.2. Sample Digestion and Pb Separation

Unleached and leached rock powders were digested in a closed vessel using a 1:10 mixture of concentrated HNO_3 and HF acids on a hotplate at ~120°C over ~48 hours. During this period, the sample solutions were ultrasonicated for ~30 minutes to ensure complete digestion, after which they were dried, re-digested in 10 mL of 6M HCl for ~24 hours and dried again. In preparation for Pb chemistry, the samples were re-dissolved in 2 mL of 0.5M HBr. As a final precaution, sample solutions were ultrasonicated for ~20 minutes and centrifuged at 14,500 rpm (14,100 × *g*) for 6 minutes before being loaded onto a pre-cleaned and conditioned 200 µL column of fresh AG1-X8 100-200 mesh resin (Bio-Rad Laboratories, USA). The matrix was washed out with 0.5M HBr after which Pb was eluted in 6M HCl [*Weis et al.*, 2006]; this column chemistry results in close to 100% recovery of Pb [*D. Weis, unpublished data*]. To assess the efficiency of the Pb purification and potential matrix effects, a second set of leached triplicates of 11 samples was subjected to two passes through the same anion-exchange resin. After chemical purification, the eluted Pb fraction was dried, a small quantity of concentrated HNO_3 was added to destroy any organic material eluted from the resin along with the Pb, and it was dried again. In preparation for isotopic analyses, the dried Pb fractions were re-dissolved in 1 mL of 0.05N sub-boiled HNO_3 in an ultrasonic bath. Seven total procedural blanks, including leaching, were measured by ID-TIMS using a [205]Pb spike; their Pb concentrations were between 50 to 160 pg (average 100

pg), which is negligible in comparison to the Pb content of the sample powders analyzed (52 to 428 ng).

2.4.3. Mass Spectrometry

2.4.3.1. Pb Concentrations

The Pb concentrations of leached and unleached sample powders, as well as of each acid-leaching step solution and bulk leachates were measured to determine the amount of Pb present at each step of the acid-leaching procedure. The analyses were performed on an ELEMENT2 high-resolution (HR)-ICP-MS (Thermo Finnigan, Germany) and were quantified using external calibration curves and indium (In) as an internal standard. Standard solutions were prepared from a 1000 ppm Specpure® (Alfa Aesar®, Johnson Matthey Company, USA) Pb standard solution. Samples and standards were diluted and run in 0.15M HNO_3. All analyses were normalized to the internal standard and blank subtracted.

2.4.3.2. Pb Isotopic Compositions

The Pb isotopic analyses were performed on a Nu Plasma MC-ICP-MS (Nu Instruments Ltd, UK) under dry plasma conditions using a membrane desolvator (Nu DSN100) for sample introduction. Analyses were made by static multi-collection with masses 202 to 208 measured in collectors L2 to H4, respectively. Instrumental mass fractionation was monitored and corrected on-line using a Specpure® Tl standard solution with a $^{205}Tl/^{203}Tl$ = 2.3885. This in-house value provides SRM-981 Pb standard (NIST, USA) ratios within error of the triple spike isotopic values [*Galer and Abouchami*, 1998] and has remained constant since instrument installation (fall 2002). The potential ^{204}Hg isobaric interference on the ^{204}Pb ion beam was monitored at mass 202 and, when necessary, was corrected for assuming natural abundances ($^{202}Hg/^{204}Hg$ = 4.35) adjusted for instrumental mass fractionation. As is standard practice for all MC-ICP-MS analyses at the PCIGR, all samples and standards were prepared fresh for each analytical session, which can be particularly important for Pb-Tl solutions [*Kamenov et al.*, 2004]. Standard solutions were prepared by combining the SRM-981 Pb standard and the Tl standard solutions to give a

[Pb]/[Tl] of ~4 and diluted with 0.05M HNO_3 to obtain an optimal ^{208}Pb ion beam of 8V (and no less than 2V). Samples were also run in 0.05M HNO_3 with Tl added to match the standard [Pb]/[Tl] of ~4. Matching of [Pb]/[Tl] is done to ensure that sample and standard solutions are matrix-matched as much as possible. To accomplish this, the Pb content of each solution was determined by HR-ICP-MS analysis of a small aliquot prior to isotopic analysis of the sample by MC-ICP-MS.

Sample analysis followed a modified sample-standard bracketing protocol in which the SRM-981 Pb standard was run after every second sample. The results were then normalized off-line to the triple spike values ($^{206}Pb/^{204}Pb$ = 16.9405, $^{207}Pb/^{204}Pb$ = 15.4963, and $^{208}Pb/^{204}Pb$ = 36.7219) [*Galer and Abouchami*, 1998], using the ln-ln method as described in *Albarède et al.* [2004]. For sessions where a systematic drift in the SRM-981 isotopic ratio reference values was observed (i.e., drift >2SD on the average of the analyses for the day), the sample-standard bracketing normalization was used instead. In all cases, the agreement between the two normalization methods was excellent (better than 2×10^{-3}, or <50 ppm) for all Pb isotopic ratios.

During the course of this study, 176 analyses of the SRM-981 Pb standard yielded mean values of $^{206}Pb/^{204}Pb$ = 16.9421 ± 0.0030, $^{207}Pb/^{204}Pb$ = 15.4985 ± 0.0025, and $^{208}Pb/^{204}Pb$ = 36.7190 ± 0.0078, which are within error of the triple spike values [*Galer and Abouchami*, 1998]. Reproducibility of the SRM-981 Pb standard on a per session basis was significantly better (±30, ±42 and ±60 ppm/amu for $^{208}Pb/^{204}Pb$, $^{207}Pb/^{204}Pb$ and $^{206}Pb/^{204}Pb$, respectively).

2.5. Results

All the analyses acquired during the course of this study are presented in Tables 2.2 to 2.6 and the results are illustrated in Figures 2.1 to 2.8. For the four samples indicated in section 3.1 that were studied in detail for characterization of the acid-leaching procedure, we report the Pb isotopic compositions for selected individual leachate solutions, which were

chosen to cover, as best as possible, the entire leaching profile. For the last leaching steps, the Pb isotopic compositions are not reported as their Pb contents were insufficient (<<7 ng) for analysis. In addition, we subjected six splits each of powder from five Hawaiian and six Kerguelen samples to acid-leaching following the procedure described in section *2.3.1*. To assess the influence of residual sample matrix (e.g., Ca, Al, Fe, Mg) still present in the Pb fraction after anion-exchange chromatography on the accuracy and reproducibility of the Pb isotopic compositions, one-half of these same powder splits were passed 1x on columns and the other half was passed 2x, as described in section *2.3.2*.

2.5.1. Sequential Leaching

Throughout the multi-step acid-leaching procedure, the Hawaiian basalts lost ~35% of their initial weight and the Kerguelen basalts lost ~60%, which is consistent with the higher degree of alteration presented by the older Kerguelen basalts [*Hanano et al.*, 2009]. For both Hawaiian and Kerguelen samples, the amount of Pb (as well as Sr, Nd and Hf) that is leached out decreases significantly in the first 1–2 steps and then slowly decreases with each progressive step (Tables 2.2 and 2.3; Figures 2.1, 2.2 and 2.3). Leaching removes up to 70–80% of the original Pb content of each sample. Unleached sample powders are isotopically more radiogenic than their respective leached sample residues, with the exception of the submarine Kerguelen basalt (ODP leg 183, sample 1140A-31R-1, 57-61), and fall along a mixing line formed by the leached sample residues and the respective bulk leachate solutions. Most of the foreign Pb (~40 to 50% for the Hawaiian and submarine Kerguelen tholeiites and ~25% for the subaerial Kerguelen Archipelago basalts) is removed during the first leaching step (Figures 2.1, 2.2 and 2.3), as demonstrated by the similarity between the Pb isotopic compositions of the first leachate solutions and the bulk leachate solutions. As the number of acid-leaching steps increases, the relative amount of Pb that is removed becomes increasingly smaller (<1.5%), after 3–4 steps for the Mauna Loa and Mont Crozier basalts and after 6–7 steps for the Mauna Kea and Northern Kerguelen Plateau basalts, respectively (Tables 2.2 and 2.3).

Table 2.2. Pb content and Pb Isotopic Composition of Each Leaching Step Solution for Two Hawaiian Basalts

Fraction	ng Pb in Each Fraction	% Pb in Each Fraction	Column Passes	^{206}Pb/^{204}Pb	2 SE	^{207}Pb/^{204}Pb	2 SE	^{208}Pb/^{204}Pb	2 SE
				Sample J2-020-23 (Mauna Loa)					
Unl.[a]	572.6	100	1	18.3052	0.0067	15.5121	0.0021	38.1726	0.0016
B.L.Homog.[b]	313.7	54.8	1	18.3463	0.0006	15.5306	0.0006	38.2486	0.0016
B.L.Homog.	313.7	54.8	2	18.3473	0.0007	15.5319	0.0006	38.2538	0.0017
B.L.Acid[c]	269.1	47.0	1	18.4045	0.0008	15.5575	0.0007	38.3594	0.0019
B.L.Acid	269.1	47.0	2	18.4026	0.0005	15.5553	0.0005	38.3528	0.0014
1st	340.5	59.5	1	18.3978	0.0013	15.5552	0.0012	38.3484	0.0031
2nd	18.6	3.2	1	18.2983	0.0014	15.5096	0.0012	38.1544	0.0036
3rd	12.1	2.1	1	18.2192	0.0021	15.4716	0.0019	37.9844	0.0046
4th	9.2	1.6	1	18.2400	0.0025	15.4816	0.0020	38.0073	0.0056
5th	6.7	1.2		– [d]	–	–	–	–	–
6th	3.8	0.7		–	–	–	–	–	–
1st H$_2$O	-	-		–	–	–	–	–	–
2nd H$_2$O	2.4	0.4		–	–	–	–	–	–
Total [e]	393.2	68.7							
Leach. Res.[f]	179.4	31.33	1	18.1799	0.0007	15.4577	0.0006	37.9441	0.0015
				Sample SR0954-8.00 (Mauna Kea)					
Unl.	258.8	100	1	18.6083	0.0025	15.4969	0.0029	38.1771	0.0028
B.L.Homog.	138.6		1	18.6633	0.0008	15.4987	0.0008	38.2166	0.0020
B.L.Homog. rep.[g]	138.6		1	18.6735	0.0036	15.5084	0.0030	38.2398	0.0060
B.L.Acid	139.7		1	18.6610	0.0008	15.5037	0.0007	38.2191	0.0017
1st	105.5	40.8	1	18.6687	0.0013	15.5020	0.0013	38.2270	0.0041
2nd	14.5	5.6	1	18.6288	0.0019	15.4962	0.0017	38.1966	0.0040
3rd	16.3	6.3	1	18.6219	0.0012	15.4942	0.0011	38.1924	0.0033
4th	11.3	4.3		–	–	–	–	–	–
5th	11.1	4.3		–	–	–	–	–	–
6th	9.2	3.5	1	18.6317	0.0024	15.4984	0.0020	38.1959	0.0058
7th	4.7	1.8	1	18.6477	0.0036	15.5139	0.0031	38.2144	0.0082
8th	5.5	2.1		–	–	–	–	–	–
1st H$_2$O	2.6	1.0		–	–	–	–	–	–
2nd H$_2$O	2.6	1.0		–	–	–	–	–	–
Total	183.2	70.8							
Leach. Res.	75.6	29.2	1	18.6091	0.0011	15.4874	0.0010	38.1790	0.0029

[a]Unl., unleached rock powders.
[b]B.L.Homog., bulk leachate solution homogenized (acid + fine powder particles).
[c]B.L.Acid, bulk leachate solution without the fine powder particles.
[d]Dashes indicate no isotopic analysis performed.
[e]The Pb content of the bulk leachate solutions does not equal the sum of the individual leaching steps because they were measured on different aliquots of the same powders.
[f]Leach. Res., leached powder residues.
[g]Replicate analyses of the same sample solution.
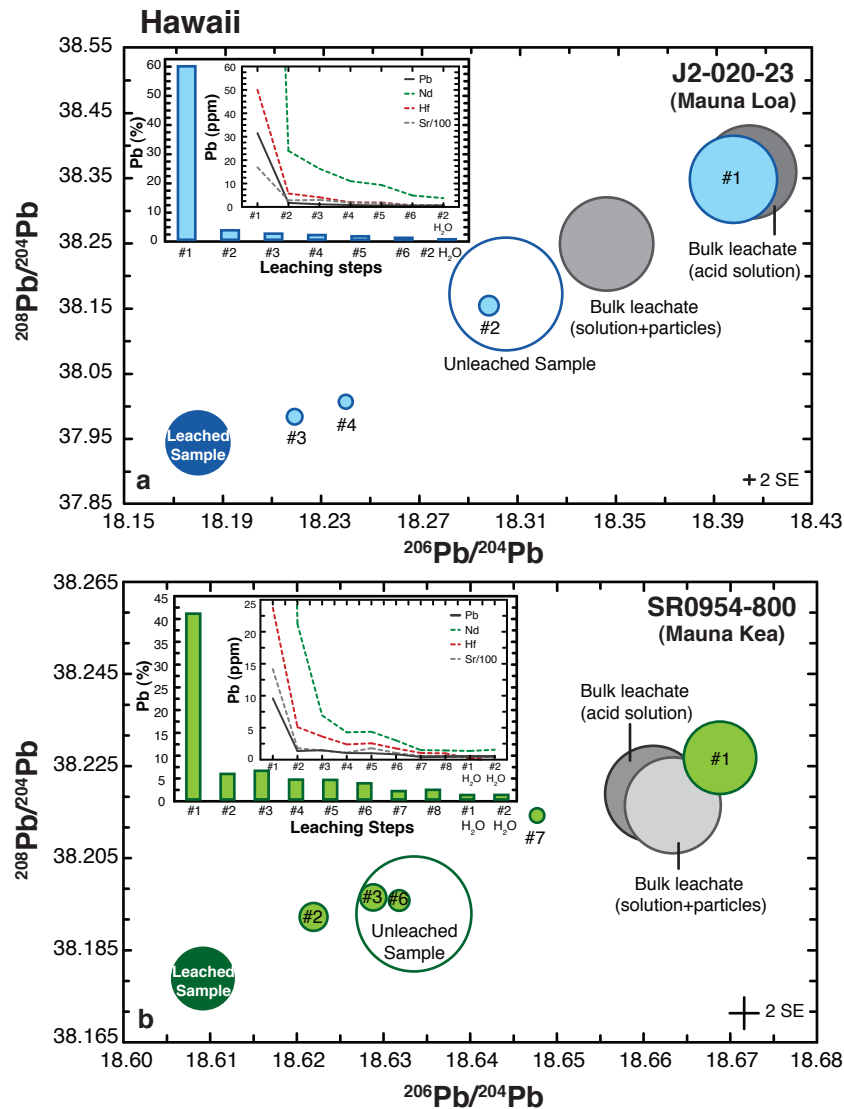
Figure 2.1. Diagrams of $^{208}Pb/^{204}Pb$ versus $^{206}Pb/^{204}Pb$ showing the results of the leaching experiments for two tholeiitic Hawaiian basalts: (a) sample J2-020-23 (Mauna Loa) and (b) sample SR0954-8.00 (Mauna Kea). Each circle represents the Pb isotopic composition for each individual leaching fraction and the size of the circle reflects the relative amount of Pb present in the fraction. The open circles indicate the analyses of the unleached sample powders and correspond to 100% of the Pb content in the sample. The filled circles without outlines (labeled as "Leached Sample") indicate analyses of the leached sample residues, and the symbol size corresponds to the amount of Pb that remained after the entire leaching procedure. The smaller filled circles indicate the analyses of leachates and the number labeled adjacent to each of these circles refers to the leaching step (see inset diagrams). The dark and light grey outlined circles represent the bulk leachate solution recovered throughout the leaching procedure; the size of these two circles is the same, as the Pb content is equivalent at the scale of the figure. The lighter grey circle refers to the isotopic composition of the acid solution plus silt size particles that were removed during leaching, whereas the darker grey circle refers to the isotopic composition of the acid solution alone, after separation of the particles by centrifugation. In the right lower corner of each panel, the average 2SE of the Pb isotopic analysis for each experiment is indicated. The inset diagrams show the percentage of Pb that was eliminated at each leaching step (histogram) and the amount of Pb (ppm) present in each leachate (line graph), as well as the amounts of Sr, Nd and Hf (also in ppm) for comparison (see chapter 3).

Table 2.3. Pb Content and Isotopic Composition of Each Leaching Step Solution for Two Kerguelen Basalts

Fraction	ng Pb in Each Fraction	% Pb in Each Fraction	Column Passes	$^{206}Pb/^{204}Pb$	2 SE	$^{207}Pb/^{204}Pb$	2 SE	$^{208}Pb/^{204}Pb$	2 SE
				Sample OB93-165 (Mont Crozier)					
Unl.[a]	1827.8	100	1	18.6045	0.0017	15.5817	0.0018	39.3219	0.0036
B.L.Homog.[b]	443.3		1	18.6066	0.0009	15.5790	0.0008	39.3221	0.0024
B.L.Homog.	443.3		2	18.6118	0.0006	15.5846	0.0005	39.3402	0.0015
B.L.Acid [c]	419.8		1	18.6045	0.0016	15.5882	0.0018	39.3534	0.0048
B.L.Acid	419.8		2	18.6025	0.0006	15.5872	0.0007	39.3482	0.0019
B.L.Acid rep.[d]	419.8		2	18.5987	0.0007	15.5830	0.0006	39.3352	0.0018
1st	445.8	24.4	1	18.6128	0.0011	15.5872	0.0009	39.3470	0.0026
2nd	96.8	5.3	1	18.5939	0.0007	15.5787	0.0006	39.2950	0.0017
3rd	28.5	1.6	1	18.6016	0.0015	15.5811	0.0012	39.2880	0.0034
4th	45.3	2.5		– [e]	–	–	–	–	–
5th	21.9	1.2		–	–	–	–	–	–
6th	22.2	1.2	1	18.6014	0.0017	15.5786	0.0017	39.2741	0.0049
7th	8.6	0.5	1	18.6286	0.0042	15.5839	0.0030	39.2643	0.0086
8th	8.3	0.5		–	–	–	–	–	–
1st H$_2$O	3.2	0.2		–	–	–	–	–	–
2nd H$_2$O	1.8	0.1		–	–	–	–	–	–
Total [f]	682.3	37.3							
Leach. Res.[g]	1145.6	62.7	1	18.5959	0.0010	15.5769	0.0008	39.2961	0.0020
				Sample ODP Leg 183, 1140A-31R-1, 57-61 (Northern Kerguelen Plateau)					
Unl.	572.5	100.00	1	18.5451	0.0008	15.5619	0.0009	38.9056	0.0029
B.L.Homog.	332.7		1	18.5409	0.0011	15.5624	0.0013	38.9003	0.0042
B.L.Homog.	332.7		2	18.5420	0.0025	15.5622	0.0031	38.9019	0.0105
B.L.Acid	314.2		1	18.5428	0.0010	15.5625	0.0010	38.9025	0.0027
B.L.Acid	314.2		2	18.5431	0.0026	15.5623	0.0030	38.9039	0.0099
1st	262.6	45.9	1	18.5487	0.0011	15.5685	0.0011	38.9182	0.0030
2nd	59.9	10.5	1	18.5484	0.0008	15.5646	0.0007	38.9090	0.0019
3rd	27.3	4.8	1	18.5461	0.0012	15.5635	0.0012	38.8882	0.0028
4th	19.9	3.5	1	18.5436	0.0022	15.5627	0.0023	38.8781	0.0064
5th	15.6	2.7		–	–	–	–	–	–
6th	14.9	2.6	1	18.5521	0.0012	15.5648	0.0011	38.8814	0.0031
7th	11.9	2.1	1	18.5635	0.0018	15.5659	0.0017	38.8893	0.0056
8th	7.5	1.3	1	18.5741	0.0027	15.5648	0.0023	38.8627	0.0064
9th	8.8	1.5	1	18.5856	0.0018	15.5723	0.0016	38.9003	0.0040
10th	5.1	0.9	1	18.6111	0.0032	15.5922	0.0029	38.8502	0.0067
11th	5.6	1.0		–	–	–	–	–	–
12th	4.8	0.8		–	–	–	–	–	–
13th	5.1	0.9		–	–	–	–	–	–
14th	3.1	0.5		–	–	–	–	–	–
1st H$_2$O	2.6	0.4		–	–	–	–	–	–
2nd H$_2$O	2.0	0.3		–	–	–	–	–	–
Total	456.8	79.8							
Leach. Res.	115.7	20.2	1	18.5575	0.0006	15.5648	0.0007	38.9405	0.0020

[a]Unl., unleached rock powders.
[b]B.L.Homog., bulk leachate solution homogenized (acid + fine powder particles).
[c]B.L.Acid, bulk leachate solution without the fine powder particles.
[d]Replicate analyses of the same sample solution.
[e]Dashes indicate no isotopic analysis performed.
[f]The Pb content of the bulk leachate solutions does not equal the sum of the individual leaching steps because they were measured on different aliquots of the same powders.
[g]Leach. Res., leached powder residues.
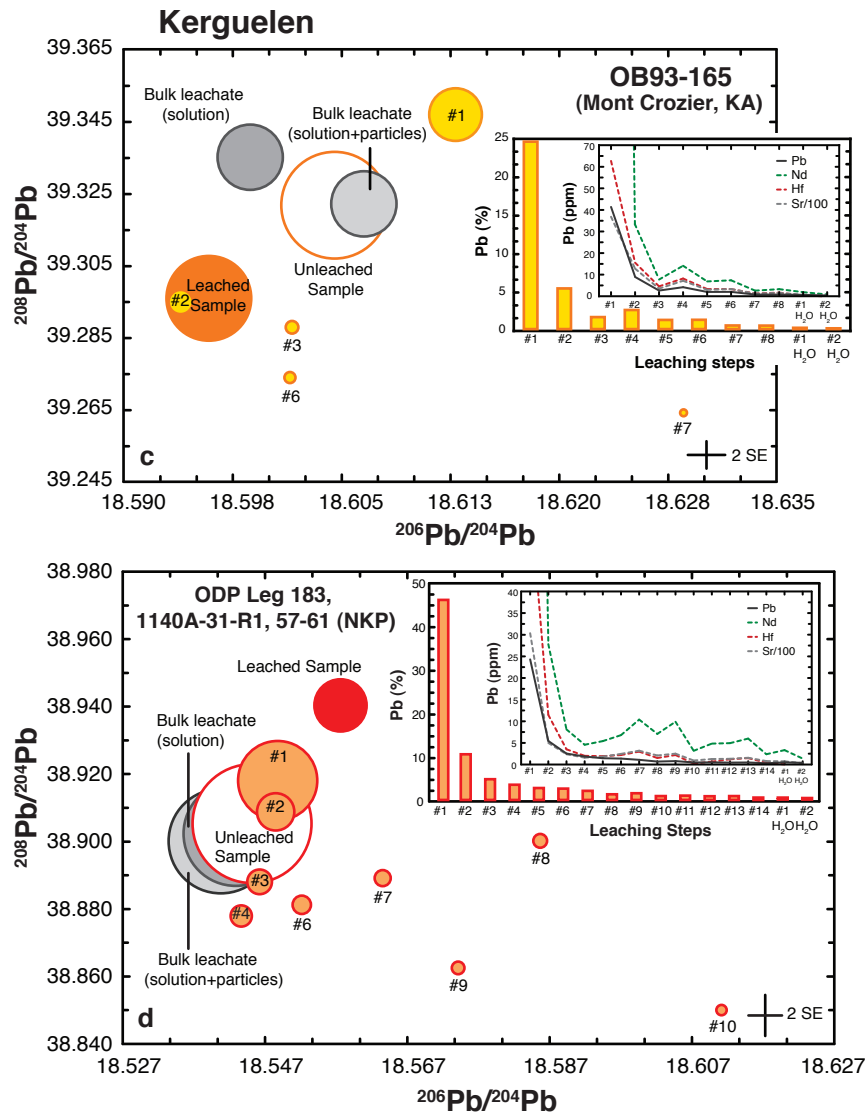
Figure 2.2. Diagrams of ^{208}Pb/^{204}Pb versus ^{206}Pb/^{204}Pb showing the results of the leaching experiments for two Kerguelen basalts: (a) sample OB93-165 (Mont Crozier, Kerguelen Archipelago) and (b) sample 1140A-31-R1, 57-61 (ODP Leg 183, Northern Kerguelen Archipelago). Color coding, symbol sizing, labelling, and insets as described in the legend to Figure 2.1. KA = Kerguelen Archipelago, NPK = Northern Kerguelen Plateau.
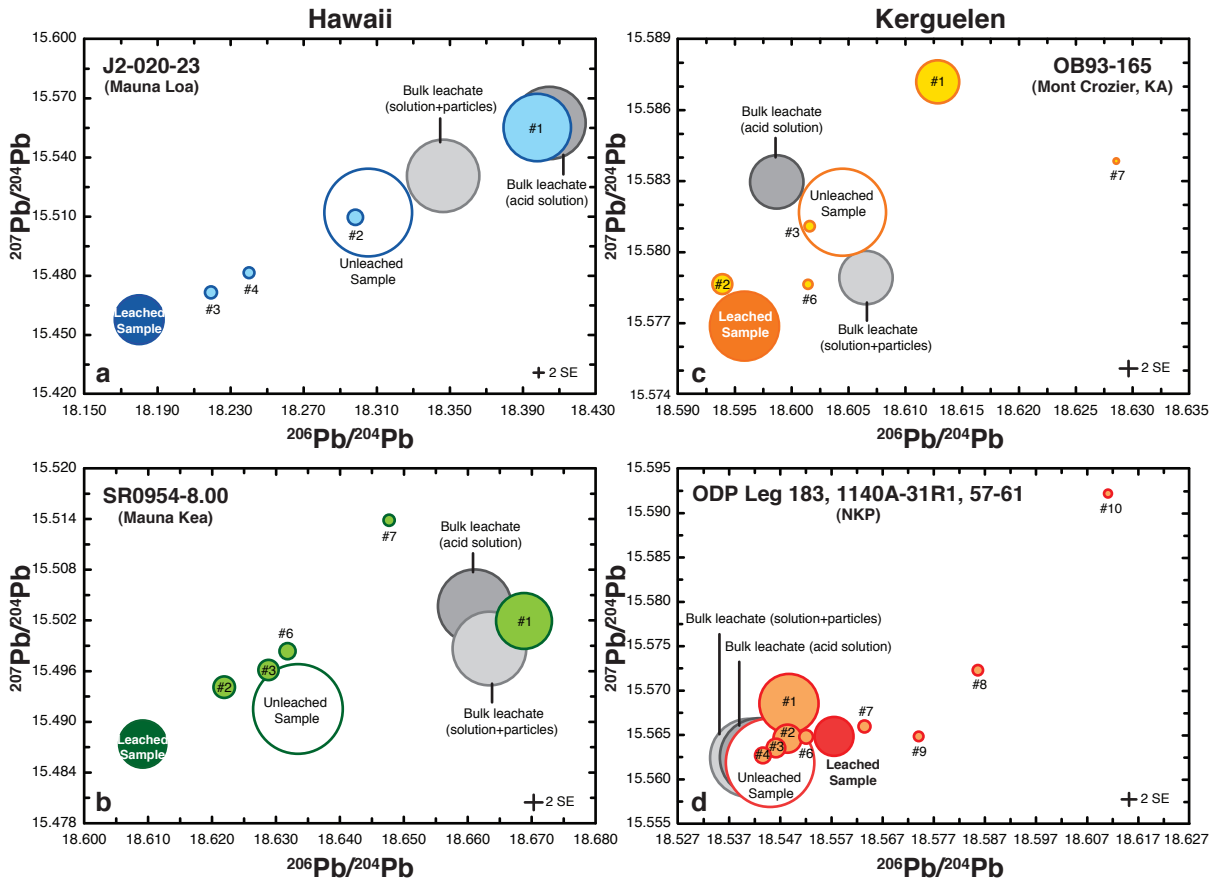
Figure 2.3. Diagrams of $^{207}Pb/^{204}Pb$ versus $^{206}Pb/^{204}Pb$ showing the results of the leaching experiments: (a) Hawaiian basalt sample J2-020-23, (b) Hawaiian basalt sample SR0954-8.00, (c) Kerguelen basalt sample OB93-165 and (d) Northern Kerguelen Plateau basalt sample 1140A-31-R1, 57-61. Colour coding, symbol sizing and labeling as described in the legend to Figure 2.1; abbreviations as indicated in the legend to Figure 2.2.

For the Hawaiian basalts (Figures 2.1, 2.3a and 2.3b), the Pb isotopic compositions of the individual leachate solutions generally plot along a mixing trend between a more radiogenic end-member and the leached sample residue. In contrast, for the Kerguelen basalts (Figures 2.2, 2.3c and 2.3d), the Pb isotopic compositions of the individual leachate solutions after leaching step #5 deviate from the mixing line formed by the residual leached sample powder and bulk leachate solutions. The leachate solutions corresponding to higher leaching steps are insignificant in terms of their Pb content (Figures 2.1 to 2.3). Nevertheless, these leachate solutions yield more radiogenic Pb isotope ratios, which indicates the presence of an additional minor component.

With the exception of three Hawaiian samples, the unleached sample powders show better reproducibility (e.g., 122 and 93 ppm on $^{206}Pb/^{204}Pb$ for samples SR954-8.00 and OB93-165, respectively) than their respective leached sample residues (e.g., 254 and 230 ppm on $^{206}Pb/^{204}Pb$ for the same two samples) (Tables 2.4 to 2.6). In a $^{208}Pb/^{204}Pb$ vs. $^{206}Pb/^{204}Pb$ diagram (Figure 8a), the individual leaching trends have steeper slopes than the "Kea-mid8" and "Kea-hi8" groups of HSDP-2 basalts defined by *Eisele et al.* [2003]. The isotopic compositions of the unleached powders for three Hawaiian basalts (J2-019-04, J2-020-23, SR0705-0.15) yield much higher dispersion and plot distinctly outside the fields of their respective volcano (Figure 8), which reflects the presence of a much higher proportion of contamination and secondary components (Figure 2.6; and see section 2.5.1 below). The Hawaiian basalts, despite significantly younger ages and less alteration than the Kerguelen basalts, show much larger differences between the Pb isotopic compositions of unleached powders, bulk leachate solutions and their residue.

The number of acid-leaching steps affects the final Pb isotopic reproducibility of a sample. In Figure 2.4, we compare results for an alkalic basalt (OB93-165) from the Kerguelen Archipelago, for which powder splits were subjected either to six-acid leaching steps (3 aliquots) or eight acid-leaching steps (7 aliquots). The Pb isotopic compositions of the powder splits that were subjected to six acid-leaching steps have a reproducibility of 230 ppm on $^{206}Pb/^{204}Pb$, whereas those subjected to eight steps have a reproducibility of 136 ppm

Table 2.4. Pb Isotopic Compositions of Tholeiitic Basalts From Mauna Loa and Mauna Kea

Sample	Acid Leaching Steps	% Weight Loss	Column Passes	$^{206}Pb/^{204}Pb$	2 SE	$^{207}Pb/^{204}Pb$	2 SE	$^{208}Pb/^{204}Pb$	2 SE
Mauna Loa									
SW-70 -1 [a]	–	–	1	18.1092	0.0014	15.4842	0.0016	37.9295	0.0045
SW-70 -2	–	–	1	18.1059	0.0020	15.4824	0.0023	37.9235	0.0079
SW-70 -3	–	–	1	18.0993	0.0014	15.4759	0.0016	37.9069	0.0051
Ext. Reprod.[b] (ppm)				558		566		619	
SW-70 -I[c]	6	39.15	1	18.0721	0.0007	15.4841	0.0008	37.9454	0.0023
SW-70 -II	6	34.50	1	18.0562	0.0009	15.4590	0.0011	37.8660	0.0033
SW-70 -III	6	35.50	1	18.0551	0.0008	15.4568	0.0009	37.8588	0.0029
Ext. Reprod. (ppm)				1053		1960		2536	
J2-020-23 -1	–	–	1	18.3052	0.0016	15.5121	0.0021	38.1726	0.0067
J2-020-23 -I	7	37.28	1	18.1801	0.0007	15.4571	0.0006	37.9415	0.0018
J2-020-23 -II	7	26.76	1	18.1772	0.0005	15.4539	0.0006	37.9323	0.0014
J2-020-23 -III	7	38.45	1	18.1797	0.0012	15.4568	0.0013	37.9401	0.0041
J2 020 23 -III rep.[d]	7	38.45	1	18.1800	0.0009	15.4571	0.0008	37.9414	0.0022
Ext. Reprod. (ppm)				153		198		230	
J2-020-23 -a [e]	7	37.39	2	18.1799	0.0008	15.4568	0.0007	37.9401	0.0020
J2-020-23 -b	7	36.21	2	18.1805	0.0008	15.4573	0.0009	37.9418	0.0026
J2-020-23 -c	7	30.74	2	18.1809	0.0013	15.4576	0.0013	37.9437	0.0042
J2-020-23 -c rep	7	30.74	2	18.1779	0.0013	15.4544	0.0013	37.9355	0.0036
Ext. Reprod. (ppm)				146		187		185	
J2-019-04 -1	–	–	1	18.4951	0.0012	15.5703	0.0014	38.4676	0.0042
J2-019-04 -I	7	34.78	1	18.1796	0.0008	15.4583	0.0008	37.9751	0.0022
J2-019-04 -II	7	34.83	1	18.1774	0.0007	15.4558	0.0006	37.9677	0.0018
Ext. Reprod. (ppm)				170		227		278	
J2-019-04 -a	7	28.89	2	18.1806	0.0009	15.4601	0.0009	37.9795	0.0024
Mauna Kea (HSDP-2)									
SR0705-0.15 -1	–	–	1	18.5130	0.0009	15.5042	0.0009	38.1661	0.0028
SR0705-0.15 -2	–	–	1	18.6619	0.0013	15.5289	0.0011	38.2650	0.0037
SR0705-0.15 -3	–	–	1	18.7945	0.0020	15.5518	0.0023	38.3567	0.0073
Ext. Reprod. (ppm)				15096		3065		4983	
SR0705-0.15 -I	6	40.05	1	18.3372	0.0017	15.4662	0.0020	38.0123	0.0067
SR0705-0.15 -II	6	38.63	1	18.3201	0.0010	15.4768	0.0011	38.0054	0.0029
SR0705-0.15 -III	6	37.02	1	18.3475	0.0017	15.4686	0.0020	38.0264	0.0063
Ext. Reprod. (ppm)				1514		719		564	
SR0768-11.20 -1	–	–	1	18.5598	0.0015	15.4854	0.0019	38.1574	0.0064
SR0768-11.20 -I	11	30.63	1	18.5380	0.0011	15.4819	0.0011	38.1435	0.0031
SR0768-11.20 -II	11	27.31	1	18.5338	0.0006	15.4776	0.0006	38.1313	0.0019
SR0768-11.20 -III	10	33.72	1	18.5373	0.0010	15.4817	0.0009	38.1422	0.0027
Ext. Reprod. (ppm)				243		309		351	
SR0768-11.20 -a	9	31.42	2	18.5374	0.0014	15.4801	0.0016	38.1426	0.0049
SR0768-11.20 -b	9	32.67	2	18.5357	0.0017	15.4817	0.0020	38.1379	0.0062
SR0768-11.20 -c	9	29.72	2	18.5376	0.0011	15.4813	0.0013	38.1422	0.0039
Ext. Reprod. (ppm)				115		106		137	
SR0954-8.00 -1	–	–	1	18.6336	0.0014	15.4921	0.0012	38.1946	0.0034
SR0954-8.00 -2	–	–	1	18.6346	0.0012	15.4921	0.0011	38.1943	0.0033
SR0954-8.00 -3	–	–	1	18.6323	0.0010	15.4908	0.0011	38.1898	0.0034
Ext. Reprod. (ppm)				122		98		142	
SR0954-8.00 -I	6	27.60	1	18.5986	0.0012	15.4811	0.0016	38.1574	0.0043
SR0954-8.00 -II	6	19.09	1	18.6031	0.0013	15.4832	0.0014	38.1641	0.0050
SR0954-8.00 -III	6	49.92	1	18.6020	0.0014	15.4804	0.0013	38.1561	0.0041
Ext. Reprod. (ppm)				254		186		225	
SR0954-8.00 -a	6	28.64	2	18.6100	0.0006	15.4874	0.0006	38.1787	0.0018
SR0954-8.00 -b	6	28.75	2	18.6089	0.0008	15.4864	0.0008	38.1761	0.0019
SR0954-8.00 -c	6	31.82	2	18.6075	0.0010	15.4869	0.0009	38.1764	0.0027
Ext. Reprod. (ppm)				135		62		74	
SR0956-18.35 -1	–	–	1	18.5075	0.0009	15.4786	0.0009	38.1409	0.0025
SR0956-18.35 -I	9	34.93	1	18.4892	0.0006	15.4748	0.0005	38.1281	0.0014
SR0956-18.35 -II	8	34.62	1	18.4864	0.0009	15.4717	0.0009	38.1182	0.0026
Ext. Reprod. (ppm)				210		283		370	
SR0956-18.35 -a	8	35.45	2	18.4857	0.0010	15.4742	0.0011	38.1250	0.0033

[a]Numbers 1, 2, and 3 refer to complete procedural duplicates of unleached samples.
[b]Ext. Reprod., external reproducibility of the set of the same type of analyses (i.e., 1, 2, and 3; I, II, and III; and a, b, and c), expressed in ppm (2 SD on the mean of individual analyses of each set of triplicatesof the same sample: 2 SD/mean × 10⁶).
[c]Roman numerals I, II, and III refer to complete procedural duplicates of leached samples that were passed once on anion exchange columns.
[d]Replicate analyses of the same sample solutions by MC-ICP-MS are indicated by rep.
[e]Letters a, b, and c refer to complete procedural duplicates of leached samples that were passed twice on anion exchange columns.

Table 2.5. Pb Isotopic Compositions of Subaerial Alkalic Basalts From Mont Crozier on the Kerguelen Archipelago

Sample	Acid Leaching Steps	% Weight Loss	Column Passes	^{206}Pb/^{204}Pb	2 SE	^{207}Pb/^{204}Pb	2 SE	^{208}Pb/^{204}Pb	2 SE
OB93-165 -1 [a]	–	–	1	18.6054	0.0015	15.5830	0.0012	39.3245	0.0037
OB93-165 -2	–	–	1	18.6038	0.0015	15.5812	0.0017	39.3212	0.0034
OB93-165 -3	–	–	1	18.6037	0.0011	15.5811	0.0010	39.3207	0.0028
OB93-165 -3 rep.[b]	–	–	1	18.6050	0.0009	15.5815	0.0013	39.3212	0.0043
Ext. Reprod. (ppm) [c]				93		114		90	
OB93-165 -I [d]	6	36.20	1	18.5969	0.0010	15.5788	0.0010	39.3010	0.0030
OB93-165 -II	6	35.49	1	18.5930	0.0010	15.5769	0.0012	39.2908	0.0036
OB93-165 -III	6	34.67	1	18.5936	0.0009	15.5751	0.0010	39.2894	0.0033
Ext. Reprod. (ppm)				230		239		324	
OB93-165 -A2 [e]	8	50.44	1	18.5892	0.0007	15.5765	0.0007	39.2840	0.0023
OB93-165 -A3	8	50.44	1	18.5895	0.0009	15.5763	0.0010	39.2853	0.0032
OB93-165 -B2	8	45.31	1	18.5895	0.0014	15.5778	0.0018	39.2870	0.0055
OB93-165 -B3	8	45.31	1	18.5868	0.0021	15.5750	0.0026	39.2786	0.0091
OB93-165 -C2	8	41.31	1	18.5868	0.0015	15.5749	0.0017	39.2803	0.0059
OB93-165 -C3	8	41.31	1	18.5871	0.0011	15.5746	0.0010	39.2778	0.0028
OB93-165 -C3 rep	8	41.31	1	18.5881	0.0018	15.5744	0.0019	39.2773	0.0064
Ext. Reprod. (ppm)				136		158		199	
OB93-165 -a [f]	7	62.00	2	18.5890	0.0008	15.5758	0.0009	39.2823	0.0025
OB93-165 -b	7	52.49	2	18.5924	0.0008	15.5756	0.0011	39.2878	0.0031
OB93-165 -b rep	7	52.49	2	18.5920	0.0009	15.5775	0.0011	39.2890	0.0026
OB93-165- c	7	62.65	2	18.5920	0.0009	15.5770	0.0010	39.2898	0.0031
Ext. Reprod. (ppm)				172		120		172	
OB93-165 -A1	8	50.44	2	18.5898	0.0015	15.5773	0.0019	39.2851	0.0065
OB93-165 -B1	8	45.31	2	18.5868	0.0014	15.5749	0.0015	39.2808	0.0049
OB93-165 -C1	8	41.31	2	18.5892	0.0028	15.5765	0.0035	39.2833	0.0120
Ext. Reprod. (ppm)				175		161		110	
OB93-177 -1	–	–	1	18.4802	0.0013	15.5682	0.0015	39.1292	0.0044
OB93-177 -I	7	55.99	1	18.4459	0.0009	15.5606	0.0009	39.0594	0.0022
OB93-177 -II	6	36.86	1	18.4493	0.0010	15.5609	0.0010	39.0603	0.0026
OB93-177 -III	4	80.64	1	18.4534	0.0010	15.5615	0.0009	39.0610	0.0025
Ext. Reprod. (ppm)				410		57		43	
OB93-177 -a	6	61.99	2	18.4528	0.0014	15.5624	0.0014	39.0639	0.0035
OB93-177 -b	5	54.36	2	18.4534	0.0008	15.5630	0.0008	39.0654	0.0020
OB93-177 -c	5	45.91	2	18.4480	0.0008	15.5598	0.0011	39.0583	0.0021
Ext. Reprod. (ppm)				322		220		191	
OB93-202 -1	–	–	1	18.4917	0.0009	15.5734	0.0010	39.1247	0.0029
OB93-202 -I	7	62.62	1	18.4957	0.0008	15.5724	0.0007	39.1123	0.0015
OB93-202 -II	5	52.21	1	18.4934	0.0007	15.5728	0.0007	39.1090	0.0017
Ext. Reprod. (ppm)				176		35		118	
OB93-202 -a	5	58.25	2	18.4976	0.0009	15.5740	0.0009	39.1166	0.0025

[a]Numbers 1, 2, and 3 refer to complete procedural duplicates of unleached samples.
[b]Replicate analyses of the same sample solutions by MC-ICP-MS are indicated by rep.
[c]Ext. Reprod., external reproducibility of the set of the same type of analyses (i.e., 1, 2, and 3; I, II, and III; and a, b, and c), expressed in ppm (2 SD on the mean of individual analyses of each set of triplicates of the same sample: 2 SD/mean × 10^6).
[d]Roman numerals I, II, and III refer to complete procedural duplicates of leached samples that were passed once on anion exchange columns.
[e]Capital letters A2, A3, B2, B3, C2, and C3 refer to portions of three leached duplicates that were passed once on anion exchange columns, and capital letters A1, B1, and C1 refer to fractions of three leached duplicates that were passed twice on Pb anion exchange.
[f]Letters a, b, and c refer to complete procedural duplicates of leached samples that were passed twice on anion exchange columns.

48
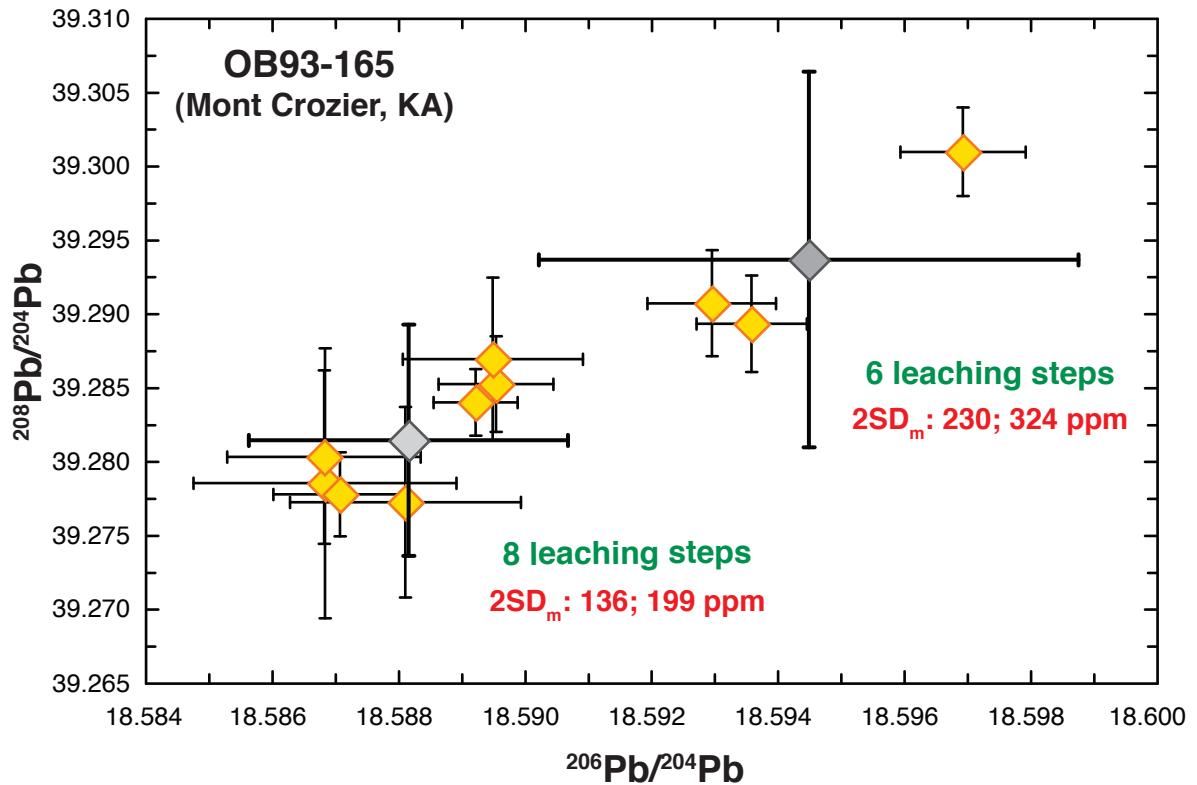
Figure 2.4. Diagram of ^{208}Pb/^{204}Pb versus ^{206}Pb/^{204}Pb showing the reproducibility of the Pb isotopic compositions of powder splits from the same alkalic basalt (OB93-165) from the Kerguelen Archipelago that were subjected to six acid-leaching steps (three aliquots) and eight acid-leaching steps (seven aliquots). All these samples were purified once through Pb anion exchange columns prior to analysis by MC-ICP-MS. The error bars on each individual symbol represent the 2 SE of the individual run. The average (mean) Pb isotopic composition and 2 SD for each set of aliquots subjected to different numbers of leaching steps are represented by the larger grey symbols with thicker error bars. The number of acid-leaching steps is indicated as well as the external reproducibility (2 SD$_m$ in parts per million (ppm)) of ^{206}Pb/^{204}Pb and ^{208}Pb/^{204}Pb.

Table 2.6. Pb Isotopic Compositions of Subaerial Tholeiitic Transitional Basalts From Mont des Ruches, Mont Fontaine, and Mont Bureau on the Kerguelen Archipelago and of a Submarine Tholeiitic Basalt from ODP Leg 183, Site 1140, on the Northern Kerguelen Plateau

Sample	Acid Leaching Steps	% Weight Loss	Column Passes	$^{206}Pb/^{204}Pb$	2 SE	$^{207}Pb/^{204}Pb$	2 SE	$^{208}Pb/^{204}Pb$	2 SE
Mont Des Ruches									
BY96-27 -1 [a]	–	–	1	18.2551	0.0006	15.5272	0.0005	38.8273	0.0014
BY96-27 -2	–	–	1	18.2543	0.0011	15.5273	0.0010	38.8260	0.0029
BY96-27 -3	–	–	1	18.2534	0.0011	15.5258	0.0011	38.8210	0.0035
Ext. Reprod.[b] (ppm)				95		110		171	
BY96-27 -I [c]	6	29.46	1	18.2539	0.0014	15.5201	0.0016	38.7853	0.0055
BY96-27 -II	6	30.03	1	18.2542	0.0010	15.5211	0.0010	38.7885	0.0031
BY96-27 -III	6	31.34	1	18.2495	0.0006	15.5167	0.0006	38.7737	0.0021
Ext. Reprod. (ppm)				288		301		402	
BY96-31 -1	–	–	1	18.3490	0.0008	15.5516	0.0010	39.0494	0.0042
BY96-31 -I	11	44.32	1	18.3222	0.0014	15.5514	0.0017	39.0013	0.0055
BY96-31 -II	10	41.67	1	18.3225	0.0019	15.5497	0.0022	38.9980	0.0075
Ext. Reprod. (ppm)				28		155		118	
BY96-31 -a [d]	12	58.54	2	18.3258	0.0015	15.5528	0.0014	39.0097	0.0037
BY96-31 -b	12	54.62	2	18.3200	0.0012	15.5479	0.0010	38.9925	0.0029
BY96-31 -c	11	41.74	2	18.3228	0.0018	15.5510	0.0007	39.0034	0.0007
Ext. Reprod. (ppm)				318		320		445	
Mont Fontaine									
BY96-86 -1	–	–	1	18.3610	0.0008	15.5436	0.0007	39.0256	0.0022
BY96-86 -1rep.[e]	–	–	1	18.3624	0.0014	15.5448	0.0017	39.0217	0.0037
Ext. Reprod. (ppm)				106		110		138	
BY96-86 -I	13	58.93	1	18.3803	0.0008	15.5397	0.0007	39.0083	0.0019
BY96-86 -II	10	59.20	1	18.3776	0.0012	15.5387	0.0009	39.0034	0.0027
Ext. Reprod. (ppm)				212		85		178	
BY96-86 -a	9	55.45	2	18.3788	0.0009	15.5406	0.0009	39.0084	0.0021
Mont Bureau									
GM92-48 -1	–	–	1	18.4760	0.0013	15.5660	0.0012	38.5495	0.0036
GM92-48 -1rep	–	–	1	18.4748	0.0008	15.5639	0.0008	38.5457	0.0024
Ext. Reprod. (ppm)				90		196		142	
GM92-48 -I	10	59.85	1	18.4475	0.0014	15.5199	0.0014	38.6163	0.0043
GM92-48 -II	9	60.08	1	18.4472	0.0015	15.5179	0.0014	38.6113	0.0040
GM92-48 -III	11	61.24	1	18.4454	0.0014	15.5170	0.0013	38.6106	0.0036
Ext. Reprod. (ppm)				123		194		160	
Northern Kerguelen Plateau: ODP Leg 183, Site 1140									
1140A-31R-1, 57-61 -1	–	–	1	18.5451	0.0008	15.5619	0.0009	38.9056	0.0029
1140A-31R-1, 57-61 -I	13	64.01	1	18.5583	0.0012	15.5637	0.0010	38.9384	0.0027
1140A-31R-1, 57-61 -II	13	54.72	1	18.5519	0.0015	15.5570	0.0015	38.9214	0.0046
1140A-31R-1, 57-61 -III	10	50.99	1	18.5567	0.0009	15.5631	0.0008	38.9349	0.0023
Ext. Reprod. (ppm)				359		475		461	
1140A-31R-1, 57-61 -a	10	49.73	2	18.5571	0.0008	15.5636	0.0007	38.9383	0.0020
1140A-31R-1, 57-61 -b	11	54.89	2	18.5622	0.0009	15.5642	0.0008	38.9369	0.0021
1140A-31R-1, 57-61 -c	14	59.99	2	18.5594	0.0013	15.5646	0.0012	38.9420	0.0032
Ext. Reprod. (ppm)				274		68		134	

[a]Numbers 1, 2, and 3 refer to complete procedural duplicates of unleached samples.
[b]Ext. Reprod., external reproducibility of the set of the same type of analyses (i.e., 1, 2, and 3; I, II, and III; and a, b, and c), expressed in ppm (2 SD on the mean of individual analyses of each set of triplicates of the same sample: 2 SD/mean × 10^6).
[c]Roman numerals I, II, and III refer to complete procedural duplicates of leached samples that were passed once on anion exchange columns.
[d]Letters a, b, and c refer to complete procedural duplicates of leached samples that were passed twice on anion exchange columns.
[e]Replicate analyses of the same sample solutions by MC-ICP-MS are indicated by rep.

(Table 2.5). Comparable improvements in reproducibility were observed for $^{207}Pb/^{204}Pb$ and for $^{208}Pb/^{204}Pb$. Although just within error, the average isotopic composition of the powder splits that were subjected to eight acid-leaching steps is slightly less radiogenic (i.e., further from the composition of the unleached powder and leachate solutions) than the average of those that were leached six times.

2.5.2 Pb Purification

The matrix elimination experiments show differences between full procedural sample triplicates that were processed once and twice by anion-exchange chromatography (Tables 2.4 to 2.6, Figure 2.5). Sample triplicates subjected to the same number of acid-leaching steps (six for the Hawaiian sample and eight for the Kerguelen sample) that were purified twice yield Pb isotopic compositions that are in general more reproducible (e.g., 135 and 74 ppm difference in $^{206}Pb/^{204}Pb$ and $^{208}Pb/^{204}Pb$ for Hawaii and 175 and 110 ppm for Kerguelen, respectively) than the triplicates that were purified only once (e.g., 254 and 225 ppm difference in $^{206}Pb/^{204}Pb$ and $^{208}Pb/^{204}Pb$ for Hawaii and and 136 and 199 ppm for Kerguelen, respectively). The differences in reproducibility are more significant for the Hawaiian sample and may reflect greater matrix effects (see section 2.5.2 below).

The number of acid-leaching steps that the powder splits are subjected to affects the relative differences in the measured isotopic ratios of the samples processed once vs. twice on columns. For the Mont Crozier sample OB93-165 (Figure 2.7a), the difference in the Pb isotopic ratios of powder splits that were purified once or twice decreases with an increasing number of acid-leaching steps. For the Mauna Loa samples J2-019-04 and J2-020-23 (Figure 2.6a), the powder splits were subjected to seven acid-leaching steps and show negligible difference in their isotopic compositions after one and two passes on the Pb anion-exchange columns, whereas for the Mauna Kea sample SR0954-8.00 (Figures 2.6a and 2.6b), where the powder splits were subjected to six leaching steps, the Pb isotopic signatures are clearly distinct.

51
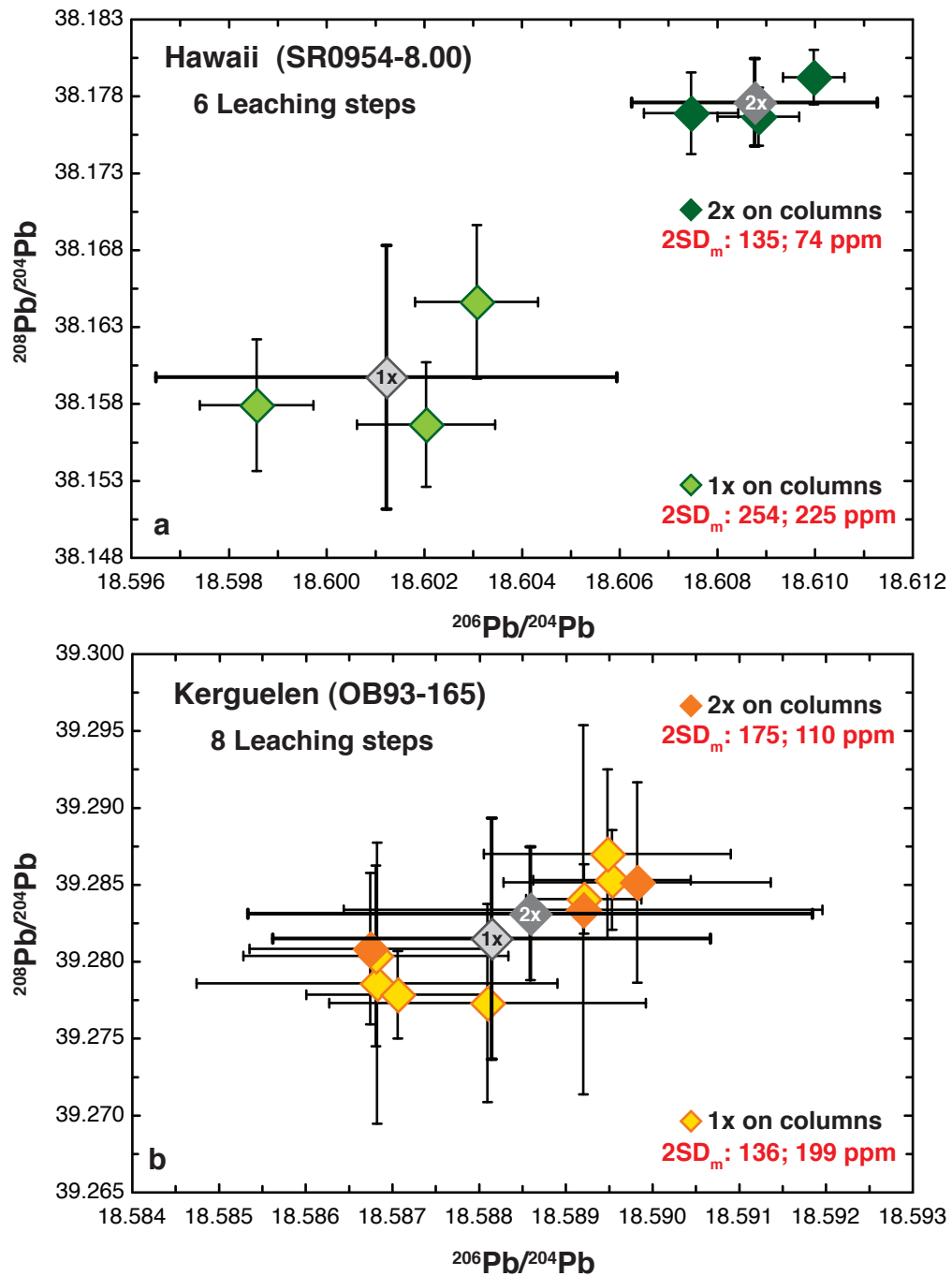
Figure 2.5. Diagrams of $^{208}Pb/^{204}Pb$ versus $^{206}Pb/^{204}Pb$ for powder aliquots of (a) a tholeiitic Hawaiian basalt (sample SR0954-8.00 (Mauna Kea)) and (b) an alkalic Kerguelen basalt (sample OB93-165 (Mont Crozier)) showing the effect of purifying samples by anion exchange chromatography. For each sample, the powder aliquots were subjected to the same number of acid-leaching steps (six steps for the Hawaiian sample and eight steps for the Kerguelen sample) and processed once or twice through the Pb anion-exchange columns prior to analysis by MC-ICP-MS. The error bars on the individual symbols represent the 2 SE of individual run. The average Pb isotopic compositions and 2 SD for the different groups of analyses are represented by the larger grey symbols and thicker error bars. Also identified are the number of acid-leaching steps that each group of powders was subjected to, as well as their reproducibility (2 SD_m expressed in ppm) for $^{206}Pb/^{204}Pb$ and $^{208}Pb/^{204}Pb$.

Finally, all triplicates, from Hawaiian and Kerguelen samples, that were processed twice on columns show more radiogenic Pb isotopic compositions (Tables 2.4 to 2.6). The results for the triplicates of Mauna Kea sample SR0954-8.00 that were subjected to one pass vs. two passes on columns are not within error of each other (Figures 2.5a and 2.6b). For the Kerguelen Archipelago basalts, the differences in Pb isotopic compositions for samples with one- vs. two-passes on columns are within error (Figures 2.5b and 2.7a). For the submarine basalt on the Northern Kerguelen Plateau (Figure 2.7b), even though the powder splits were subjected to higher numbers of acid-leaching steps (10–14), the relationship between one vs. two passes on columns is preserved.

2.6. Discussion

2.6.1. Implications of Sequential Acid-Leaching

Acid-leaching of whole rock powders of oceanic basalts leaves a residue of plagioclase and clinopyroxene ± olivine and oxides that provides the closest estimate of the magmatic isotopic compositions [e.g., *Mahoney*, 1987; *Regelous et al.*, 2003; *Hanano et al.*, 2009]. For both the Hawaiian and Kerguelen basalts examined in this study, the relationship between full procedural triplicates of unleached and leached samples defines trends that are oblique to calculated mass fractionation lines (Figures 2.6 and 2.7). These trends result from the removal by acid-leaching of foreign Pb hosted in low-temperature alteration minerals or in any potential contaminant (i.e., drilling mud, secondary minerals related to seawater alteration) [*Hanano et al.*, 2009].

For the tholeiitic Hawaiian basalts, the difference in the Pb isotopic compositions between full procedural triplicates of unleached and leached sample splits reflects the incorporation of a local contaminant, such as seawater Pb as represented by Pacific Fe-Mn nodules [*Abouchami and Galer*, 1998; *Eisele et al.*, 2003] (Figure 2.6a). For the two submarine tholeiites from Mauna Loa (J2-019-04 and J2-020-23), the compositions of the unleached and leached sample splits trend towards the field of the Pacific Fe-Mn nodules
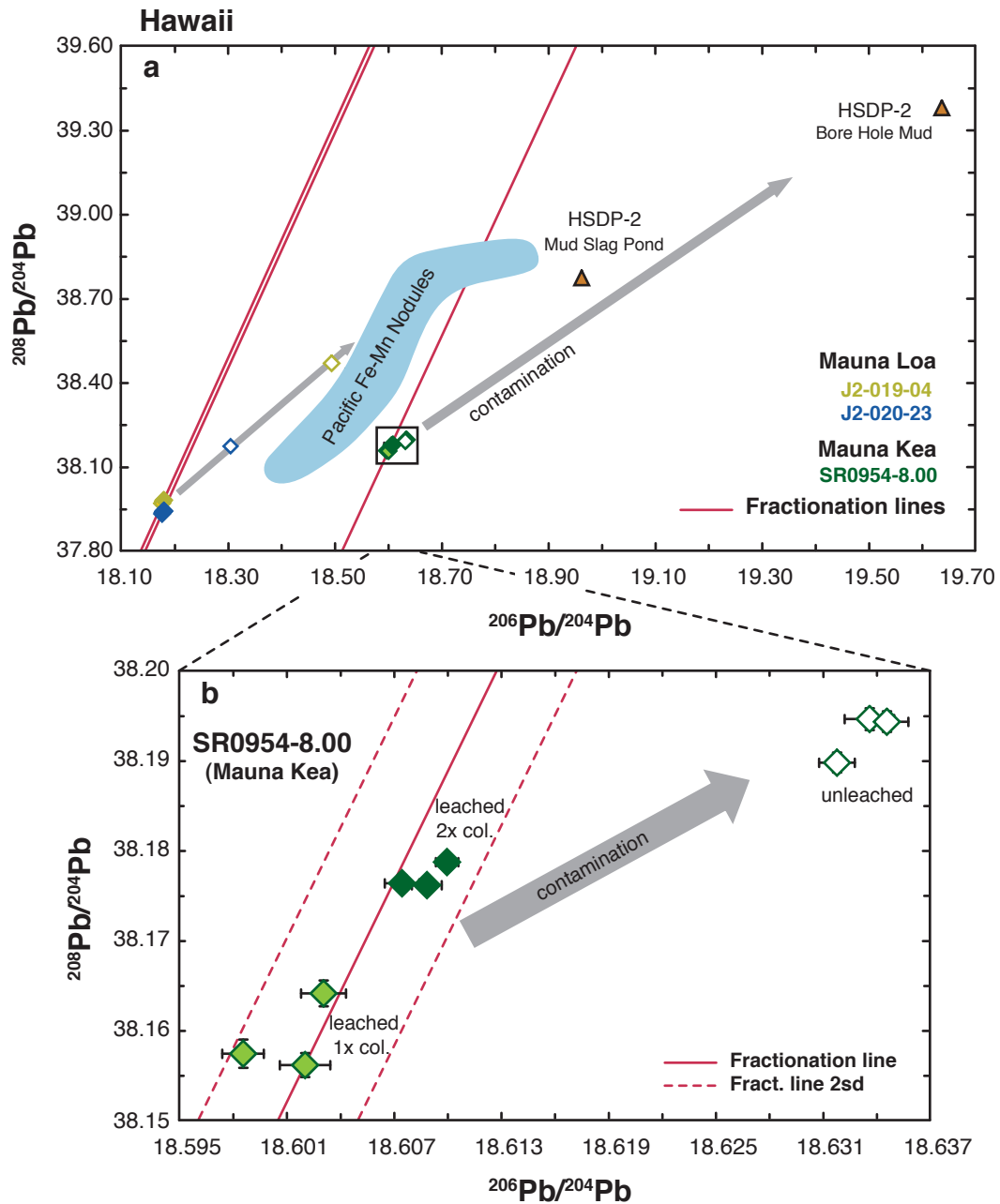
Figure 2.6. Diagrams of ^{208}Pb/^{204}Pb versus ^{206}Pb/^{204}Pb showing the isotopic compositions obtained from the acid-leaching and matrix elimination experiments for tholeiitic Hawaiian basalts (samples J2-019-04, J2-020-23, SR0954-8.00). (a) Larger scale. Potential contaminants are also reported, including seawater Pb, represented by the field for Pacific Fe-Mn nodules [*Abouchami and Galer*, 1998], and HSDP-2 borehole mud and mud from the right slag pond [*Abouchami et al.,* 2000*; Eisele et al.*, 2003], represented as triangles. Also shown are the mass fractionation lines (red solid lines) calculated for these samples. (b) Enlarged portion of Figure 6a, focusing on the isotopic results for leaching and matrix elimination experiments of sample SR0954-8.00 from Mauna Kea. The calculated mass fractionation line is shown as the red solid line and its associated 2 SD as subparallel red dashed lines. The grey arrows on both diagrams show the direction of possible contamination that could explain the relationship between the isotopic results for the leached (colored symbols) and unleached (open symbols) samples.

(Figure 2.6a), which is consistent with the observation by *Hanano et al.* [2009] of finely banded Mn-oxides filling void spaces in sample J2-019-04.

For the Mauna Kea samples collected from the HSDP-2 drill core (Figures 2.6 and 2.8), the trends of the leaching results do not intercept the field for Pacific Fe-Mn nodules indicating that seawater Pb is not a major contaminant. The trends point towards a much more radiogenic contaminant, with potentially variable Pb isotopic compositions, such as the drilling mud used during HSDP-2 (bore hole mud and mud from the right slag pond [*Abouchami et al.*, 2000; *Eisele et al.*, 2003]). Distinct patches of barite/celestite have been identified within sample SR0954-8.00 [*Hanano et al.*, 2009], thus despite the careful sample washing procedures employed for the HSDP sample suite prior to crushing [*Rhodes and Vollinger*, 2004], unleached HSDP-2 samples may be contaminated by interaction with drilling mud. The distinctly larger differences in Pb isotopic compositions between unleached and leached powder splits observed for the Hawaiian basalts compared to the Kerguelen basalts (Figures 2.8a and 2.8b) is likely accounted for by contamination of the HSDP-2 samples with drilling mud and by interaction with seawater for the Mauna Loa samples. These larger differences were surprising as the Hawaiian basalts are much younger (≤500 ka vs. 24-34 Ma) and significantly less altered than the Kerguelen basalts.

For the Kerguelen Archipelago basalts, the unleached powder splits plot within 2σ error of each other and typically have more radiogenic Pb isotopic compositions than the leached splits (Figures 2.7a and 2.8b). The results for the leached powder splits for sample OB93-165 (Figure 2.7a) trend towards less radiogenic isotopic compositions. This trend is systematic and correlates with an increasing number of leaching steps, which is consistent with progressive removal of secondary alteration minerals by sequential acid leaching. For this subaerial alkalic basalt, the trend corresponds to a mixing line with an unidentified component associated with alteration. All the other Kerguelen samples show comparable alteration systematics (Figure 2.8b), except the Mount Bureau sample GM92-48. Identification of the contaminant in the subaerial basalts from the Kerguelen Archipelago is more difficult to trace than that for the submarine basalts and may be related to the wide
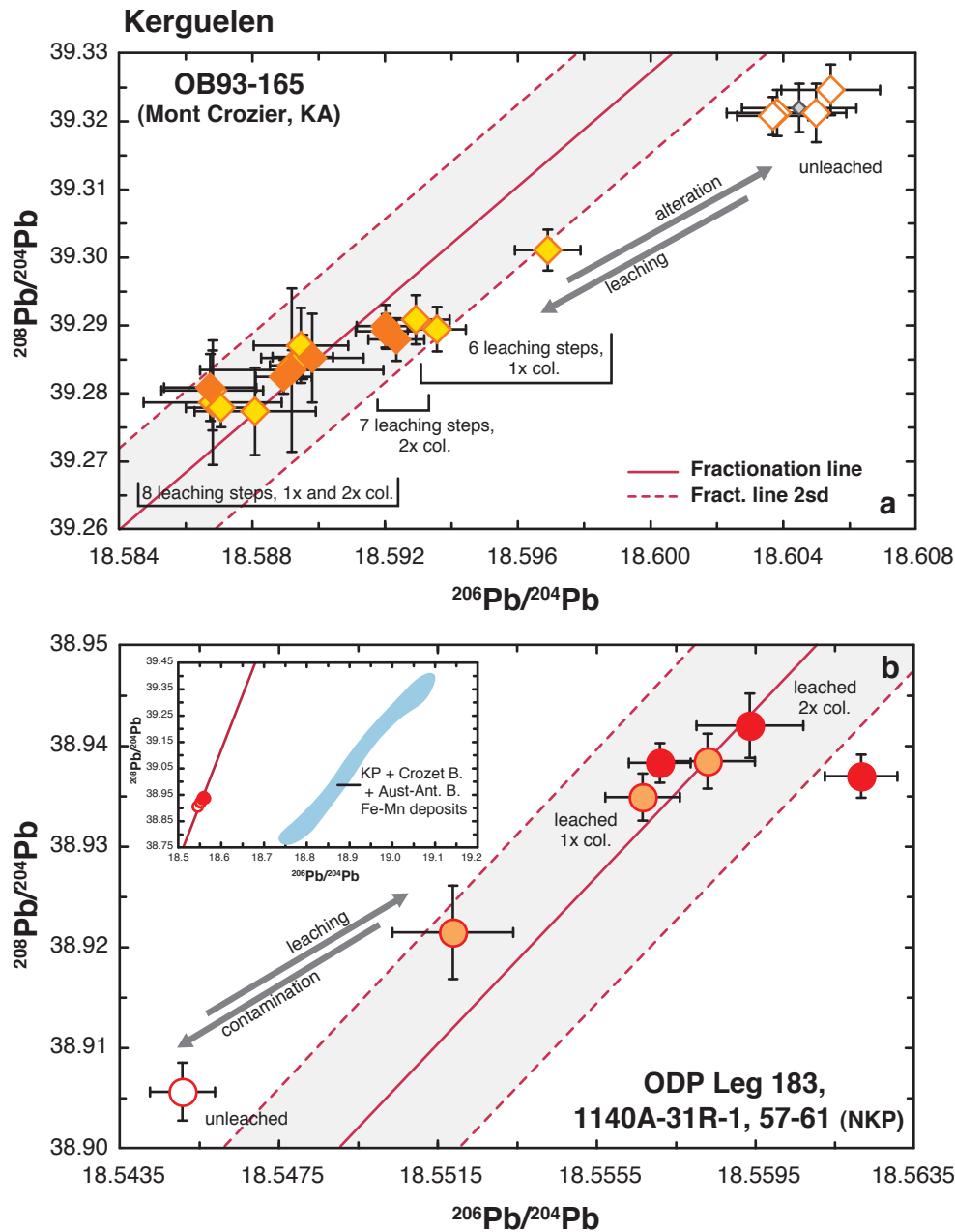
Figure 2.7. Diagrams of ^{208}Pb/^{204}Pb versus ^{206}Pb/^{204}Pb showing the isotopic compositions obtained with the acid-leaching and matrix elimination experiments for Kerguelen basalts. (a) The results for the subaerial alkalic sample OB93-165 from Mont Crozier on the Kerguelen Archipelago and (b) the results for the submarine tholeiitic sample 1140A-31R-1, 57-61, recovered during ODP Leg 183 (Site 1140) from the Northern Kerguelen Plateau (NKP). Also reported are the mass fractionation lines (red solid lines) calculated for these samples and their associated 2 SD (red dashed lines); the pale grey areas represent the range of uncertainty of the calculated mass fractionation. The inset diagram in the top left of Figure 7b shows the results for sample 1140A-31R-1, 57-61, and the Pb isotopic composition of Indian Ocean seawater, which is represented by the field for Fe-Mn deposits from the Kerguelen Plateau, Crozet Basin and Australian-Antarctic Basin [*Vlastélic et al.*, 2001]. The relationship between the results for the unleached and leached duplicates in these experiments cannot be explained by interaction with seawater.

variety of secondary minerals (carbonates, oxides, sulfides, quartz, clays, epidotes, zeolites) produced during subsequent hydrothermal alteration of the subaerial basalts [*Nougier et al.*, 1982; *Verdier*, 1989; *Hanano et al.*, 2009].

In contrast to all the other studied Hawaiian and Kerguelen basalts, the submarine tholeiite (ODP leg 183, 1140A-31R-1, 57-61) from the Northern Kerguelen Plateau (Figures 2.2, 2.3 and 2.7b) shows more radiogenic isotopic compositions for the leached sample splits than for the unleached sample. The reason for this reverse leaching behaviour is enigmatic, especially as the field for Indian seawater Pb is distinctly more radiogenic (Figure 2.7b). Thus, interaction with seawater Pb, as represented by the Fe-Mn deposits from the Kerguelen Plateau, Crozet Basin and Australian-Antarctic Basin [*Vlastélic et al.*, 2001], cannot account for this observation.

2.6.2. Effect of Matrix Elimination

The accuracy of radiogenic isotope ratio measurements by MC-ICP-MS can be affected by non-spectral interferences (matrix effects that affect the ionization and transmission of the analyte and instrumental mass bias) due to residual sample matrix [e.g., *Thirlwall*, 2002; *Woodhead*, 2002; *Barling and Weis*, 2008]. Samples for isotope ratio analysis by MC-ICP-MS thus need to be as pure as possible to obtain accurate high-precision results. Another possible source of inaccuracy could be mass fractionation during Pb anion-exchange chromatography [*Blichert-Toft et al.*, 2003], as under certain circumstances, incomplete elution of the Pb fraction leads to lighter (less radiogenic) Pb isotopic compositions. In this case, if a significant difference was to be observed in the measured Pb isotopic ratios for a sample that was purified once and twice on columns (with close to 100% recovery in the Pb chemistry), then the twice-purified Pb fraction would be isotopically lighter than the once-purified Pb fraction.

In this study, all samples processed twice on columns have heavier isotopic ratios (i.e., more radiogenic) than those processed once, thus we observe the opposite relationship
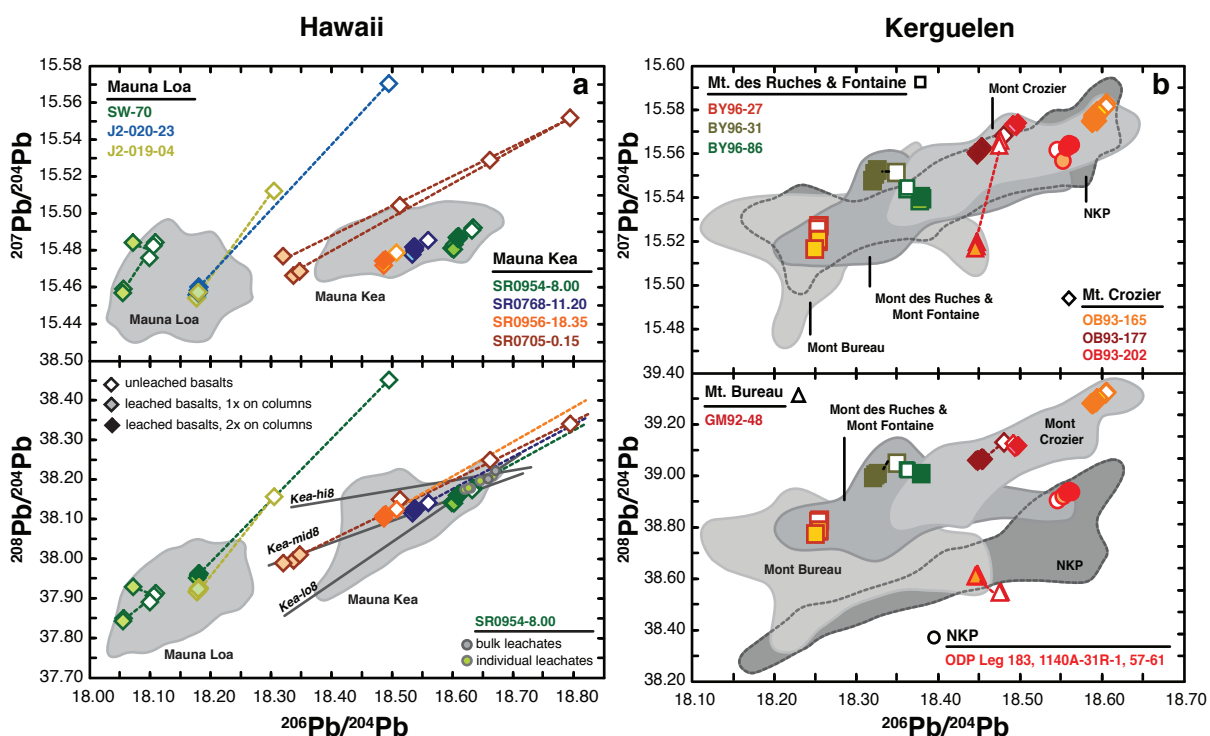
Figure 2.8. Diagrams of $^{207}Pb/^{204}Pb$ versus $^{206}Pb/^{204}Pb$ and $^{208}Pb/^{204}Pb$ versus $^{206}Pb/^{204}Pb$ for leached and unleached samples from this study compared to fields for reported compositions of Hawaiian and Kerguelen basalts. (a) Hawaii. Fields for high-precision Pb isotopic compositions by TS-TIMS [*Abouchami et al.*, 2000; *Eisele et al.*, 2003] and MC-ICP-MS [*Blichert-Toft et al.*, 2003; *Wanless et al.*, 2006; *Weis,* D. unpublished data, 2005] are reported for basalts from Mauna Loa and Mauna Kea volcanoes. Lines for Kea-lo8, Kea-mid8 and Kea-hi8 are those defined by *Eisele et al.* [2003] on HSDP-2 basalts. Results for Hawaiian basalts analyzed in this study are shown as individual symbols (the analytical uncertainty for individual samples is smaller than the symbol sizes). Open symbols correspond to unleached samples, light-coloured symbols (with dark outlines) correspond to leached samples purified once on Pb anion-exchange columns, and dark-coloured symbols indicate leached samples passed twice on Pb anion exchange columns. For reference, dashed lines connect results for unleached and leached samples (colour-coded to match the corresponding symbols); they have been extrapolated to more radiogenic values for the HSDP-2 samples to clearly show the difference in slope compared to the Pb-Pb arrays of *Eisele et al.* [2003]. (b) Kerguelen. Fields for Pb isotopic compositions by TIMS [*Yang et al.*, 1998; *Doucet et al.*, 2002] and MC-ICP-MS [*Doucet et al.*, 2005; *Weis,* D. unpublished data, 2005] are reported for basalts from the Kerguelen Archipelago and Northern Kerguelen Plateau [*Weis and Frey*, 2002]. Results for the Kerguelen basalts analyzed in this study are shown as individual symbols. Analytical uncertainty, colour coding and legend are as noted above. In both diagrams, note the significantly reduced dispersion of high-precision Pb isotopic ratios for leached samples compared to results from unleached samples and TIMS analyses.

58

of what would be expected from column fractionation experiments [*Blichert-Toft et al.*, 2003] (Figures 2.6b and 2.7b). These observed differences between the two types of triplicates (purified 1x and 2x on columns), which are more pronounced in the tholeiitic basalts (Hawaiian and submarine Northern Kerguelen Plateau basalts), appear to fall along the calculated mass fractionation lines (within their 2σ deviations). However, these differences are best explained by a non-spectral matrix effect as *Barling and Weis* [2008] show that the presence of magnesium and calcium in the matrix leads to lighter Pb isotopic compositions.

The lack of a mass fractionation effect produced during chromatography is also supported by the Pb isotopic results for the transitional and alkalic basalts from the Kerguelen Archipelago, which have comparable CaO, but lower MgO and higher NaO and SiO$_2$ contents than the Hawaiian basalts. For these Kerguelen basalts, the Pb isotopic compositions for full procedural triplicates of leached powder splits that were purified once and twice on Pb anion-exchange columns are within error of each other (Tables 2.5 and 2.6). In addition, their 2σ mean deviations (≤160 ppm for ^{206}Pb/^{204}Pb and ^{208}Pb/^{204}Pb for the alkalic basalt OB93-165, Figure 7a) are within instrumental external reproducibility (≤200 ppm).

One possible explanation for the occurrence of a non-spectral matrix effect due to residual sample matrix during processing of the tholeiitic basalts may lie in their relatively low Pb concentrations (sub-ppm to ppm range) compared to the alkalic basalts (Table 2.1) and thus the amount of sample powder (mg) that is purified. For the tholeiitic samples, more sample powder is needed to ensure enough Pb for MC-ICP-MS analysis after leaching and chromatography. All of the sample splits for which the leached residue exceeded ~170 mg (e.g., 250-300 mg for Mauna Kea [HSDP-2] samples and 130-190 mg for the NKP sample) show differences in Pb isotopic compositions when passed once and twice on columns. Full procedural sample triplicates where less sample was loaded (e.g., 150-170 mg for the Mauna Loa samples, and 76-130 mg for the Kerguelen Archipelago samples) show smaller to negligible differences (i.e., within errors) in Pb isotopic compositions for one and two passes

on columns. Larger sample sizes, still well below column saturation, mean that more sample matrix is loaded into the columns and this may not be effectively removed with just a single pass through columns [*Barling and Weis*, 2008]. Thus, for oceanic tholeiitic basalts, a second pass of chemical separation may be needed to reduce the sample matrix to negligible levels.

2.7. Conclusions

Acid-leaching and matrix elimination experiments on the Pb isotopic compositions of ocean island basalts from Hawaii and Kerguelen yield the following conclusions:

- Acid-leaching removes the effects of contamination and alteration that disturb the magmatic Pb isotopic composition of OIB, which is essential for evaluating the isotopic composition of the mantle source of these basalts.

- In most cases, acid-leaching leads to distinctly less radiogenic (>500 ppm) Pb isotopic ratios of the samples compared to unleached samples and is associated with a slight decrease in reproducibility.

- Independent of basalt composition (i.e., tholeiitic vs. alkalic), leaching results in 35-60% weight loss throughout the entire process and 70-80% of the Pb is lost in the first three acid-leaching steps.

- The reproducibility of Pb isotopic compositions of OIB improves with the number of acid-leaching steps that the samples are subjected to, even if most of the Pb is leached out in the first steps.

- Another factor controlling the reproducibility of Pb isotopic compositions of leached oceanic basalts is matrix elimination through column chromatography. Samples purified twice on columns show more radiogenic Pb isotopic compositions. The effect is stronger for tholeiitic (Hawaiian and Kerguelen Plateau basalts) than for alkalic (Kerguelen Archipelago) compositions.

- The difference in the Pb isotopic compositions of leached samples that are passed once vs. twice through chromatography is not due to fractionation on the anion-exchange columns, but instead depends on the specific basalt composition (i.e., the Pb concentration of the sample). Whenever a relatively large amount of material

(>170 mg) needs to be dissolved for analysis due to low Pb concentrations (sub-ppm to ppm), a second chemical purification step is recommended to avoid matrix effects.

- All steps are crucial during sample processing for obtaining accurate, high-precision Pb isotopic compositions, to discern the mantle sources and components of ocean island basalts.

Chapter 3

The Effects of Acid Leaching on the Sr-Nd-Hf Isotopic Compositions of Ocean Island Basalts [1]

3.1. Synopsis

The ability to conduct multi-isotopic analyses (e.g., Sr-Nd-Hf-Pb) on the same sample is critical for studies that evaluate the mantle source components of oceanic basalts. The isotopic compositions of relatively immobile elements, such as Nd (and other REE) and Hf, are considered to be relatively resistant to alteration, however, accurate Sr and Pb isotopic analyses of oceanic basalts require thorough acid leaching prior to dissolution. A detailed study of the Sr, Nd and Hf isotopic systematics of acid-leached oceanic basalts from Hawaii and Kerguelen was undertaken to assess how acid leaching affects their isotopic compositions. Most of the Sr, Nd and Hf was removed in the first acid leaching steps. Hawaiian basalts lose up to 35% and 40% of their total Sr and Hf contents, respectively, whereas for Kerguelen basalts the corresponding losses are 63% and ~70%. Acid leaching leads to significant loss of the original Nd content (up to 90%), which cannot be solely explained by the elimination of alteration phases and is likely related to preferential removal of the REE in the constituent silicate minerals (e.g., plagioclase, clinopyroxene). The leached residues yield Sr isotopic ratios significantly less radiogenic than their respective unleached powders and Nd-Hf isotopic compositions that are within analytical uncertainty of the respective unleached powders. This study shows that multi-isotopic analyses on the same acid-leached sample aliquot can produce reliable results for use in the discrimination of mantle source components of oceanic basalts.

3.2. Introduction

The combination of analyses of different isotopic systems (e.g., Sr-Nd-Hf-Pb) on samples of oceanic basalts constitutes a powerful tool for the determination and characterization of their mantle sources and components [e.g., *Gast et al.*, 1964; *Tatsumoto*, 1966, 1978; *White and Hofmann*, 1982; *Dupré and Allègre*, 1983; *Hart*, 1984; *White*, 1985; *Hamelin et al.*, 1986; *Zindler and Hart*, 1986; *Weaver*, 1991; *Hofmann*, 1997; 2003; *Stracke et al.*, 2005]. Inherent to their emplacement in an oceanic environment, oceanic basalts are susceptible to seawater alteration, and the effects of this alteration on Rb-Sr and U-Pb isotope systematics have long been recognized [e.g., *Hart et al.*, 1974; *Hawkesworth and*

Morrison, 1978; *Cohen and O'Nions*, 1982; *Verma*, 1992; *Staudigel et al.*, 1995; *Krolikowska-Ciaglo et al.*, 2005]. Another well known cause of disturbance of the isotopic compositions of basalts, especially for Pb isotopes, is contamination during crushing and grinding [e.g., *Woodhead and Hergt*, 2000; *McDonough and Chauvel*, 1991; *Weis et al.*, 2005]. To overcome the chemical disturbance caused by alteration, plus possible contamination during sample handling, careful acid leaching of samples prior to dissolution and analysis has proven to be an effective and essential step in sample processing for mantle geochemistry studies [e.g., *Manhès et al.*, 1978; *Dupré and Allègre*, 1980; *McDonough and Chauvel*, 1991; *Eisele et al.*, 2003; *Stracke et al.*, 2003; *Weis et al.*, 2005; *Thompson et al.*, 2008; *Hanano et al.*, 2009; *Nobre Silva et al.*, 2009].

Given the geochemical nature of Nd and Hf (rare earth element (REE) and high field strength element (HFSE), respectively), they are considered to be relatively immobile elements in aqueous solutions and their isotopic compositions to be relatively resistant to alteration [e.g., *Cohen and O'Nions*, 1982; *Verma*, 1992; *Staudigel et al.*, 1995; *Lassiter et al.*, 1996; *Chauvel and Blichert-Toft*, 2001; *Mattielli et al.*, 2002; *Krolikowska-Ciaglo et al.*, 2005]. Also, in contrast to Sr, which is relatively abundant in seawater, the concentrations of Nd and Hf in seawater are very low [e.g., *Faure*, 1986]. Hence, an acid-leaching treatment prior to chemical separation for Nd and Hf isotopic analysis is not considered to be a requirement. Several studies, however, do show evidence for some mobility of Nd (and other REE) during hydrothermal alteration [e.g., *Ludden and Thompson*, 1979; *Cotten et al.*, 1995; *Staudigel et al.*, 1995; *Bau et al.*, 1996; *Smith et al.*, 2000; *Kempton et al.*, 2002]. Furthermore, the $^{143}Nd/^{144}Nd$ and $^{176}Hf/^{177}Hf$ ratios of basalts may be affected to some extent by seawater alteration under some specific conditions [e.g., *Kempton et al.*, 2002; *Thompson et al.*, 2008].

Depending on the sample collection method in studies of oceanic basalts (i.e., by hammering an outcrop, dredging along the slope of a seamount, ridge, or ocean floor, or by drilling), the sample sizes available for geochemical analysis can range from kilograms to less than a few grams. To properly characterize the sample and avoid any sample

heterogeneity effect, it is important that multi-isotopic analyses are performed on the same sample aliquot (same sample powders, chips, and/or glasses). This means that sequenced chemical separations should be performed on a single dissolution of each leached sample. A wide variety of leaching protocols are used by different laboratories [e.g., *Mahoney*, 1987; *McDonough and Chauvel*, 1991; *Weis and Frey*, 1991; *Stracke and Hegner*, 1998; *Abouchami et al.*, 2000; *Thirlwall*, 2000; *Eisele et al.*, 2003; *Stracke et al.*, 2003; *Baker et al.*, 2004; *Weis et al.*, 2005], but not all leaching techniques seem to provide results with the desired reproducibility for high-precision isotopic studies and interlaboratory comparison [*Abouchami et al.*, 2000; *Eisele et al.*, 2003; *Stracke et al.*, 2003; *Baker et al.*, 2004; 2005; *Albarède et al.*, 2005]. The recent improvements in precision and reproducibility offered by the current generations of multiple collector mass spectrometers (TIMS and MC-ICP-MS) have enabled researchers to discriminate different isotopic trends within data sets that previously were within analytical uncertainty, especially for Pb and Hf. The question then arises, to what extent, if any, are the Nd and Hf isotopic compositions of OIB affected by acid leaching?

To complement an earlier study on the effect of acid leaching and matrix elimination on Pb isotopes of samples from ocean island basalts [*Nobre Silva et al.*, 2009], we carried out a comprehensive study of the Sr, Nd and Hf isotopic systematics of two Hawaiian and two Kerguelen oceanic basalts (0-1.7 wt% LOI) that were subjected to multi-step acid leaching (up to 14 steps). Here we report the Sr, Nd, and Hf elemental contents and isotope compositions for the unleached and respective leached powders (residues), as well as for the acid solutions (leachates) of each leaching step and the bulk leachates (all solutions combined). A full suite of trace element concentrations on both unleached and leached powders was also measured for one of the basalts. These data are used to assess the effects of our leaching procedure on basaltic rock compositions.

3.3. Samples

For this study, we selected two Hawaiian and two Kerguelen basalts amongst the 14 analyzed by *Nobre Silva et al.* [2009]. We focused on these samples as they are

Table 3.1. Summary of Sample Geochemical Characteristics, Hawaii and Kerguelen

Sample	Eruption Environment	Depth[a] (mbsl/masl)	Rock Type	SiO$_2$ (wt%)	MgO (wt%)	Na$_2$O (wt%)	K$_2$O (wt%)	Pb (ppm)	Sr (ppm)	Nd (ppm)	Hf (ppm)	A.I.[b]	LOI[c]	Age (Ma)[d]	References
Hawaiian Basalts															
Mauna Loa (Southwest Rift Zone)															
J2-020-23	submarine	489	tholeiitic basalt	50.14	6.50	2.72	0.52	2.00	306	32.08	6.60	-0.87	0.99	-	J. M. Rhodes (unpublished data, 2003)
Mauna Kea (HSDP-2 [e])															
SR0954-8.00	submarine	3009.2	tholeiitic basalt	47.67	18.03	1.65	0.23	0.66	239	15.43	2.95	-1.31	0.85	0.55	*Rhodes and Vollinger* [2004]
Kerguelen Basalts															
Mont Crozier															
OB93-165	subaerial	515	alkalic basalt	50.91	3.54	3.52	1.45	6.34	417	36.30	5.99	0.67	-	24.5	D. Weis (unpublished data, 2005)
Northern Kerguelen Plateau															
ODP Leg 183, 1140A 31R-1 57-61	submarine	270.07	tholeiitic basalt	49.64	5.54	2.64	0.49	1.52	262	20.4	3.75	-0.81	1.65	34.3	*Weis and Frey* [2002]

[a]mbsl = meters below sea level, for submarine basalts; masl = meters above sea level, for subaerial basalts.
[b]A.I. = alkalinity index (AI = total alkalis - (SiO2 x 0.37 - 14.43)) [*Rhodes,* 1996].
[c]LOI = weight loss-on-ignition after 30 min at 1020ºC.
[d]Ages from Mauna Kea samples: *Sharp and Rennes* [2005]; Mont Crozier and Mont Bureau: *Nicolaysen et al.* [2000]; Mont des Ruches and Mont Fontaine: *Doucet et al.* [2002]; Site 1140: *Duncan* [2002].
[e]HSDP2 = Hawaii Scientific Drilling Project, phase 2.

representative of basalts typically analyzed for radiogenic isotopic compositions from these two islands and span a wide range of MgO (3.5–18.0 wt%) with relatively weak alteration (e.g., 0.85–1.65 wt% LOI). The samples are: J2-020-23 from the Mile High Section of Mauna Loa volcano, SR0954-8.00 from the Mauna Kea volcano collected from the Hawaii Scientific Drilling Project (HSDP), OB93-165 from Mont Crozier on the Courbet Peninsula of the Kerguelen Archipelago, and 1140A-31R-1, 57-61 cm recovered during ODP Leg 183 on the Northern Kerguelen Plateau (see Table 3.1 for additional sample characterization). To assess the effects of our multistep acid leaching procedure on the elemental concentrations and Sr, Nd, and Hf isotopic compositions of these four samples, all column separations and analyses were performed on the same chemical digestions of all sample fractions (i.e., unleached and leached sample powders, leachate solutions collected at each leaching step, and respective accumulate bulk leachates) as the Pb isotopic analyses published by *Nobre Silva et al.* [2009].

3.4. Analytical Techniques

3.4.1. Sample preparation

All chemical digestion and separation were carried out in Class 1000 clean laboratories and the mass spectrometric analyses were performed in Class 10,000 laboratories at the Pacific Centre for Isotopic and Geochemical Research (PCIGR) at the University of British Columbia. Sample handling in all labs was carried out in Class 100 laminar flow hoods. All reagents used for leaching, dissolution and separation were sub-boiled, all dilutions were made using $\geq$18.2 MΩ·cm de-ionized water, and all labware was acid-washed prior to use. The acid leaching procedure used follows that of *Weis et al.* [2005] and is detailed by *Nobre Silva et al.* [2009]. Briefly, the sample powders were acid-leached using 10 mL of 6 M HCl in screw-top Savillex® beakers, in a warm (~50ºC) ultrasonic bath (40 kHz) for 20 min. Immediately after, the supernatant (leachate solution) was decanted without centrifugation, to ensure the removal of the silt to fine-size particle fraction, which is mostly dominated by secondary alteration phases. The whole process was repeated (6 to 14 times for the samples in this study) until the leachate was clear and free of fine-size particles.

For all sample specimens, Sr, Nd and Hf elemental concentrations and isotopic compositions were determined on a single dissolution, using methods similar to those described in *Weis et al.* [2005, 2006, and 2007]; the total Sr, Nd and Hf procedural blanks were of the order of 200, 60, and 30 pg, respectively. The results are reported in Tables 3.2 and 3.3. In Table 3.4, a summary of the percentages of powder and elemental losses is presented.

3.4.2. Mass Spectrometry

3.4.2.1 Sr, Nd, and Hf Abundances

To determine the amount of Sr, Nd, and Hf present at each step of the acid-leaching procedure, and consequently how much is lost, the respective concentrations were measured on a 10% aliquot of the unleached sample powders, individual leachates and bulk leachate solutions. The analyses were performed on an ELEMENT2 high-resolution (HR)-ICP-MS (Thermo Finnigan, Germany) and were quantified using external calibration curves and indium (In) as an internal standard. Multi-element (Sr, Nd, and Hf) standard solutions were prepared from 1000 ppm Specpure® (Alfa Aesar®, Johnson Matthey Company, USA) single element standard solutions. Samples and standards were diluted accordingly ([Sr] and [Hf] = 1–500 ppb; [Nd] 0.1–25 ppb) and run in 0.15M HNO_3. All analyses were normalized to the internal standard and blank subtracted.

3.4.2.2 Sr, Nd, and Hf Isotopic Compositions

All Sr and Nd isotopic ratios were measured on a TRITON (Thermo Finnigan) thermal ionization mass spectrometer (TIMS) in static mode with relay matrix rotation on single Ta (Sr) or double Re-Ta (Nd) filaments. Sr and Nd isotopic compositions were corrected for mass fractionation with the exponential law using $^{86}Sr/^{88}Sr$ = 0.1194 and $^{146}Nd/^{144}Nd$ = 0.7219, respectively. The data were then normalized using the average of the corresponding standard (NIST SRM 987 for Sr and La Jolla for Nd) ran in the barrel, relative to the values of NIST SRM 987 $^{87}Sr/^{86}Sr$ = 0.710248 and La Jolla $^{143}Nd/^{144}Nd$ = 0.511858 [*Weis et al.*, 2006]. During the course of the analyses presented in this study, the average

value of the SRM 987 Sr standard was 0.710244 ± 0.000027 (n = 11) and the La Jolla Nd standard was 0.511854 ± 0.000014 (n = 9).

Hf isotopic compositions were determined on a Nu Plasma (Nu021; Nu Instruments Ltd, UK) multiple collector inductively coupled plasma mass spectrometer (MC-ICP-MS), under dry plasma conditions using a membrane desolvator (Nu DSN100) for sample introduction, following the analytical procedures detailed by *Weis et al.* [2007]. All analyses were obtained in static multi-collection mode, with interference corrections for ^{176}Lu and ^{176}Yb on ^{176}Hf, and ^{174}Yb on ^{174}Hf, respectively. All sample and standard solutions were prepared fresh for each analytical session and sample analysis followed a modified sample-standard bracketing protocol in which the JMC 475 standard solution was run after every two samples to monitor for any systematic daily drift of the standard value. Hf isotopic ratios were corrected for instrumental mass fractionation by exponentially normalizing to ^{179}Hf/^{177}Hf = 0.7325. The sample results were then normalized to the ^{176}Hf/^{177}Hf value of 0.282160 [*Vervoort and Blichert-Toft*, 1999] using the daily average of the JMC 475 Hf standard. The JMC 475 Hf standard analyzed over the period of the analyses gave an average value of ^{176}Hf/^{177}Hf = 0.282181 ± 0.000008 (n = 32).

3.5. Results

Throughout the multistep acid-leaching procedure, the Hawaiian basalts lose ~35% of their initial weight (up to 8 acid steps; Tables 3.2 and 3.4) and Kerguelen basalts lose up to 60% (up to 14 acid steps; Tables 3.3 and 3.4). For all samples, the largest amount of Sr, Nd and Hf is leached out in the first 1-2 acid leaching steps (Figure 1), as is the Pb. Overall, leaching removes up to 35% of the total Sr content and 40% of the Hf content for Hawaiian basalts, and up to 63% and ~70% of the Sr and Hf contents, respectively, for the Kerguelen basalts (Tables 3.2, 3.3, and 3.4). With the exception of one Hawaiian basalt, all samples lose ~90% of their initial Nd content during leaching. Similar proportions of Sr and Nd losses after acid leaching have been reported for basalts from the first drilling phase of the HSDP [*Hauri et al.*, 1996].

Table 3.2. Sr, Nd, and Hf Elemental Contents and Isotopic Compositions of Unleached Whole-rock Powders, Leachate Solutions, and Leached Residues for Hawaiian Basalts

Sample	Sr				Nd				Hf			
	Total ng in Each Fraction	% Sr in Each Fraction	$^{87}Sr/^{86}Sr$	2 SE[a]	Total ng in Each Fraction	% Nd in Each Fraction	$^{143}Nd/^{144}Nd$	2 SE[a]	Total ng in Each Fraction	% Hf in Each Fraction	$^{176}Hf/^{177}Hf$	2 SE[a]
Sample J2-020-23 (Mauna Loa)												
Unleached [b]	85466	100	0.703818	9	8960	100	0.512943	7	1843	100	0.283189	33
B.L.Homog.[c]	29768	34.8	0.703930	10	4754	53.1	0.512934	9	647	35.1	–	–
B.L.Acid [d]	18415	21.5	0.704203	9	4395	49.0	0.512931	8	503	27.3	0.283109	10
1st	18266	21.4	0.704310	9	4490	50.1	0.512943	8	540	29.3	–	–
2nd	3033	3.55	0.703782	8	259	2.89	0.512938	7	61.9	3.36	–	–
3rd	3233	3.78	0.703671	9	176	1.97	0.512948	12	44.5	2.41	–	–
4th	2012	2.35	–	–	121	1.35	–	–	21.8	1.18	–	–
5th	1738	2.03	0.703687	8	101	1.13	0.512956	18	20.4	1.11	–	–
6th	669	0.783	0.703704	8	52.8	0.589	0.512939	14	7.35	0.40	–	–
1st H_2O	– [e]	–	–	–	–	–	–	–	–	–	–	–
2nd H_2O	343	0.401	–	–	18.8	0.209	–	–	0.450	0.024	–	–
Total [f]	29294	34.3			5218	58.2			696	37.8		
Leach. Res.[g]	56172	65.7	0.703683	10	3742	41.8	0.512948	7	1147	62.2	0.283084	6
Sample SR0954-8.00 (Mauna Kea)												
Unleached	94286	100	0.703728	8	6085	100	0.513009	8	1164	100	0.283158	12
B.L.Homog.	19718	20.9	0.704556	8	6944	114	0.512997	9	407.7	35.0	–	–
B.L.Acid	19579	20.8	0.704634	9	7020	115	0.512614	10	406.5	34.9	–	–
1st	15597	16.5	0.704511	9	4902	80.6	0.512995	7	261.7	22.5	–	–
2nd	1951	2.07	0.703831	8	229	3.77	–	–	55.00	4.73	–	–
3rd	1548	1.64	0.703661	17	76.3	1.25	0.513027	42	39.91	3.43	–	–
4th	1175	1.25	–	–	46.2	0.759	–	–	25.80	2.22	–	–
5th	1978	2.10	0.703570	7	48.0	0.789	0.512872	112	28.10	2.41	–	–
6th	1130	1.20	–	–	32.6	0.536	–	–	18.90	1.62	–	–
7th	635	0.673	0.703592	9	16.2	0.266	–	–	11.35	0.975	–	–
8th	601	0.637	–	–	15.7	0.258	–	–	10.75	0.924	–	–
1st H_2O	245	0.260	–	–	6.80	0.112	–	–	0.800	0.069	–	–
2nd H_2O	222	0.236	–	–	7.80	0.128	–	–	-	-	–	–
Total	25083	26.6			5381	88.4			452	38.9		
Leach. Res.	69203	73	0.703535	9	704.4	11.6	0.513000	3	711	61	0.283120	5

[a]2 SE, indicates the uncertainty in the last digits of the measured isotopic ratios
[b]Unleached, unleached rock powders.
[c]B.L.Homog., bulk leachate solution homogenized (acid + fine powder particles).
[d]B.L.Acid, bulk leachate solution without the fine powder particles.
[e]Dashes indicate no isotopic analysis performed.
[f]Total = sum of the elemental contents of all individual leaching steps. The Sr, Nd, and Hf contents of the bulk leachate solutions does not equal the sum of the individual leaching steps because they were measured on different aliquots of the same sample powders. Note: the elemental contents (ng) of the unleached powders are calculated from the initial amounts of powder and the respective sample concentrations (see Table 3.1). The contents of the bulk and individual leachate solutions are those measured by HR-ICP-MS on a 10% aliquot of each solution. The elemental contents (ng) of the leached residues are calculated by mass balance between the total ng in the starting unleached powders and the sum of the elemental contents in all the individual leachate solutions.
[g]Leach. Res., leached powder residues.

Table 3.3. Sr, Nd, and Hf Elemental Contents and Isotopic Compositions of Unleached Whole-rock Powders, Leachate Solutions, and Leached Residues for Kerguelen Basalts

Sample	Sr				Nd				Hf			
	Total ng in Each Fraction	% Sr in Each Fraction	87Sr/86Sr	2 SE[a]	Total ng in Each Fraction	% Nd in Each Fraction	143Nd/144Nd	2 SE[a]	Total ng in Each Fraction	% Hf in Each Fraction	176Hf/177Hf	2 SE[a]
Sample OB93-165 (Mont Crozier)												
Unleached [b]	120221	100	0.705340	8	10465	100	0.512621	6	1727	100	0.282850	6
B.L.Homog.[c]	37016	30.8	0.705430	10	9088	86.8	0.512617	7	488	28.3	0.282849	9
B.L.Acid [d]	34489	28.7	0.705440	9	9196	87.9	–	–	334	19.4	–	–
1st	39774	33.1	0.705414	7	8774	83.8	0.512626	8	677	39.2	0.282761	15
2nd	13813	11.5	0.705303	8	357	3.41	0.512632	10	168	9.72	0.282835	8
3rd	3808	3.17	0.705297	9	83.5	0.798	0.512633	10	49.3	2.85	–	–
4th	7740	6.44	– [e]	–	153	1.46	–	–	88.5	5.12	–	–
5th	3289	2.74	0.705291	8	75.7	0.723	0.512062	11	36.7	2.13	–	–
6th	3607	3.00	–	–	79.7	0.762	–	–	36.1	2.09	–	–
7th	1297	1.08	0.705284	9	27.8	0.265	0.512632	40	13.8	0.796	–	–
8th	1661	1.38	–	–	35.3	0.337	–	–	18.2	1.05	–	–
1st H2O	313	0.261	–	–	9.60	0.092	–	–	1.35	0.078	–	–
2nd H2O	194	0.161	–	–	4.10	0.039	–	–	–	–	–	–
Total [f]	75495	62.8			9599	91.7			1089	63.1		
Leach. Res.[g]	44726	37.2	0.705298	10	866	8.28	0.512625	6	638	36.9	0.282849	6
ODP Leg 183, 1140A-31R-1, 57-61 (Northern Kerguelen Plateau)												
Unleached	103438	100	0.704422	8	8037	100	0.512808	7	1481	100	0.283020	5
B.L.Homog.	54762	52.9	0.704545	8	6289	78.3	0.512809	7	885	59.8	0.283023	5
B.L.Acid	46404	44.9	0.704668	8	6143	76.4	0.512806	7	779	52.6	0.282962	10
1st	32782	31.7	0.704720	6	5745	71.5	0.512818	8	672	45.4	0.282908	18
2nd	5508	5.32	0.704615	8	307	3.8	0.512213	19	127	8.55	0.283023	6
3rd	2567	2.48	0.704629	9	87.7	1.1	-	-	37.9	2.56	–	–
4th	1718	1.66	-	-	49.5	0.6	-	-	21.6	1.46	–	–
5th	1981	1.92	0.704548	9	58.6	0.7	-	-	20.7	1.40	–	–
6th	2652	2.56	-	-	73.4	0.9	-	-	23.7	1.60	–	–
7th	3483	3.37	0.704300	8	113	1.4	-	-	32.5	2.19	–	–
8th	2263	2.19	-	-	76.6	1.0	-	-	16.4	1.11	–	–
9th	2773	2.68	0.704226	8	109	1.4	0.512806	20	24.2	1.63	–	–
10th	1014	0.98	-	-	35.0	0.4	-	-	2.20	0.148	–	–
11th	1399	1.35	0.704227	8	53.2	0.7	0.512833	22	7.19	0.486	–	–
12th	1455	1.41	0.704228	10	54.4	0.7	0.512712	34	13.3	0.898	–	–
13th	1688	1.63	–	–	64.8	0.8	–	–	16.0	1.08	–	–
14th	850	0.821	–	–	25.8	0.3	–	–	4.65	0.314	–	–
1st H2O	373	0.360	–	–	16.7	0.2	–	–	0.15	0.010	–	–
2nd H2O	154	0.149	–	–	6.85	0.1	–	–	–	–	–	–
Total	62660	60.6			6876	85.6			1019	68.8		
Leach. Res.	40778	39.4	0.704222	23	1161	14.4	0.512839	6	462	31.2	0.283028	5

[a] 2 SE, indicates the uncertainty in the last digits of the measured isotopic ratios

[b] Unleached, unleached rock powders.

[c] B.L.Homog., bulk leachate solution homogenized (acid + fine powder particles).

[d] B.L.Acid, bulk leachate solution without the fine powder particles.

[e] Dashes indicate no isotopic analysis performed.

[f] Total = sum of the elemental contents of all individual leaching steps. The Sr, Nd, and Hf contents of the bulk leachate solutions does not equal the sum of the individual leaching steps because they were measured on different aliquots of the same sample powders. Note: the elemental contents (ng) of the unleached powders are calculated from the initial amounts of powder and the respective sample concentrations (see Table 3.1). The contents of the bulk and individual leachate solutions are those measured by HR-ICP-MS on a 10% aliquot of each solution. The elemental contents (ng) of the leached residues are calculated by mass balance between the total ng in the starting unleached powders and the sum of the elemental contents in all the individual leachate solutions.

[g] Leach. Res., leached powder residues.

71

Figure 3.1. Variation of Pb, Sr, Nd, and Hf concentrations throughout the leaching procedure for basalts from (a) Mauna Loa, (b) Mauna Kea, (c) Mont Crozier, and (d) the Northern Kerguelen Plateau. Elemental concentrations (ppb) refer to the abundances in each leachate solution measured by HR-ICP-MS. The Sr abundances are divided by 100 to allow for plotting on the same graph as the other elements.

The Hawaiian and Kerguelen basalts present a similar pattern of Sr isotopic variation throughout the leaching process (Figure 3.2). The magnitudes of the isotopic variations at each leaching step are different between the four samples as they are dependent on the amount of fine particles (mostly alteration phases and contaminants) that are removed when decanting the individual leachate solutions. The leached powder residues of all four samples yield less radiogenic Sr isotopic compositions than the respective unleached powders. The Sr isotopic compositions of the individual leachate solutions and unleached powders, of both Hawaiian and Kerguelen basalts, generally plot along a mixing trend between a more radiogenic end-member (represented by the bulk leachate solutions and 1st leachate solution) and the leached sample residue (Figure 3.2).

For both Hawaiian and Kerguelen basalts, no significant difference (i.e., outside individual analytical error) is observed between the Nd isotopic compositions of the unleached rock powders, the bulk leachate solutions, the individual leachate solutions, and the leached residues (Figure 3.3). For each individual sample, the results for nearly all sample fractions plot within error of each other. The few exceptions with lower ^{143}Nd/^{144}Nd represent a very minor relative proportion of the whole sample Nd content (e.g., leachate #2 for sample 1140A-31R-1, 57-61; leachate #5 for sample OB93-165; and a bulk leachate solution for sample SR0954-8.00). After acid leaching, the leached powder residues of both Hawaiian and Kerguelen basalts yield similar Nd isotopic compositions to those of their respective unleached sample powders.

Statistically acceptable Hf runs (i.e., >1.5 V on the ^{177}Hf beam) could only be obtained for the Kerguelen samples. This was because during the course of analysis of the leachate solutions, we encountered tungsten (W) interference problems on some of the Hawaiian samples processed in a tungsten carbide (WC) crusher and mill. In addition, the Hf contents of some fractions were not sufficient to provide good runs, hence no data is reported. For the two Kerguelen samples, the Hf isotope compositions of the unleached sample powders, bulk leachate solutions, and leached sample residues are within error of each other (Figure 3.4). In both cases, the first leachate solution yields lower ^{176}Hf/^{177}Hf
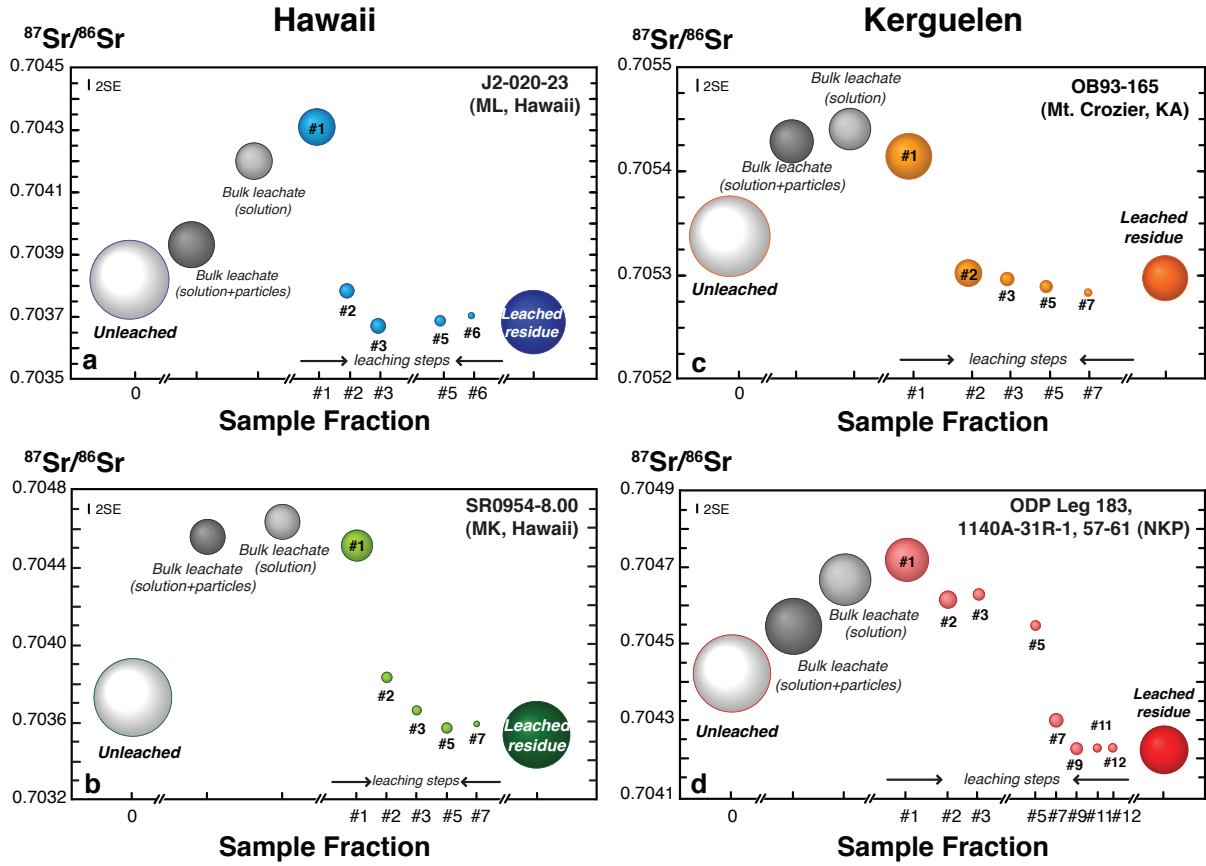
Figure 3.2. $^{87}Sr/^{86}Sr$ variations throughout the acid leaching procedure for basalts from (a) Mauna Loa, (b) Mauna Kea, (c) Mont Crozier, and (d) the Northern Kerguelen Plateau. The numbers refer to the respective acid leaching step (see Tables 3.1 and 3.3). The size of the spheres is proportional to the amount of Sr in each sample fraction. The analytical uncertainty of each analysis is smaller than the symbol sizes. In the top left corner of the diagrams, the average 2SE of the Sr isotopic analysis of each experiment is shown.
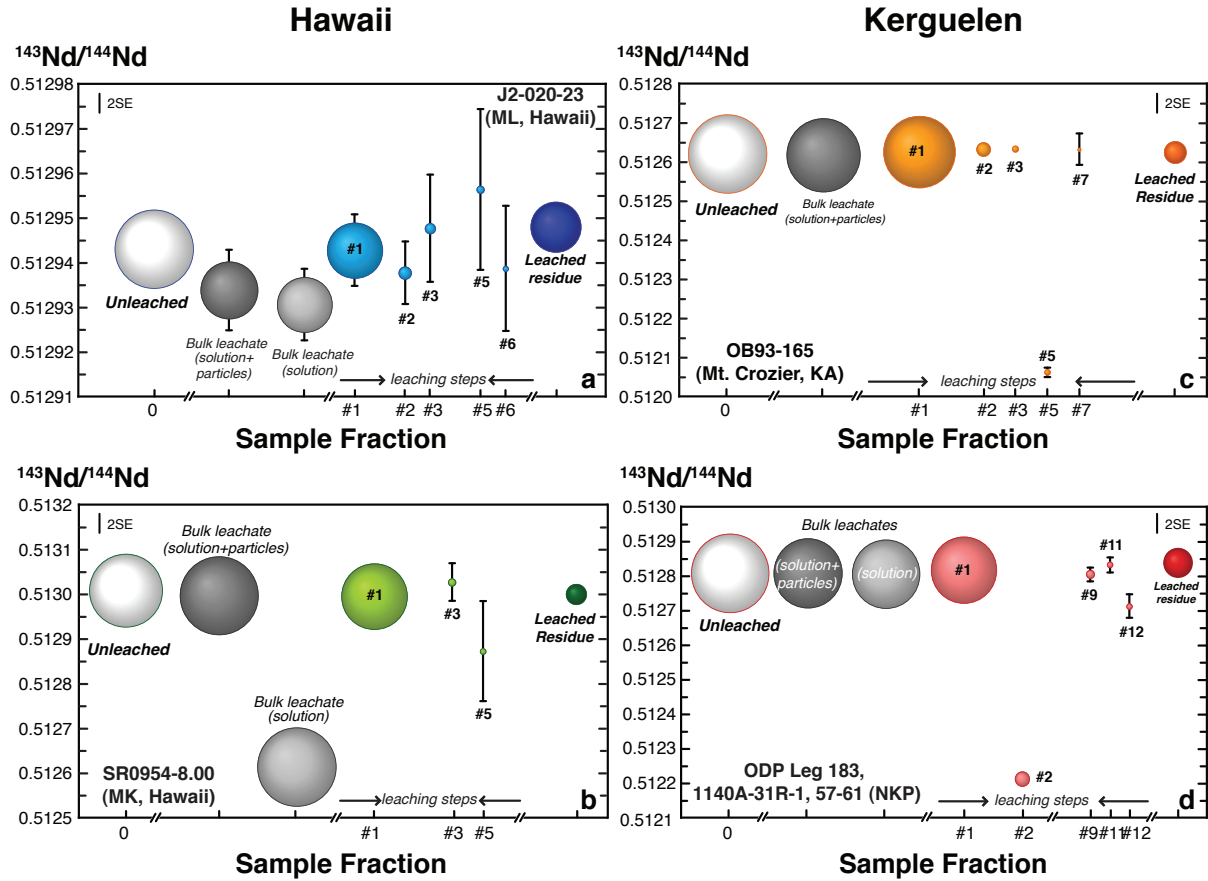
Figure 3.3. ^{143}Nd/^{144}Nd variations throughout the acid leaching procedure for basalts from (a) Mauna Loa, (b) Mauna Kea, (c) Mont Crozier, and (d) Northern Kerguelen Plateau. Symbol colours and sizes are as described in the caption of Figure 3.2. The analytical uncertainty is smaller than the symbol sizes, except where represented. The average 2 SE of the Nd isotopic analysis of each experiment is shown in the upper corners of the diagrams.
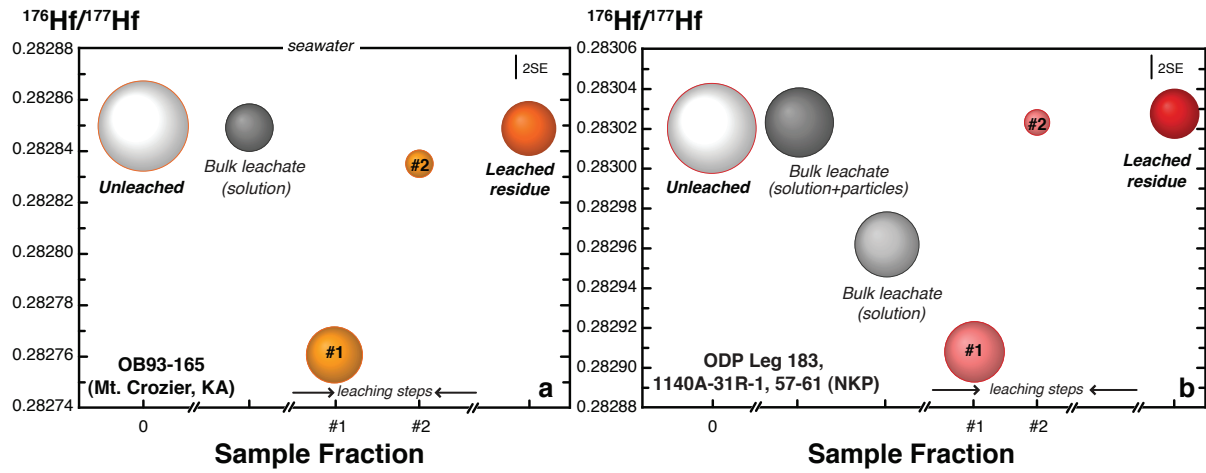
Figure 3.4. ^{176}Hf/^{177}Hf variations throughout the acid leaching procedure for basalts from (a) Mont Crozier and (b) the Northern Kerguelen Plateau basalts. Symbol colours and sizes are as described in the caption of Figure 3.2. The average 2 SE of the Hf isotopic analysis of each experiment is shown in the upper right corner of the diagrams. Note the non-overlapping range of Hf isotopic ratios between the two diagrams.

values. After acid leaching, the leached powder residues of both Hawaiian and Kerguelen basalts yield identical Hf isotopic compositions to those of their respective unleached sample powders (Tables 3.2 and 3.3).

3.6. Discussion

3.6.1. Effects of Acid Leaching of OIB in Sr-Pb Isotopic Space

The bulk leachate solutions consist of acid, a combination of secondary mineral phases, and any contaminant removed from the sample by the acid leaching process. The isotopic compositions of the bulk leachate solutions are thus a proxy for the total alteration and contaminant removed with the acid leaching procedure, whereas those of the leached residues can be considered to represent the original isotopic composition of the samples. In multi-isotopic space, the bulk leachate solutions and leached residues are hence expected to lie along mixing trends that encompass the isotopic compositions of the initial unleached rock powders and that provide insight about the nature of the contaminant. In Figures 3.5 and 3.6, we combine the Sr isotopic results of our leaching experiments with their respective Pb isotopic compositions from *Nobre Silva et al.* [2009], and discuss the plausibility of several natural contaminants to explain the mixing trends defined by the bulk leachates and the leached sample residues.

The differences between the Sr and Pb isotopic compositions of the unleached and leached rock powders of the submarine tholeiites from Mauna Loa (sample J2-020-23) and Mauna Kea (sample SR0954-8.00) reflect exchange with a more radiogenic contaminant (Figures 3.2a, 3.2b, and 3.5). Given their high Sr contents and radiogenic Sr isotopic compositions, possible natural contaminants to consider for these two Hawaiian basalts are seawater, local deep-sea sediments and/or Fe-Mn crusts, or a mixture of each. A distal contaminant that must also be considered, and that has been identified in soil horizons of Hawaiian lavas, is wind-blown Chinese loess into the central north Pacific [e.g. *Kennedy et al.*, 1998; *Abouchami et al.*, 2000; *Jones et al.*, 2000].

Table 3.4. Summary of the Weight and Relevant Element % Losses During the Multi-step Acid Leaching Procedure

Each leaching step Sample	Initial Weight (g)	# Acid Leaching Steps	Final Weight (g)	Weight Loss (%)	Pb Loss (%)	Sr Loss (%)	Nd Loss (%)	Hf Loss (%)
Mauna Loa								
J2-020-20	0.2793	6	0.1828	34.6	68.7	34.3	58.2	37.8
Mauna Kea								
SR0954-8.00	0.3945	8	0.259	34.3	70.8	26.6	88.4	38.9
Mont Crozier								
OB93-165	0.2883	8	0.106	63.2	37.3	62.8	91.7	63.1
Northern Kerguelen Plateau								
ODP Leg 183, 1140A-31R-1, 57-61	0.3948	14	0.1598	59.5	76.1	60.6	85.6	68.8

In Pb-Sr isotopic space, the leaching experiments for the Mauna Loa basalt (sample J2-020-23) produce a shallow trend defined by the leached sample residue, unleached sample powder, bulk leachates, and individual leachate solutions (Figure 3.5a). This trend reflects a larger difference in the Pb isotopic values of the leached fractions relative to their Sr isotopic compositions. Mixing between the fresh basaltic rock sample and a contaminant with a high Pb content is thus needed to explain this "leaching" trend. Given their very low Pb contents, Pacific Ocean seawater ([Sr] = ~ 8 ppm [after *Faure*, 1986]; $^{87}Sr/^{86}Sr$ = 0.70918 [*Thomas et al.*, 1996]; [Pb]$_{1000–2000\,m}$ = ~5 x 10^{-5} ppm [after *Chester*, 2003]) and authigenic carbonate deposits can be ruled out as viable contaminants (see mixing curves in Figure 3.5a). Fe-Mn deposits, which are efficient scavengers of trace metals, have very elevated Pb contents (e.g., Central Pacific Fe-Mn deposits: 997 – 1054 ppm [after *Ling et al.*, 1997]). Even a contribution of 1% of Fe-Mn oxides would be too high to explain the observed trend between the sample and leachate fractions (Figure 3.5a). Chinese eolian loess has elemental and isotopic compositions ([Sr] = ~200 ppm [after *Nakai et al.*, 1993]; $^{87}Sr/^{86}Sr$ = 0.717 [after *Kennedy et al.*, 1998]; [Pb] = ~20 ppm [after *Gallet et al.*, 1996]; $^{206}Pb/^{204}Pb$ = 18.775 [after *Jones et al*, 2000]) suitable to explain the trend produced by leaching. However, incorporation of as much as 15% of loess into the fresh lava would be needed (Figure 3.5a). This is a very large amount of sediment to be incorporated into a basalt erupted in a submarine environment and thus unlikely to be the sole explanation for the observed trend. A preferred explanation is incorporation of a composite mixture of deep-sea interbedded clay-bearing carbonate sediments, similar in composition to those now subducting at the Izu-Bonin trench [*Hauff et al.*, 2003; *Plank et al.*, 2007], and some minor Fe-Mn oxides, deposited on the surface of the basalt (Figure 3.5a).

For the HSDP-2 Mauna Kea submarine tholeiite (sample SR0954-8.00), the isotopic trend produced by the acid leaching reflects interaction of the basalt with a highly radiogenic contaminant, different than that discussed above for the submarine Mauna Loa basalt (Figures 3.2b and 3.5b). Several previous studies have suggested possible contamination of the HSDP samples by drilling mud [e.g., *Hauri et al.*, 1996; *Abouchami et al.*, 2000; *Eisele et al.*, 2003; *Nobre Silva et al.*, 2009]. *Hanano et al.* [2009] also identified distinct patches of
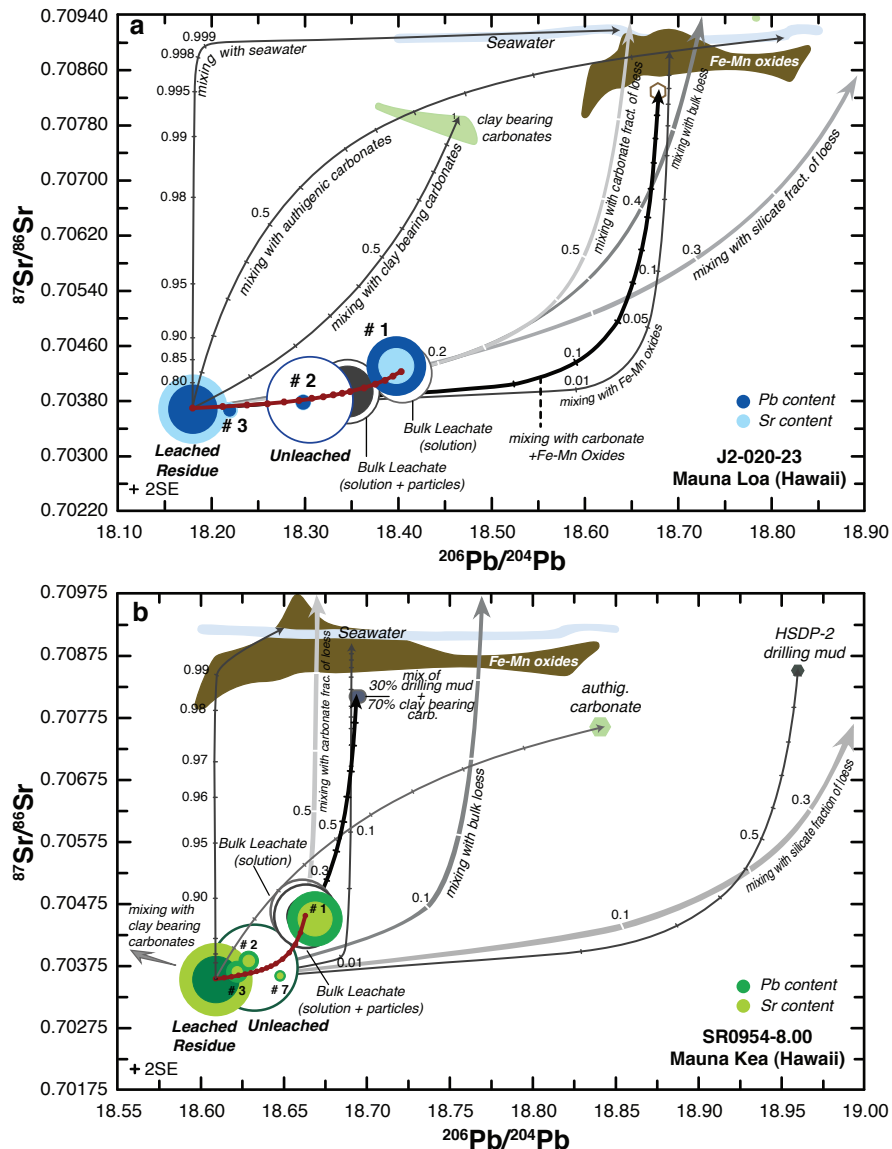
Figure 3.5. $^{87}Sr/^{86}Sr$ versus $^{206}Pb/^{204}Pb$ diagrams showing the relationships between the unleached sample powders, leached residues, and leachate solutions for the two Hawaiian basalts compared to the isotopic compositions of possible external contaminants. Pb isotopic compositions and concentrations are from *Nobre Silva et al.* [2009]. In both diagrams, the size of the symbols is proportional to the Sr (lighter colour) and Pb (darker colour) contents in each sample fraction. The analytical uncertainty of each analysis is represented by the 2 SE, which is much smaller than the symbol sizes. (a) The results for the Mauna Loa sample (J2-020-23) and several possible contaminants: seawater (elemental abundances (EA): *Faure* [1986]; isotopic compositions (IC): *Abouchami and Galer* [1998] and *Eisele et al.*, [2003]); authigenic carbonates (EA: *Faure* [1986] and *Chester* [2003]; IC: same as seawater); Fe-Mn oxides (EA and IC: *Ling et al.* [1997]); deep-sea interbedded clay-bearing carbonate sediments such as those now subducting at the Izu-Bonin trench (EA and IC: *Hauff et al.* [2003] and *Plank et al.* [2007]); Chinese loess (EA: *Nakai et al.* [1993] and *Gallet et al.* [1996]; IC: *Kennedy et al.* [1998] and *Jones et al.* [2000]). The thick red line represents the mixing trend between the leached sample residue and the bulk leachate solutions (circles indicate 10% increments). (b) The results for the Mauna Kea sample (SR0954-8.00) and three external contaminants: seawater, carbonates, HSDP-2 bulk mud [*Abouchami et al.*, 2000], and a mixture of clay-bearing carbonates plus drilling mud. The mixing trend between each of these contaminants and the leached sample residue are shown. All unlabelled tick marks on the mixing curves indicate 10% increments.

barite/celestite within a thin section of this sample. This is unexpected given the careful sample washing procedures employed for the HSDP sample suite prior to crushing [*Rhodes*, 1996; *Rhodes and Vollinger*, 2004]. The bulk mud used during HSDP-2 has distinctly more radiogenic Sr and Pb isotopic compositions [*Abouchami et al.*, 2000; *Eisele et al.*, 2003], however its Pb isotopic composition is too radiogenic to explain the trend defined by the leached sample residue, unleached sample powder, bulk leachates and individual leachate solutions of the Mauna Kea basalt (SR0954-8.00) (Figure 3.5b). Interaction of loess particles with this sample could potentially account for the observed trend produced by leaching. Based on its Pb isotopic composition, the carbonate fraction of Asian loess has been considered a possible source of the radiogenic Pb contamination of Hawaiian basalts recovered during the HSDP [*Abouchami et al.*, 2000; *Eisele et al.*, 2003]. However, as much as 25% of the carbonate fraction of the loess alone would be needed (Figure 3.5b). This represents an excessively large amount of sediment to be incorporated into the sample, and requires a process that would facilitate interaction with the carbonate fraction of the loess, but not with the silicate fraction. Another alternative is the interaction of the fresh basalt with 20% of drilling mud and deep sea carbonates mixed in a proportion of 30:70 (black thick mixing curve in Figure 3.5b). However, 20% is also a large amount of a contaminant to be incorporated into the basalt. A more plausible explanation for the observed trend is interaction of the basaltic rock sample with a combination of distinct end-members, including the drilling muds used during the HSDP-2.

Acid leaching of the submarine tholeiite from the Northern Kerguelen Plateau (sample 1140A-31R-1, 57-61) lowers its Sr isotopic composition (Figures 3.2 and 3.6b). In contrast, its Pb isotopic composition increases after being acid leached [*Nobre Silva et al.*, 2009]. This implies that the contaminant being leached out has more radiogenic $^{87}Sr/^{86}Sr$ values, but less radiogenic Pb isotopic compositions, than those of the basalt. Given the low Pb content and radiogenic Sr and Pb isotopic compositions of seawater, alteration of this basalt by Indian Ocean seawater or contamination with carbonated sediments (Figure 3.6a) cannot account for this opposite behaviour during leaching. Assuming that the isotopic compositions of the drilling muds used during the ODP Leg 183 are comparable to those
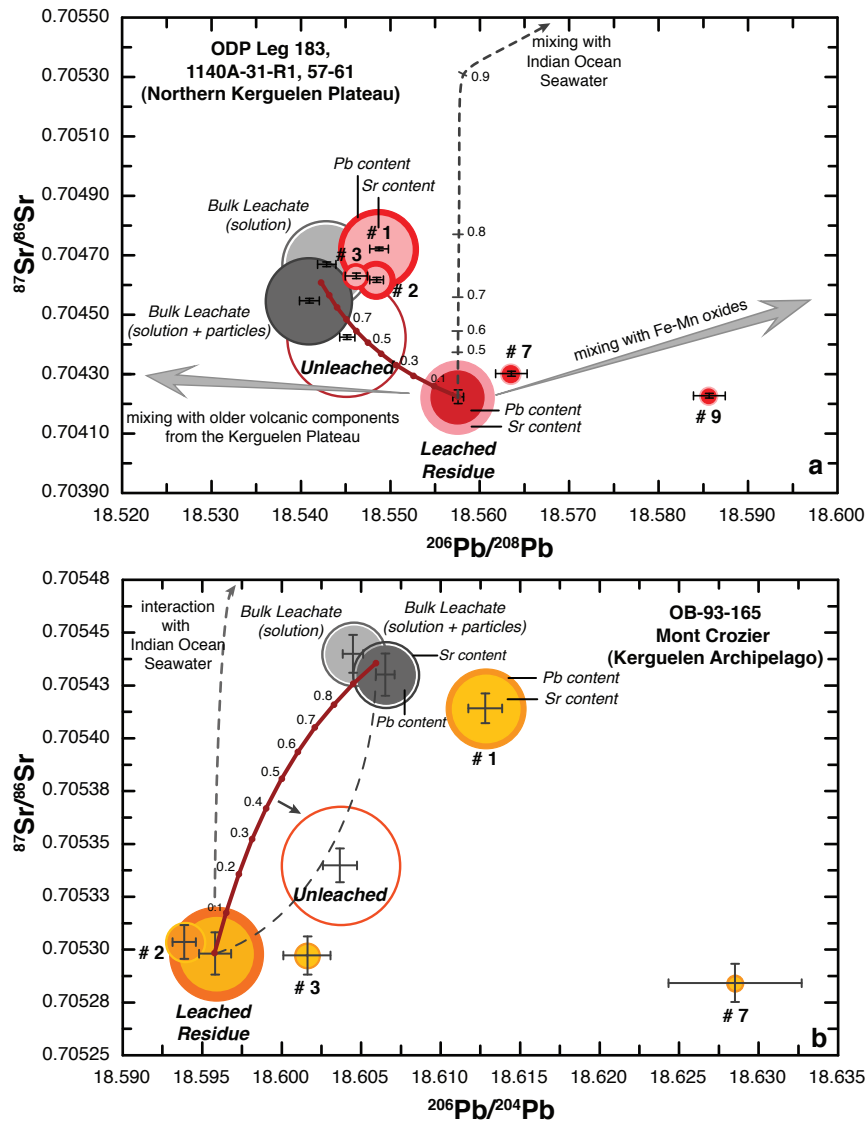
Figure 3.6. $^{87}Sr/^{86}Sr$ versus $^{206}Pb/^{204}Pb$ diagrams showing the isotopic compositions of each sample fraction obtained throughout the leaching procedure for the Kerguelen basalts compared to the isotopic compositions of possible external contaminants. Pb isotopic compositions and concentrations are from *Nobre Silva et al.* [2009]. In both diagrams, the size of the symbols is proportional to the Sr (lighter colour) and Pb (darker colour) contents in each sample fraction. The analytical uncertainty of each individual analysis is represented by the black error bars centered on the respective symbol. (a) The relationship between the Sr and Pb isotopic compositions of the leached and unleached powders, individual leaching steps, and bulk leachate solutions of the Northern Kerguelen Plateau basalt (ODP Leg 183, 1140A-31-R1-57-61). The thick red line with 10% increments represents the mixing trend between the leached sample residue and the bulk leachate solutions. Mixing lines are shown between the leached sample residue and Indian Ocean seawater (dashed line) (EA: *Faure* [1986]; IC: *Vlastélic et al.* [2001]], Fe-Mn oxides, drilling muds, and volcanic components weathered from older parts of the Kerguelen Plateau (grey arrow) (e.g., CKP: *Frey et al.* [2002a] and *Neal et al.* [2002]]. (b) The relationship between the Sr and Pb isotopic compositions of the leached and unleached powders, individual leaching steps, and bulk leachate solutions of the Mont Crozier basalt (OB93-165). The thick red line with 10% increments shows the mixing trend between the leached sample residue (proxy for the fresh sample) and the bulk leachate solutions (proxy for the total alteration removed). The black dashed line passing though the unleached sample (altered basalt) represents the trend that would be expected between a simple binary mixing between the "fresh sample" and the "alteration removed".

used by the HSDP (i.e., highly radiogenic in Pb), contamination by the drilling muds cannot be the cause for the observed differences in the isotopic compositions of the unleached and leached powders of sample 1140A-31R-1, 57-61 (Figure 3.6a). Volcanic components released during weathering of older parts of the Kerguelen Plateau (e.g., the ca. 100 Ma Central Kerguelen Plateau), could also potentially be a viable source of contamination by deposition after eruption and emplacement of the Northern Kerguelen Plateau. However, the high Sr and relatively low Pb contents of the Central Kerguelen Plateau basalts, as well as their much less radiogenic Pb isotopic compositions [*Frey et al*. 2002a; *Neal et al*., 2002], indicates that they alone are not viable contaminants (Figure 3.6a). The combined information given by the Sr and Pb isotopic compositions of the leaching experiment with sample ODP Leg 183, 1140A-31R-1, 57-61, does not allow the identification the exact nature of its unradiogenic Pb contaminant. As with the other basalts in this study, the most probable scenario is that the source of contamination of this basalt is a composite one.

In contrast to the submarine basalts in this study, the unleached rock powder of the subaerial Kerguelen Archipelago basalt from Mont Crozier (sample OB93-165) does not plot along the mixing trend defined by the leached sample residue and the bulk and first leachate solutions (Figure 3.6b). The scatter observed in the Pb isotope values of the individual leachate solutions compared with their Sr isotopic compositions (Figure 3.6a; and chapter 2 Figure 2.2a]) suggests an additional source of variability. This is consistent with the progressive removal at each step of the leaching procedure of a variety of secondary alteration minerals (carbonates, oxides, sulfides, clays, epidote, zeolites [e.g., *Nougier et al*., 1982; *Verdier*, 1989; *Hanano et al*., 2009]). The different Pb isotopic compositions of each leaching step relative to their Sr isotopic compositions suggest that the alteration minerals removed during the acid-leaching procedure may have been formed by more than one alteration process, including surficial chemical and physical weathering, possible interaction with seawater transported by hydrothermal fluids, or interaction with sea spray.

3.6.2. Effects of Acid Leaching on Trace Element Abundances and Nd-Hf Isotopic Compositions of OIB

Both Hawaiian and Kerguelen basalts lose a large relative amount (~90%) of Nd during the acid leaching procedure (Tables 3.2, 3.3, and Figure 3.1). Comparing the trace element abundances of unleached and leached powder splits of the Mont Crozier basalt (sample OB93-165; Table 3.5 and Figure 3.7), the elements that are the most affected (i.e., showing the highest proportion of removal) by the leaching process are Cs, Rb, Th, U, Pb, and the rare earth elements (REE), especially the light REE. The LREE abundances in the leached powder splits are ~5 times less than in the original unleached powder splits, whereas the heavy REE are only a factor of ~1.5 less abundant. This extraction and fractionation of the REE by acid leaching has been previously noted by other authors [e.g., *Verma*, 1992; *Thompson et al.*, 2008].

A surprising effect of the leaching process is the higher concentrations of Nb and Ta in the leached powder splits than in the unleached splits (Figure 3.7). The elemental concentrations in the leached powder splits are measured on a residue weight of about ~0.2 g (vs. ~0.4 g for the unleached splits) that represents what is left after differential mineral removal by acid leaching. Nb and Ta are high field strength elements and are predominantly concentrated in primary Fe-Ti oxide minerals, such as titanomagnetite or ilmenite. The resistance of these minerals to the acid-leaching process will promote the concentration of Nb and Ta relative to other elements in the final powder residue, hence the leached residues will have higher concentrations of these elements than the unleached powders.

The trace element abundances measured on the leached powder splits are ~2–5 times less variable than the abundances measured on the unleached powder splits (e.g., %RSD$_{unl/leach}$ = 4.45 for La; = 1.94 for Lu). This demonstrates the reproducibility of the leaching process and that mineral phases are not randomly removed from the altered crystalline basalt. The acid leached residue of whole rock powders of oceanic basalts is composed mainly of plagioclase and clinopyroxene ± olivine and Fe-Ti oxides [e.g.,

Table 3.5. ICP-MS Trace Element Abundances in ppm of Unleached and Leached Splits of the Mont Crozier, Kerguelen Archipelago, Basalt

Element	Unleached OB93-165					Leached OB93-165					Unleach./Leach.
	Split 1	Split 2	Split 3	average	SD	Split A	Split B	Split C	average	SD	
Li	4.2	4.9	5.2	4.8	0.53	4.0	3.9	3.6	3.8	0.19	1.2
Sc	22	23	24	23	1.0	28	27	26	27	1.13	0.85
V	292	298	339	310	26	146	142	137	141	4.8	2.2
Co	34	35	37	35	1.8	21	21	21	21	0.19	1.7
Ni	17	19	19	18	1.1	9.3	9.3	9.3	9.3	0.01	2.0
Cu	61	71	72	68	6.4	0.9	0.9	0.9	0.9	0.01	76
Zn	92	104	110	102	9.2	51	51	50	51	0.81	2.0
Ga	25	27	28	27	1.7	23	23	24	23	0.42	1.1
Rb	25	30	31	29	2.9	28	28	27	27	0.59	1.0
Sr	459	483	507	483	24	441	444	441	442	1.76	1.1
Y	31	32	34	32	1.5	16	16	15	16	0.21	2.1
Zr	252	288	283	275	20	249	241	256	249	7.74	1.1
Nb	30	31	36	32	3.0	45	43	42	43	1.94	0.75
Mo	1.9	2.1	2.4	2.1	0.28	1.1	1.0	1.0	1.0	0.02	2.1
Cd	0.19	0.21	0.22	0.21	0.02	0.12	0.12	0.11	0.12	0.00	1.8
Sn	1.7	1.7	2.0	1.8	0.17	0.83	0.86	0.89	0.86	0.03	2.1
Cs	0.07	0.08	0.09	0.08	0.01	0.03	0.03	0.02	0.03	0.00	3.1
Ba	320	351	355	342	19	342	340	358	347	9.99	0.99
La	34	37	38	37	2.1	6.9	7.1	7.1	7.0	0.09	5.2
Ce	75	78	83	79	4.0	15	15	15	15	0.22	5.1
Pr	8.8	9.1	9.7	9.2	0.45	2.0	2.0	2.0	2.0	0.04	4.6
Nd	35	37	39	37	1.8	9.4	9.1	9.1	9.2	0.18	4.0
Sm	7.5	7.8	8.2	7.8	0.38	2.7	2.6	2.6	2.6	0.04	3.0
Eu	2.4	2.5	2.7	2.5	0.14	2.2	2.2	2.3	2.2	0.02	1.1
Gd	7.2	7.6	7.9	7.6	0.37	3.1	3.0	3.0	3.0	0.08	2.5
Tb	1.1	1.2	1.2	1.2	0.06	0.53	0.52	0.52	0.53	0.01	2.2
Dy	6.5	6.7	7.1	6.8	0.33	3.4	3.3	3.3	3.3	0.08	2.0
Ho	1.3	1.3	1.4	1.3	0.07	0.71	0.67	0.68	0.69	0.02	1.9
Er	3.4	3.5	3.7	3.6	0.14	2.0	1.9	1.9	1.9	0.04	1.8
Tm	0.46	0.48	0.52	0.49	0.03	0.29	0.28	0.29	0.29	0.00	1.7
Yb	2.9	3.0	3.2	3.0	0.16	2.0	1.9	1.9	1.9	0.04	1.6
Lu	0.43	0.44	0.46	0.44	0.02	0.30	0.29	0.29	0.29	0.01	1.5
Hf	6.3	7.2	7.1	6.9	0.48	6.2	5.9	6.0	6.0	0.14	1.1
Ta	2.0	2.2	2.6	2.3	0.30	3.5	3.4	3.4	3.4	0.04	0.65
Pb	2.7	2.8	2.9	2.8	0.12	1.9	2.0	2.0	1.9	0.03	1.4
Th	4.4	4.7	4.8	4.6	0.22	2.4	2.2	2.3	2.3	0.11	2.0
U	1.1	1.1	1.2	1.1	0.05	0.71	0.71	0.73	0.72	0.01	1.6

Mahoney, 1987; *Regelous et al.*, 2003: *Hanano et al.*, 2009]. The chondrite-normalized REE patterns of the leached powder splits of sample OB93-165 (Figure 3.7) are consistent with removal of olivine, pyroxene, and some plagioclase, and with plagioclase being the main mineral left after acid leaching (e.g., positive Eu anomaly). The irregular trace element pattern of the leached powder residues reflects the selective removal of some elements relative to others. This indicates that the elemental abundances measured on the leached residue powders cannot be considered representative of the primary magma elemental concentrations. The REE, given their ionic radii (La: 1.16 Å; Lu: 0.97 Å) and valence (+3), do not readily substitute for other elements in the lattices of early crystallizing minerals (olivine and pyroxene) of a mafic melt [e.g., *Krauskopf and Bird*, 1995]. Instead, the REE are mostly located in non-structural sites and defects, where the bonds are most easily broken. Hence, the observation that the REE, especially the LREE, are more easily leached out likely reflects their relatively weak bonding in the mineral structures. As a result, the REE are easily remobilized and preferentially concentrated into the leachable secondary mineral phases during alteration [*Verma*, 1992], which subsequently allows for their differential removal by the acid leaching process.

Previous studies have suggested that Nd and Hf isotope ratios of oceanic basaltic rocks are to some extent modified by alteration, generally becoming slightly lower in the altered rock [e.g., *Kempton et al.*, 2002; *Thompson et al.*, 2008]. Despite the large relative amounts of Nd (and other REE) lost during the acid leaching procedure, there is very little effect on the Nd isotopic compositions (Figure 3.3). Seawater has Nd isotopic composition that varies among and within the ocean basins (mean $^{143}Nd/^{144}Nd_{Pacific\ Ocean}$ = ~0.5125 [*Piepgras and Wasserburg,* 1980]; mean $^{143}Nd/^{144}Nd_{Indian\ Ocean}$ = ~0.5123 [*Albarède et al.*, 1997a]) and that is overall significantly lower than the Nd isotopic composition of oceanic basalts. However, given the very low Nd concentrations in seawater (~2.6 x 10^{-6} ppm [*Faure*, 1986]), seawater-basalt interaction will not produce a significant change in the REE content and Nd isotopic compositions of the basalts unless the water/rock ratios are greater than 10^5 [*Ludden and Thompson*, 1979]. For each of the four samples in this study, the unleached and leached sample powders, bulk and individual leachate solutions mostly plot within analytical
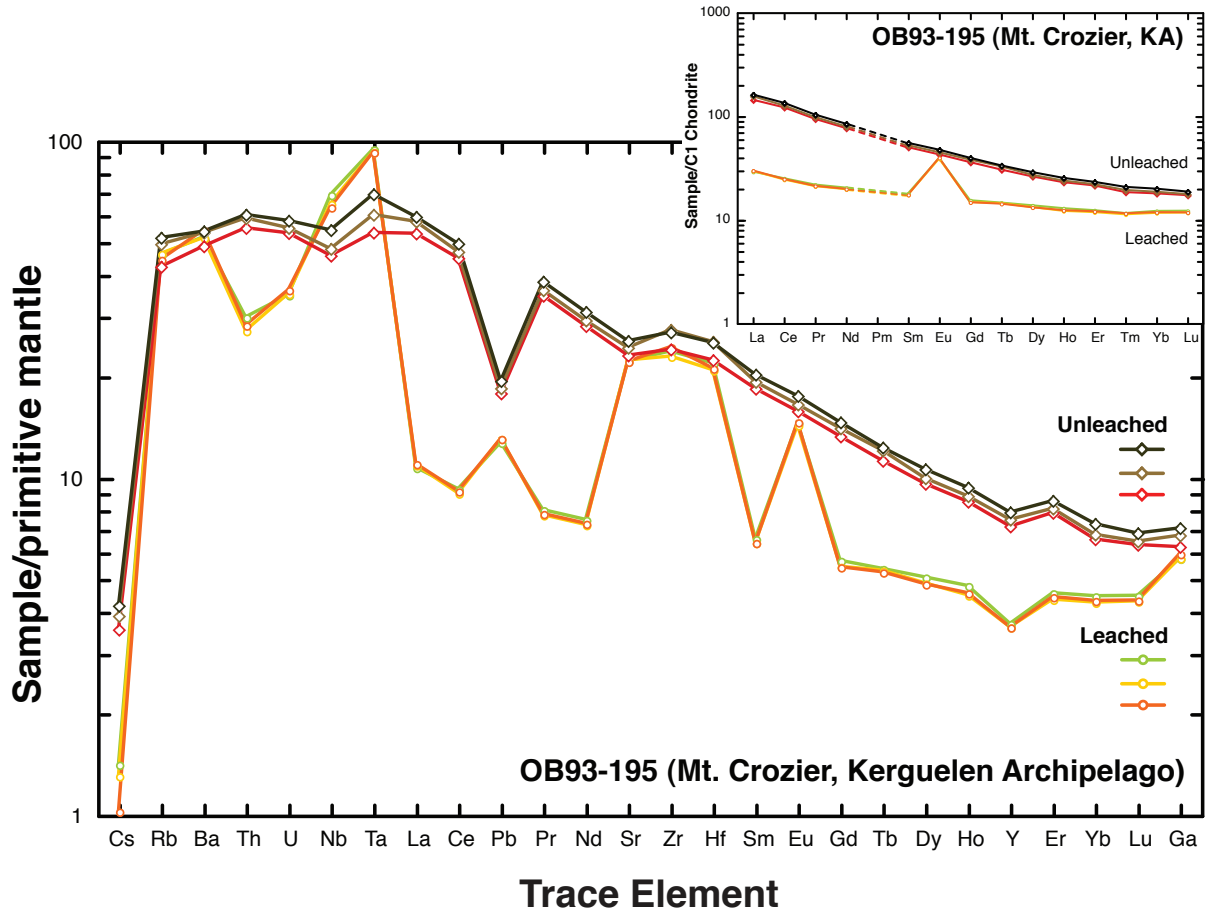
Figure 3.7. Extended primitive mantle-normalized trace element diagram showing the results for three unleached powder splits (diamonds) and three leached powders splits (circles) of sample OB93-165 from the Kerguelen Archipelago. The inset diagram shows the chondrite-normalized rare earth element patterns for the same powder splits. Normalizing values are from *McDonough and Sun* [1995].

uncertainty of each other, except for a few leachate solutions that present lower isotopic compositions. The cause of the lower isotopic compositions of these odd fractions is unknown, but may be due to some heterogeneity in the secondary alteration phases.

Reliable Hf isotopic data could only be obtained for the Kerguelen basalts (Figure 3.4). The Hf isotopic compositions of both the unleached and leached sample powders are the same within analytical uncertainty. The Hf isotopic composition of seawater (mean $^{176}Hf/^{177}Hf_{Indian\ Ocean}$ = ~0.28288 [*David et al.*, 2001]) is significantly different from that of ocean island basalts, being more radiogenic than the Kerguelen Archipelago basalt and less radiogenic than the Northern Kerguelen Plateau basalt. However, given the geochemical nature of Hf (high field strength element) and its low concentration in seawater (~7 x 10^{-6} ppm [*Faure*, 1986; *Chester*, 2003]), no change in the Hf isotopic compositions of the basalts is expected.

3.7. Conclusions

The results of this study on the effects of acid leaching of whole-rock powders on radiogenic isotopes (Pb-Sr-Nd-Hf) commonly used to discern and characterize the mantle sources of oceanic basalts demonstrate that accurate multi-isotopic analysis can be acquired on the same sample aliquots after an acid leaching treatment. The Sr isotopic ratios of all leached sample residues (submarine or subaerial) are significantly less radiogenic than their respective unleached powders. The higher $^{87}Sr/^{86}Sr$ ratios of the unleached powders are generally related to seawater interaction/alteration and (in the case of cored samples) drilling mud contamination. Seawater alone cannot explain the Sr and Pb isotopic compositional differences between unleached and leached powders of the submarine tholeiites, and interaction with other external contaminants such as Fe-Mn oxides, deep-sea sediments, and loess is also likely. For all the samples, the Nd and Hf isotopic compositions of leached and unleached powders are within analytical uncertainty of each other, despite the significant losses (~90%) of Nd (and other REE) and to a lesser extent Hf. Given these relatively significant elemental losses, care should be taken to ensure that enough material is available to measure isotopic compositions with the required precision after acid leaching of the

samples. Due to the trace element losses and REE fractionation during acid leaching, the elemental abundances measured on leached sample powders are not reliable magmatic elemental signatures. Hence, for calculation of initial isotopic ratios at the time of crystallization, parent/daughter ratios should be determined from elemental concentration ratios measured on unleached sample powders.

CHAPTER 4

The Ninetyeast Ridge and its Relation to the Kerguelen, Amsterdam and St. Paul Hotspots in the Indian Ocean

4.1. Synopsis

The Ninetyeast Ridge, a 5000 km long north-south oriented submarine volcanic ridge in the eastern Indian Ocean, is interpreted to have formed from magmatism associated with the deep-seated Kerguelen mantle plume as the Indian plate drifted rapidly northward during the Late Cretaceous. Basalts recovered along the ridge have the characteristic Dupal geochemical signatures of Indian Ocean basalts, but debate concerning the nature and number of components in the mantle source contributing to the formation of these basalts persists. New MC-ICP-MS (Pb, Hf) and TIMS (Sr, Nd) isotopic analyses were determined for tholeiites representative of the ~180 m of basaltic basement recovered from three drill sites (758: 82 Ma; 757: 58 Ma, 756: 43 Ma) along the Ninetyeast Ridge during ODP Leg 121. No systematic isotopic variation is observed along the ridge, which is inconsistent with the hypothesis of an aging mantle plume origin for the ridge. The Pb-Hf-Sr-Nd isotopic compositions are generally intermediate between those of the volcanic products of the Kerguelen and Amsterdam-St. Paul hotspots and define mixing trends between components with relatively enriched and depleted signatures. At least three, possibly four, source components are required to explain the observed isotopic variability along the Ninetyeast Ridge. The unradiogenic isotopic signatures of some Ninetyeast Ridge basalts (e.g., $^{87}Sr/^{86}Sr$ = 0.70381 – 0.70438) are not related to Indian MORB compositions and are consistent with the presence of a relatively depleted component in a deep mantle source. A similar source component is also identified in other Indian ocean island basalts (e.g., Crozet, Réunion) that are characterized by strong EM-1-like compositions. The Pb-Hf-Sr-Nd isotopic compositions of the Ninetyeast Ridge basalts are consistent with the presence of a mixture of recycled sediments and lower continental crust together with altered oceanic crust in their mantle source, hence supporting a deep origin for the EM-1-like Dupal signatures encountered in ocean island basalts.

4.2. Introduction

Hotspot tracks refer to linear, age-progressive ocean island–seamount chains and volcanic aseismic ridges across the ocean floor. They are considered to be the surface

manifestation of the interaction between focused, relatively fixed mantle melting anomalies and the motion of an overriding lithospheric plate [*Wilson*, 1963; *Morgan*, 1971, 1972]. The distinct chemistry (as compared to ocean ridge basalts), longevity (up to 100 Myr; *Coffin and Eldholm* [1994]; *Ernst et al.* [2005]) and volume of these intraplate volcanic features appear to result from melting within the conduit (or tail) of deep-seated mantle plumes, most probably originated at the core-mantle boundary [e.g., *Morgan*, 1971, 1972; *Stacey and Loper*, 1983; *Richards et al.*, 1989; *Farnetani and Samuel*, 2005]. The geometry and longevity of hotspot tracks, whether or not hotspots are considered to be fixed [e.g., *Morgan*, 1971, 1972] or advected by mantle flow [e.g., *Steinberger*, 2000; *O'Neill et al.*, 2003], are used to calculate models of plate motion [e.g., *Morgan*, 1972] and estimate cooling rates of the core [e.g., *Stacey and Loper*, 1984; *Davies*, 1988; *Sleep*, 1990]. The geochemistry of hotspot-related volcanic rocks provides information about the compositions and evolution of the mantle regions that are sampled by the mantle plumes [e.g., *Wasserburg and DePaolo*, 1979; *Campbell and Griffiths*, 1990; *DePaolo et al.*, 2001; *Jellinek and Manga*, 2004; *Bryce et al.*, 2005; *DePaolo and Weis*, 2007].

Located in the eastern Indian Ocean (Figure 4.1), the ~5000 km long Ninetyeast Ridge is the longest linear feature on earth. Together with the Chagos-Laccadive Ridge, which is related to the Réunion hotspot, the Ninetyeast Ridge is the main hotspot track used to define the motion of the Indian Ocean plate [e.g., *Morgan* 1981; *Royer et al.*, 1991; *Weis et al.*, 1992; *Müller et al.*, 1993]. Its origin has long been subject of debate, with many tectonic settings (e.g., horst structure, overthrusted plate boundary, interaction between a spreading center and transform fault, hotspot track) being proposed for its formation [e.g., *Whitford and Duncan*, 1978; *Royer et al.*, 1991; and references therein]. Following the DSDP (Legs 22 and 26) and ODP (Leg 121: Sites 756–8) drilling campaigns on the Ninetyeast Ridge during the late 1970s and late 1980s, a general consensus was reached that the ridge formed from enhanced volcanism generated during ~44 Myr of hotspot volcanism related to the Kerguelen mantle plume at the edge of the Indian Plate as the plate moved rapidly northward during the Late Cretaceous to Late Eocene [*Whitford and Duncan*, 1978; *Royer et al.*, 1991; *Duncan*, 1991; *Frey et al.*, 1991; *Weis and Frey*, 1991].
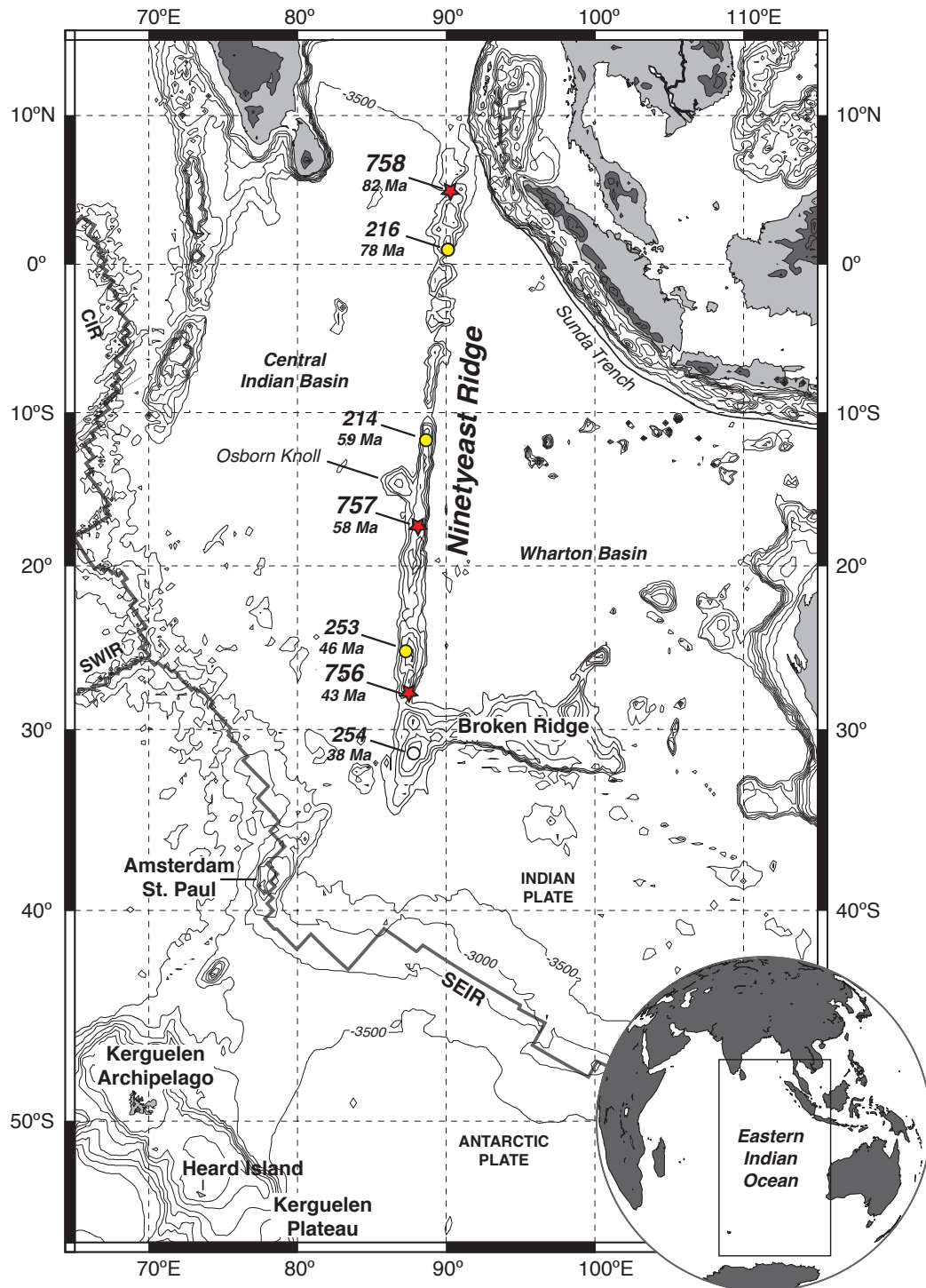
Figure 4.1. Bathymetry map (500 m interval contours) of the eastern Indian Ocean showing the major topographic features of the ocean basin (drawn using the now extinct online map creator from GEOMAR: www.aquarius.geomar.de). The yellow circles on the Ninetyeast Ridge are the DSDP Legs 22 and 26 drill Site (216, 214, 253 and 254) locations where basement was recovered, and the red stars are the ODP leg 121 drill Site (758, 757, and 756) locations. SEIR, SWIR, and CIR refer to the Southeast Indian Ridge; the Southwest Indian Ridge; and Central Indian Ridge, respectively.

The identity and number of the mantle sources and respective components involved in the generation of the Ninetyeast Ridge is however still debated. *Saunders et al.* [1991] and *Weis and Frey* [1991] interpreted the isotopic compositions of the Ninetyeast Ridge basalts as indicating mixing between at least three mantle components: a depleted mid-ocean ridge basalt (MORB)-like component, an enriched Kerguelen hotspot–type component, and a component comparable to that sampled by Amsterdam-St. Paul volcanic rocks. They interpreted the differences in the isotopic compositions of basalts from each drill site as indicative of different relative proportions of each mantle component due to the changes in tectonic setting, from hotspot-centred volcanism at Site 758 (in the northern end of the ridge) to hotspot-ridge interaction volcanism at Site 756 (in the southern end). A different view of the isotopic compositions of the Ninetyeast Ridge was presented by *Class et al.* [1993], who interpreted the increase in initial $^{206}Pb/^{204}Pb$ with decreasing eruption age, from Site 758 (~82 Ma) to Site 757 (~58 Ma) to Site 756 (~43 Ma), as reflecting the systematic compositional evolution of a single homogeneous plume by secular changes in isotopic ratios resulting from radioactive decay in the source. They proposed that this source is presently best characterized by the low $^{87}Sr/^{86}Sr$ and high $^{143}Nd/^{144}Nd$ and $^{206}Pb/^{204}Pb$ end-member of Heard Island volcanic rocks [*Barling and Goldstein*, 1990]. However, the compositional trend with time detected by *Class et al.* [1993] is not observed in the Sr and Nd isotopic systems. For example, Site 758 lavas have intermediate Sr and Nd isotopic compositions compared to those of Sites 756 and 757 [*Weis and Frey*, 1991; *Weis et al.*, 1992; *Frey and Weis*, 1995].

Since ODP Leg 121 in 1988, when the Ninetyeast Ridge basement was successfully drilled at three Sites (756, 757, 758) and subjected to comprehensive geochemical studies, the precision of Pb and Hf isotopic analyses determined by multiple collector inductively coupled plasma mass spectrometry (MC-ICP-MS) [e.g., Pb: *Belshaw et al.*, 1998; *Rehkämper and Halliday*, 1998; *White et al.*, 2000; *Weis et al.*, 2005; Hf: *Blichert-Toft et al.*, 1997; *Vervoort and Blichert-Toft*, 1999] has provided substantial improvement over the precision achieved by conventional thermal ionization mass spectrometry (TIMS) (ppm vs. ‰ range). In recent years, numerous studies have significantly increased the trace element and isotopic

datasets for other parts of the Kerguelen large igneous province (the Cretaceous Kerguelen Plateau, after ODP Leg 183; e.g., *Frey et al.* [2000a]; *Neal et al.* [2002]; *Weis and Frey* [2002]; *Ingle et al.* [2003]; Cenozoic flood basalts on the Kerguelen Archipelago; e.g., *Doucet et al.* [2005]), Amsterdam–St. Paul hotspot [e.g., *Doucet et al.*, 2004; *Graham et al.*, 2006; *Nicolaysen et al.*, 2007] and Indian Ridges [e.g., *Mahoney et al.*, 2002; *Escrig et al.*, 2004; *Hanan et al.*, 2004; *Meyzen et al.*, 2005]. These results have lead to a better understanding and new interpretations of the genesis of Kerguelen plume and Indian MORB compositions.

An "enriched" component with continental geochemical affinities has long been recognized amongst oceanic basalts from the Indian and South Atlantic oceans [*Dupré and Allègre*, 1983]. The nature of this geographically widespread isotopic domain, characterized by high $^{87}Sr/^{86}Sr$, high $^{207}Pb/^{204}Pb$ and $^{208}Pb/^{204}Pb$ for a given $^{206}Pb/^{204}Pb$ and termed Dupal [*Hart*, 1984], is not well understood. Based on the coincidence of the Dupal maxima with a low seismic velocity zone at the core-mantle boundary, a deep origin for the Dupal anomaly has been advocated [e.g., *Castillo*, 1988; *Wang and Wen*, 2004; *Wen*, 2006]. According to this hypothesis, the surfacing of the Dupal anomaly through the upwelling of long-lived mantle plumes, like the Kerguelen mantle plume [*Weis and Frey*, 1991; *Weis et al.*, 1991], is responsible for the contamination of the Indian sub-oceanic asthenosphere [*Storey et al.*, 1989; *Barling et al.*, 1994]. In contrast, the results of recent Sr-Nd-Pb-Hf-Os isotopic studies on the Indian ridges argue against the involvement of recycling of subducted oceanic crust and sediments, and instead favor a shallow origin for this regional anomaly by entrainment of lower continental crust into the Indian upper mantle during the rifting of Gondwana [e.g., *Escrig et al.*, 2004; *Hanan et al.*, 2004; *Meyzen et al.*, 2005]. *Regelous et al.* [2009] proposed a similar model to explain the Dupal anomaly in the South Atlantic. Basalts from the Cretaceous Kerguelen Plateau and Broken Ridge show geochemical evidence of interaction between the basaltic magmas with continental material [*Mahoney et al.*, 1995; *Frey et al.*, 2002a] and fragments of Indian continental crust have been found in some Kerguelen Plateau basalts from Elan Bank [e.g., *Weis et al.*, 2001; *Nicolaysen et al.*, 2001; *Frey et al.*, 2002a; *Ingle et al.*, 2002]. The existing isotopic results for basalts from the Ninetyeast Ridge

indicate that they exhibit the distinctive Dupal isotopic signature [*Dupré and Allègre*, 1983; *Hart*, 1984; *Weis and Frey*, 1991], however, continental signatures such as the ones identified in the Cretaceous Kerguelen Plateau have not been encountered in the lavas from the Ninetyeast Ridge nor in those from the Kerguelen Archipelago [e.g., *Weis and Frey*, 1991; *Frey et al.*, 2000a and b; *Doucet et al.*, 2002].

In this paper, we present new high-precision isotope compositions acquired by MC-ICP-MS (Pb, Hf) and TIMS (Sr, Nd) on acid-leached samples recovered during ODP Leg 121. This is the first comprehensive study to report Hf isotopic data for the Ninetyeast Ridge, although a few Hf results were reported by *Barry et al.* [2002; 2003]. In light of the new geochemical results that characterize the southeastern Indian Ocean mantle, we use this new multi-isotopic dataset to: 1) test the current interpretations regarding the mantle sources involved in the formation of the Ninetyeast Ridge; and 2) better discern the interaction between the Kerguelen mantle plume and the Southeast Indian Ridge, and the involvement of the Amsterdam-St. Paul hotspot during this period of evolution of the Indian Ocean basin. Finally, together with the geochemistry available from other parts of the Kerguelen large igneous province that has erupted Dupal-like basalts since ~115 Ma, and other Indian Ocean islands, we evaluate the geochemistry of the Ninetyeast Ridge to establish the source and age of the Dupal anomaly.

4.3. Geographic and Geological Setting

The Ninetyeast Ridge is a major submarine aseismic volcanic ridge, located in the eastern Indian Ocean along the 90˚E meridian (Figure 4.1). It is ~5000 km long, extending from ~17˚N, where it is buried beneath a ~5 km pile of sediments of the Bengal Fan [e.g., *Mukhopadhyay and Krishna*, 1995], to 34˚S, where it intersects with Broken Ridge [e.g., *Royer et al.*, 1991; *Mukhopadhyay and Krishna*, 1995; *Krishna et al.*, 2001]. The Ninetyeast Ridge rises to a maximum height of ~3.5 km above the surrounding ocean floor (Figure 4.2) and has an average width of 200 km, except for a ~700 km segment south of ~7˚S, where it is ~100 km wide [e.g., *Peirce et al.*, 1989; *Royer et al.*, 1991]. Near 15˚S, a circular
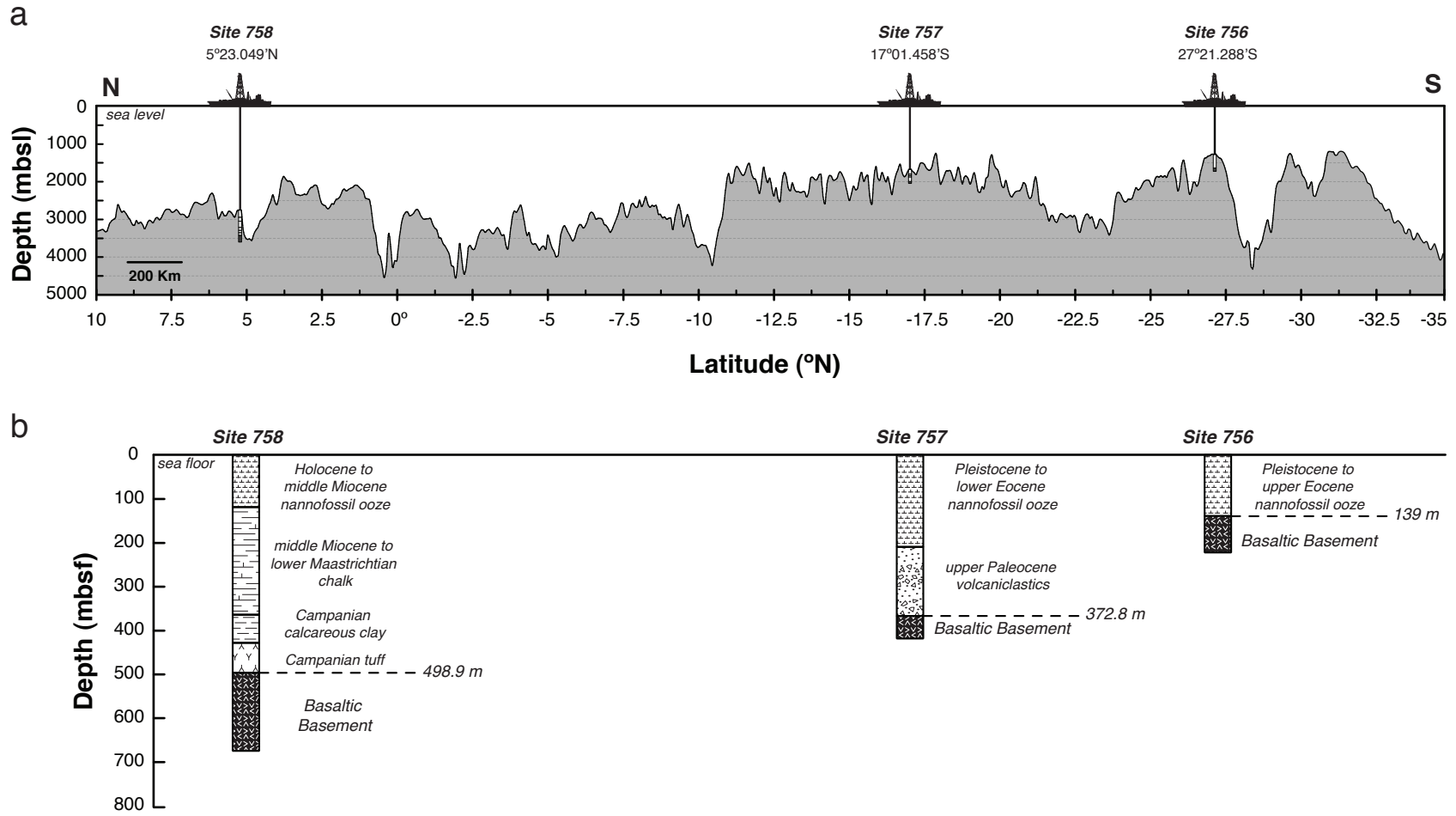
Figure 4.2. (a) Topographic profile along the Ninetyeast Ridge (north–south). Vertical exaggeration = 171x. Profile drawn using GeoMapApp: http://www.geomapapp.org. (b) Schematic summary of the core stratigraphy with depth (in meters below sea floor – mbsf) at Sites 758, 757, and 756 drilled during ODP Leg 121 [*Shipboard Scientific Party*, 1989].

topographic rise with a radius of ~150 km (Osborn Knoll) stands out to the west of the ridge. This structure is believed to be the result of seafloor spreading [*Krishna et al.*, 1995].

Along its length, the ridge can be divided into distinct morphological segments that reflect its emplacement within the complex tectonic evolution of the Indian Ocean basin [*Royer et al.*, 1991; *Krishna et al.*, 1995, 1999] and the tectonic forces that the ridge has been subjected to [e.g., *Subrahmanyam et al.*, 2008]. North of 2.5˚S, the ridge is formed by a wide series of en echelon blocks separated by areas of abyssal seafloor (Figure 4.1), and is interpreted to have been generated by intraplate volcanism on the Indian plate [*Royer et al.*, 1991]. From 2.5˚S to 15˚S, the ridge becomes narrow, linear and continuous (Figure 4.1), reflecting its emplacement at the transform boundary between the Antarctic (or a short-lived microplate) and Australian plates [*Royer et al.*, 1991]. South of ~15˚S, the ridge again becomes wider, comprised by a slightly less linear succession of shallow volcanic edifices (Figure 4.1), interpreted to have been emplaced near the edge of the Indian plate [*Royer et al.*, 1991]. In addition to these three segments, *Krishna et al.* [1999] considered another segment, from 11˚S to 17˚S, which, based on the paleomagnetic anomalies and continuity of the ridge at those latitudes, they interpreted as resulting from on-axis volcanism.

The Ninetyeast Ridge separates two distinct domains of the Indian Ocean basin (Figure 4.1): the Central Indian Basin to the west, where seafloor ages decrease from north to south, and the Wharton Basin to the east, where seafloor ages decrease from south to north [*Duncan*, 1978; *Royer et al.*, 1991]. Paleomagnetic, paleontological and radiometric studies on samples recovered during DSDP and ODP cruises, indicate that the Ninetyeast Ridge formed at paleolatitudes near 50˚S (drill Sites 217 to 757) and 43˚S (drill Site 756) [*Klootwijk et al.*, 1991], and that the basement rocks become systematically older in a northward direction, from ~38 Ma at DSDP Site 254 (~30.97˚S) to ~82 Ma at ODP Site 758 (~5.38˚S) [*Duncan*, 1978; 1991; *Royer et al.,* 1991]. These ages are roughly contemporaneous with those of the adjacent Central Indian basin seafloor, indicating emplacement on very young oceanic crust at/or close to a spreading centre [*Royer et al.*, 1991]. The slight obliquity of the Ninetyeast Ridge relative to the fracture zone pattern of the

Indian Basin suggests that the location of the ridge was not controlled primarily by the location of the fracture zones [*Royer et al.*, 1991].

4.4. Previous Petrologic and Geochemical Results

Petrologic studies on the samples recovered during DSDP and ODP cruises indicate that most of the Ninetyeast Ridge basement rocks consist of enriched tholeiitic basalts and few intermediate differentiated rocks (oceanic andesites at Site 214), affected by variable degrees of post-magmatic, low-temperature alteration [e.g., *Thompson et al.*, 1974; *Frey and Sung*, 1974; *Frey et al.*, 1991; *Saunders et al.*, 1991; *Frey and Weis*, 1995]. The effects of late-stage alteration, arising from alkali mobility are strongly reflected on the anomalously high total alkali (Na_2O+K_2O) content of some ODP Site 757 and 756 samples, as well as on their trace element abundances (Figures 4.3 and 4.4). Although these samples lie in the alkalic field in Figure 4.3, they are in fact altered tholeiitic basalts (see *Frey et al.* [1991] for more detailed discussion). The trachytic groundmass texture of some Ninetyeast Ridge lavas (DSDP sites) suggests they reached thermal and chemical equilibrium in relatively shallow magma chambers [*Thompson et al.*, 1974; *Ludden et al.*, 1980]. The high abundance of vesicles and cavities in most Ninetyeast Ridge basalts is consistent with eruption in a subaerial environment or at shallow water depths. The exception is Site 758, where all samples are pillow and massive basalts with quenched textures, denoting a submarine eruption environment [*Shipboard Scientific Party*, 1989; *Frey et al.*, 1991; *Saunders et al.*, 1991]. Although all basalts recovered from the Ninetyeast Ridge basement have been moderately to highly altered (H_2O^+ contents typically > 1 wt%) in a low-temperature environment under both reducing and oxidizing conditions, many of their geochemical characteristics reflect the original magma compositions [*Thompson et al.*, 1974; *Frey et al.*, 1991; *Saunders et al.*, 1991]. Trace element and isotope compositions of the Ninetyeast Ridge basalts are intermediate between Indian MORB and Indian Ocean island basalts (Kerguelen Archipelago, at ~55˚S, Amsterdam and St. Paul islands, at ~38˚S) [e.g., *Hekinian*, 1974; *Frey and Sung*, 1974; *Frey et al.*, 1991; *Saunders et al.*, 1991; *Weis and Frey*, 1991; *Weis et al.*, 1992; *Frey and Weis*, 1995]. Together with the large volumes of
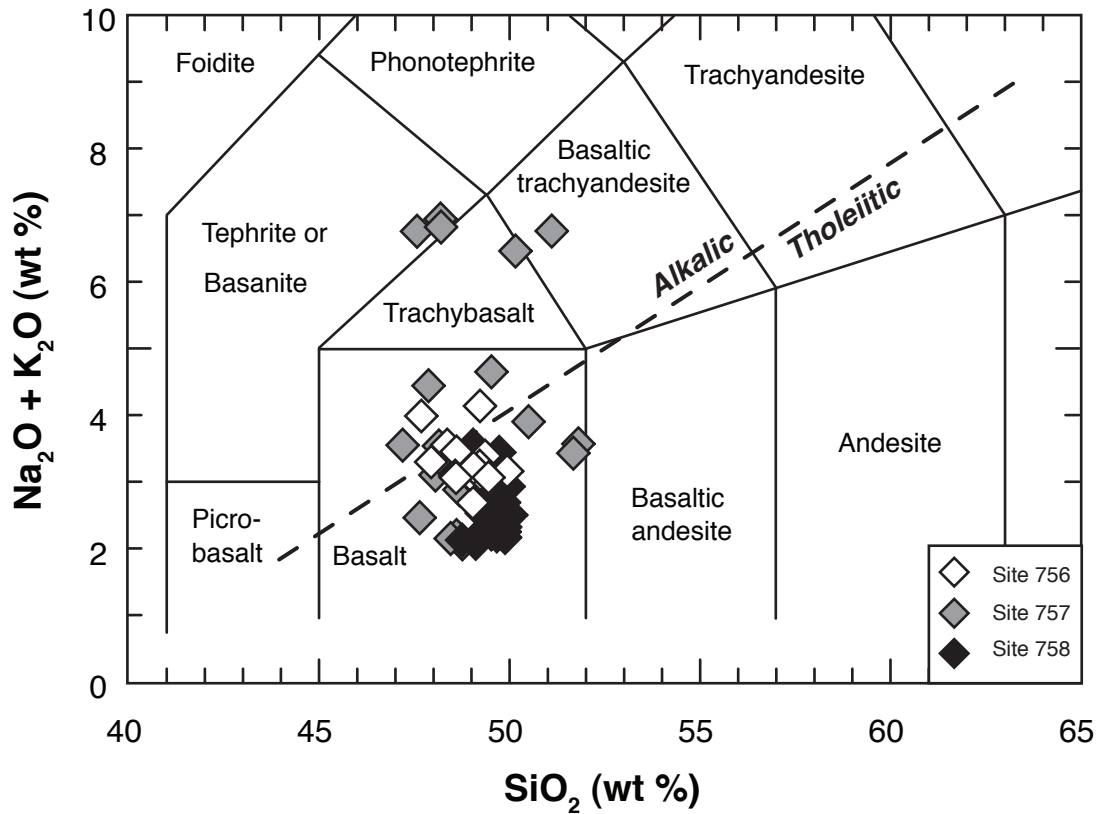
Figure 4.3. Total alkalis versus silica diagram (after *LeBas et al.* [1986]) showing the compositional range of the Ninetyeast Ridge basalts recovered during ODP Leg 121 at Sites 758, 757, and 756 [*Frey et al.*, 1991]. The tholeiitic-alkalic dividing line is from Macdonald and Katsura (1964). The distinctly higher alkali content of some samples reflects K_2O enrichment during postmagmatic alteration and not the true magmatic values of the basalts (see text and discussion of *Frey et al.* [1991] for details).

magma involved in the genesis of the Ninetyeast Ridge ($\sim$27 x 10^6 km^3, *Schubert and Sandwell* [1989]), these characteristics are consistent with derivation from enhanced magmatism of enriched composition, such as that associated with a mantle plume source [e.g., *Thompson et al.*, 1974; *Ludden et al.*, 1980; *Frey et al.*, 1991; *Weis and Frey*, 1991; *Saunders et al.*, 1991; *Frey and Weis*, 1995; 1996].

4.5. Samples and Methods

4.5.1. Samples

Thirty-eight samples of tholeiitic basalts from the Ninetyeast Ridge recovered during ODP Leg 121, previously analyzed and reported by *Weis and Frey* [1991], were analyzed. These samples encompass basalts representative of the different flow units from ODP drill Sites 756 (n=10), 757 (n=12) and 758 (n=16), and they cover a sampling distance of $\sim$3630 km along the ridge. Each drill site is located on different segments/sections of the ridge (Figure 4.1) and at each site basement was found at different depths (meters below sea floor (mbsf)) reflecting the increasing sediment cover with increasing basement age (Figure 4.2). At Site 758 ($\sim$5.23°N, $\sim$82 Ma) this site, in hole 758A, 178 meters were drilled through basaltic flows, which were first encountered 498.9 mbsf. Twenty-nine flow units were identified; the 16 samples here analyzed are from 14 of those units. At Site 757 ($\sim$17.01°S, $\sim$58 Ma), in hole 757C, basement was encountered 372.8 mbsf and 52 meters of basaltic flows were drilled. Nineteen flow units were identified and the 12 samples here analyzed are from nine of those units. At Site 756 ($\sim$27.35°S, $\sim$43 Ma), in hole 756C, 8.7 meters were drilled through basaltic basement, which was first encountered at 150.2 mbsf. In hole 756D, basement was first encountered 139 mbsf, and 82 meters of basaltic flows were drilled. Two and 14 flow units were identified for each hole, respectively. The 10 samples here analyzed are from nine of those units. A summary of the pertinent geochemical characteristics of these samples is presented in Tables 4.1 and 4.2. Detailed petrographic descriptions can be found in *Frey et al.* [1991] and their previously analyzed Pb, Sr and Nd isotopic compositions in *Weis and Frey* [1991].

Table 4.1. Summary of the Geochemical Characteristics of the Ninetyeast Ridge Basalts Sampled During ODP Leg 121

Sample ID [Core, section, interval (cm)]	Flow Unit[a]	Depth within core (mbsf)	Eruption Environment	Age[b] (Ma)	SiO_2 (wt%)	MgO (wt%)	FeO_t (wt%)	Na_2O (wt%)	K_2O (wt%)	Mg#[c]	A.I.[d]	Vol.[e] (wt%)	Zr/Nb	Zr/Y	La/Yb
Site 756 (27°21.253'S; 27°21.288'S)															
121-756C-10N-1, 32-36*	F1	150.62	subaerial	43	49.24	6.28	11.29	2.79	0.49	0.36	-0.51	1.65	13.33	4.95	3.41
121-756D-4R-1, 35-39	F1	139.35	subaerial	43	47.68	4.89	13.12	3.10	0.91	0.27	0.80	1.65	13.11	5.22	2.95
121-756D-4R-1, 85-89*	F2	139.85	subaerial	43	47.94	5.53	13.47	2.80	0.51	0.29	0.00	2.20	13.17	5.37	2.99
121-756D-6R-1, 6-10*	F4	158.36	subaerial	43	48.60	5.30	12.91	2.82	0.64	0.29	-0.09	3.17	12.57	5.38	3.48
121-756D-6R-2, 9-13*	F5	159.89	subaerial	43	49.05	6.80	11.16	2.73	0.49	0.38	-0.50	2.68	13.09	4.54	3.19
121-756D-6R-2, 13-17*	F5	159.93	subaerial	43	48.57	6.92	11.08	2.87	0.23	0.38	-0.44	2.45	12.89	4.25	3.01
121-756D-7R-1, 100-104	F6	169.00	subaerial	43	49.22	6.43	9.92	3.75	0.41	0.39	0.38	2.63	12.46	5.73	3.53
121-756D-8R-1, 20-23	F7	177.90	subaerial	43	49.44	6.69	11.26	2.54	0.53	0.37	-0.79	4.12	10.50	4.86	3.84
121-756D-10R-1, 99-103	F12	197.99	subaerial	43	49.93	6.71	10.41	2.65	0.52	0.39	-0.88	3.10	12.80	4.58	3.09
121-756D-12R-3, 139-143	F14	220.19	subaerial	43	49.21	7.11	10.89	3.00	0.25	0.40	-0.53	1.97	13.22	4.22	2.79
Site 757 (17°01.389'S)															
121-757C-9R-1, 105-109*	F2	383.05	subaerial	58	48.76	5.88	6.14	1.93	0.14	0.49	-1.54	2.38	14.29	3.84	2.96
121-757C-9R-5, 34-38	F4	387.11	subaerial	58	48.14	4.76	6.17	2.54	1.00	0.44	0.16	4.05	13.14	4.74	3.37
121-757C-9R-6, 102-105	F5	388.62	subaerial	58	48.05	5.60	6.06	1.98	1.12	0.48	-0.25	3.62	16.25	4.77	3.34
121-757C-9R-7, 78-82	F5	389.5	subaerial	58	47.64	5.14	7.32	1.82	0.64	0.41	-0.74	2.58	18.08	4.02	2.95
121-757C-9R-8, 54-59	F5	390.64	subaerial	58	48.68	5.97	6.18	1.89	0.99	0.49	-0.70	2.92	13.24	4.71	2.80
121-757C-10R-1, 86-90	F6	392.56	subaerial	58	48.15	5.18	5.34	2.20	1.16	0.49	-0.03	5.70	14.17	3.95	2.83
121-757C-10R-3, 2-6	F8	394.56	subaerial	58	48.20	5.28	5.25	5.15	1.67	0.50	3.42	7.69	12.50	2.70	3.16
121-757C-11R-2, 10-14	F12	402.95	subaerial	58	49.52	6.94	7.50	3.03	1.62	0.48	0.76	7.90	12.67	4.13	3.15
121-757C-11R-2, 51-56	F13	403.36	subaerial	58	50.15	5.88	8.04	4.48	1.98	0.42	2.33	7.15	14.75	5.00	3.09
121-757C-12R-1, 100-104*	F18	412.10	subaerial	58	51.80	5.18	6.85	2.80	0.77	0.43	-1.17	2.57	17.05	5.51	3.61
121-757C-12R-2, 0-5	F18	412.45	subaerial	58	50.49	5.38	8.85	2.62	1.28	0.38	-0.35	2.02	16.88	5.34	3.28
121-757C-12R-4, 24-29	F19	415.30	subaerial	58	51.10	5.28	8.01	4.63	2.13	0.40	2.28	5.13	17.01	6.32	4.09
Site 758 (5°23.049'N)															
121-758A-55R-5, 82-86	F1	505.42	submarine	82	49.52	7.96	9.49	2.14	0.08	0.46	-1.67	2.06	17.78	2.68	1.42
121-758A-56R-1, 64-68	F1	509.04	submarine	82	49.49	8.18	9.68	2.37	0.12	0.46	-1.40	2.39	18.39	3.33	1.45
121-758A-58R-6, 21-25*	F2	534.42	submarine	82	49.97	8.08	14.65	2.78	0.15	0.36	-1.13	4.48	15.59	3.35	1.79
121-758A-59R-2, 58-62*	F2	538.49	submarine	82	49.61	8.39	11.27	2.36	0.14	0.43	-1.43	3.29	15.44	2.97	1.66
121-758A-60R-1, 122-126	F3	547.12	submarine	82	49.85	9.00	11.81	2.60	0.09	0.43	-1.33	3.82	14.81	3.42	2.11
121-758A-62R-1, 130-134	F4	565.60	submarine	82	48.75	8.15	7.38	2.01	0.11	0.52	-1.48	3.18	14.71	3.47	1.90
121-758A-62R-3, 80-84	F5	568.01	submarine	82	49.35	9.43	10.98	2.89	0.17	0.46	-0.77	5.38	16.48	3.55	2.37
121-758A-65R-1, 51-55	F10	593.21	submarine	82	49.81	9.11	10.36	2.81	0.10	0.47	-1.09	5.76	15.18	4.40	2.27
121-758A-67R-4, 31-35	F14	616.25	submarine	82	49.88	9.51	10.76	2.47	0.07	0.47	-1.49	5.12	15.69	3.96	1.91
121-758A-69R-3, 53-57	F17	633.39	submarine	82	49.11	9.60	10.14	1.97	0.11	0.49	-1.67	4.35	17.22	2.78	1.77
121-758A-70R-1, 71-75	F18	640.11	submarine	82	49.27	9.60	10.07	2.82	0.09	0.49	-0.89	6.15	15.00	4.24	2.23
121-758A-70R-2, 129-133	F19	642.19	submarine	82	49.49	10.21	10.02	2.36	0.08	0.50	-1.44	6.16	13.08	3.58	2.02
121-758A-71R-1, 127-131	F20	649.87	submarine	82	49.64	9.57	9.67	2.50	0.13	0.50	-1.31	5.24	16.19	3.82	2.06
121-758A-71R-3, 64-68	F22	652.20	submarine	82	49.88	9.26	9.95	2.12	0.05	0.48	-1.86	4.15	15.00	3.32	1.75
121-758A-73R-1, 82-86	F27	668.42	submarine	82	49.90	8.94	9.67	2.13	0.06	0.48	-1.85	5.02	-	-	1.61
121-758A-73R-4, 105-109	F29	673.08	submarine	82	49.74	8.92	10.78	2.24	0.11	0.45	-1.63	3.92	-	-	7.45

[a]Defined on-board on the basis of macroscopic and thin-section criteria [*Peirce et al.*, 1989].

[b]Average $^{40}Ar/^{39}Ar$ ages for each site [*Duncan*, 1991].

[c]Mg# is molar $Mg/(Mg + Fe^{2+})$.

[d]A.I. is Alkalinity Index [= (total alkali - 0.37*SiO2 + 14.43)] and represents a measure of the deviation of a sample from the alkalic-tholeiitc boundary defined by *MacDonald and Katsura* [1964]. Positive values are most probably due to the high alteration degree of those samples and do not reflect the basalt type. See *Frey et al.* [1991] for details and discussion.

[e]Vol. = Sum of volatiles (H_2O^+, H_2O^-, CO_2).

*samples for which the U content is too low and was recalculated based on a model Th/U = 4 prior to calculation of the initial Pb ratios (see text for details).

Major and trace element geochemical data is from *Frey et al.* [1991].

Table 4.2. Parent-Daughter Concentrations and Ratios of the Ninetyeast Ridge Basalts Sampled During ODP Leg 121

Sample ID [Core, section, interval (cm)]	Flow Unit [a]	Th (ppm)	U (ppm)	Pb (ppm)	Th/U	Rb (ppm)	Sr (ppm)	Rb/Sr	Sm (ppm)	Nd (ppm)	Sm/Nd	Lu (ppm)	Hf (ppm)	Lu/Hf
Site 756 (27°21.253'S; 27°21.288'S)														
121-756C-10N-1, 32-36*	F1	1.26	0.10	0.59	12.6	6.50	188	0.03	4.66	17.20	0.27	0.39	3.69	0.11
121-756D-4R-1, 35-39	F1	1.17	-	-	-	10.0	195	0.05	4.81	16.90	0.28	0.48	4.18	0.11
121-756D-4R-1, 85-89*	F2	1.33	0.10	0.56	13.3	15.0	181	0.08	5.10	16.80	0.30	0.46	4.08	0.11
121-756D-6R-1, 6-10*	F4	1.70	0.08	0.40	21.3	19.0	166	0.11	5.40	18.70	0.29	0.46	4.23	0.11
121-756D-6R-2, 9-13*	F5	0.71	0.09	0.41	7.9	33.0	171	0.19	3.97	12.90	0.31	0.37	2.98	0.12
121-756D-6R-2, 13-17*	F5	0.70	0.09	0.37	7.8	1.10	174	0.01	4.18	14.00	0.30	0.42	3.12	0.13
121-756D-7R-1, 100-104	F6	1.01	0.38	0.80	2.7	2.90	200	0.01	4.67	16.80	0.28	0.44	3.83	0.11
121-756D-8R-1, 20-23	F7	0.75	0.22	0.93	3.4	13.0	153	0.08	3.93	14.50	0.27	0.38	2.98	0.13
121-756D-10R-1, 99-103	F12	0.66	0.24	0.86	2.8	16.0	156	0.10	3.89	13.50	0.29	0.34	2.96	0.11
121-756D-12R-3, 139-143	F14	0.68	0.17	0.79	4.0	1.90	163	0.01	4.17	13.40	0.31	0.40	2.91	0.14
Site 757 (17°01.389'S)														
121-757C-9R-1, 105-109*	F2	0.33	0.07	0.14	4.7	1.40	176	0.01	1.57	5.70	0.28	0.18	1.14	0.16
121-757C-9R-5, 34-38	F4	0.24	0.13	0.37	1.8	11.0	313	0.04	1.35	5.20	0.26	0.15	0.98	0.15
121-757C-9R-6, 102-105	F5	0.28	0.16	0.53	1.8	35.0	215	0.16	1.70	4.60	0.37	0.17	1.07	0.16
121-757C-9R-7, 78-82	F5	0.43	0.15	0.38	2.9	18.0	181	0.10	1.50	5.30	0.28	0.19	1.12	0.17
121-757C-9R-8, 54-59	F5	0.24	0.11	0.34	2.2	22.0	184	0.12	1.44	5.10	0.28	0.17	1.14	0.15
121-757C-10R-1, 86-90	F6	0.09	0.11	0.28	0.8	17.0	247	0.07	1.07	4.00	0.27	0.14	0.71	0.20
121-757C-10R-3, 2-6	F8	0.25	0.13	0.29	1.9	17.0	559	0.03	1.60	5.90	0.27	0.18	0.85	0.21
121-757C-11R-2, 10-14	F12	0.35	0.19	0.49	1.8	19.0	324	0.06	1.82	6.10	0.30	0.21	1.35	0.16
121-757C-11R-2, 51-56	F13	0.34	0.18	0.46	1.9	20.0	292	0.07	1.67	6.00	0.28	0.19	1.41	0.13
121-757C-12R-1, 100-104*	F18	1.53	0.30	0.37	5.1	7.80	164	0.05	3.77	14.40	0.26	0.46	3.67	0.13
121-757C-12R-2, 0-5	F18	1.48	0.45	0.79	3.3	20.0	160	0.13	3.70	14.30	0.26	0.51	3.45	0.15
121-757C-12R-4, 24-29	F19	1.89	0.47	1.35	4.0	14.0	150	0.09	4.30	16.00	0.27	0.48	4.52	0.11
Site 758 (5°23.049'N)														
121-758A-55R-5, 82-86	F1	0.17	0.07	0.13	2.4	0.40	122	0.00	1.79	5.00	0.36	0.28	1.24	0.23
121-758A-56R-1, 64-68	F1	0.23	0.08	0.21	2.9	1.40	127	0.01	1.90	5.30	0.36	0.28	1.40	0.20
121-758A-58R-6, 21-25*	F2	0.73	0.09	0.97	8.1	1.10	143	0.01	4.22	14.20	0.30	0.60	3.03	0.20
121-758A-59R-2, 58-62*	F2	0.26	0.04	0.20	6.5	2.20	127	0.02	2.44	7.66	0.32	0.36	1.77	0.20
121-758A-60R-1, 122-126	F3	0.43	0.14	0.32	3.1	0.60	131	0.00	2.55	9.00	0.28	0.35	1.72	0.20
121-758A-62R-1, 130-134	F4	0.23	0.08	0.56	2.9	0.90	139	0.01	1.66	5.50	0.30	0.23	1.25	0.18
121-758A-62R-3, 80-84	F5	0.27	0.20	0.51	1.4	0.70	157	0.00	3.40	10.90	0.31	0.37	2.31	0.16
121-758A-65R-1, 51-55	F10	0.33	0.12	0.30	2.8	0.40	157	0.00	2.61	9.00	0.29	0.27	2.18	0.12
121-758A-67R-4, 31-35	F14	0.19	0.13	0.75	1.5	0.20	144	0.00	2.74	10.40	0.26	0.37	2.40	0.15
121-758A-69R-3, 53-57	F17	0.28	0.10	0.21	2.8	0.70	114	0.01	2.40	8.30	0.29	0.33	1.49	0.22
121-758A-70R-1, 71-75	F18	0.22	0.12	0.41	1.8	0.10	140	0.00	2.33	8.30	0.28	0.31	1.83	0.17
121-758A-70R-2, 129-133	F19	0.25	0.12	0.33	2.1	0.50	125	0.00	2.20	7.80	0.28	0.28	1.68	0.17
121-758A-71R-1, 127-131	F20	0.27	0.11	0.30	2.5	0.80	130	0.01	2.10	7.90	0.27	0.27	1.56	0.17
121-758A-71R-3, 64-68	F22	0.33	0.11	0.37	3.0	0.10	122	0.00	2.30	7.30	0.32	0.32	1.74	0.18
121-758A-73R-1, 82-86	F27	0.41	0.11	0.43	3.7	0.00	121	0.00	2.30	7.00	0.33	0.37	1.81	0.20
121-758A-73R-4, 105-109	F29	0.26	0.11	1.46	2.4	1.50	113	0.01	2.50	8.30	0.30	0.36	1.74	0.21

[a]Defined on-board on the basis of macroscopic and thin-section criteria [*Peirce et al.*, 1989].

*samples for which the U content is too low and was recalculated based on a model Th/U = 4 prior to calculation of the initial Pb ratios (see text for details).

Trace element data is from *Frey et al.* [1991].
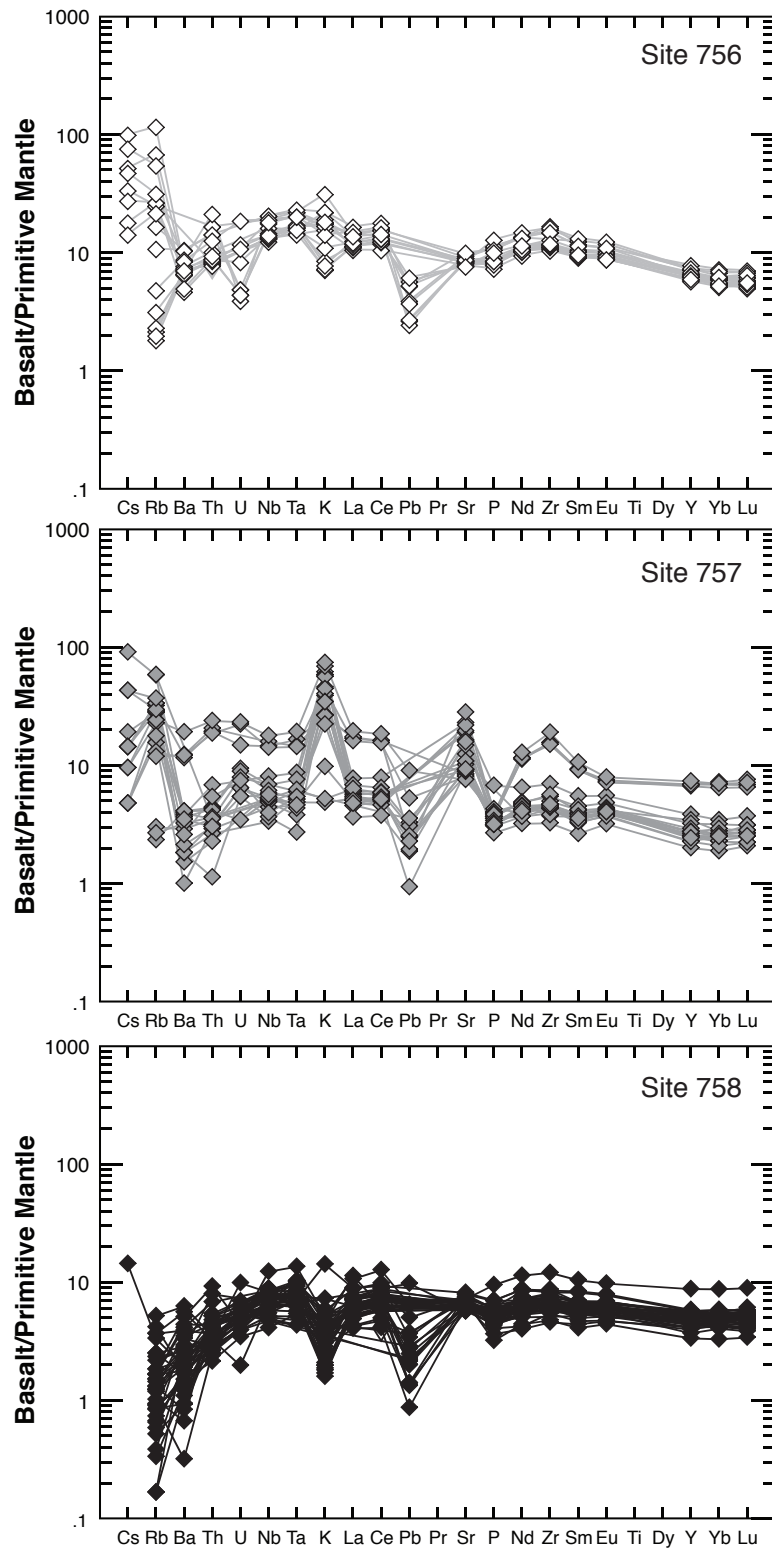
Figure 4.4. Extended primitive mantle-normalized incompatible trace element abundances of the Ninetyeast Ridge basalts collected during ODP Leg 121. Data is from *Frey et al.* [1991]. Normalizing values are from *McDonough and Sun* [1995].

4.5.1.1. Summary of Alteration Features and Secondary Mineralogy of Samples

The majority of the basalts recovered at Site 756 are aphyric to sparsely plagioclase-phyric, and all have undergone some extent of alteration that led to the pervasive replacement of groundmass by clay minerals and infilling of many of the vesicles (summarized from *Shipboard Scientific Party* [1989]). The alteration degree is moderate, ranging between 20 and 40% volume of alteration phases. Plagioclase phenocrysts are commonly slightly altered to a pale green clay mineral and the rare olivine phenocrysts are completely replaced by green smectite-vermiculite or red iddingsite. In the groundmass, olive is altered to iddingsite, smectite and vermiculite. Two styles of alteration are found in these basalts [*Shipboard Scientific Party*, 1989; *Frey et al.*, 1991; *Saunders et al.*, 1991]. The earlier alteration mineral assemblage is bluish to greenish grey in colour and is mainly constituted by saponitic smectites. This non-oxidative alteration resulted in the loss of K and Rb from the bulk rock, which is characteristic of subaerial alteration of basalt and submarine alteration at >150°C. The later, oxidative, alteration mineral assemblage is brown to orange grey in colour and is constituted by calcite, saponite-glauconite and Fe-Mn oxides, which typically affects the uppermost basalts of the oceanic crust. Zeolite minerals are not found in basalts from Site 756.

All basalts recovered at Site 757 are moderately (~20 vol%) to highly (40-50 vol%) plagioclase-phyric, vesicular basalts [*Shipboard Scientific Party*, 1989]. The plagioclase phenocrysts are typically zoned. Alteration to potassium feldspar in several samples reflects addition of K during postmagmatic alteration. Other phenocryst phases include clinopyroxene and olivine, the latter being completely replaced by green smectite with chlorite and iddingsite. The degree of alteration of these basalts varies from moderate to high (up to 80%), which resulted in pervasive replacement of the groundmass by green or brown smectites/chlorites, and Fe-oxides/hydroxides. Veins, cavities and vesicles are filled by calcite, smectites, Fe-oxides/hydroxides, opal or chalcedony, and zeolites (natrolite and analcite), which are more abundant in the lower flow units [*Shipboard Scientific Party*, 1989; *Frey et al.*, 1991]. The presence of zeolite minerals and chalcedony is indicative of

hydrothermal alteration of these basalts. The occurrence of oxidative alteration, as observed in Site 756 basalts, is restricted to the uppermost flow units.

Basalts from Site 758 are predominantly aphyric to sparcely plagioclase-phyric, and all are highly altered [*Shipboard Scientific Party*, 1989; *Frey et al.*, 1991; *Saunders et al.*, 1991]. The groundmass is pervasively replaced by brown and green chlorite-smectites, whereas the phenocrysts, when present, are only slightly affected. Black, brown and green smectites, chlorite-smectites, calcite, quartz and ankerite are part of the mineral assemblage filling the vesicles and fractures. In contrast to the basalts from the previous sites, late stage oxidative alteration is not evident in the Site 758 basalts.

4.5.2. Analytical Techniques

Whole-rock powders of ODP Leg 121 basalts were analyzed for Pb, Hf, Sr, and Nd isotopic compositions at the Pacific Centre for Isotopic and Geochemical Research (PCIGR) at the University of British Columbia. To remove the alteration phases and obtain reproducible Pb isotopic compositions of oceanic basalts [e.g., *Hanano et al.*, 2009], all sample powders were thoroughly acid-leached with 6 M HCl prior to digestion and isotopic analysis, following the sequential acid leaching procedure described in *Weis et al.* [2005] and in *Nobre Silva et al.* [2009; 2010]. The leached sample powders were digested in a mixture of concentrated sub-boiled HF and HNO_3 acids in sealed Teflon® vessels and then processed through a sequence of chromatographic ion-exchange columns for Pb, Sr, Nd and Hf purification. For all samples, the Pb, Sr, Nd and Hf isotopic compositions were determined on a single dissolution of each sample, using methods similar to those described by *Weis et al.* [2006; 2007] and the results are reported in Tables 4.4 and 4.5.

Pb and Hf isotopic compositions were determined on a Nu Plasma (Nu Instruments Ltd, UK) multiple collector inductively coupled plasma mass spectrometer (MC-ICP-MS), under dry plasma conditions using a membrane desolvator (Nu DSN100) for sample introduction [*Weis et al.,* 2006; 2007]. All analyses were obtained in static multi-collection mode, with interference corrections for ^{204}Hg on ^{204}Pb, ^{176}Lu and ^{176}Yb on ^{176}Hf, and ^{174}Yb

on ^{174}Hf. All sample and standard solutions were prepared fresh for each analytical session and sample analysis followed a modified sample-standard bracketing procedure in which the standard solution (NIST SRM 981 for the Pb analyses, JMC 475 for the Hf analyses) was run after every two samples, to monitor for any systematic in-run drift of the standard value.

Pb isotopic ratios were corrected online for instrumental mass fractionation using a Specpure® Tl standard solution with a ^{205}Tl/^{203}Tl = 2.3885. All Pb sample solutions were analyzed with similar [Pb]/[Tl] ($\approx$4) as the SRM 981 Pb standard solution, to ensure that sample and standard solutions were matrix-matched with respect to Tl. To accomplish this, the Pb content of a small aliquot of each solution was determined by HR-ICP-MS, on an ELEMENT2 (Thermo Finnigan, Germany) prior to isotopic analysis. Samples were run with an optimal ^{208}Pb ion beam of 8V and no less than 2V, to limit the significance of the ^{204}Hg interference on ^{204}Pb and ensure a better analytical precision altogether. The fractionation-corrected Pb isotopic ratios were then normalized off-line to the SRM 981 triple-spike values (^{206}Pb/^{204}Pb = 16.9405 ± 15, ^{207}Pb/^{204}Pb = 15.4963 ± 16, and ^{208}Pb/^{204}Pb = 36.7219 ± 44; *Abouchami et al.*, [2000]), using the ln-ln method as described in *White et al.* [2000] and *Albarède et al.* [2004]. During the period of analysis, the SRM 981 Pb standard yielded mean values ± 2SD of ^{206}Pb/^{204}Pb = 16.9414 ± 0.0067, ^{207}Pb/^{204}Pb = 15.4962 ± 0.0032, and ^{208}Pb/^{204}Pb = 36.7121 ± 0.0104 (n = 30), which are within 2SD of the triple spike values [*Abouchami et al.*, 2000].

Hf isotopic ratios were corrected for instrumental mass fractionation by exponentially normalizing to ^{179}Hf/^{177}Hf = 0.7325 [*Patchett and Tatsumoto*, 1984]. The sample results were then normalized to the ^{176}Hf/^{177}Hf value of 0.282160 of *Vervoort and Blichert-Toft* [1999] using the daily average of the JMC 475 Hf standard. The JMC 475 Hf standard analyzed over the period of analysis gave an average value of ^{176}Hf/^{177}Hf = 0.282161 ± 0.000010 (n = 112).

Two new Hawaiian rock samples used as in-house reference materials, Kil-93 and Ko'olau, collected and made available by Marc Norman (ANU), were processed together

with the sample set. Kil-93 is a quenched sample from the Pu'u O'o 10 May 1993 eruption. ICP-MS trace element concentrations for this sample have been determined by *Eggins et al.* [1997] and major element compositions have been reported by *Garcia et al.* [2000]. Ko'olau is a tholeiitic basalt from a flow near the base of the Makapu'u section on Oahu. Although no geochemical data has been published for this sample, it should be comparable to flows 1, 2, 3 of *Frey et al.* [1994]. In Table 3 we report the first Pb, Sr, Nd, Hf isotopic compositions for these samples. These values are in good agreement with the values acquired over three years at the PCIGR for these samples (Table 4.3).

All Sr and Nd isotopic ratios were measured on a TRITON (Thermo Finnigan) thermal ionization mass spectrometer (TIMS) in static mode with relay matrix rotation on single Ta (Sr) or double Re-Ta (Nd) filaments, respectively. Sr and Nd isotopic compositions were corrected for mass fractionation using $^{86}Sr/^{86}Sr = 0.1194$ and $^{146}Nd/^{144}Nd = 0.7219$ using an exponential law. The data was then normalized using the average of the corresponding standard (NIST SRM 987 for Sr and La Jolla for Nd) in the barrel, relative to the values of $^{87}Sr/^{86}Sr = 0.710248$ and $^{143}Nd/^{144}Nd = 0.511858$ [*Weis et al.*, 2006]. During the course of these analyses, the average value of the SRM 987 Sr standard was 0.710249 ± 0.000015 (n = 23) and the La Jolla Nd standard was 0.511851 ± 0.000003 (n = 28).

For more accurate comparison between our data and the literature isotopic data shown and discussed here, all literature data have been renormalized to the respective accepted standard values used in this study [*Vervoort and Blichert-Toft*, 1999; *Abouchami et al.*, 2000; *Weis et al.*, 2006].

4.5.3. Age-Correction of the Isotopic Ratios of the Ninetyeast Ridge Samples

To account for in-situ decay of ^{87}Rb, ^{147}Sm, ^{176}Lu, $^{238-235}U$ and ^{232}Th since crystallization, age corrections were applied to the measured (present-day) Sr, Nd, Hf, and Pb isotopic ratios from Sites 756 (43 Ma), 757 (58 Ma) and 758 (82 Ma) (ages from *Duncan* [1991]). For Rb, Sm and Lu, we consider the elemental abundances measured on unleached

Table 4.3. Pb-Sr-Nd-Hf Isotopic Compositions by MC-ICP-MS and TIMS of Hawaiian Basalt Reference Materials Analyzed in this Study

Reference Materials	Acid Leaching Steps	% Weight Loss	^{206}Pb/^{204}Pb	Error (2SE)	^{207}Pb/^{204}Pb	Error (2SE)	^{208}Pb/^{204}Pb	Error (2SE)	^{87}Sr/^{86}Sr	Error (2σ)	^{143}Nd/^{144}Nd	Error (2σ)	^{176}Hf/^{177}Hf	Error (2SE)
Kil-93	10	42.06	18.4107	0.0011	15.4749	0.0010	38.0712	0.0029	0.703590	8	0.512976	6	0.283108	5
Ko'olau	5	53.98	17.8396	0.0007	15.4364	0.0006	37.7458	0.0018	0.704103	8	0.512759	6	0.282961	4
Ko'olau dup.	9	41.12	17.8413	0.0008	15.4384	0.0008	37.7517	0.0022	0.704082	8	–	–	0.282953	5
Average Isotopic Compositions and 2SD Over Three Years (2007 - 2010) at the PCIGR														
Kil-93 (n = 10)	10	35.32	18.4083	0.0050	15.4737	0.0036	38.0667	0.0094	0.703589	15	0.512975	20	0.283104	7
Ko'olau (n = 6)	10	50.35	17.8405	0.0058	15.4364	0.0028	37.7451	0.0096	0.704101	22	0.512758	9	0.282959	19

powders to be more representative of the primary elemental concentrations than those measured on leached samples [*Nobre Silva et al.*, 2010]. For the Rb-Sr, Sm-Nd and Lu-Hf isotope systems, the elemental abundances measured on the unleached powders [*Frey et al.*, 1991] were used for the age-correction calculations, as the parent:daughter concentration ratios for these samples are typical of values expected for ocean island basalts.

The U, Th, and Pb elemental concentrations in the Ninetyeast Ridge basalts have been disturbed by the extensive post-eruptive alteration [e.g., *Frey et al.*, 1991; *Saunders et al.*, 1991]. The measured ratios of some samples are very high (up to 21.3, see Tables 4.1 and 4.2), and most likely result from U loss during hydrothermal alteration, as other trace element ratios not involving U are less affected (Figure 4.5). For this reason, age-correction of Pb isotope ratios using the U abundances from unleached sample powders of these samples is likely to be unreliable. This assumption is supported by the tight linear trends of measured ^{208}Pb/^{206}Pb for basalts from each site (Figure 4.6a and 4.6b), which become widely dispersed after correction to initial ^{208}Pb/^{206}Pb values (Figure 4.6c and 4.6d). For the samples exhibiting high Th/U (samples indicated by * in Tables 4.1, 4.2 and 4.4, and surrounded by dashed field in Figures 4.5c, 4.5d, 4.6c and 4.6d), we estimated U abundances assuming that Th/U = 4, based on the Kerguelen and ocean island basalts average values for this elemental ratio [*O'Nions and McKenzie*, 1993; *Weis et al.*, 1998; *Doucet et al.*, 2002]. The subsequent age-corrected Pb isotopic data is more coherent, as outlying samples now plot within the main trends of each site (Figures 4.6e and 4.6f). Previous studies where age-corrections were made using the measured U concentrations showed age progressions in initial Pb isotope ratios between the three sites [*Weis et al.*, 1991; *Class et al.*, 1993]. These variations with age are not seen in the data in this study. To properly compare the new (MC-ICP-MS) and old (TIMS) data sets, we applied the same rationale to the TIMS Pb isotope data (i.e., recalculated the initial Pb isotopic ratios for the samples exhibiting high Th/U; Figure 4.6).
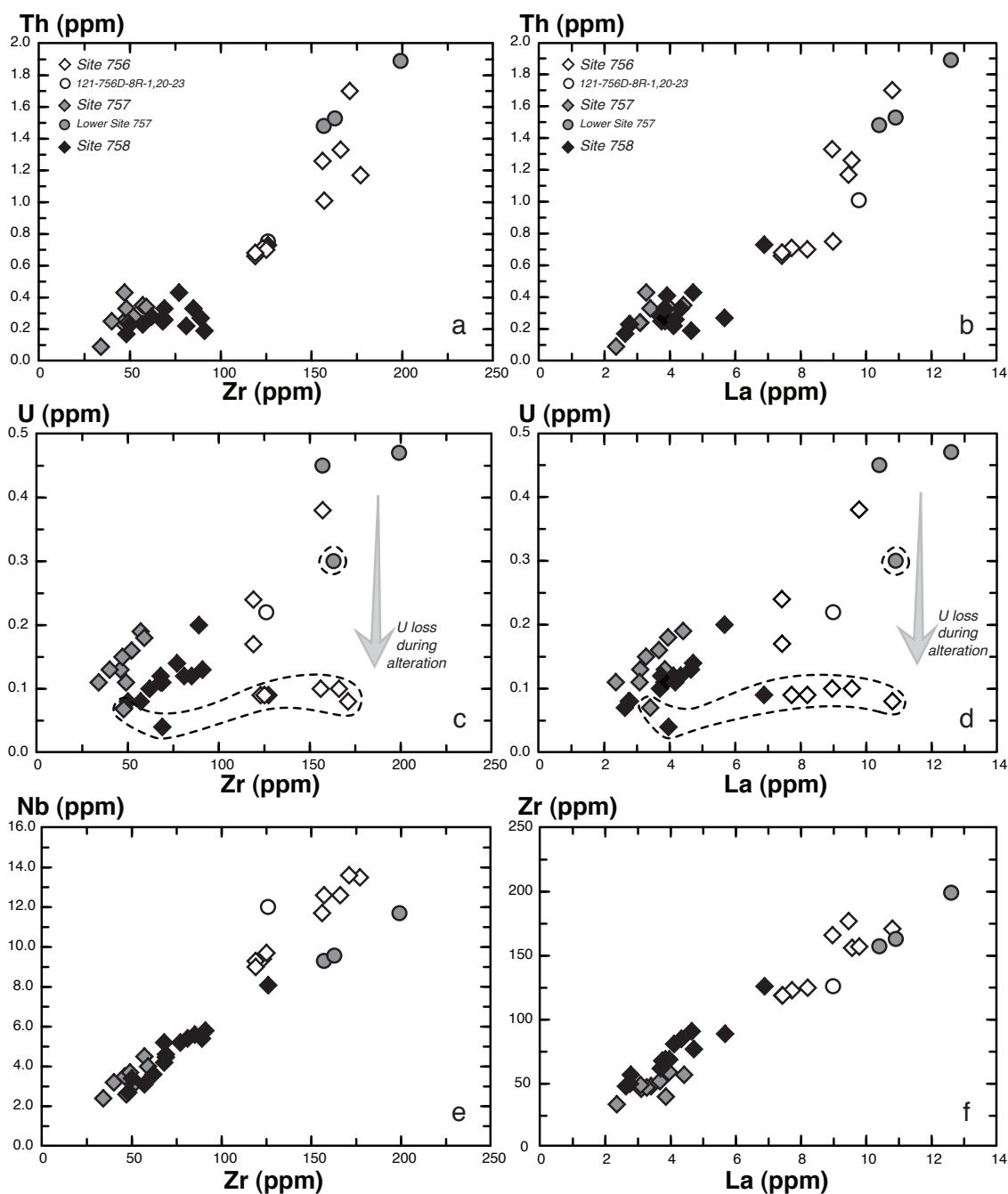
Figure 4.5. Incompatible trace element concentration variations for the ODP Leg 121 basalts. (a) Th versus Zr; (b) Th versus La; (c) U versus Zr; (d) U versus La; (e) Nb versus Zr; (f) Zr versus La. White-, grey-, and black-filled diamonds represent basalts from Site 756, 757 and 758 respectively. Grey circles with black outlines represent basalts from the lower flow units of Site 757, which are characterized by higher trace element concentrations. The white circle with black outline represents a basalt from Site 756 that has distinctive geochemical compositions in comparison to other basalts from the same drill site. Note the significant loss of U due to alteration of some of the Ninetyeast Ridge basalts relative to other alteration resistant incompatible elements (Th, Nb, Zr, La). Samples enclosed by the dashed fields (diagrams c and d) correspond to the samples that exhibit high Th/U (samples indicated by * in Tables 1 and 2) and for which age-correction calculations were performed using the estimated U concentrations based on Th/U = 4 (see text for details).

4.6. Results

4.6.1. Site 758 (~5.38°N; ~82 Ma)

Samples from the 178 m of basaltic basement penetrated in drill hole 758A yield the least radiogenic and the largest variation of Pb isotopic compositions observed within the three Ninetyeast Ridge drill sites ($^{206}Pb/^{204}Pb_m$ = 18.326 – 18.686, $^{206}Pb/^{204}Pb_i$ = 18.049 – 18.533; $^{207}Pb/^{204}Pb_m$ = 15.542 – 15.585, $^{207}Pb/^{204}Pb_i$ = 15.521 – 15.568; $^{208}Pb/^{204}Pb_m$ = 38.618 –38.974, $^{208}Pb/^{204}Pb_i$ = 38.280 – 38.822; where the subscripts m and i refer to the measured and initial ratios, respectively) (Table 4.4, Figures 4.6, 4.8 and 4.9). Their Hf isotopic compositions are also the most variable amongst the Ninetyeast Ridge basalts ($^{176}Hf/^{177}Hf_m$ = 0.283029 – 0.283132, $^{176}Hf/^{177}Hf_i$ = 0.28299 – 0.28308) (Table 4.5, Figure 4.7b and 4.7d). In contrast, very little variation is observed in the Sr ($^{87}Sr/^{86}Sr_m$ = 0.704318 – 0.704502, $^{87}Sr/^{86}Sr_i$ = 0.70431 – 0.70449) and Nd isotopic compositions ($^{143}Nd/^{144}Nd_m$ = 0.512854 – 0.512888, $^{143}Nd/^{144}Nd_i$ = 0.51275 – 0.51278) throughout the basement stratigraphy of hole 758A (Table 4.5, Figure 4.7a and 4.7c). Based on Pb and Hf isotopic variations, three distinct groups of flows can be identified in hole 758A (Figure 4.8c). The lowermost flows (units 29 to 14) show the least variable Pb isotopic compositions and have some of the least radiogenic Hf isotopic values (units 29 and 19) and the most radiogenic Nd isotope ratios (units 29, 27, and 22) measured within this core (Figure 4.8a). The middle section (flow units 14 to 3) is characterized by a systematic increase of Pb and Sr isotopic ratios upwards with stratigraphic position, whereas Hf and Nd isotopic compositions evolve to less radiogenic compositions. The upper section (flow units 3 to 1) shows larger Pb, Hf and Nd isotopic variations than the underlying flow units (Figure 4.8a). The Sr isotope values increase slightly upwards until flow unit 5, and then decrease in the upper part of the core, toward the average $^{87}Sr/^{86}Sr$ value (0.70441) for this drill hole.

Four samples (121-758A-58R-6, 21-25 cm; 121-758A-55R-5, 82-86 cm; 121-758A-56R-1, 64-68 cm; 121-758A-59R-2, 58-62 cm) have considerably lower $^{206}Pb/^{204}Pb$ and $^{208}Pb/^{204}Pb$ values than the rest of Site 758 core samples (Figures 4.6 and 4.8a). Sample 121-758A-58R-6, 21-25 cm is highly enriched in Fe_2O_3, TiO_2, P_2O_5, V, Zn, Y and most of the

Table 4.4. Pb Isotopic Compositions by MC-ICP-MS from the Ninetyeast Ridge Basalts ODP Leg 121

Sample ID	Acid Leaching Steps	% Weight Loss	^{206}Pb/^{204}Pb[d]	Error (2SE)	^{207}Pb/^{204}Pb[d]	Error (2SE)	^{208}Pb/^{204}Pb[d]	Error (2SE)	(^{206}Pb/^{204}Pb)$_i$[e]	(^{207}Pb/^{204}Pb)$_i$[e]	(^{208}Pb/^{204}Pb)$_i$[e]	^{208}Pb*/^{204}Pb*[f]
Site 756												
121-756C-10N1, 32-36*	17	59.92	18.6697	0.0007	15.5468	0.0007	38.9793	0.0023	18.4406	15.5360	38.6780	1.0150
121-756C-10N1, 32-36 dup.*[a]	17	50.23	18.6704	0.0011	15.5475	0.0010	38.9811	0.0030	18.4412	15.5368	38.6797	1.0151
121-756D-4R1, 35-39 [ag.][b]	17	70.51	18.7110	0.0011	15.5534	0.0010	38.9823	0.0025	-	-	-	1.0109
121-756D-4R1, 35-39 [ag.] dup.	19	71.86	18.7140	0.0009	15.5559	0.0010	38.9887	0.0029	-	-	-	1.0112
121-756D-4R1, 35-39 [wc][b]	14	84.26	18.7186	0.0017	15.5510	0.0015	38.9803	0.0042	-	-	-	1.0098
121-756D-4R1, 35-39 [wc] dup.	19	80.40	18.7138	0.0010	15.5529	0.0008	38.9813	0.0022	-	-	-	1.0105
121-756D-4R1, 85-89*	15	78.17	18.6918	0.0016	15.5457	0.0018	38.9691	0.0040	18.4370	15.5337	38.6339	1.0115
121-756D-4R1, 85-89 rep.*[c]	-	-	18.6922	0.0017	15.5468	0.0014	38.9684	0.0038	18.4374	15.5349	38.6332	1.0114
121-756D-6R1, 6-10*	19	60.98	18.6630	0.0023	15.5444	0.0025	38.9636	0.0078	18.2072	15.5230	38.3640	1.0141
121-756D-6R2, 9-13*	13	71.02	18.7011	0.0019	15.5533	0.0014	39.0452	0.0042	18.5151	15.5446	38.8005	1.0186
121-756D-6R2, 9-13 dup.*	13	71.81	18.6972	0.0019	15.5522	0.0016	39.0394	0.0045	18.5111	15.5435	38.7947	1.0184
121-756D-6R2, 13-17*	13	64.30	18.6958	0.0016	15.5506	0.0013	39.0284	0.0039	18.4926	15.5411	38.7611	1.0174
121-756D-7R1, 100-104	14	82.31	18.6859	0.0016	15.5536	0.0013	38.9931	0.0037	18.4819	15.5440	38.8148	1.0147
121-756D-8R1, 20-23	17	69.48	18.7232	0.0013	15.5756	0.0013	39.2427	0.0036	18.6212	15.5709	39.1283	1.0372
121-756D-10R1, 99-103	13	64.57	18.6924	0.0016	15.5481	0.0015	38.9941	0.0043	18.5726	15.5425	38.8858	1.0141
121-756D-12R3, 139-143	16	71.90	18.6626	0.0024	15.5444	0.0015	38.9423	0.0048	18.5703	15.5400	38.8209	1.0118
Site 757												
121-757C-9R1, 105-109*	10	68.50	18.7011	0.0039	15.5804	0.0033	38.9499	0.0090	18.3594	15.5643	38.5009	1.0085
121-757C-9R1, 105-109 dup.*	11	68.32	18.6986	0.0015	15.5796	0.0016	38.9476	0.0050	18.3570	15.5634	38.4986	1.0085
121-757C-9R5, 34-38	17	83.18	18.7749	0.0058	15.5965	0.0049	38.9921	0.0117	18.5709	15.5869	38.8683	1.0051
121-757C-9R6, 102-105	10	75.94	18.7213	0.0021	15.5798	0.0023	38.9177	0.0085	18.5463	15.5715	38.8170	1.0029
121-757C-9R7, 78-82	9	53.17	18.7155	0.0008	15.5809	0.0008	38.9496	0.0022	18.4866	15.5701	38.7340	1.0069
121-757C-9R8, 54-59	12	70.93	18.6941	0.0076	15.5785	0.0051	38.9295	0.0166	18.5065	15.5696	38.7951	1.0071
121-757C-10R1, 86-90	13	65.97	18.7946	0.0016	15.5921	0.0018	38.9820	0.0050	18.5664	15.5813	38.9207	1.0019
121-757C-10R3, 2-6	13	91.61	19.1841	0.0067	15.6122	0.0053	39.1105	0.0137	18.9218	15.5999	38.9448	0.9754
121-757C-11R2, 10-14	10	68.35	18.7584	0.0045	15.5898	0.0037	39.0155	0.0094	18.5331	15.5792	38.8792	1.0093
121-757C-11R2, 51-56	19	83.77	18.9097	0.0049	15.5906	0.0040	39.0220	0.0099	18.6819	15.5798	38.8806	0.9941
121-757C-12R1, 100-104*	9	51.97	18.8259	0.0011	15.5774	0.0010	39.0713	0.0027	18.2246	15.5490	38.2809	1.0080
121-757C-12R2, 0-5	10	57.48	18.7548	0.0015	15.5687	0.0012	39.0489	0.0033	18.4240	15.5531	38.6913	1.0132
121-757C-12R2, 0-5 dup.	10	69.79	18.7587	0.0014	15.5709	0.0014	39.0466	0.0036	18.4278	15.5553	38.6890	1.0126
121-757C-12R4, 24-29	10	83.96	18.8101	0.0031	15.5744	0.0028	39.1964	0.0073	18.6062	15.5648	38.9284	1.0229
Site 758												
121-758A-55R5, 82-86	10	48.48	18.4879	0.0030	15.5421	0.0027	38.7290	0.0076	18.0485	15.5212	38.3788	1.0078
121-758A-56R1, 64-68	13	52.40	18.4691	0.0017	15.5467	0.0013	38.6945	0.0037	18.1584	15.5319	38.4014	1.0062
121-758A-58R6, 21-25*	7	62.41	18.3261	0.0015	15.5689	0.0014	38.6178	0.0044	18.1731	15.5616	38.4170	1.0136
121-758A-59R2, 58-62*	10	57.72	18.3307	0.0015	15.5688	0.0014	38.6269	0.0044	18.0664	15.5562	38.2799	1.0141
121-758A-60R1, 122-126	16	63.08	18.6862	0.0017	15.5852	0.0019	38.9741	0.0053	18.3268	15.5681	38.6119	1.0127
121-758A-60R1, 122-126 dup.	10	56.91	18.6833	0.0019	15.5840	0.0017	38.9657	0.0039	18.3240	15.5668	38.6036	1.0121
121-758A-62R1, 130-134	13	59.76	18.6421	0.0022	15.5706	0.0021	38.9323	0.0056	18.3425	15.5650	38.8217	1.0130
121-758A-62R3, 80-84	14	72.57	18.6334	0.0042	15.5729	0.0037	38.8938	0.0105	18.3119	15.5575	38.7514	1.0098
121-758A-65R1, 51-55	14	63.05	18.5804	0.0012	15.5635	0.0011	38.8710	0.0027	18.2528	15.5479	38.5754	1.0131
121-758A-67R4, 31-35	18	73.96	18.4967	0.0023	15.5535	0.0018	38.7987	0.0051	18.3551	15.5468	38.7308	1.0145
121-758A-69R3, 53-57	12	62.19	18.5748	0.0032	15.5598	0.0032	38.8016	0.0114	18.1853	15.5412	38.4437	1.0062
121-758A-70R1, 71-75	12	59.65	18.5264	0.0019	15.5620	0.0019	38.8358	0.0058	18.2870	15.5506	38.6918	1.0152
121-758A-70R2, 129-133	10	65.54	18.4821	0.0024	15.5652	0.0026	38.7936	0.0079	18.1850	15.5510	38.5905	1.0155
121-758A-71R1, 127-131	17	63.64	18.5240	0.0023	15.5721	0.0017	38.8112	0.0062	18.2242	15.5579	38.5697	1.0128
121-758A-71R3, 64-68	11	42.74	18.4952	0.0013	15.5659	0.0009	38.8528	0.0026	18.2521	15.5543	38.6135	1.0205
121-758A-73R1, 82-86	13	63.29	18.5197	0.0033	15.5626	0.0025	38.7785	0.0068	18.3106	15.5526	38.5228	1.0098
121-758A-73R4, 105-109	10	63.99	18.5943	0.0031	15.5591	0.0038	38.8064	0.0102	18.5327	15.5561	38.7586	1.0046

[a]Pb isotopic ratios normalized to the SRM 981 Pb standard solution TS-TIMS reference values of *Abouchami et al.* [2000]; the 2σ error is the absolute error value of the individual sample analysis (internal error).

[b]Initial isotopic ratios calculated for leached samples on the basis of the ^{40}Ar/^{39}Ar eruption age measured for basalts from Sites 756 (43 Ma), 757 (58 Ma) and 758 (82 Ma) [*Duncan*, 1991].

[c]^{208}Pb*/^{206}Pb* defined as (^{208}Pb/^{204}Pbsample - 29.475)/(^{206}Pb/^{204}Pbsample - 9.037) by *Galer and O'Nions* [1985].

*samples for which the U content is too low and was recalculated based on a model Th/U = 4 prior to calculation of the initial Pb ratios (see text for details).

[d]dup. = full procedural duplicate analysis of the same starting sample powder.

[e][ag] = samples crushed in agate mill, [wc] = samples crushed in tungsten-carbide mill.

[f]rep. = replicate analysis of the same sample solution on the MC-ICP-MS.
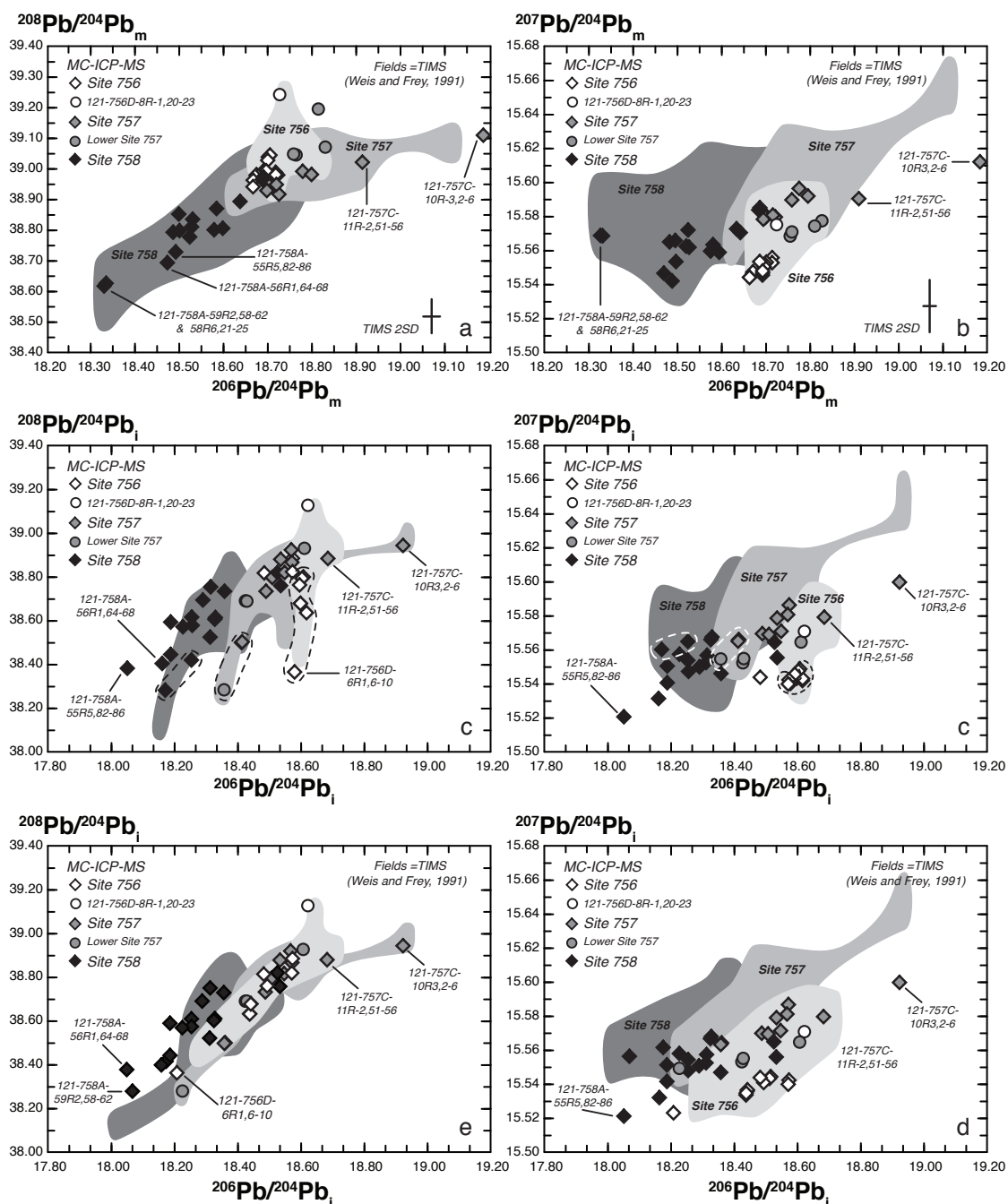
Figure 4.6. Diagrams of $^{208}Pb/^{204}Pb$ and $^{207}Pb/^{204}Pb$ versus $^{206}Pb/^{204}Pb$ showing the comparison between the MC-ICP-MS results from this study (symbols) and published TIMS results (shaded grey fields) from *Weis and Frey* [1991] for the Ninetyeast Ridge, ODP Leg 121 basalts. (a) and (b) show the present-day (measured) Pb isotope values. Note that the analytical uncertainty of all MC-ICP-MS measurements is smaller than the symbol sizes. The 2SD uncertainty of the TIMS measurements is shown at the bottom right corner of the plots. (c) and (d) show the initial ratios, where the age-corrections are 82 Ma (Site 758), 58 Ma (Site 757), and 43 Ma (756). Dashed fields enclose the samples that exhibit high Th/U and consequently show unreliable age-corrected values. (e) and (f) show the initial ratios calculated using the estimated U concentrations for the samples with high Th/U (see text for details). In all diagrams, samples with distinct compositions relative to the compositional average of each drill core (outliers) are labeled.

114

rare earth elements (REE), and has very low abundances of Al_2O_3, CaO, Ni and Cr, compared to other Site 758 core samples [*Frey et al.*, 1991]. In contrast, the other three samples are not distinctive in either major element and/or trace element characteristics, but yield slightly higher Hf isotopic values (Figures 4.7 to 4.9).

4.6.2. Site 757 (~17°S; ~58 Ma)

Within the ~50 m of basalts recovered in hole 757C, Pb and Sr isotopic compositions show relatively little variation throughout the stratigraphy of the hole ($^{206}Pb/^{204}Pb_m = 18.694 – 18.826$, $^{206}Pb/^{204}Pb_i = 18.225 – 18.922$; $^{207}Pb/^{204}Pb_m = 15.569 – 15.597$, $^{207}Pb/^{204}Pb_i = 15.549 – 15.587$; $^{208}Pb/^{204}Pb_m = 38.918 – 39.196$, $^{208}Pb/^{204}Pb_i = 38.281 – 38.928$; $^{87}Sr/^{86}Sr_m = 0.704396 – 0.704886$, $^{87}Sr/^{86}Sr_i = 0.70422 – 0.70466$) (Figures 4.6, 4.7, and 4.8b). In contrast, the Hf and Nd isotopic compositions are more variable ($^{143}Nd/^{144}Nd_m = 0.512788 – 0.512822$, $^{143}Nd/^{144}Nd_i = 0.51272 – 0.51276$; $^{176}Hf/^{177}Hf_m = 0.282994 – 0.283034$, $^{176}Hf/^{177}Hf_i = 0.28296 – 0.28301$) (Figures 4.6, 4.8 and 4.9) and two stratigraphic groups with distinct Hf isotope values can be identified (Figure 4.9b). The lower group encompasses samples from flow units 19 to 12 and display higher average ε_{Hf} and ε_{Nd} values (+9.2 and 3.4, respectively), whereas the upper group encompasses samples from flow units 8 to 2 and yields lower average ε_{Hf} and ε_{Nd} values (+8.4 and 3.1, respectively). Site 757 basalts display the widest range of Sr and Nd isotope compositions among the Ninetyeast Ridge basalts and their Nd and Hf isotopes are the least radiogenic of the three drill sites (Table 4.5, Figure 4.7).

Two samples from Site 757 (121-757C-10R-3, 2-6 cm and 121-757C-11R-2, 51-56 cm) have distinctly higher Pb and Sr isotopic values (Tables 4.4 and 4.5), extending considerably the range of Pb and Sr isotopic variations for this site. These samples are located in the middle to lower part of the core (flow units 8 and 13, respectively) and are strongly altered (H_2O^+ up to 7.2 wt%), highly plagioclase-phyric basalts, where the plagioclase megacrysts show K-feldspar and albite reaction rims [*Frey et al.*, 1991]. We

Table 4.5. Sr-Nd-Hf Isotopic Compositions by TIMS from the Ninetyeast Ridge Basalts ODP Leg 121

Sample ID	$^{87}Sr/^{86}Sr^a$	Error (2σ)	$^{87}Sr/^{86}Sr_i^b$	$^{143}Nd/^{143}Nd^a$	Error (2σ)	ε_{Nd}^c	$^{143}Nd/^{143}Nd_i^b$	$\varepsilon_{Nd_i}^d$	$^{176}Hf/^{177}Hf^a$	Error (2SE)	ε_{Hf}^c	$^{176}Hf/^{177}Hf_i^b$	$\varepsilon_{Hf_i}^d$
Site 756													
121-756C-10N1, 32-36	0.703868	9	0.703807	0.512902	6	5.2	0.512856	5.3	0.283070	4	10.5	0.283057	11.1
121-756C-10N1, 32-36 dup.[e]	0.703858	8	0.703797	0.512894	6	5.0	0.512848	5.2	0.283071	8	10.6	0.283058	11.1
121-756D-4R1, 35-39 [ag.][f]	0.703907	8	0.703816	0.512893	7	5.0	0.512845	5.1	0.283058	5	10.1	0.283044	10.6
121-756D-4R1, 35-39 [ag.] dup.	0.703916	6	0.703825	0.512896	7	5.0	0.512848	5.2	0.283065	7	10.4	0.283052	10.9
121-756D-4R1, 35-39 [wc][f]	0.703904	7	0.703813	0.512903	7	5.2	0.512855	5.3	0.283062	8	10.3	0.283049	10.8
121-756D-4R1, 35-39 [wc] dup.	0.703899	6	0.703808	0.512891	8	4.9	0.512843	5.1	0.283068	7	10.5	0.283054	11.0
121-756D-4R1, 85-89	0.703899	8	0.703753	0.512902	6	5.2	0.512851	5.2	0.283082	8	11.0	0.283069	11.5
121-756D-6R1, 6-10	0.703864	8	0.703662	0.512904	6	5.2	0.512855	5.3	0.283076	5	10.7	0.283063	11.3
121-756D-6R2, 9-13	0.703895	7	0.703554	0.512893	7	5.0	0.512841	5.0	0.283060	7	10.2	0.283046	10.7
121-756D-6R2, 9-13 dup.	0.703899	8	0.703558	0.512886	7	4.8	0.512834	4.9	0.283064	6	10.3	0.283049	10.8
121-756D-6R2, 13-17	0.703896	7	0.703885	0.512896	6	5.0	0.512845	5.1	0.283069	6	10.5	0.283054	10.9
121-756D-6R2, 13-17 rep.[g]	-	-	-	-	-	-	-	-	0.283064	5	10.3	0.283048	10.7
121-756D-7R1, 100-104	0.703951	7	0.703925	0.512878	7	4.7	0.512831	4.8	0.283045	14	9.7	0.283032	10.2
121-756D-8R1, 20-23	0.704379	7	0.704229	0.512820	8	3.6	0.512774	3.7	0.283016	6	8.6	0.283001	9.1
121-756D-10R1, 99-103	0.703891	10	0.703710	0.512890	7	4.9	0.512841	5.0	0.283057	8	10.1	0.283043	10.6
121-756D-12R3, 139-143	0.703813	7	0.703792	-	-	-	-	-	0.283074	6	10.7	0.283058	11.1
Site 757													
121-757C-9R1, 105-109	0.704396	8	0.704377	0.512799	6	3.1	0.512736	3.4	0.282997	7	8.0	0.282972	8.4
121-757C-9R1, 105-109 dup.	0.704415	7	0.704396	0.512811	7	3.4	0.512748	3.6	0.283001	6	8.1	0.282976	8.5
121-757C-9R5, 34-38	0.704525	8	0.704584	0.512792	7	3.0	0.512732	3.3	0.283013	8	8.5	0.282989	9.0
121-757C-9R6, 102-105	0.704654	7	0.704266	-	-	-	-	-	0.283009	7	8.4	0.282984	8.8
121-757C-9R7, 78-82	0.704501	7	0.704264	0.512794	7	3.1	0.512730	3.2	0.283018	7	8.7	0.282991	9.0
121-757C-9R8, 54-59	0.704653	7	0.704368	0.512788	6	2.9	0.512724	3.1	0.283006	11	8.3	0.282982	8.8
121-757C-10R1, 86-90	0.704707	5	0.704543	0.512802	7	3.2	0.512741	3.5	0.282994	7	7.9	0.282963	8.1
121-757C-10R3, 2-6	0.705775	8	0.705702	0.512799	8	3.1	0.512737	3.4	0.283010	16	8.4	0.282976	8.5
121-757C-10R3, 2-6 dup.	0.705781	8	0.705708	0.512805	6	3.3	0.512743	3.5	0.282995	6	7.9	0.282961	8.0
121-757C-11R2, 10-14	0.704776	8	0.704636	0.512808	6	3.3	0.512740	3.4	0.283033	7	9.2	0.283008	8.0
121-757C-11R2, 51-56	0.705589	7	0.705426	0.512811	7	3.4	0.512748	3.6	0.283033	12	9.2	0.283012	9.7
121-757C-12R1, 100-104	0.704427	7	0.704314	0.512818	7	3.5	0.512758	3.8	0.283033	6	9.2	0.283013	9.8
121-757C-12R1, 100-104 rep.	-	-	-	-	-	-	-	-	0.283029	5	9.1	0.283010	9.7
121-757C-12R2, 0-5	0.704518	8	0.704220	0.512820	5	3.6	0.512761	3.9	0.283030	5	9.1	0.283006	9.6
121-757C-12R2, 0-5 dup.	0.704526	9	0.704228	0.512822	5	3.6	0.512763	3.9	0.283034	5	9.3	0.283011	9.8
121-757C-12R4, 24-29	0.704878	9	0.704655	0.512809	7	3.3	0.512748	3.6	0.283025	10	8.9	0.283008	9.7
121-757C-12R4, 24-29 dup.	0.704886	8	0.704663	0.512810	4	3.4	0.512749	3.6	-	-	-	-	-
Site 758													
121-758A-55R5, 82-86	0.704405	7	0.704394	0.512888	7	4.9	0.512772	4.7	0.283132	10	12.7	0.283081	12.8
121-758A-56R1, 64-68	0.704416	8	0.704379	0.512876	6	4.7	0.512760	4.4	0.283117	6	12.2	0.283072	12.5
121-758A-58R6, 21-25	0.704426	6	0.704400	-	-	-	-	-	0.283034	7	9.3	0.282990	9.6
121-758A-59R2, 58-62	0.704425	9	0.704366	0.512854	6	4.2	0.512751	4.3	0.283130	10	12.7	0.283084	12.9
121-758A-60R1, 122-126	0.704481	7	0.704466	0.512857	6	4.3	0.512766	4.5	0.283064	5	10.3	0.283018	10.6
121-758A-60R1, 122-126 dup.	0.704482	10	0.704466	-	-	-	-	-	0.283062	7	10.3	0.283017	10.5
121-758A-62R1, 130-134	0.704475	8	0.704453	-	-	-	-	-	0.283103	6	11.7	0.283061	12.1
121-758A-62R3, 80-84	0.704502	8	0.704487	0.512865	6	4.4	0.512764	4.5	0.283035	11	9.3	0.282999	9.9
121-758A-65R1, 51-55	0.704425	8	0.704416	0.512871	5	4.6	0.512777	4.8	0.283055	8	10.0	0.283027	10.9
121-758A-67R4, 31-35	0.704440	8	0.704435	-	-	-	-	-	0.283061	14	10.2	0.283026	10.9
121-758A-69R3, 53-57	0.704390	9	0.704369	0.512871	6	4.6	0.512778	4.8	0.283073	7	10.6	0.283023	10.7
121-758A-70R1, 71-75	0.704425	7	0.704423	-	-	-	-	-	0.283060	15	10.2	0.283022	10.7
121-758A-70R2, 129-133	0.704351	8	0.704338	-	-	-	-	-	0.283038	12	9.4	0.283000	9.9
121-758A-71R1, 127-131	0.704345	7	0.704324	0.512867	6	4.5	0.512781	4.9	0.283087	9	11.1	0.283048	11.6
121-758A-71R3, 64-68	0.704335	9	0.704332	0.512886	8	4.8	0.512784	4.9	0.283075	5	10.7	0.283034	11.1
121-758A-73R1, 82-86	0.704318	7	-	0.512886	7	4.8	0.512779	4.8	0.283097	9	11.5	0.283051	11.7
121-758A-73R4, 105-109	0.704343	8	0.704310	0.512876	6	4.6	0.512778	4.8	0.283029	11	9.1	0.282983	9.3

[a]Measured Sr isotopic ratio normalized to the NBS-987 standard solution mean of the wheel: $^{87}Sr/^{86}Sr = 0.710256$; the 2σ error is the absolute error value of the individual sample analysis (internal error) and reported as x10[6].

Measured Nd isotopic ratio normalized to the La Jolla standard solution mean of the wheel: $^{143}Nd/^{144}Nd = 0.511852$; the 2σ error is the absolute error value of the individual sample analysis (internal error) and reported as x10[6].

Measured Hf isotopic ratio normalized to the JMC475 standard solution, based on the mean of the daily analyses: $^{176}Hf/^{177}Hf = 0.282160$; the 2σ error is the absolute error value of the individual sample analysis (internal error) and reported as x10[6].

[b]Initial Sr, Nd and Hf isotopic ratios calculated for leached samples on the basis of the $^{40}Ar/^{39}Ar$ eruption age measured for basalts from Sites 756 (43 Ma), 757 (58 Ma) and 758 (82 Ma) [*Duncan*, 1991].

[c]εNd and εHf are calculated using present-day $^{143}Nd/^{144}Nd$ and $^{176}Hf/^{177}Hf$ values for CHUR = 0.512638 and 0.282772, respectively.

[d]ε_{Nd_i} and ε_{Nd_i} are calculated using both sample and CHUR $^{143}Nd/^{144}Nd$ and $^{176}Hf/^{177}Hf$ values corrected for the age of eruption.

[e]dup. = full procedural duplicate analysis of the same starting sample powder.

[f][ag] = samples crushed in agate mill, [wc] = samples crushed in tungsten–carbide mill.

[g]rep. = replicate analysis of the same sample solution on the MC-ICP-MS.

116
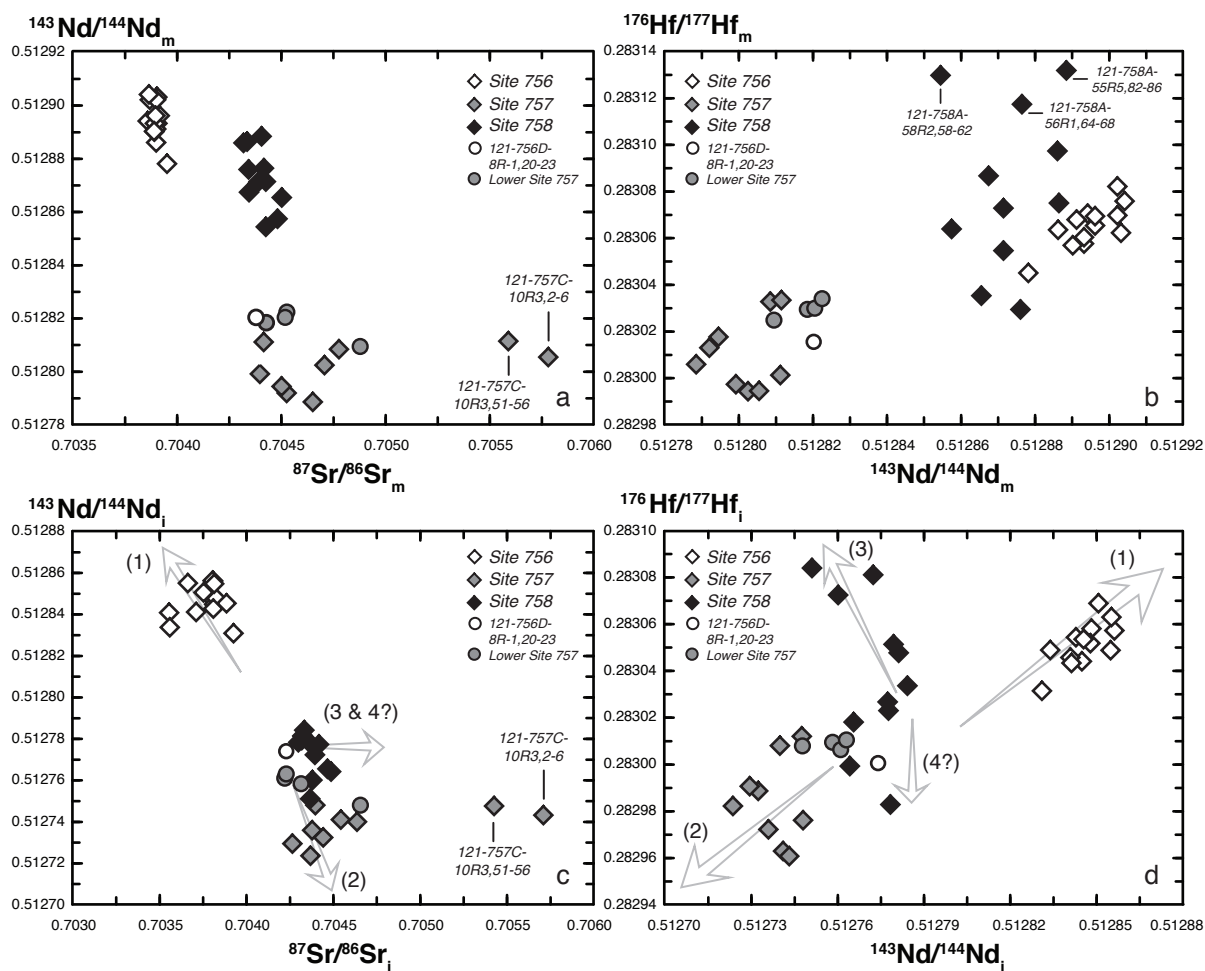
Figure 4.7. Diagrams of $^{143}Nd/^{144}Nd$ versus $^{87}Sr/^{86}Sr$ and $^{176}Hf/^{177}Hf$ versus $^{143}Nd/^{144}Nd$ for the Ninetyeast Ridge, ODP Leg 121 basalts. (a) and (b) show the measured ratios by MC-ICP-MS and TIMS; (c) and (d) show the calculated initial ratios, respectively. Note that the analytical uncertainty of all measurements is smaller than the symbol sizes. In all diagrams, the samples with distinct isotopic compositions relative to the compositional average of each drill core (outliers) are labeled. Numbers (1, 2, 3, 4) refer to the inferred components necessary to explain the isotopic variability within the Ninetyeast Ridge basalts and the arrows point towards the possible direction of such components (see text for details).

suspect that these particular secondary alteration phases may be more resistant to acid leaching and were not fully removed by the sequential acid-leaching procedure. Even excluding these samples, Site 757 basalts have the most radiogenic $^{87}Sr/^{86}Sr$ compositions observed amongst the three Ninetyeast Ridge sites.

4.6.3. Site 756 (~27.35°S; ~43 Ma)

The samples representing the 82 m of basaltic flows recovered at Site 756 display little variation in their Pb, Hf, Sr and Nd isotopic compositions throughout the stratigraphy of the drill hole (Figures 4.6 to 4.9). Their Pb isotopic ratios form a cluster with very narrow variation ($^{206}Pb/^{204}Pb_m$ = 18.663 – 18.719, $^{206}Pb/^{204}Pb_i$ = 18.207 – 18.573; $^{207}Pb/^{204}Pb_m$ = 15.544 – 15.577, $^{207}Pb/^{204}Pb_i$ = 15.523 –15.545; $^{208}Pb/^{204}Pb_m$ = 38.942 – 39.045, $^{208}Pb/^{204}Pb_i$ = 38.364 – 38.886) of intermediate compositions between those of basalts from Sites 757 and 758 (Table 4.4, Figure 4.6). Their Hf isotope compositions ($^{176}Hf/^{177}Hf_m$ = 0.283045 – 0.283082, $^{176}Hf/^{177}Hf_i$ = 0.28303 – 0.28307) overlap mostly with those of basalts from Site 758 (Table 4.5, Figures 4.7 to 4.9). The $^{87}Sr/^{86}Sr$ ratios of Site 756 basalts show limited variation ($^{87}Sr/^{86}Sr_m$ = 0.703813 – 0.703951, $^{87}Sr/^{86}Sr_i$ = 0.70355 – 0.70393) and are the least radiogenic values measured within basalts from the Ninetyeast Ridge (Table 4.5, Figures 4.7 to 4.9), whereas their Nd isotope values ($^{143}Nd/^{144}Nd_m$ = 0.512878 – 0.512904, $^{143}Nd/^{144}Nd_i$ = 0.51283 – 0.57286) are amongst the most radiogenic, together with some of the Site 758 basalts (Table 4.5, Figures 4.7 to 4.9). Overall, three shifts in isotopic compositions are identified for this drill hole. From flow unit 14 (at the bottom of the hole) to flow unit 7 (~180 mbsf), there is a slight increase in the Sr isotope ratios coupled with a decrease of Hf and Nd isotopes. These trends are then reversed upwards to flow unit 4, shifting once again to values closer to the average compositions for this site, until flow unit 1.

Sample 121-756D-8R-1, 20-23 cm (flow unit 7), recovered at ~180 mbsf, has distinct isotopic compositions compared to the rest of Site 756 basalts. It has considerably higher $^{87}Sr/^{86}Sr_m$ (0.704379), similar to Site 758 samples, yields lower $^{143}Nd/^{144}Nd_m$ (0.512820) and $^{176}Hf/^{177}Hf_m$ (0.283016), similar to some Site 757 samples, and has higher $^{207}Pb/^{204}Pb$ and
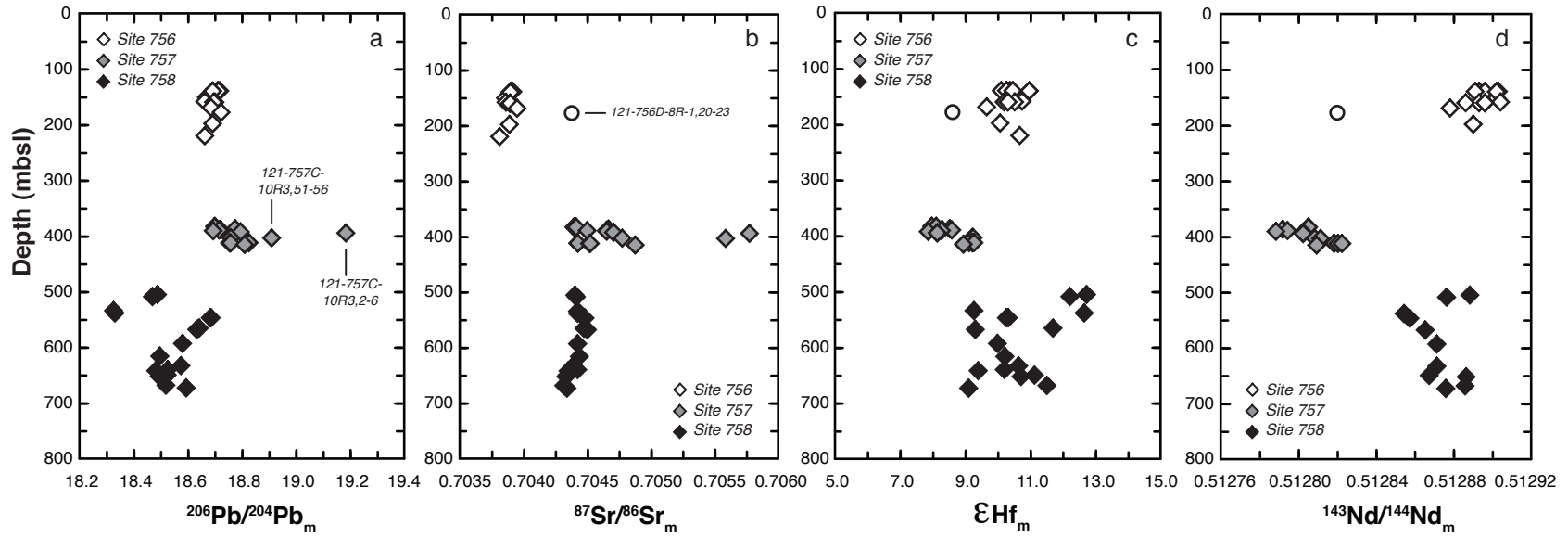
Figure 4.8. Comparison of the measured (a) $^{206}Pb/^{204}Pb_m$; (b) $^{87}Sr/^{86}Sr_m$; (c) εHf_m; and (d) $^{143}Nd/^{144}Nd_m$ variations as a function of drilling depth in meters below sea level (mbsl) between the three Ninetyeast Ridge ODP Leg 121 drill sites. Symbols and colour coding as described in previous Figures. Note that the analytical uncertainty of all measurements is smaller than the symbol sizes.

$^{208}Pb/^{204}Pb$ values for a given $^{206}Pb/^{204}Pb$ than the other Ninetyeast Ridge samples (Figures 4.6 and 4.8c). This sample was interpreted by *Frey et al.* [1991] as being derived from a compositionally different parent magma than the other Site 756 samples.

4.6.4. Comparison Between Sites

Whether considering the measured or the initial Pb-Hf-Sr-Nd isotopic ratios, basalts from Site 756 display the smallest ranges of variations compared to basalts from the other Ninetyeast Ridge sites. They generally have intermediate compositions to those of Sites 758 and 757, whereas basalts from Site 757 present the greater range of variation and some of the most extreme isotopic signatures within the Ninetyeast Ridge (Figures 4.6 to 4.9). In contrast to the previous TIMS dataset, which led *Class et al.* [1993, 1996] to propose a single homogeneous "aging" plume source model for the Ninetyeast Ridge, reanalysis of the tholeiites representative of the ~180 m of basaltic basement recovered during ODP Leg 121 shows that there are no systematic short-term (intra-site) or long-term (inter-site) isotopic evolution trends (Figures 4.9 and 4.10). The isotopic compositions of the Ninetyeast Ridge basalts do not correlate with stratigraphic position throughout the cores at each individual site (i.e., eruption age), nor with distance (i.e., emplacement age) along the ridge. The absence of a temporal trend in the isotopic compositions of the Ninetyeast Ridge basalts is consistent with the involvement of distinct mantle components, intrinsic or not to the plume-source, throughout the volcanic history of the ridge [*Saunders et al.*, 1991; *Weis and Frey*, 1991; *Frey and Weis*, 1995; 1996].

The considerable isotopic differences between basalts from the Ninetyeast Ridge sites likely reflect: 1) variability inherent to the source of the magmas erupting at each volcanic centre at a given time, or 2) interaction and mixing of source derived magmas with extraneous material. In multi-isotopic diagrams, basalts from each drill site define distinct isotopic compositional fields with very little overlap and each site trends toward a different end-member composition (Figures 4.6 to 4.8). Simple binary mixing relations cannot explain the distribution of the isotopic compositions observed amongst the Ninetyeast Ridge basalts
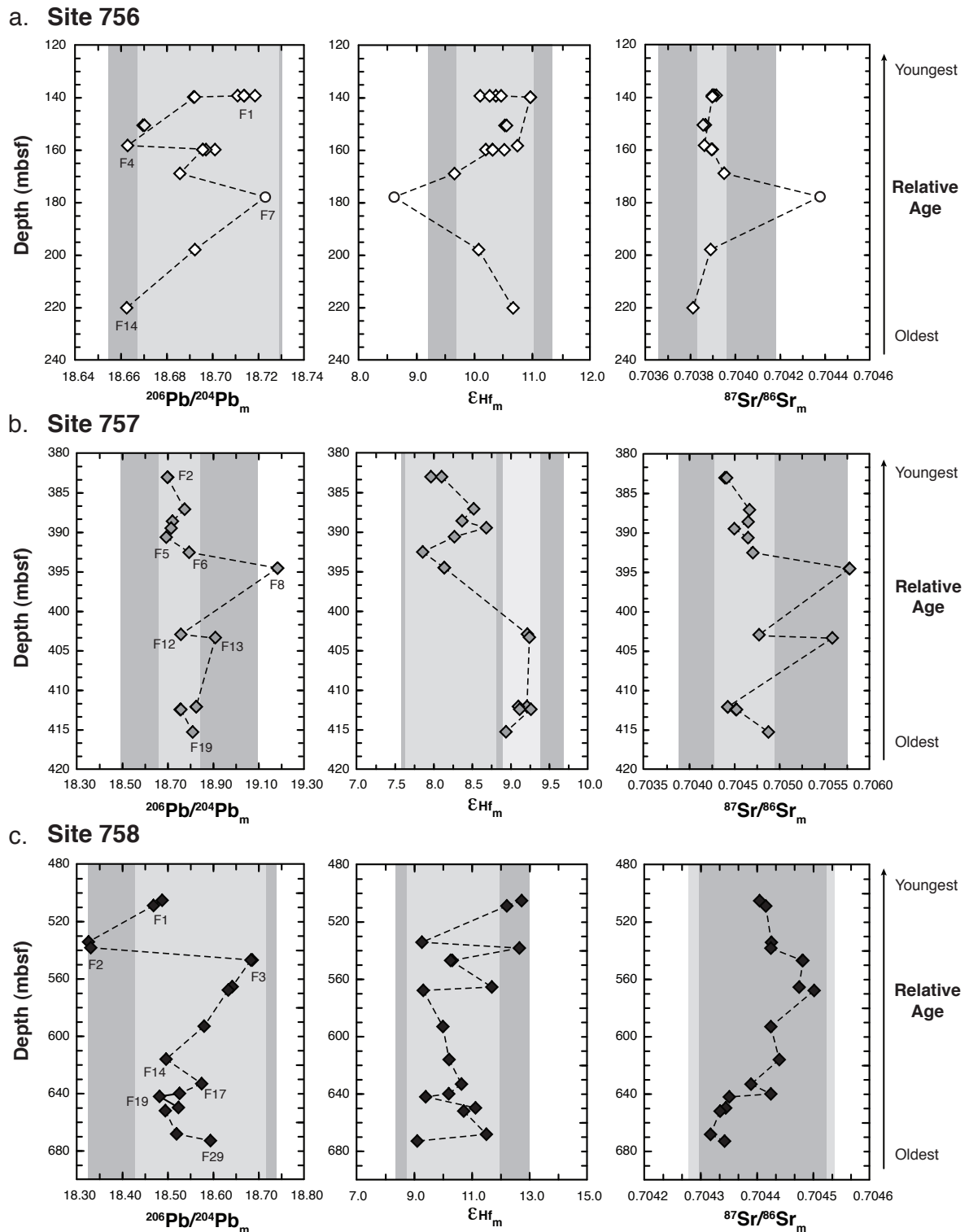
Figure 4.9. Variations of the measured $^{206}Pb/^{204}Pb$, ε_{Hf}, and $^{87}Sr/^{86}Sr$ as a function of drilling depth in meters below sea floor (mbsf) for each individual drill site. (a) Site 756; (b) Site 757; (c) Site 758. In all plots, the dark grey areas correspond to the ± 2SD of the mean of the respective data set, and the light grey areas correspond to the ± 2SD of the mean minus outliers of the respective data set. Labels F1, F2, etc. refer to the flow units the samples belong to (see Table 4.1).

and at least three distinct components are required. To account for the isotopic compositions of most of Site 756 and some of Site 758 basalts, a relatively depleted component with unradiogenic $^{87}Sr/^{86}Sr$ values and $^{207}Pb/^{204}Pb$, intermediate $^{206}Pb/^{204}Pb$ and $^{208}Pb/^{204}Pb$ values, and relatively radiogenic Nd and Hf isotopic compositions is required. An enriched component with radiogenic Hf isotopic compositions, unradiogenic $^{206}Pb/^{204}Pb$ and $^{208}Pb/^{204}Pb$ values, and intermediate Sr and Nd isotopic compositions is necessary to account for most of the isotopic compositions of Site 758 samples, the sample from flow unit 7 of Site 756 and part of the Site 757 samples. A third component, relatively enriched with unradiogenic Hf and Nd isotopic compositions and radiogenic Sr and Pb isotopic compositions, is required to account for the isotopic compositions of some of Site 757 lavas. The isotopic compositional fields defined by the samples from each site appear to converge toward a common, shared composition, with $^{206}Pb/^{204}Pb_i \approx 18.55$, $^{87}Sr/^{86}Sr_i \approx 0.70425$, $^{143}Nd/^{144}Nd_i \approx 0.51278$, $^{176}Hf/^{177}Hf_i \approx 0.28315$ (e.g., Figure 4.7 and 4.9). This may reflect an additional end-member composition present within the Ninetyeast Ridge source region or may be an artifact resulting from mixing of the other distinct components [e.g., *Douglas and Shilling*, 2000].

4.7. Discussion

4.7.1. Defining the Mantle Source Components of the Ninetyeast Ridge Basalts

Previous studies interpreted the isotopic variations in the Ninetyeast Ridge basement samples to reflect mixing between at least three components [*Saunders et al.*, 1991; *Weis et al.*, 1991]. *Saunders et al.* [1991] and *Weis and Frey* [1991] recognized that two of these components were best represented by the compositions attributed to the Kerguelen and Amsterdam-St. Paul mantle plumes. However, whereas *Weis and Frey* [1991] considered the third component to be a Indian MORB-like depleted component, *Saunders et al.* [1991] argued that there was no obvious contribution from a MORB source component to the Ninetyeast Ridge basalts. The isotopic compositions of the Ninetyeast Ridge basalts from these previous studies did not define clear mixing arrays, which indicated that they were not derived from simple mixing between any of the identified components. The new high-

Figure 4.10. Variation of initial isotopic compositions of the Ninetyeast Ridge drilled basalts as a function of latitude. (a) $^{206}Pb/^{204}Pb_i$; (b) ε_{Hfi}; (c) $^{87}Sr/^{86}Sr_i$; and (d) ε_{Ndi}. Large black, grey and white diamond symbols with black outlines represent the ODP Leg 121 data from this study. The other diamond symbols without outlines correspond to literature data for the DSDP samples [*Frey and Weis*, 1995]. Data for other nearby Indian Ocean island basalts (OIB) and MORB are also shown for context, at their appropriate latitude: Amsterdam and St. Paul islands [*Doucet et al.*, 2004]; Mont Crozier: (D. Weis, unpublished data); Site 1138 [*Neal et al.*, 2002; *Ingle et al.*, 2003]; Indian MORB [*Chauvel and Blichert-Toft*, 2001; *Mahoney et al.*, 2002; *Nicolaysen et al.*, 2007]. For convenience, the Kerguelen plume derived volcanic products Mont Crozier (which represents the present composition of the Kerguelen plume tail mantle source) and Site 1138 (which represents the composition in the Kerguelen plume head mantle source) are shown at the same latitude. Dashed lines mark the different segments along the Ninetyeast Ridge as defined by *Royer et al.* [1991] and *Krishna et al.* [1999].
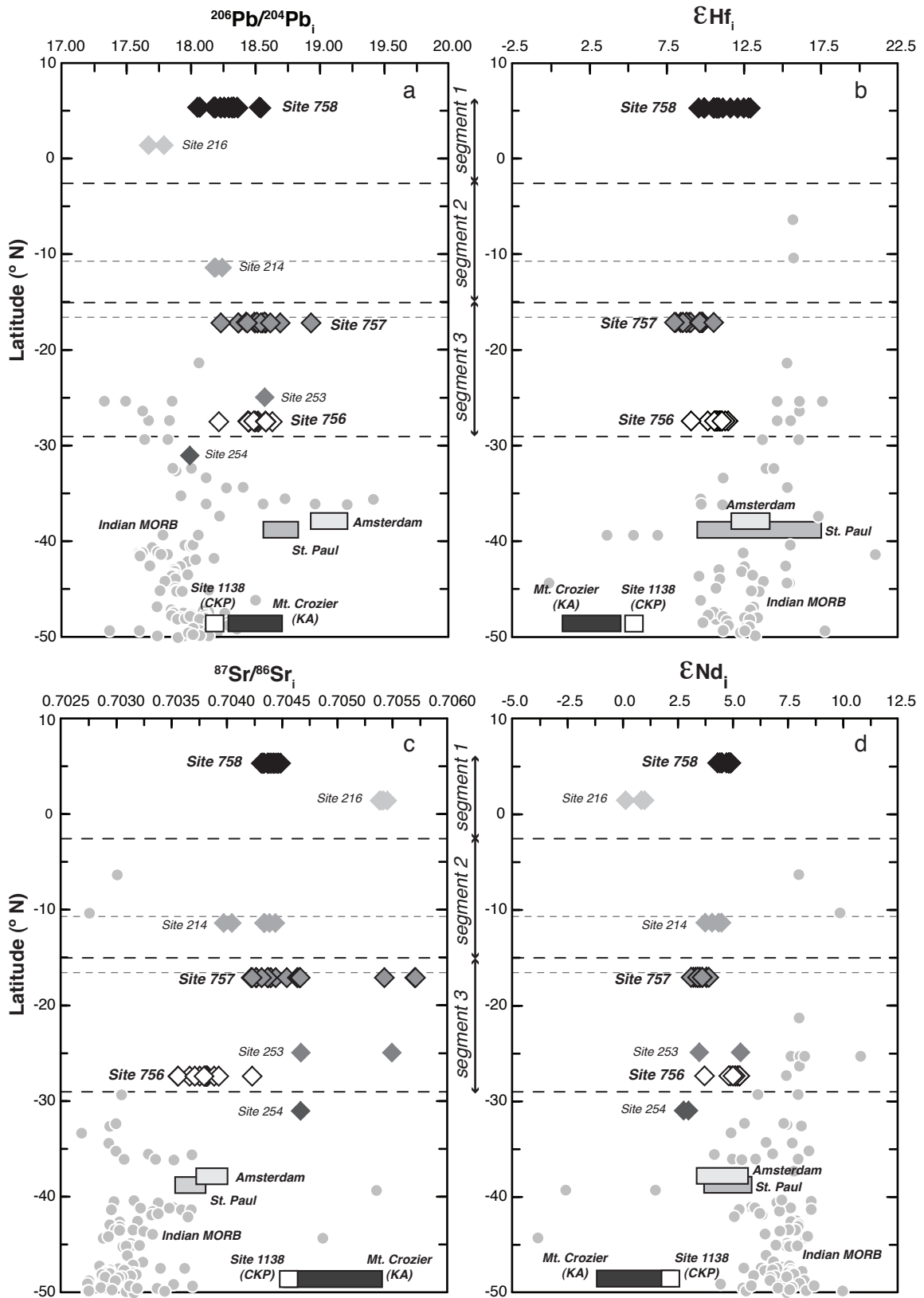
Figure 4.10.

precision Pb-Hf-Sr-Nd isotope dataset also indicates the presence of three, possibly four, components contributing to the compositions of the Ninetyeast Ridge basalts. However, in contrast to the older TIMS dataset, the newly determined Pb isotopic compositions from Site 758 and 757 basalts define linear arrays that may be interpreted as binary mixing arrays, and the compositions for Site 756 show relatively little variation (Figures 4.6 and 4.7). In light of the new isotopic dataset of the Ninetyeast Ridge basalts, the question arises as to how the components identified compare to the more recent end-member compositions now attributed to the Kerguelen [*Neal et al.*, 2002; *Ingle et al.*, 2003] and Amsterdam mantle plume sources [*Doucet et al.*, 2004] and MORB.

4.7.1.1. Is the Relatively Depleted Ninetyeast Ridge Component Indian MORB?

The tholeiitic basalts of the Ninetyeast Ridge erupted during a period characterized by higher spreading rates (18–20 cm/yr; e.g., *Müller et al.*, [2008]) when the Kerguelen hotspot was considered to be relatively close to the spreading axis of the newly forming Southeast Indian Ridge [e.g., *Frey et al.*, 1991; *Royer et al.*, 1991; *Frey and Weis*, 1995]. Any contribution from depleted asthenospheric mantle, resultant from plume-ridge interaction as volcanism on the Ninetyeast Ridge evolved from an intraplate setting to near-axis and on axis settings, can be discriminated by the isotopic compositions of the basalts forming at the different segments of the Ninetyeast Ridge. Basalts from Site 758, together with DSDP Site 216 basalts, erupted in the northern segment of the ridge (Figure 4.10) that formed as intraplate volcanism on the Indian plate [*Royer et al.*, 1991; *Krishna et al.*, 1999]. As a result, basalts from this segment of the ridge should yield the strongest enriched plume signatures within the Ninetyeast Ridge, as the MORB influence would be smaller or non-existent [e.g., *Frey and Weis*, 1995]. Site 757 basalts erupted during the period when the Kerguelen hotspot was coincident with the Wharton spreading center (60 to 54 Ma; *Krishna et al.* [1999]). These basalts should show a more diluted plume signature, given the higher degree of possible interaction with the surrounding depleted astenospheric mantle. Site 756, located on the southern segment of the Ninetyeast Ridge, is thought to have formed on the edge of the Indian plate [*Royer et al.*, 1991; *Krishna et al.*, 1999]. Basalts forming at this

tectonic environment should yield the most variable isotopic signatures, reflecting the variable degrees of mixing between the enriched plume material and the depleted mantle.

Linear regressions through the Pb isotopic compositions of each Ninetyeast Ridge site produce three linear arrays of slightly different slopes (Figure 4.11). These arrays are best interpreted as binary mixing trends between source components that lie along the radiogenic and unradiogenic extensions of the arrays [e.g., *Abouchami et al.*, 2000; *Eisele et al.*, 2003]. When comparing the initial Pb isotopic compositions of the Ninetyeast Ridge basalts and other Indian Ocean basalts (Figure 4.11a), the arrays defined by basalts from Site 757 and Site 756 intersect the Indian MORB compositional field, represented by compositions of basalts from the Southeast Indian Ridge (excluding the segments on the Amsterdam-St. Paul Plateau), Central Indian Ridge, and Southwest Indian Ridge. However, the same is not true when considering the measured Pb isotopic compositions. For example, all Ninetyeast Ridge basalts have higher $^{208}Pb/^{206}Pb$ for a given $^{207}Pb/^{206}Pb$ than MORB, and none of the arrays intersect the Indian MORB field (Figure 4.11b). In diagrams of $^{87}Sr/^{86}Sr$, $^{143}Nd/^{144}Nd$, and $^{176}Hf/^{177}Hf$ versus $^{206}Pb/^{204}Pb$, the arrays (not shown) defined by each of the Ninetyeast Ridge sites also do not trend towards Indian MORB. Instead, they are mostly parallel to the MORB compositional field (Figures 4.12 and 4.13). Additionally, together with other Indian Ocean island basalts, the Ninetyeast Ridge basalts plot at higher $^{176}Hf/^{177}Hf$ for a given $^{143}Nd/^{144}Nd$ compared to the mantle array [*Vervoort and Blichert-Toft*, 1999] (Figure 4.13b), which reflects derivation from a source with higher time-integrated Lu/Hf relative to Sm/Nd than the MORB source.

The depleted isotopic signatures observed in the Ninetyeast Ridge hence cannot be accounted for by mixing with depleted Indian asthenospheric mantle, in contrast to basalts from the Northern Kerguelen Plateau that formed ~50 km away from the southeast Indian Ridge at >34 Ma and whose compositions reveal incorporation of asthenospheric mantle by the Kerguelen plume [*Weis and Frey*, 2002]. Although the ridge formed close to a spreading axis, MORB was not entrained by plume-derived material to form the Ninetyeast Ridge. This is in good agreement with fluid dynamical models that predict the absence of upper mantle

Figure 4.11. Diagrams of (a) initial $^{208}Pb/^{204}Pb$ versus $^{206}Pb/^{204}Pb$, and (b) measured $^{208}Pb/^{206}Pb$ versus $^{207}Pb/^{206}Pb$ for the Ninetyeast Ridge basalts compared to other Indian Ocean basalts. Dashed lines represent the regression lines through the compositions from each Ninetyeast Ridge site; The small grey circles represent basalts from all the Indian Ocean spreading centres: SEIR [*Chauvel and Blichert-Toft*, 2001; *Mahoney et al*., 2002; *Nicolaysen et al.*, 2007]; CIR [*Rehkämper and Hofmann*, 1997; *Nauret et al.*, 2006]; SWIR [*Mahoney et al*., 1992; J*anney et al*., 2005; *Meyzen et al*., 2005]. Red arrows represent two cases of 100 Ma evolution (tick marks represent 20 Ma increments) by radiogenic decay of a compositionally homogeneous source considering compositions similar to those of Site 1138 (proxy for the Kerguelen plume head composition) and of Mont Crozier (proxy for the Kerguelen plume tail composition), respectively. Black arrow represents a similar evolution trajectory for an average Indian MORB source. Data sources for the Indian Ocean island basalts compositional fields: Amsterdam and St. Paul islands [*Doucet et al*., 2004]; Kerguelen Archipelago [*Weis et al*., 1998; *Frey et al.*, 2002b; *Doucet et al*., 2005; *Xu et al.*, 2007]; Mont Crozier (D. Weis unpublished data, 2001); ODP Sites 747, 749, 750 on the Central and South Kerguelen Plateau and Broken Ridge [*Mahoney et al*., 1995; *Frey et al.*, 2002b]; ODP Sites 1136 and 1138 on the South and Central Kerguelen Plateus [*Neal et al*., 2002; *Ingle et al.*, 2003]; Heard Island [*Barling et al*., 1990; 1994]; Crozet [*Mahoney et al*., 1996; *Salters and White*, 1998]; Réunion [*Vlastélic et al.*, 2007, 2009; *Bosh et al*., 2008]; DSDP Sites 214, 216, and 253 [*Frey and Weis*, 1995]. Global isotopic end-members DMM, EM-1 and EM-2 are from *Zindler and Hart* [1986], C is from *Hanan et al.* [1996; 2004] and Fozo is from *Stracke et al.* [2005]. NRHL refers to the Northern Hemisphere Reference Line as defined by *Hart* [1984].
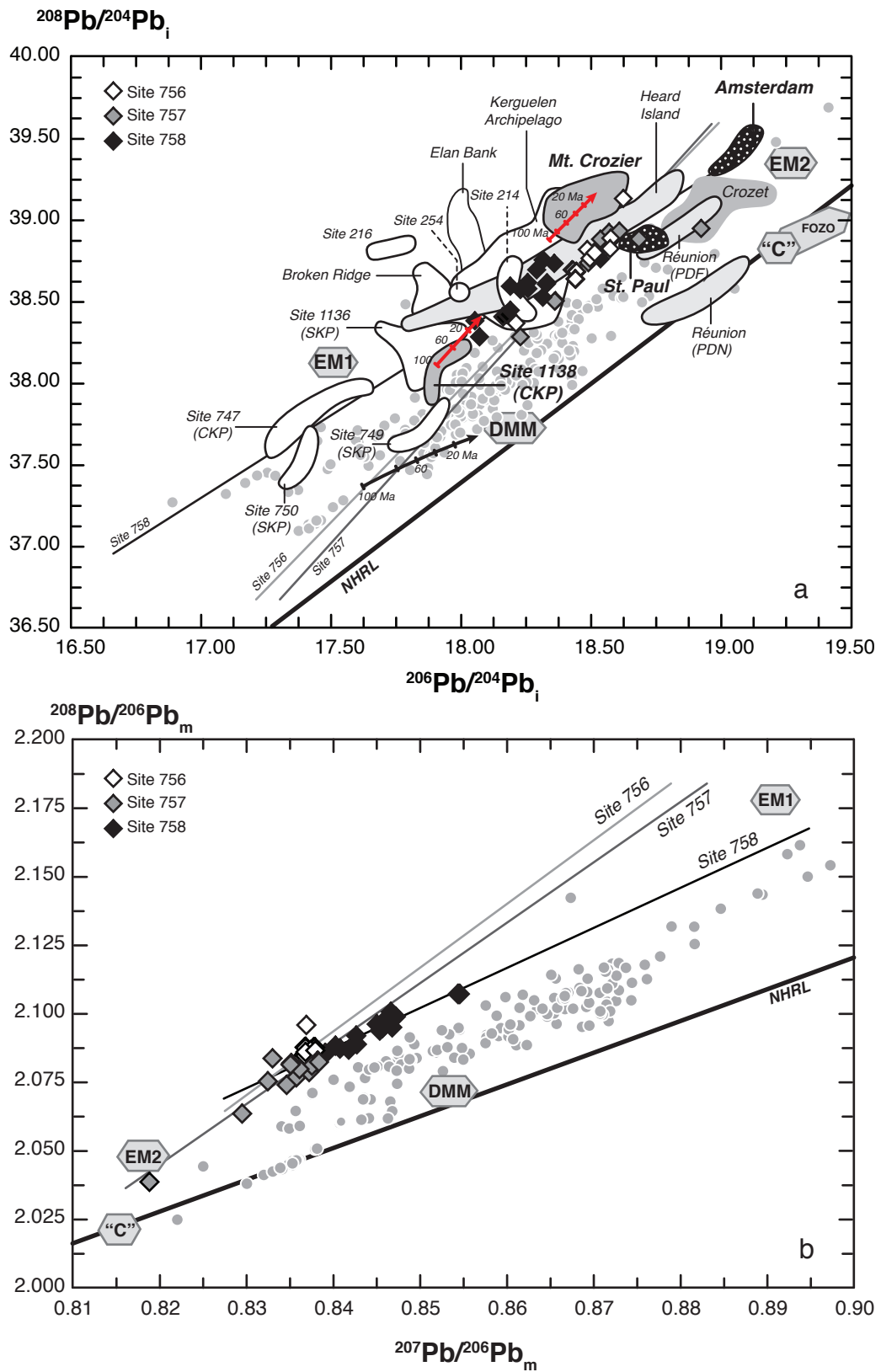
Figure 4.11.

entrainment by plume heads and consequent absence of MORB contribution in plume-related basalts [*Farnetani et al.*, 2002; *Farnetani and Samuel*, 2005]. Thus, the relatively depleted component responsible for the more depleted signatures within the Ninetyeast Ridge basalts is likely intrinsic to the heterogeneous upwelling mantle source.

4.7.1.2. Are the Ninetyeast Ridge Enriched Components Related to the Kerguelen and Amsterdam-St. Paul Mantle Plumes?

The geochemical similarities between basalts from the Ninetyeast Ridge and those derived from the geographically proximal Kerguelen and Amsterdam–St. Paul hotspots led to the interpretation that they must be genetically related [e.g., *Saunders et al.*, 1991; *Weis and Frey*, 1991; *Frey and Weis*, 1995; 1996]. Geochronological studies and plate tectonic reconstructions provide temporal and spatial evidence that relate the Ninetyeast Ridge to the long-lived (~120 m.y.) Kerguelen mantle plume [e.g., *Duncan*, 1991; *Royer et al.*, 1991; *Klootwijk et al.*, 1991; *Duncan and Storey*, 1992]. Association of the Amsterdam–St. Paul hotspot to the Ninetyeast Ridge is supported by the lower paleolatitudes measured on the basaltic cores of the drill sites at the southern end of the ridge compared to the other drill sites on the ridge [*Klootwijk et al.*, 1991], and the existence of a volcanic chain connecting the southern end of the ridge and the northeast part of the Amsterdam–St. Paul plateau (Figure 4.1). This volcanic trail may be an older trace of the Amsterdam–St. Paul hotspot [e.g., *Royer and Schlich*, 1988]. The activity of the Amsterdam–St. Paul hotspot is considerably more recent than that of Kerguelen [*Nicolaysen et al.*, 2000]. Although volcanism on the Amsterdam–St. Paul plateau is younger than 5 Ma [*Scheirer et al.*, 2000], it is possible that volcanic activity of Amsterdam–St. Paul started as early as ~40–45 Ma, a time period when the newly formed Southeast Indian Ridge separated Broken Ridge from the Kerguelen Plateau, and when the southern end of the Ninetyeast Ridge formed [e.g., *Mutter and Cande*, 1983; *Munschy et al.*, 1992; *Frey and Weis*, 1996].

A deep-seated origin for the long-lived Kerguelen mantle plume is supported by recent tomographic studies [e.g., *Montelli et al.*, 2004, 2006]. Recent geochemical studies have shown a compositional distinction between the volcanic products of the Kerguelen

plume head and tail [e.g., *Mattielli et al.*, 2002; *Neal et al.*, 2002; *Ingle et al.*, 2003; *Weis and Frey*, 2002]. The Kerguelen plume head source is, at present, best represented by the compositions of the Cretaceous basalts recovered on Site 1138, ODP Leg 183, [*Neal et al., 2002*; *Ingle et al.*, 2003], whereas the Kerguelen plume tail source is best represented by the compositions ca. 24 Ma mildly alkalic basalts from Mont Crozier on the Courbet Peninsula of the Kerguelen Archipelago [*Mattielli et al.*, 2002; *Weis and Frey*, 2002; *Ingle et al.*, 2003; D. Weis, unpublished data]. The distinct isotopic compositions of these components are not related by radiogenic ingrowth in the source (red arrows; Figures 4.11 to 4.13). Instead they reflect distinct heterogeneities intrinsic to the Kerguelen plume source [e.g., *Neal et al., 2002*; *Ingle et al.*, 2003]. Similarly, the Amsterdam–St. Paul mantle plume is likely to be compositionally heterogeneous in space and time [*Doucet et al.*, 2004; *Nicolaysen et al.*, 2007]. Evidence for this is based on the isotopic differences between the young Amsterdam and St. Paul volcanoes that were interpreted as resulting from sampling of different chemical domains present within the Amsterdam–St. Paul mantle plume itself [*Doucet et al.*, 2004].

The isotopic compositions of the Ninetyeast Ridge basalts generally plot between the compositional fields defined by basalts from the Southern and Central Kerguelen Plateaus and the Kerguelen Archipelago / Amsterdam and St. Paul islands (Figures 4.11 to 4.13). The Pb isotope ratios of the ~82 Ma and ~58 Ma basalts from Sites 758 and 757, respectively, overlap for the most part with those of the (29 to <1 Ma) basalts from the Kerguelen Archipelago [e.g., *Weis et al.*, 1998; *Doucet et al.*, 2002; *Frey et al.*, 2002b] and <1 Ma basalts from Heard Island [*Barling and Goldstein*, 1990, *Barling et al.*, 1994]. Their Sr, Hf, and Nd isotopic compositions are mostly intermediate between the more enriched compositions of the Kerguelen Archipelago and the compositions observed today on basalts from Amsterdam Island [*Doucet et al.*, 2004]. The ~43 Ma old basalts from Site 756 have Pb-Sr-Hf-Nd isotopic compositions that cluster close to those of the recent (<0.04 Ma) basalts from St. Paul island [*Doucet et al.*, 2004] (Figures 4.11 to 4.13). The intermediate isotopic compositions of the Ninetyeast Ridge basalts relative to the volcanic products of the Kerguelen mantle plume and Amsterdam-St. Paul hotspot are consistent with the Ninetyeast Ridge being related to volcanic activity of these two hotspot systems.

Figure 4.12. Variations of (a) $^{87}Sr/^{86}Sr_i$ and (b) $^{176}Hf/^{177}Hf_i$ with $^{206}Pb/^{204}Pb_i$ for the Ninetyeast Ridge basalts compared to other Indian Ocean basalts. Data sources for compositional fields are as indicated in Figure 4.11. plus: Heard Island (Barling et al. unpublished, 2002); Réunion [*Albarède et al.*, 1997b; *Pietruszka et al.*, 2009]. In both diagrams, grey lines with arrows represent the mixing trajectories between a common mantle component of compositions intermediate to those of C and Fozo and enriched mantle compositions produced by incorporation of: 1) clastic sediments derived from upper continental crust, to produce compositions similar to EM-2 (after *Chauvel et al.* [1992]); 2) lower continental crust to produce compositions similar to EM-1 (after *Escrig et al*. [2004], and *Meyzen et al*. [2005]); 3) 1.5–2 Ga altered oceanic crust (90%) plus pelagic sediments (10%) to produce compositions similar to EM-1 (after *Rehkämper and Hofmann* [1997], and *Kempton et al.* [2002]); and 4) a mixture of altered oceanic crust and pelagic sediments (90%) plus lower continental crust (10%) deep into the mantle source of OIB (after *Willbold and Stracke* [2006; 2010]). Data sources for the used compositions are as follows: old altered oceanic crust, *Rehkämper and Hofmann* [1997], and *Stracke et al*. [2003]; clastic sediments, *Plank and Langmuir* [1998], and *Chauvel et al*. [2008]; pelagic sediments, *Rehkämper and Hofmann* [1997], and *Kempton et al*. [2002]; lower continental crust (Proterozoic Eastern Ghats Belt, India), *Rickers et al*. [2001]. Tick marks on mixing trends correspond to 10% increments.
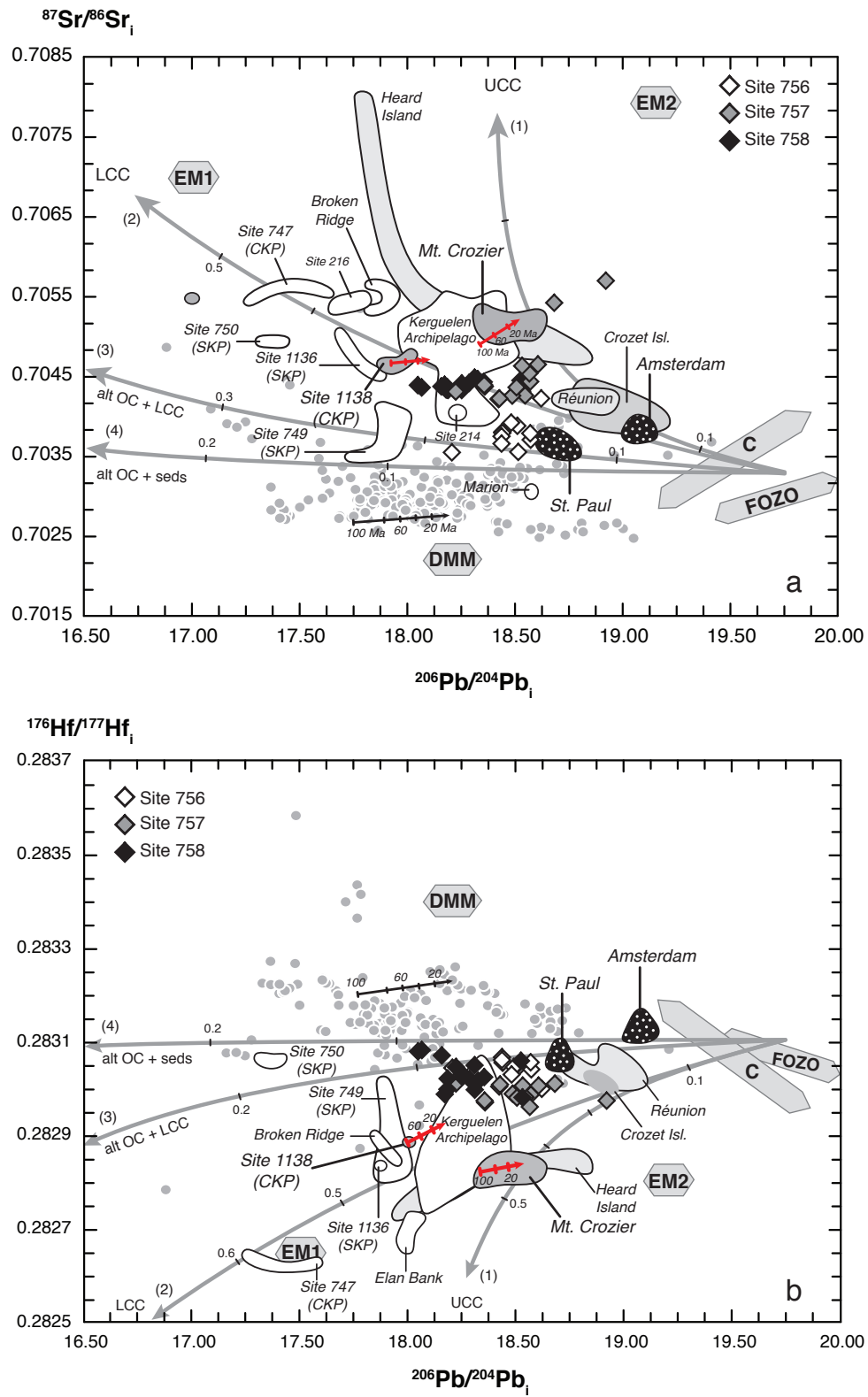
Figure 4.12.

However, despite the compositional similarities between the Ninetyeast Ridge basalts and the volcanic products of both Kerguelen and Amsterdam-St. Paul mantle plumes, simple mixing of the compositions measured to date within these hotspot systems cannot explain the isotopic variability of the Ninetyeast Ridge basalts. The calculated mixing arrays do not indicate direct mixing between any of the potential components (Figures 4.11 to 4.13). Instead they indicate mixing between components of intermediate compositions. This may be because the mantle source(s) sampled by the Ninetyeast Ridge are compositionally more complex than previously assumed. This complexity is also evidenced by the distinct isotopic compositions of the volcanic products of varying age associated with the Kerguelen and Amsterdam-St. Paul mantle plumes. Hence, to assume a Kerguelen and/or Amsterdam–St. Paul mantle plume origin for the Ninetyeast Ridge implies that these mantle plumes are compositionally heterogeneous in time and space, having components that are common and others that are not.

4.7.2. Implications for the Source of Indian Ocean Basin Volcanic Rocks and the Dupal Anomaly

The geochemical heterogeneity observed among ocean island basalts (OIB) is commonly assumed to derive from melting of distinct mantle components or some mixture of these [e.g., *White*, 1985; *Zindler and Hart*, 1986; *Hart et al.*, 1992; *Hanan and Graham*, 1996; *Stracke et al.*, 2005; *Willbold and Stracke*, 2006; 2010]. Basalts from the Ninetyeast Ridge show a marked Dupal signature (high $^{87}Sr/^{86}Sr$, and high $^{207}Pb/^{204}Pb$ and $^{208}Pb/^{204}Pb$ for a given $^{206}Pb/^{204}Pb$), characteristic of oceanic basalts from the Indian Ocean [*Hart*, 1984]. Relative to Indian MORB, the ~82 – 43 Ma basalts from the Ninetyeast Ridge are enriched in $^{208}Pb/^{204}Pb$, $^{207}Pb/^{204}Pb$ and $^{87}Sr/^{86}Sr$, and depleted in $^{176}Hf/^{177}Hf$ and $^{143}Nd/^{144}Nd$ (Figures 4.11 to 4.13). Their Pb-Hf-Sr-Nd isotopic compositions are very similar to those of other ocean island basalts within the Indian Ocean (Figures 4.11 to 4.13). The compositional trends defined by the individual Ninetyeast Ridge sites are to some extent part of larger trends containing other Indian Ocean island basalts, which suggests that any local mixing is part of a broader regional scale of mixing between several distinct components in the Indian Ocean
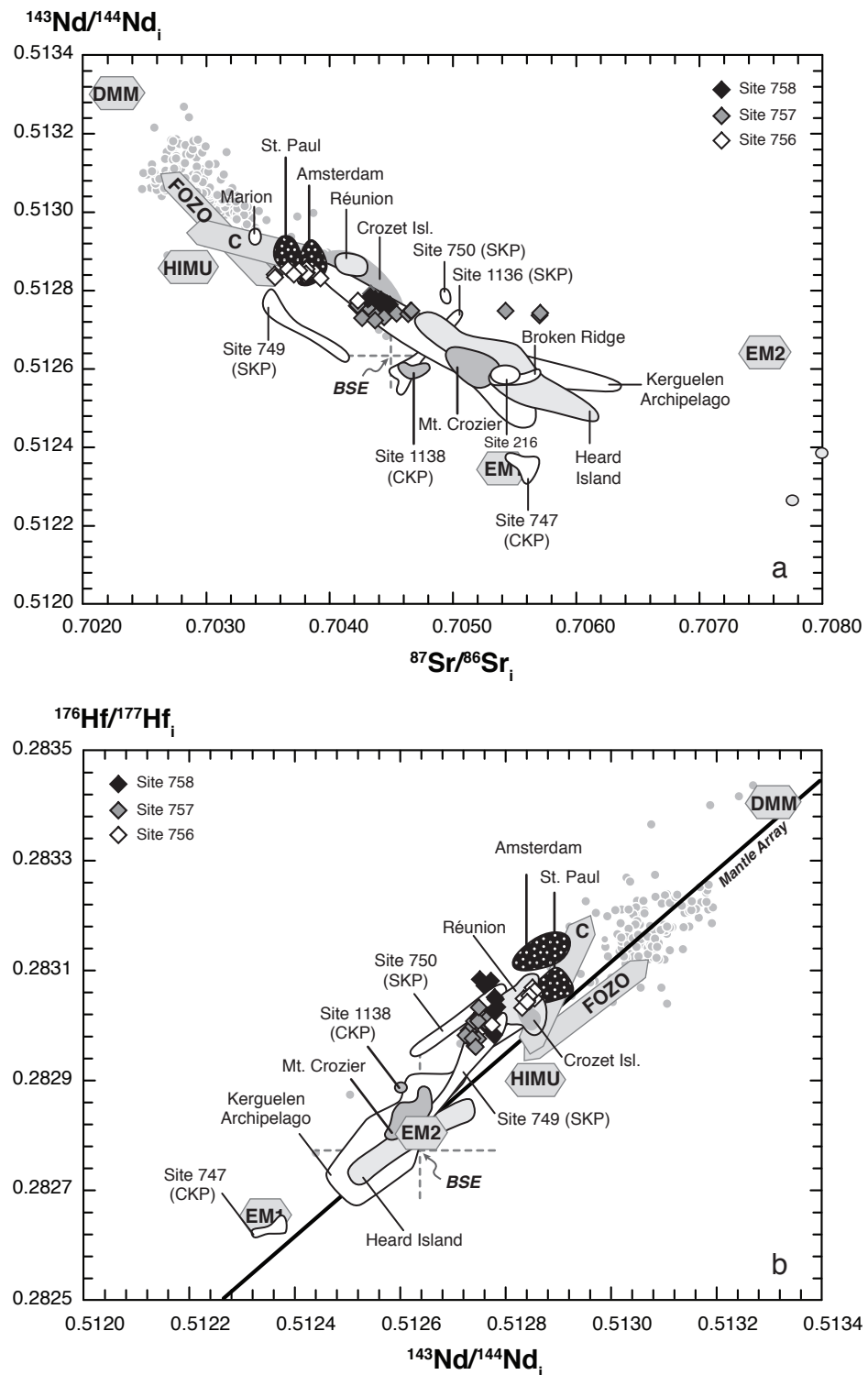
Figure 4.13. (a) $^{87}Sr/^{86}Sr_i$ versus $^{143}Nd/^{144}Nd_i$ and (b) $^{143}Nd/^{144}Nd_i$ versus $^{176}Hf/^{177}Hf_i$ of the Ninetyeast Ridge basalts compared to other Indian Ocean basalts and to the global isotopic end-members. Data sources for compositional fields are as described in Figures 4.11. and 4.12. Mantle array as defined by *Chauvel et al.* [2008].

mantle. Specifically, the close isotopic similarity of the Ninetyeast Ridge basalts to those from Réunion, Crozet, Amsterdam and St. Paul islands, indicates derivation from compositionally similar deep sources.

Together with other Indian Ocean basalts, the Ninetyeast Ridge samples converge at isotopic compositions that are intermediate between the values for the common components "C" [*Hanan and Graham*, 1996; *Hanan et al.*, 2004] and FOZO [*Hart et al.*, 1992; *Stracke et al.*, 2005]. From these common compositions, Indian Ocean OIB form arrays that fan out towards enriched mantle (EM) compositions that are mostly intermediate to those of EM-2 (high $^{87}Sr/^{86}Sr$, variable $^{208}Pb/^{204}Pb$, intermediate and almost constant $^{206}Pb/^{204}Pb$ and low $^{143}Nd/^{144}Nd$ and $^{176}Hf/^{177}Hf$) and EM-1 (high $^{87}Sr/^{86}Sr$ and $^{208}Pb^*/^{206}Pb^*$, low $^{206}Pb/^{204}Pb$, and lower $^{143}Nd/^{144}Nd$ and $^{176}Hf/^{177}Hf$) (Figures 4.11 to 4.13). Recycling of upper continental crust material in the form of clastic marine sediments together with altered oceanic crust via subduction is considered to be the mechanism responsible for the trace element and isotopic compositions of EM-2 basalts [*Weaver*, 1991; *Chauvel et al.*, 1992; *Willbold and Stracke*, 2006; *Jackson et al.*, 2007; *Porter and White*, 2009]. However, the type of recycled material leading to EM-1, Dupal-like, source characteristics is the subject of considerable debate. Any plausible source capable of generating EM-1-like isotopic compositions must have had high time-integrated Rb/Sr, Th/U and low U/Pb, Sm/Nd and Lu/Hf. Possible candidates of recycled material in the EM-1 source include: pelagic sediment with oceanic crust [e.g., *Weaver*, 1991; *Chauvel et al.*, 1992; *Eisele et al.*, 2002], incorporation and dispersal of delaminated metasomatized subcontinental lithospheric mantle prior to continental rifting [e.g., *Storey et al.*, 1992; *Mahoney et al.*, 1996; *Douglass et al.*, 1999; *Borisova et al.*, 2001; *Kempton et al.*, 2002; *Janney et al.*, 2005; *Geldmacher et al.*, 2008; *Goldstein et al.*, 2008], recycled lower continental crust by delamination [*Escrig et al.*, 2004; *Hanan et al.*, 2004; *Meyzen et al.*, 2005] or by subduction erosion [*Willbold and Stracke*, 2006; 2010].

The isotopic compositions of most Ninetyeast Ridge basalts are distributed close to the EM-1 trend together with basalts from the Kerguelen and Amsterdam Plateaus and the Afanasy-Nikitin Rise. However, the intermediate character of the enriched end-member of

the Indian Ocean OIB array formed by basalts from Heard Island, Kerguelen Archipelago, Réunion, Crozet, and Amsterdam islands, led *Barling and Goldstein* [1990] to question the compositional individuality of the EM components. The authors proposed that EM-1 and EM-2 represent extreme compositions of a continuous spectrum of isotopic compositions that reflect mantle contaminated by recycled continental crust material of different compositions into the OIB source. Models that assume a lithospheric mantle or lower continental crust material contribution to the EM-1 component advocate for its shallow incorporation into the asthenospheric mantle. Alternatively, *Willbold and Stracke* [2006, 2010] provide a model where upper and lower continental crust are concomitantly recycled together with oceanic lithosphere, deep into the OIB source, at erosive plate margins, and thus generate the multiple EM-type trace element and isotopic signatures observed in OIB.

In the Indian Ocean basin, EM-1-like compositions are found in both OIB and MORB, leading to the question of whether this ubiquitous isotopic anomaly in Indian Ocean basalt results from a deep or shallow origin. Additional questions are whether or not the EM-1-like signatures of Indian Ocean OIB and MORB result from the presence of the same contaminant into their respective sources; and if they are related to the same process(es). If lower continental crust eroded during subduction is the material responsible for EM-1-like signatures [*Willbold and Stracke*, 2006; 2010], and assuming that this material is likely to be recycled into the upper mantle as well as into the deeper mantle [e.g., *Clift and Vannuchi*, 2004], EM-1 signatures in MORB should be randomly distributed in other oceans and not be restricted to the Indian Ocean, South Atlantic Ocean, and the Gakkel Ridge in the Arctic Ocean [e.g., *Hart*, 1984; *Escrig et al.*, 2004; *Regelous et al.*, 2009; *Goldstein et al.*, 2008]. This suggests that although the EM-1 characteristics in OIB and MORB in the Indian Ocean may be related to the same type of material, they are generated by different processes. A shallow origin, by delamination of subcontinental lithospheric mantle and lower continental crust may explain the EM-1-like compositions of MORB in young oceans [*Escrig et al.*, 2004; *Hanan et al.*, 2004; *Meyzen et al.*, 2005; *Janney et al.*, 2005; *Geldmacher et al.*, 2008; *Goldstein et al.*, 2008], whereas a deep origin by deep recycling of upper and lower

continental crust may explain the EM characteristics of OIB [*Willbold and Stracke*, 2006; 2010].

There is evidence for interaction and incorporation of continental material at shallow depth by basalts related to the Kerguelen plume head at the onset of continental rifting. Depletion of Nb, Ta and Th relative to primitive mantle concentrations is found in some samples from the Kerguelen Plateau and Broken Ridge, which together with their extreme isotopic compositions indicates contamination by subcontinental lithospheric mantle or lower continental crust [e.g., *Mahoney et al.*, 1995; *Frey et al.*, 2002a]. In addition, garnet-biotite gneiss and fluvial conglomerates were recovered at Elan Bank, Site 1137 [*Weis et al.*, 2001; *Ingle et al.*, 2002]. In contrast, basalts formed in intraplate settings (Ninetyeast Ridge and Kerguelen Archipelago; *Frey et al.* [2002b]; *Weis et al.* [2001]) lack such evidence of shallow-level contamination. Although the isotopic signatures of the Ninetyeast Ridge basalts could be consistent with some lower crust contribution (Figures 4.11 to 4.13), they do not display the diagnostic Nb and Ta depletions [e.g., *Frey et al.*, 1991; *Frey and Weis*, 1995]. According to Late Cretaceous plate reconstructions, the Ninetyeast Ridge did not form close to continental plate margins [*Royer et al.*, 1991; *Müller et al.*, 1993; *Steinberger*, 2000]. This provides a geological explanation for the lack of shallow-level contamination and indicates that any isotopic continental "flavour" in the Ninetyeast Ridge basalts is inherited from its deep source. The Pb, Hf, Sr and Nd isotopic compositions of the Ninetyeast Ridge basalts are best explained by contribution of a mixture of pelagic sediments and lower continental crust recycled together with altered oceanic crust into its deep and compositionally heterogeneous mantle source.

4.8. Conclusions

High-precision Pb-Hf-Sr-Nd isotopic analysis of the basalts recovered from the 5000 km long submarine Ninetyeast Ridge during ODP Leg 121 (Sites 756, 757 and 758) define tight compositional fields for each site and are inconsistent with an age-progressive isotopic evolution along the ridge. The distinct compositional fields defined by the Ninetyeast Ridge basalts reflect mixing between components with relatively depleted and enriched signatures.

Indian asthenospheric mantle does not contribute to the depleted component, which instead is likely to be inherited from a deep mantle source. The Ninetyeast Ridge basalts have isotopic compositions intermediate to those of the volcanic products of the Kerguelen and Amsterdam-St. Paul hotspots, yet simple mixing of the compositions measured to date within these hotspot systems cannot explain this isotopic variability. A Kerguelen and/or Amsterdam–St. Paul mantle plume origin for the Ninetyeast Ridge implies that the plume sources are compositionally heterogeneous in time and space. At a regional scale, the isotopic variability of the Ninetyeast Ridge basalts, together with other Indian OIB, is part of larger mixing trends between several distinct components in the Indian Ocean. Most of the isotopic variability of Indian OIB can be accounted by mixing between the common mantle component (C or Fozo) and enriched mantle compositions (mostly between EM-1 and EM-2). The EM–1, Dupal-like characteristics of Indian MORB and Indian OIB that formed at the onset of continental rifting can be ascribed to shallow level contamination by lower continental crust and/or subcontinental lithospheric mantle and some upper crust material. In contrast, no evidence for such shallow contamination is found in the Ninetyeast Ridge basalts and other OIB formed in intraplate setting. The current isotopic and trace element dataset of the Ninetyeast Ridge basalts is not consistent with both the entrainment of Indian mantle asthenosphere into its source, and the presence of upper continental crustal material, which rules out the possibility of shallow contamination. Instead, the EM-1-like characteristics of the Ninetyeast Ridge basalts are best explained by some contribution of lower continental crust and pelagic sediments in their deep mantle source.

CHAPTER 5

Pb-Sr-Nd Systematics of the Early Mauna Kea Shield Phase and Insight Into the Deep Mantle Beneath the Pacific Ocean

5.1. Synopsis

In this study, we present high-precision Pb, Sr and Nd isotopic compositions of 40 basalts recovered during the final drilling phase of the Hawai'i Scientific Drilling Project (HSDP2-B and -C). The samples are from the last 408 metres of the 3500 metre-long drill core and represent ages >650 ka in the stratigraphic record of Mauna Kea volcano. Two sample groups can be distinguished based on their isotopic variability compared to the rest of the core. Over a depth interval of 210 m (3098.2 to 3308.2 m) the samples show very restricted Pb, Sr and Nd isotopic variation (e.g., 5x and 3x smaller variation for $^{206}Pb/^{204}Pb$ and $^{86}Sr/^{87}Sr$, respectively, than observed for younger samples). Samples from the bottom 170 metres show the largest range of $^{206}Pb/^{204}Pb$ (18.304–18.693) and $^{208}Pb/^{204}Pb$ (37.923–38.270) compared to the rest of the core. These older lavas extend the $^{206}Pb/^{204}Pb$ and $^{208}Pb/^{204}Pb$ record of Mauna Kea both to significantly more radiogenic values, similar to the isotopic compositions shown by "ancestral" Kilauea lavas, and to significantly less radiogenic values, similar to those observed in Mauna Kea and Kohala post-shield lavas. The two sample groups identified also define two tight arrays in diagrams of $^{208}Pb/^{204}Pb$ - $^{206}Pb/^{204}Pb$. The majority of these older Mauna Kea basalts plot along the "Kea-mid8" array [*Eisele et al.*, 2003] that encompasses ~75% of the Mauna Kea drill core. Some samples from the two groups, characterized by low-SiO_2 lie within the "Kea-hi8" array, indicating that a component characterized by high $^{208}Pb*/^{206}Pb*$, was already being sampled early in Mauna Kea's history. Compared to the previous 3100 m of drill core, the more restricted Pb, Sr and Nd isotopic compositions of the samples recovered during HSDP2-B indicate sampling of a more homogeneous source domain during the time interval represented by the eruption of these basalts. Similar to Mauna Loa, the earlier stages (older lavas) of Mauna Kea volcanism are isotopically more variable than subsequent stages. Overall, the isotopic heterogeneity in Mauna Kea shield lavas can be explained by mixing variable proportions of four isotopically distinct components intrinsic to the Hawaiian mantle plume. These components are: the more radiogenic "Kea" component, a high $^{208}Pb*/^{206}Pb*$ (producing low-SiO_2 basalts) component similar to Loihi, and two components with less radiogenic Pb isotopic compositions. Besides being a common and long-lived component in the Hawaiian

plume, the isotopic similarities of "Kea" to the common mantle component "C", and the fact that it is positioned at the convergence between other Pacific Ocean island basalt groups, suggests that "Kea" is a common composition in the deep mantle beneath the Pacific Ocean basin.

5.2. Introduction

The age-progressive Hawaiian-Emperor volcanic chain in the Pacific Ocean is the classic example of intraplate hotspot volcanism attributed to a deep-seated mantle plume [e.g., *Morgan*, 1971; *Courtillot et al.*, 2003; *DePaolo and Weis*, 2007]. This simple tectonic setting, together with the distant location from plate margins and large rates of magma flux, make Hawaiian volcanoes one of the best places to study the chemical evolution and structure of mantle plumes and consequently of the deep mantle [e.g., *DePaolo et al.*, 2001; *Bryce et al.*, 2005]. As the Pacific plate moves across the Hawaiian plume, at a velocity of 9–10 cm/yr, individual volcanoes grow and evolve through several stages (pre-shield, shield, post-shield, and a much later one, rejuvenated) as they sample different areas of the melting-region of the plume [e.g., *Clague and Dalrymple*, 1987]. The geochemistry of continuous eruptive sequences of individual volcanoes hence provides a record of the geochemical time-series of the melting region of the plume [e.g., *Hauri et al.*, 1996; *Lassiter et al.*, 1996; *DePaolo et al.*, 2001; *Bryce et al.*, 2005].

Isotopic compositional variations occur over various time scales during the eruptive life of a Hawaiian volcano. Both short-term (decadal to centennial) and long-term (millennial) isotopic variations have been recognized in the shield lavas of Hawaiian volcanoes [e.g., Kilauea, *Pietruska and Garcia*, 1999; *Marske et al.*, 2007; 2008], Mauna Loa, *DePaolo et al.*, 2001, Mauna Kea, *Eisele et al.*, 2003; *Kurz et al.*, 2004, Kauai, *Salters et al.*, 2006; *Fekiacova et al.*, 2007], all within the larger time scale (≥1Myr) of volcano growth and compositional evolution [e.g., *Frey et al.*, 1990; *Garcia et al.*, 2006]. The ~3500 km long volcanic core recovered by the Hawaii Scientific Drilling Project (HSDP) constitutes the longest stratigraphically controlled record of the magmatic output of a single

long-lived volcano sampled thus far. The analysis of the temporal geochemical covariations within the first ~3100 m of core has allowed for the identification of compositional heterogeneities within the Hawaiian plume as well as their maximum and minimum sizes [e.g., *Blichert-Toft et al.*, 2003; *Eisele et al.*, 2003; *Abouchami et al.*, 2005; *Bryce et al.*, 2005]. In addition, direct comparison with lavas from other Hawaiian volcanoes erupted at equivalent stages of volcano growth has led to the formulation of new models for the chemical structure (i.e., distribution of heterogeneities within the plume conduit) of the Hawaiian plume and its deep mantle source [e.g., *DePaolo et al.*, 2001; *Blichert-Toft et al.*, 2003; *Kurz et al.*, 2004; *Abouchami et al.*, 2005; *Bryce et al.*, 2005; *Farnetani and Hofmann*, 2010]

The last ~400 m of the HSDP sampled a series of submarine tholeiitic basalts erupted in the early shield-building stage of Mauna Kea. In this study, we use the Pb, Sr, and Nd isotopic analysis of 40 whole rock samples to identify short-term isotopic fluctuations that reflect compositional heterogeneities sampled in the early phase of growth of Mauna Kea. We examine the >650 kyr isotopic record of the magmatic history of Mauna Kea to evaluate both the short- and long-term isotopic variations within the core, and provide constraints on the chemical structure of the Hawaiian mantle plume and deep Pacific mantle.

5.3. Hawaii Scientific Drilling Project: Geological Setting and Core Stratigraphy

The Hawaii Scientific Drilling Project was a multidisciplinary international scientific effort to test the models of growth and chemical evolution of Hawaiian volcanoes as they drift over the mantle plume by systematically sampling a continuous stratigraphic sequence of lavas from a large Hawaiian volcano [*Stolper et al.*, 1996; *DePaolo et al.*, 2001]. The HSDP drill sites were located on the northeast side of the island of Hawaii, on the east flank of the Mauna Kea volcano, near Hilo Bay in an abandoned rock quarry adjacent to the Hilo International Airport (Figure 5.1). Mauna Kea was the targeted volcano as it is the youngest Hawaiian volcano that has completed its life cycle of major growth stages (pre-shield, shield,
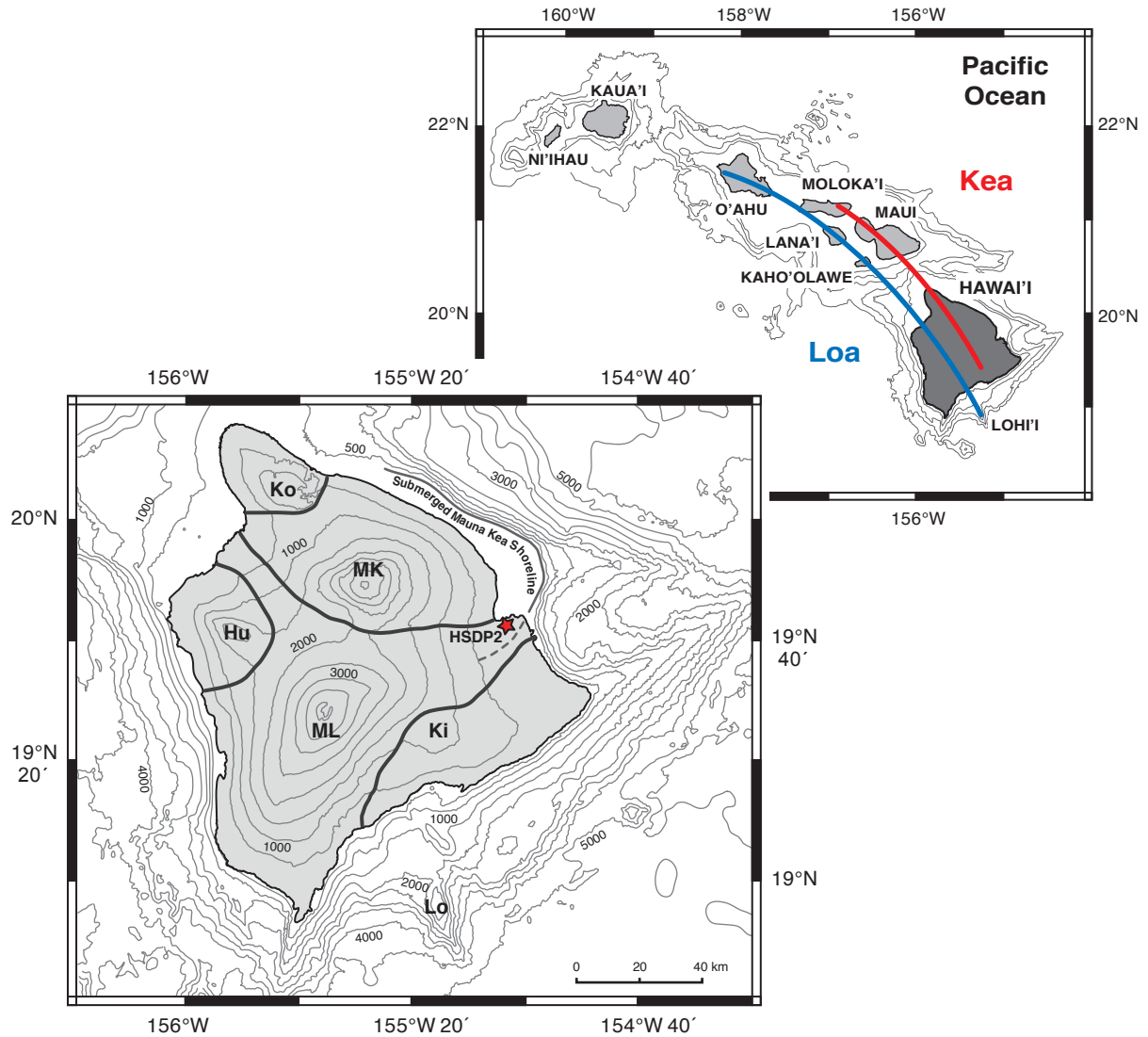
Figure 5.1. Location maps of the Hawaiian Islands and HSDP2 drill site. (a) Overview map of the Hawaiian Islands, showing the Loa and Kea volcano trends. (b) Enlarged view of the topography and bathymetry (500 m interval contours) of the island of Hawai'i (maps drawn using GeoMapApp: http://www.geomapapp.org). The boundaries of the five volcanoes (Ko, Kohala; Hu, Hualalai; MK, Mauna Kea; ML, Mauna Loa; Ki, Kilauea) are shown, as well as the submerged shoreline of Mauna Kea. The location of the Hawai'i Scientific Drilling Project deep hole (HSDP2) drilled during 1999 and 2004-2007 is identified by the red star, near Hilo Bay. The Loihi seamount (Lo) occurs to the southeast of the Big Island.

post-shield) of a typical Hawaiian volcano [e.g., *Clague and Dalrymple*, 1987; *Stolper et al.*, 1996; *Garcia et al.*, 2007; *Stolper et al.*, 2009]. At this location, almost 250 metres of Mauna Loa lavas overlie Mauna Kea lavas and thus also allowed for a comparative study of the lavas of the two consecutive volcanoes.

The first phase of the project (HSDP1) was carried out in 1993 with a "pilot hole" to a depth of 1052 metres below sea level (mbsl) to evaluate the feasibility of the project. The success of the HSDP1 [e.g., *Stolper et al.*, 1996] led to the deep drilling of the HSDP2, a ~3500 metre long core that was recovered in two phases over a total period of almost five years. The main drilling phase of the HSDP2 was carried out throughout 1999, during which time the hole reached 3110 metres below sea level (mbsl) [*Garcia et al.*, 2007]. The second drilling phase was accomplished in two stages. Starting in 2003 with the enlargement of the hole's diameter, coring began in late 2004 and proceeded until early 2005 (phase 2-B). Coring restarted in late 2006 and reached completion in early 2007 at 3508 mbsl (phase 2-C) [*Stolper et al.*, 2009].

On the basis of observed contacts and/or variations in mineralogical, lithological, and structural features, a total of 389 lithological units were identified within the HSDP2 core [*Stolper et al.*, 2009]. Five depth zones were recognized (Figure 5.2): (1) *subaerial Mauna Loa lavas* (surface to 246 mbsl), mostly composed of tholeiitic flow units, all with Mauna Loa geochemical characteristics, and some interspersed sedimentary units [*Rhodes and Vollinger*, 2004; *Garcia et al.*, 2007, *Stolper et al.*, 2009]; (2) *subaerial Mauna Kea lavas* (246 to 1079 mbsl), composed of interbedded alkalic and tholeiitic flow units belonging to Mauna Kea's Hamakua volcanic series formed during its post-shield phase (down to ~340 mbsl), and by tholeiitic flow units interspersed with some sedimentary units, marking the end of the shield phase of Mauna Kea's volcanic cycle [*Rhodes and Vollinger*, 2004]; (3) *shallow submarine Mauna Kea lavas* (1079 to 1984 mbsl), mostly comprising hyaloclastite debris flows and few massive tholeiitic flow units; (4) *deep submarine Mauna Kea lavas* (1984 to 3098 mbsl), mostly composed of pillow lavas and few hyaloclastite and massive flow units, all of tholeiitic composition; and (5) *submarine Mauna Kea lavas from the final phase of*
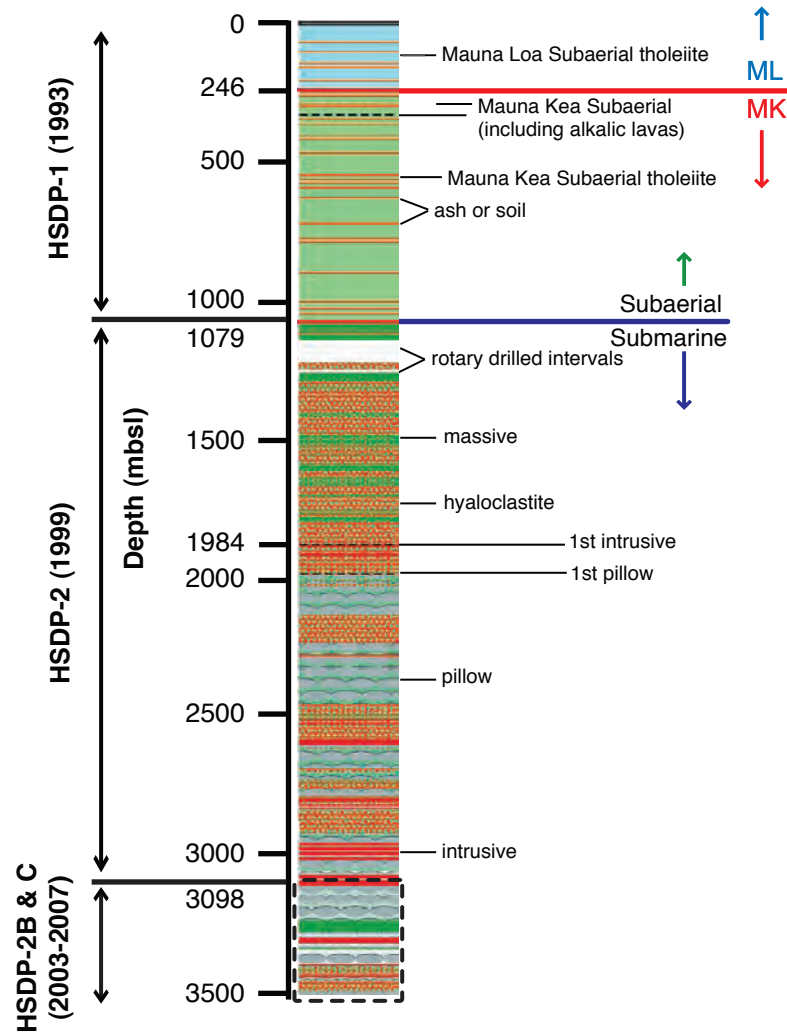
Figure 5.2. Simplified lithologic column of the HSDP2 drill core (adapted from *Stolper et al.* [2009]). The different lithologies are represented by different patterns as indicated. The depth scale is in metres below sea level (mbsl) and key depths are identified: boundary between Mauna Loa (ML) and Mauna Kea (MK) lavas; transition between subaerial and submarine MK lavas; first occurrence of intrusive rocks and pillow lavas. The dashed box highlights the stratigraphic levels drilled during phases B and C of the HSDP2, from where the samples analyzed in this study were recovered.

drilling (3098 to 3508 mbsl). In this final phase of drilling (HSDP2–B and –C), 44 flow and intrusive units were identified, consisting primarily of submarine pillow lavas (~60%), with lesser amounts of hyaloclastites (~17%), massive volcanic units (~12%), pillow breccias (~10%), and intrusive units (~1%) [*Stolper et al.*, 2009].

The youngest dated Mauna Kea sample in the core of the HSDP2 main phase, an alkalic basalt at ~277 mbsl, has a $^{40}Ar/^{39}Ar$ age of 236 ± 16 kyr and the deepest dated sample, at a depth of 2789 mbsl, has a $^{40}Ar/^{39}Ar$ age of 683 ± 82 kyr [*Sharp and Renne*, 2005]. Assuming a linear fit to the $^{40}Ar/^{39}Ar$ ages, *Sharp and Renne* [2005] determined mean accumulation rates of ~9 m/kyr and ~0.9 m/kyr for the shield and post-shield sequences, respectively, over the 400 kyr of volcanism recorded by the ~2.7 km thick section of Mauna Kea basalts. Based on the linear shield lavas accumulation rates, the bottom of the main phase of the HSDP2 drill core was estimated to be ~635 kyr [*Sharp and Renne,* 2005]. No ages have been determined on samples from the last drilling phase. Assuming the same shield lavas accumulation rates, the ages of these deeper samples are inferred to range between ~647 and ~694 kyr (Table 5.1).

5.4. Previous Geochemical Results from the HSDP2

The samples within the Mauna Kea section of the HSDP2 core show a bimodal distribution of their SiO_2 contents (<50 wt% and ≥50 wt%), evident both from whole rock XRF compositions [*Rhodes and Vollinger*, 2004] and from glass electron microprobe analysis [*Stolper et al.*, 2004; 2009]. Different correlations between SiO_2 and glass volatile content, incompatible trace element concentrations and isotope ratios led to the division of the HSDP core into distinct geochemical groups [*Huang and Frey*, 2003; *Rhodes and Vollinger*, 2004; *Stolper et al.*, 2004]. Samples in the high-SiO_2 group are tholeiitic basalts and picrites. They are distributed throughout the Mauna Kea shield section, representing the majority (60 %) of basalts from Mauna Kea [*Huang and Frey*, 2003; *Rhodes and Vollinger*, 2004; *Stolper et al.*, 2004; 2009]. High-SiO_2 samples typically have high Zr/Nb values (11–13), corresponding to the type-1 magmas of *Rhodes and Vollinger* [2004]. They are

Table 5.1. Geochemical Characteristics of Basalts Sampled from the Last Drilling Phases (-B and -C) of the HSDP2 Core

Sample [Run-Interval-Unit-Core Box]	Depth (mbsl)[a]	Inferred Age[b]	Lithology[c]	Chemical Type[d]	SiO_2 (wt%)	MgO (wt%)	Na_2O (wt%)	K_2O (wt%)	P_2O_5 (wt%)	LOI[e] (wt%)	A.I.[f]	Mg#[g]	Zr/Nb	Zr/Y
HSDP-2b														
R6 - 0.85-1.2 - 2A - 1	3097.7	647.3	pillows	MK 1	50.3	7.75	2.39	0.48	0.25	0.75	-1.30	0.58	11.1	6.0
R6 - 2.15-3.0 - 3 - 1	3098.2	647.4	massive intrusive	MK 3	47.3	12.7	1.91	0.95	0.20	5.65	-0.19	0.68	10.1	5.6
R8 - 0.15-0.7 - 2B - 3	3102.4	647.9	pillows	MK 1	50.4	7.96	2.33	0.31	0.24	0.91	-1.54	0.59	11.2	5.9
R10 - 4.35-4.7 - 2D - 6	3109.4	648.7	pillows	MK 1	50.4	7.71	2.37	0.39	0.25	0.72	-1.43	0.58	11.1	5.9
R11 - 5.3-5.7 - 4 - 7	3111.5	648.9	pillow breccia	MK 1	50.4	7.72	2.35	0.37	0.25	0.86	-1.46	0.58	11.1	5.9
R13 - 0.1-0.5 - 5 - 8	3115.2	649.4	pillows	MK 1	50.2	7.77	2.49	0.33	0.25	-4.46	-1.32	0.58	11.2	5.9
R16 - 5.2-6.0 - 7 - 11	3122.5	650.2	pillows	MK 1	50.3	8.01	2.35	0.31	0.25	0.92	-1.49	0.58	11.2	6.0
R30 - 4.25-5.2 - 7 - 18	3141.2	652.4	pillows	MK 1	50.3	8.16	2.30	0.30	0.24	1.10	-1.44	0.59	11.1	5.9
R51 - 2.4-3.6 - 9 - 26	3160.8	654.7	pillows	MK 1	50.4	8.03	2.46	0.36	0.25	0.80	-1.37	0.58	11.5	5.9
R56 - 1.0-1.5 - 10 - 30	3171.1	655.8	pillow breccia	MK 1	50.2	7.86	2.27	0.34	0.25	0.86	-1.53	0.58	11.1	5.9
R57 - 5.0-5.9 - 11 - 31	3173.4	656.1	pillows	MK 1	50.2	7.91	2.28	0.33	0.25	1.04	-1.51	0.58	11.2	5.9
R60 - 7.6-8.4 - 13 - 34	3181.2	657.0	pillows	MK 1	50.4	8.14	2.28	0.37	0.24	0.65	-1.55	0.59	11.5	5.8
R80 - 2.8-3.5 - 13 - 47	3215.5	661.0	pillows	MK 1	50.3	8.00	2.35	0.32	0.23	0.70	-1.50	0.58	11.2	5.8
R93 - 1.4-2.0 - 13 - 56	3234.7	663.2	pillows	MK 1	50.1	7.97	2.35	0.33	0.24	0.75	-1.40	0.58	11.1	5.8
R101 - 4.4-4.9 - 14 - 60	3244.8	664.4	massive volcanic	MK 1	50.3	8.10	2.28	0.40	0.23	0.60	-1.47	0.59	11.3	5.8
R108 - 0.0-0.7 - 14 - 67	3263.9	666.6	massive volcanic	MK 1	50.7	7.42	2.41	0.46	0.26	0.34	-1.42	0.56	11.3	5.9
R112 - 7.1-7.7 - 14 - 72	3277.0	668.1	massive volcanic	MK 1	50.2	7.91	2.35	0.41	0.23	0.45	-1.37	0.58	11.3	5.6
R116 - 6.25-7.2 - 15 - 75	3285.8	669.2	pillows	MK 1	50.4	8.11	2.40	0.28	0.23	0.79	-1.52	0.59	11.3	5.7
R122 - 1.85-2.65 - 17 - 81	3300.1	670.8	pillows	MK 1	50.8	6.60	2.65	0.34	0.27	0.61	-1.34	0.54	11.1	6.0
R125 - 4.9-5.3 -18A - 83	3305.9	671.5	massive intrusive	MK 1	50.4	7.90	2.49	0.33	0.24	0.90	-1.37	0.58	11.2	5.9
R127 - 1.4-2.2 -19B - 85	3308.2	671.8	pillows	MK 4	50.4	6.94	2.42	0.31	0.24	1.14	-1.47	0.55	10.5	6.1
R129 - 5.8-6.5 -20B - 87	3313.5	672.4	massive intrusive	MK 1	49.8	11.7	2.19	0.30	0.20	0.36	-1.46	0.69	12.8	5.6
HSDP-2c														
R149 - 1.2 - 1.6 - 22 - 94	3333.3	674.7	pillows	MK 4	50.7	6.75	2.13	0.36	0.25	0.46	-1.83	0.55	10.9	6.3
R154 - 2.1 - 2.95 - 23 - 96	3339.5	675.4	massive volcanic	MK 1	48.3	15.6	1.78	0.27	0.16	1.10	-1.35	0.73	13.0	5.6
R155 - 2.7 - 3.5 - 23 - 97	3341.4	675.6	massive volcanic	MK 1	47.9	17.4	1.37	0.10	0.18	2.26	-1.79	0.75	12.6	5.9
R158 - 1.75 - 2.10 - 24 - 99	3348.3	676.4	pillow breccia	MK 4	50.8	6.83	1.64	0.30	0.25	0.79	-2.40	0.55	10.8	6.2
R162 - 1.55 - 2.3 - 25 - 101	3353.9	677.1	pillows	MK 4	50.7	6.85	2.10	0.37	0.24	0.76	-1.83	0.55	10.9	6.3
R163 - 2.1 - 2.6 - 26 - 102	3357.0	677.4	hyaloclastite	MK 4	49.6	9.66	1.44	0.31	0.23	0.57	-2.17	0.63	9.7	6.3
R165 - 0.75 - 1.45 - 29 - 103	3359.8	677.7	pillows	MK 4	49.2	9.72	1.87	0.28	0.22	1.18	-1.61	0.63	10.1	6.3
R168 - 3.7 - 4.15 - 30 - 106	3366.3	678.5	pillows	MK 4	49.6	9.61	1.91	0.31	0.22	0.55	-1.68	0.63	10.0	6.3
R176 - 5.93 - 6.5 - 30 - 112	3381.3	680.2	pillows	MK 4	49.5	9.55	1.93	0.34	0.22	0.35	-1.57	0.62	10.2	6.3
R184 - 1.15 - 2.1 - 32 - 121	3400.9	682.5	massive intrusive	MK 3	47.6	12.3	2.06	0.14	0.21	1.82	-0.94	0.67	10.6	5.9
R187 - 0.9 - 1.8, 2.05 - 2.5 - 33 - 123	3405.3	683.0	pillows	ML!	48.6	15.7	1.80	0.16	0.18	0.63	-1.56	0.74	13.0	5.8
R192 - 4.4 - 5.4 - 35 - 127	3418.1	684.5	massive volcanic	MK 1	47.1	20.3	1.36	0.20	0.17	0.32	-1.41	0.78	11.2	6.2
R198 - 0.5 - 1.9 -37A - 133	3435.2	686.5	pillows	MK 4	47.1	20.8	1.32	0.19	0.15	0.35	-1.45	0.79	10.9	5.9
R204 - 1.1 - 1.8 -37E - 140	3453.4	688.6	pillows	MK 4	45.9	24.2	1.24	0.15	0.13	0.29	-1.13	0.81	10.8	5.8
R205 - 7.5 - 8.15 - 40 - 142	3458.4	689.2	pillows	MK 4	45.5	25.4	1.09	0.12	0.12	0.67	-1.15	0.82	11.0	5.8
R210 - 3.3 - 3.95 - 43 - 147	3472.2	690.8	hyaloclastite	ML!	50.4	9.67	2.20	0.30	0.26	0.66	-1.69	0.64	15.1	5.8
R219 - 5.55 - 6.2, 7.25 - 7.7- 44 - 157	3500.9	694.1	pillows	ML!	50.2	9.88	1.57	0.33	0.27	0.87	-2.22	0.64	13.3	6.3
R222 - 8.0 - 8.8 - 45 - 159	3505.7	694.7	pillows	MK 4	50.0	6.89	2.54	0.35	0.26	0.56	-1.14	0.55	10.6	6.3

[a] mbsl = meters below sea level.
[b] Age of the samples infered from the model age curve of *Sharp and Renne* [2005].
[c] Five lithologic types identified by the on-side logging team [*Garcia et al.*, 2007; *Stolper at al.*, 2009].
[d] Chemical Types defined by *Rhodes and Vollinger* [2004], based on SiO_2 content and Zr/Nb.
[d] A.I. = alkalinity index (AI = total alkalis - (SiO_2 x 0.37 - 14.43)) [*Rhodes*, 1996].
[e] LOI = weight loss-on-ignition after 30 min at 1020ºC.
[f] Mg# = Mg/(Mg+Fe) after adjusting Fe^{3+}/total Fe to 0.1 [*Rhodes*, 1996; *Rhodes and Vollinger*, 2004].
All geochemical data presented in this table is from Rhodes et al. (in preparation).

characterized by high $^{208}Pb/^{204}Pb$ [*Eisele et al.*, 2003], $^{176}Hf/^{177}Hf$ [*Blichert-Toft et al.*, 2003], and $^{143}Nd/^{144}Nd$ [*Bryce et al.*, 2005], and low $^{3}He/^{4}He$ [*Kurz et al.*, 2004] and $^{87}Sr/^{86}Sr$ values [*Bryce et al.*, 2005] relative to low-SiO_2 samples. However, some high-SiO_2 basalts are characterized by low Zr/Nb values and have been considered a distinct group, the type-4 magmas of *Rhodes and Vollinger* [2004].

Samples with low SiO_2 contents are found at different levels in the stratigraphy of Mauna Kea, forming discrete groups that differ mostly in elemental abundances and isotopic compositions. The intercalated alkalic and tholeiitic basalts from the post-shield group, at the top of Mauna Kea section, are characterized by low SiO_2 and high TiO_2 contents, high incompatible element abundances, and high La/Yb, Sm/Yb, low Zr/Nb [*Huang and Frey*, 2003; *Rhodes and Vollinger*, 2004]. Their isotope compositions are generally less radiogenic, except for $^{143}Nd/^{144}Nd$ which define the high end of range of values [*Bryce et al.*, 2005]. Within the shield section, low-SiO_2 tholeiitic basalts are found near the top (above 850 mbsl) and deeper in the core section (between 1974 and 3098 mbsl). Both stratigraphic groups have identical isotopic compositions, but are discriminated by the higher Zr/Nb values of the younger basalts. These correspond to the type-2 and type-3 magmas of *Rhodes and Vollinger* [2004], respectively.

The geochemical differences between these distinct groups of samples have been inferred to reflect changes in melt production, depth of melting and differences in the source components sampled during the ~400 kyr of eruptive history of Mauna Kea as it crossed ~40 km over the Hawaiian plume [*Feigenson et al.*, 2003; *Huang and Frey*, 2003; *Rhodes and Vollinger*, 2004; *Stolper et al.*, 2004]. Correlations between the isotopic and trace element compositions of the HSDP tholeiites require that the high and low-SiO_2 groups formed from compositionally distinct source components, similar to those of Kilauea and Loihi, respectively [*Huang and Frey*, 2003; *Rhodes and Vollinger*, 2004]. The high-SiO_2 tholeiites (type-1 and -4) are inferred to derive from melting of depleted peridotite, whereas the low-SiO_2 tholeiites, located deeper in the core (type-3), are consistent with partial melting (30–40 kbar) of an isotopically enriched source, such as lherzolite [*Feigenson et al.*, 2003;

Rhodes and Vollinger, 2004; *Stolper et al.*, 2004]. The late-stage (type-2) and post-shield low-SiO$_2$ samples represent a transition to more alkalic compositions and are considered to derive from low degrees of partial melting of an isotopically depleted peridotite source, similar to the source of the high-SiO$_2$ samples, at higher pressures within the garnet stability field [*Feigenson et al.*, 2003; *Stolper et al.*, 2004].

Basalts from Mauna Kea have higher ε_{Nd}, ε_{Hf}, $^{206}Pb/^{204}Pb$, and lower $^{87}Sr/^{86}Sr$ and $^{3}He/^{4}He$ compared to Mauna Loa basalts, indicating they are derived from a more depleted source than that of Mauna Loa basalts [*Lassiter et al.*, 1996; *DePaolo et al.*, 2001; *Blichert-Toft et al.*, 2003; *Kurz et al.*, 2004; *Bryce et al.*, 2005]. The systematic differences in the isotopic compositions of Mauna Kea basalts compared to those from Mauna Loa, or between the "Kea-trend" and "Loa-trend" volcanoes [*Dana*, 1849; *Jackson et al.*, 1972], have been interpreted to reflect the compositional structure of the Hawaiian mantle plume. The Sr, Nd, Os and He isotopic differences between the Mauna Kea and Mauna Loa basalts recovered by the HSDP are consistent with a concentrically zoned melting region for the Hawaiian mantle plume [*Lassiter et al.*, 1996; *DePaolo et al.*, 2001; *Kurz et al.*, 2004; *Bryce et al.*, 2005]. However, the Pb isotopic differences are best explained by a bilaterally zoned melting region [*Abouchami et al.*, 2005]. Additional support for an axisymmetric zoning is given by the Pb isotope compositions of post-shield lavas of Hawaiian volcanoes [e.g., *Fekiacova et al.*, 2007; *Hanano et al.*, 2010].

In addition to horizontal zoning, a vertical component of heterogeneity is required in the structure of the Hawaiian plume to explain the short-term fluctuations in isotopic compositions throughout the HSDP core. Different models have been proposed to explain how the vertical heterogeneities are distributed within the plume conduit. These include: vertical streaks of at least several tens of km in length within the Hawaiian plume conduit [*Eisele et al.*, 2003], pulses of magma with different isotopic compositions, corresponding to heterogeneities within the hotter plume core derived from the base of the mantle [*Kurz et al.*, 2004; *Bryce et al.*, 2005], and heterogeneous packets of melts distributed vertically within the plume that are sampled consecutively by the volcano [*Blichert-Toft et al.*, 2003].

5.5. Samples

Forty Mauna Kea basalts from the whole rock reference suite of the deeper section of the HSDP cored during the last two drilling phases [HSDP-2B (2003–2005) and HSDP-2C (2006–2007)] were analyzed for Pb-Sr-Nd isotope compositions. A summary of the relevant geochemical characteristics of these samples is presented in Table 5.1. All basalts are tholeiitic and cover a wide range of MgO contents (6.6–25.4 wt%). The majority has high SiO_2 contents (>50 wt%) and based on their trace element contents belong to the type-1 (high SiO_2, high Zr/Nb) and type-4 (high SiO_2, low Zr/Nb) magma groups [*Rhodes and Vollinger*, 2004; Rhodes unpublished data]. Exceptions are samples R6-2.15-3.0 and R184-1.15-2.1, at 3098.2 and 3400.9 mbsl, respectively, which are most similar to type-3 samples; and samples R210-3.3-3.95 and R219-5.55-6.2, 7.25-7.7, at 3472.2 and 3500.9 mbsl, respectively, which have compositions most similar to those of Mauna Loa [*Rhodes and Vollinger*, 2004; Rhodes unpublished data].

5.6. Analytical Techniques

All isotopic analyses were performed on whole rock powders, with the exception of sample 26-102-R163-2.1-2.6, which was in glass chip form. The sample powders were prepared from rock chips that were repeatedly rinsed in deionized water and pulverized following the crushing and washing procedures described in *Rhodes* [1996] and *Rhodes and Vollinger* [2004]. Given the time gap between these two phases of sample recovery, the isotopic measurements presented in this study were obtained in two analytical sessions (mid-2006 for the 22 samples from phase -2B and early 2008 for the 18 samples from phase -2C).

Chemical purification and mass spectrometric analyses of the 40 Mauna Kea samples were carried out in Class 100 and Class 10,000 clean laboratories, respectively, at the Pacific Centre for Isotopic and Geochemical Research (PCIGR) at the University of British Columbia. For all samples, the Pb, Sr and Nd isotopic compositions were determined on the same sample solution, following the sequential chromatographic purification methods

described in *Weis et al.* [2006]. Given the importance of efficiently removing alteration phases and any extraneous Pb contaminant to get accurate and reproducible Pb isotopic compositions of oceanic basalts [*Hanano et al.*, 2009; Chapter 2, *Nobre Silva et al.*, 2009], all sample powders and glass chips were thoroughly acid leached with 6 M HCl prior to digestion and isotopic analysis, following the sequential acid leaching procedure of *Weis et al.* [2005] and *Nobre Silva et al.* [2009; 2010; Chapters 2 and 3]. The leached sample powders and chips were digested in a mixture of concentrated HF and HNO_3 acids in sealed Teflon® vessels and processed twice on Pb anion exchange columns for Pb purification. The sample fractions that were washed out from the Pb columns, containing all other sample matrix elements, were then processed on other chromatographic ion exchange columns for Sr and Nd purification [*Weis et al.*, 2006].

All Pb isotopic compositions were determined on a Nu Plasma MC-ICP-MS (Nu Instruments Ltd, UK), under dry plasma conditions using a membrane desolvator (Nu DSN100) for sample introduction. All analyses were obtained in static multi-collection mode, with masses 202 to 208 measured in collectors L2 to H4, respectively, following the procedures detailed in *Weis et al.* [2006]. Instrumental mass fractionation was monitored and corrected on-line using a Specpure® Tl standard solution with $^{205}Tl/^{203}Tl$ = 2.3885. The potential ^{204}Hg isobaric interference on the ^{204}Pb ion beam was monitored at mass 202 and, when necessary, was corrected for assuming natural abundances ($^{202}Hg/^{204}Hg$ = 4.35) adjusted for instrumental mass fractionation. All sample solutions were analyzed with the same [Pb]/[Tl] ($\approx$ 4) as the NIST SRM 981 Pb standard solution, to ensure that sample and standard solutions were matrix-matched as much as possible. To accomplish this, the Pb content of a small aliquot of each solution was determined by HR-ICP-MS, on an ELEMENT2 (Thermo Finnigan, Germany), prior to isotopic analysis. All sample and standard solutions were prepared fresh for each analytical session by adding the corresponding amount of Tl standard to the respective solution and diluting with 0.05M HNO_3 to obtain an optimal ^{208}Pb ion beam of ~8V (and no less than 2V).

Sample analysis followed a modified sample-standard bracketing protocol in which the SRM 981 Pb standard was run after every two samples. The fractionation-corrected isotopic ratios were then normalized off-line to the triple-spike values (^{206}Pb/^{204}Pb = 16.9405, ^{207}Pb/^{204}Pb = 15.4963, and ^{208}Pb/^{204}Pb = 36.7219; [*Abouchami et al.*, 2000]), using the ln-ln method as described in *White et al.* [2000] and *Albarède et al.* [2004]. During the two analytical sessions (2006, n = 140; and 2008, n = 36), analyses of the SRM 981 Pb standard yielded mean values of ^{206}Pb/^{204}Pb = 16.9406 ± 0.0013 and 16.9420 ± 0.0016, ^{207}Pb/^{204}Pb = 15.4964 ± 0.0025 and 15.4987 ± 0.0020, and ^{208}Pb/^{204}Pb = 36.7138 ± 0.0084 and 36.7156 ± 0.0062, respectively, which are within 2SD of each other and of the triple spike values [*Abouchami et al.*, 2000]. United States Geological Survey (USGS) reference material BHVO-2 and Hawaiian rock Kil-93 (sample collected in 1993 from Kilauea's summit Pu`u `O`o eruption by M. O. Garcia), processed together with the sample sets, yielded Pb isotopic ratios of ^{206}Pb/^{204}Pb = 18.6451 ± 0.0011 and 18.4066 ± 0.0008, ^{207}Pb/^{204}Pb = 15.4890 ± 0.0013 and 15.4715 ± 0.0007, and ^{208}Pb/^{204}Pb = 38.206 ± 0.004 and 38.061 ± 0.002, respectively, and are in agreement with published values for leached residues of BHVO-2 [*Weis et al.*, 2006] and with the in-house values of Kil-93 [Chapter 4, Table 4.2].

All Sr and the first batch (HSDP-2B) of Nd isotopic ratios were measured on a TRITON (Thermo Finnigan) thermal ionization mass spectrometer (TIMS) in static mode with relay matrix rotation on a single Ta and double Re-Ta filament, respectively. Sr and Nd isotopic compositions were corrected for mass fractionation using ^{86}Sr/^{88}Sr = 0.1194 and ^{146}Nd/^{144}Nd = 0.7219 using an exponential law. The data was then normalized to the average of the corresponding standard solution (NIST SRM 987 for Sr and La Jolla for Nd) analyzed during the analytical sessions, relative to the values of ^{87}Sr/^{86}Sr = 0.710248 and ^{143}Nd/^{144}Nd = 0.511858 [*Weis et al.*, 2006]. During the course of these analyses, the average ^{87}Sr/^{86}Sr value of the SRM 987 Sr standard was 0.710256 ± 0.000015 (n = 10) in 2006 and 0.710246 ± 0.000004 (n = 9) in 2008, and the average ^{143}Nd/^{144}Nd values of the La Jolla Nd standard was 0.511852 ± 0.000010 (n = 10). USGS reference material BHVO-2 and Hawaiian rock Kil-93 yielded Sr isotopic ratios of 0.703462 ± 0.000007 and 0.703582 ± 0.000009,

respectively, and Nd isotopic compositions of 0.512979 ±0.000007 and 0.512972 ± 0.000007, respectively. These are in agreement with the published values for BHVO-2 [*Weis et al.*, 2006] and with the in-house values of Kil-93 [Chapter 4, Table 4.2].

The Nd isotopic compositions of the second batch of samples (HSDP-2C) were analyzed on the Nu Plasma MC-ICP-MS under dry plasma conditions in static multi-collection mode. The analysis procedure followed that detailed in *Weis et al*. [2006], which showed a good comparison between the Nd isotopic compositions of several USGS reference materials covering a wide range of compositions obtained on the TRITON TIMS and on the Nu Plasma MC-ICP-MS at the PCIGR. Masses 140 to 150 were measured in collectors L3 to H5, respectively. Potential isobaric interferences on masses 144, 148, 150 and 142 were monitored at masses 147 (Sm) and 140 (Ce) and were, when necessary, corrected for assuming natural isotopic abundances (^{144}Sm = 0.030734, ^{147}Sm = 0.149934, ^{148}Sm = 0.112406, ^{150}Sm = 0.073796, ^{140}Ce = 0.88449, ^{142}Ce = 0.11114 [*Rosman and Taylor*, 1998]), adjusted for instrumental mass discrimination using an exponential law as monitored by the ^{146}Nd/^{144}Nd ratio. Nd isotope ratios were normalized internally for fractionation to ^{146}Nd/^{144}Nd = 0.7219 and then to the daily average value of the Rennes Nd standard solution, relative to the value of ^{143}Nd/^{144}Nd = 0.511973 [*Weis et al.,* 2006]. These analyses were acquired over two nonconsecutive days, and for each the average value for the Rennes Nd standard was 0.511986 ± 0.000009 (n = 12), and 0.512014 ± 0.000009 (n = 28), respectively. The Hawaiian Kil-93 (n = 2), processed together with the sample batch, yielded an average Nd isotopic ratio of 0.512972 ± 0.000008, which is in agreement with the value obtained on the TIMS during the first batch of HSDP2-B samples and with the in-house values of Kil-93 [Chapter 4, Table 4.2].

5.7. Results

5.7.1. Stratigraphic Variations in Pb-Sr-Nd Isotope Compositions

Basalts from the last ~400 metres (phases B and C) of the HSDP2 core yield ^{206}Pb/^{204}Pb = 18.3033 − 18.6936, ^{207}Pb/^{204}Pb = 15.4707 − 15.4993, ^{208}Pb/^{204}Pb = 37.924 −

Table 5.2. Pb Isotopic Compositions by MC-ICP-MS of Mauna Kea Samples From the Last Drilling Phases (-B and -C) of the HSDP2 Core

Sample	Depth (mbsl)[a]	$^{206}Pb/^{204}Pb$[b]	2SE	$^{207}Pb/^{204}Pb$[b]	2SE	$^{208}Pb/^{204}Pb$[b]	2SE	$^{207}Pb/^{206}Pb$	$^{208}Pb/^{206}Pb$	$^{208}Pb*/^{206}Pb*$[c]
HSDP-2b										
R6 - 0.85-1.2	3097.7	18.5913	0.0009	15.4854	0.0009	38.1905	0.0026	0.8329	2.0542	0.9386
R6 - 2.15-3.0	3098.2	18.4953	0.0006	15.4728	0.0006	38.1869	0.0019	0.8366	2.0647	0.9480
R8 - 0.15-0.7	3102.4	18.5934	0.0009	15.4871	0.0008	38.1962	0.0023	0.8329	2.0543	0.9390
R10 - 4.35-4.7	3109.4	18.5949	0.0006	15.4882	0.0005	38.2017	0.0013	0.8329	2.0544	0.9395
rep.[d]	3109.4	18.5920	0.0010	15.4850	0.0009	38.1903	0.0026	0.8329	2.0541	0.9385
R11 - 5.3-5.7	3111.5	18.5853	0.0008	15.4871	0.0008	38.1885	0.0024	0.8333	2.0548	0.9390
R13 - 0.1-0.5	3115.2	18.5868	0.0007	15.4881	0.0008	38.1939	0.0025	0.8333	2.0549	0.9394
R16 - 5.2-6.0	3122.5	18.5866	0.0009	15.4888	0.0009	38.1940	0.0024	0.8333	2.0549	0.9395
dup.[e]	3122.5	18.5857	0.0012	15.4880	0.0011	38.1934	0.0033	0.8333	2.0550	0.9395
R30 - 4.25-5.2	3141.2	18.5912	0.0005	15.4859	0.0005	38.1939	0.0016	0.8330	2.0544	0.9390
R51 - 2.4-3.6	3160.8	18.5936	0.0012	15.4883	0.0014	38.2005	0.0045	0.8330	2.0545	0.9395
R56 - 1.0-1.5	3171.1	18.5865	0.0010	15.4875	0.0011	38.1926	0.0031	0.8333	2.0549	0.9393
dup.	3171.1	18.5888	0.0010	15.4838	0.0007	38.1869	0.0024	0.8330	2.0543	0.9385
R57 - 5.0-5.9	3173.4	18.5931	0.0007	15.4883	0.0008	38.2003	0.0019	0.8330	2.0545	0.9395
R60 - 7.6-8.4	3181.2	18.5811	0.0012	15.4881	0.0013	38.1867	0.0040	0.8335	2.0551	0.9393
dup.	3181.2	18.5796	0.0010	15.4866	0.0011	38.1824	0.0036	0.8335	2.0551	0.9389
R80 - 2.8-3.5	3215.5	18.5833	0.0011	15.4894	0.0012	38.1939	0.0036	0.8335	2.0553	0.9398
rep.	3215.5	18.5815	0.0030	15.4885	0.0038	38.1914	0.0126	0.8335	2.0553	0.9397
R93 - 1.4-2.0	3234.7	18.5819	0.0010	15.4879	0.0011	38.1900	0.0031	0.8335	2.0552	0.9395
R101 - 4.4-4.9	3244.8	18.5853	0.0008	15.4854	0.0006	38.1891	0.0016	0.8332	2.0548	0.9391
R108 - 0.0-0.7	3263.9	18.5935	0.0007	15.4864	0.0007	38.1954	0.0018	0.8329	2.0542	0.9389
rep.	3263.9	18.5938	0.0007	15.4868	0.0007	38.1959	0.0020	0.8329	2.0542	0.9390
R112 - 7.1-7.7	3277.0	18.5845	0.0010	15.4853	0.0009	38.1883	0.0022	0.8332	2.0548	0.9391
R116 - 6.25-7.2	3285.8	18.5765	0.0010	15.4876	0.0011	38.1858	0.0037	0.8337	2.0556	0.9396
R122 - 1.85-2.65	3300.1	18.5960	0.0009	15.4887	0.0008	38.2020	0.0022	0.8329	2.0543	0.9394
R125 - 4.9-5.3	3305.9	18.5920	0.0012	15.4882	0.0013	38.1989	0.0041	0.8331	2.0546	0.9395
R127 - 1.4-2.2	3308.2	18.5907	0.0009	15.4985	0.0007	38.2018	0.0018	0.8337	2.0549	0.9399
rep.	3308.2	18.5910	0.0008	15.4993	0.0007	38.2042	0.0021	0.8337	2.0550	0.9401
R129 - 5.8-6.5	3313.5	18.4286	0.0007	15.4725	0.0007	38.0685	0.0019	0.8396	2.0657	0.9420
HSDP-2c										
R149 - 1.2 - 1.6	3333.3	18.6305	0.0007	15.4906	0.0007	38.2233	0.0017	0.8315	2.0517	0.9382
R154 - 2.1 - 2.95	3339.5	18.5035	0.0007	15.4780	0.0006	38.1296	0.0030	0.8365	2.0607	0.9410
R155 - 2.7 - 3.5	3341.4	18.5488	0.0010	15.4803	0.0010	38.1501	0.0030	0.8346	2.0567	0.9386
R158 - 1.75 - 2.10	3348.3	18.6296	0.0007	15.4911	0.0007	38.2242	0.0024	0.8315	2.0518	0.9384
R162 - 1.55 - 2.3	3353.9	18.6292	0.0007	15.4897	0.0006	38.2195	0.0020	0.8315	2.0516	0.9379
R163 - 2.1 - 2.6	3357.0	18.6885	0.0009	15.4941	0.0011	38.2588	0.0033	0.8291	2.0472	0.9362
R165 - 0.75 - 1.45	3359.8	18.6922	0.0008	15.4947	0.0009	38.2651	0.0026	0.8289	2.0471	0.9365
dup.	3359.8	18.6898	0.0008	15.4933	0.0006	38.2601	0.0018	0.8290	2.0471	0.9362
R168 - 3.7 - 4.15	3366.3	18.6936	0.0009	15.4969	0.0008	38.2710	0.0021	0.8290	2.0473	0.9370
R176 - 5.93 - 6.5	3381.3	18.6916	0.0007	15.4938	0.0007	38.2624	0.0018	0.8289	2.0470	0.9363
R184 - 1.15 - 2.1	3400.9	18.5289	0.0006	15.4788	0.0006	38.2058	0.0017	0.8354	2.0620	0.9466
R187 - 0.9 - 1.8, 2.05 - 2.5	3405.3	18.5929	0.0007	15.4869	0.0007	38.1756	0.0020	0.8329	2.0532	0.9369
R192 - 4.4 - 5.4	3418.1	18.6438	0.0013	15.4889	0.0010	38.2103	0.0026	0.8308	2.0495	0.9355
rep.	3418.1	18.6473	0.0007	15.4910	0.0006	38.2167	0.0017	0.8307	2.0495	0.9358
R198 - 0.5 - 1.9	3435.2	18.6297	0.0023	15.4894	0.0020	38.2193	0.0053	0.8314	2.0515	0.9379
R204 - 1.1 - 1.8	3453.4	18.5935	0.0016	15.4984	0.0014	38.2043	0.0035	0.8335	2.0547	0.9399
R205 - 7.5 - 8.15	3458.4	18.6424	0.0008	15.4933	0.0007	38.2347	0.0025	0.8311	2.0510	0.9382
R210 - 3.3 - 3.95	3472.2	18.3041	0.0009	15.4707	0.0010	37.9340	0.0027	0.8452	2.0724	0.9401
dup.	3472.2	18.3056	0.0007	15.4733	0.0006	37.9412	0.0016	0.8453	2.0727	0.9407
dup. rep.	3472.2	18.3033	0.0006	15.4712	0.0007	37.9341	0.0019	0.8453	2.0725	0.9402
R219 - 5.55 - 6.2, 7.25 - 7.7	3500.9	18.3059	0.0008	15.4733	0.0006	37.9241	0.0016	0.8453	2.0717	0.9388
R222 - 8.0 - 8.8	3505.7	18.4836	0.0008	15.4729	0.0008	38.1172	0.0027	0.8371	2.0622	0.9417

[a] mbsl = meters below sea level.
[b] Pb isotopic ratios by MC-ICP-MS, normalized to the SRM 981 TS-TIMS reference values of Galer and Abouchami [1998]; the 2SE is the absolute error value of the individual sample analysis (internal error).
[c] $^{208}Pb*/^{206}Pb*$ defined as $(^{208}Pb/^{204}Pb sample - 29.475)/(^{206}Pb/^{204}Pb sample - 9.037)$ by *Galer and O'Nions* [1985].
[d] rep = replicate analysis of the same sample solution by MC-ICP-MS.
[e] dup = full procedural duplicate analysis of the same sample.

38.271, $^{87}Sr/^{86}Sr$ = 0.703513 – 0.703631, and $^{143}Nd/^{144}Nd$ = 0.512968 – 0.513011 (Tables 5.2 and 5.3, Figure 5.3). The Pb and Nd isotopic values are in good agreement with those of *Blichert-Toft and Albarède* [2009] (see Appendix A) and are, for the most part, similar to those of the preceding, younger lavas (above ~3098 metres; Figure 5.3) [e.g., *Eisele et al.*, 2003; *Blichert-Toft et al.*, 2003; *Bryce et al.*, 2005].

Between 3097.7 and 3308.2 metres depth, the isotopic variability of these older basalts is very restricted ($^{206}Pb/^{204}Pb$ = 18.4953 – 18.5960, $^{208}Pb/^{204}Pb$ = 38.187 – 38.204, $^{87}Sr/^{86}Sr$ = 0.703595 – 0.703631, and $^{143}Nd/^{144}Nd$ = 0.512968 – 0.512990). Type-1 basalts are the most abundant in this interval and the observed range of isotopic compositions correlates with the limited variation in major and trace element contents of these basalts (Table 5.1, Rhodes unpublished data). These 210.5 metres represent the longest interval (corresponding to ~10 kyr) of restricted geochemical variation observed within the HSDP2 core; the relative variation in $^{206}Pb/^{204}Pb$, $^{86}Sr/^{87}Sr$, and $^{143}Nd/^{144}Nd$ is ~11x, ~4x, and ~3x, respectively, smaller than that observed for younger basalts. The exception is sample R6-2.15-3.0, a massive intrusive rock at 3098.2 metres depth with low SiO_2 and Zr/Nb that has isotopic compositions identical to other type-3 samples recovered during the main drill phase of the HSDP2.

In contrast, basalts from the last 192 metres of drill core (3313.5 to 3505.7 metres depth) are most similar to type-4 basalts and show significantly larger Pb isotopic variations (Figure 5.3, Tables 5.2 and 5.3). This group of 19 samples yields the largest range of Pb isotopic compositions ($^{206}Pb/^{204}Pb$ = 18.3033 – 18.6936, $^{208}Pb/^{204}Pb$ = 37.924 – 38.291) compared to basalts from the entire ~3200 metres of core above. These deeper basalts extend the Pb isotopic range ($^{206}Pb/^{204}Pb$ and $^{208}Pb/^{204}Pb$) of Mauna Kea to compositions that are both significantly more and less radiogenic than those previously observed for this volcano [e.g., *Abouchami et al.*, 2000; *Blichert-Toft et al.*, 2003; *Eisele et al.*, 2003]. This distinction is less obvious in the Sr and Nd isotopic compositions (Figure 5.3). Collectively, basalts within the the lowermost 192 meters of the core present (~2x) smaller Sr and Nd isotopic variations compared to the variations among the younger drill core samples [*Bryce et al.*,

Table 5.3. Sr and Nd Isotopic Compositions by TIMS and MC-ICP-MS of Mauna Kea Samples From the Last Drilling Phases (-B and -C) of the HSDP2 Core

Sample	Depth (mbsl)[a]	[87]Sr/[86]Sr[b]	2SE	[143]Nd/[144]Nd[c]	2SE	εNd[d]
HSDP-2b						
R6 - 0.85-1.2	3097.7	0.703582	0.000010	0.512984	0.000007	6.7
R6 - 2.15-3.0	3098.2	0.703595	0.000007	0.512968	0.000006	6.4
R8 - 0.15-0.7	3102.4	0.703577	0.000006	0.512983	0.000005	6.7
R10 - 4.35-4.7	3109.4	0.703573	0.000006	0.512980	0.000007	6.7
R11 - 5.3-5.7	3111.5	0.703565	0.000007	0.512977	0.000006	6.6
dup.[e]	3111.5	0.703571	0.000008	0.512977	0.000006	6.6
R13 - 0.1-0.5	3115.2	0.703551	0.000007	0.512972	0.000005	6.5
R16 - 5.2-6.0	3122.5	0.703564	0.000007	0.512974	0.000006	6.5
R30 - 4.25-5.2	3141.2	0.703591	0.000008	0.512990	0.000006	6.9
R51 - 2.4-3.6	3160.8	0.703568	0.000006	0.512982	0.000008	6.7
R56 - 1.0-1.5	3171.1	0.703564	0.000008	0.512975	0.000005	6.6
R57 - 5.0-5.9	3173.4	0.703572	0.000006	0.512982	0.000007	6.7
R60 - 7.6-8.4	3181.2	0.703575	0.000007	0.512987	0.000007	6.8
R80 - 2.8-3.5	3215.5	0.703574	0.000006	0.512983	0.000006	6.7
R93 - 1.4-2.0	3234.7	0.703572	0.000009	0.512980	0.000007	6.7
R101 - 4.4-4.9	3244.8	0.703587	0.000008	0.512980	0.000007	6.7
R108 - 0.0-0.7	3263.9	0.703569	0.000009	0.512972	0.000005	6.5
R112 - 7.1-7.7	3277.0	0.703561	0.000010	0.512978	0.000005	6.6
R116 - 6.25-7.2	3285.8	0.703580	0.000010	0.512969	0.000008	6.5
dup.	3285.8	0.703579	0.000008	0.512972	0.000006	6.5
R122 - 1.85-2.65	3300.1	0.703565	0.000008	0.512984	0.000006	6.7
R125 - 4.9-5.3	3305.9	0.703585	0.000006	0.512980	0.000005	6.7
R127 - 1.4-2.2	3308.2	0.703588	0.000006	0.512988	0.000006	6.8
R129 - 5.8-6.5	3313.5	0.703631	0.000007	0.512971	0.000008	6.5
HSDP-2c						
R149 - 1.2 - 1.6	3333.3	0.703559	0.000008	0.512983	0.000008	6.7
R154 - 2.1 - 2.95	3339.5	0.703551	0.000007	0.512996	0.000005	7.0
R155 - 2.7 - 3.5	3341.4	0.703564	0.000007	0.512981	0.000005	6.7
R158 - 1.75 - 2.10	3348.3	0.703566	0.000007	0.512979	0.000009	6.6
rep.[f]	3348.3	-	-	0.512980	0.000008	6.7
R162 - 1.55 - 2.3	3353.9	0.703560	0.000008	0.512986	0.000007	6.8
R163 - 2.1 - 2.6	3357.0	0.703604	0.000008	0.5129786	0.000007	6.6
R165 - 0.75 - 1.45	3359.8	0.703562	0.000010	0.512987	0.000010	6.8
dup.	3359.8	0.703563	0.000010	0.512981	0.000006	6.7
R168 - 3.7 - 4.15	3366.3	0.703556	0.000008	0.512977	0.000009	6.6
R176 - 5.93 - 6.5	3381.3	0.703557	0.000008	0.512975	0.000006	6.6
R184 - 1.15 - 2.1	3400.9	0.703513	0.000010	0.512993	0.000006	6.9
R187 - 0.9 - 1.8, 2.05 - 2.5	3405.3	0.703587	0.000007	0.512968	0.000006	6.4
R192 - 4.4 - 5.4	3418.1	0.703529	0.000009	0.512981	0.000006	6.7
R198 - 0.5 - 1.9	3435.2	0.703559	0.000009	0.512988	0.000007	6.8
R204 - 1.1 - 1.8	3453.4	0.703570	0.000009	0.512984	0.000007	6.7
R205 - 7.5 - 8.15	3458.4	0.703583	0.000007	0.512989	0.000006	6.9
R210 - 3.3 - 3.95	3472.2	0.703554	0.000009	0.513000	0.000007	7.1
dup.	3472.2	0.703567	0.000009	0.513011	0.000009	7.3
R219 - 5.55 - 6.2, 7.25 - 7.7	3500.9	0.703596	0.000007	0.513000	0.000007	7.1
R222 - 8.0 - 8.8	3505.7	0.703534	0.000009	0.512994	0.000006	6.9

[a]mbsl = meters below sea level.
[b]Sr isotopic ratios measured by TIMS, normalized to the average value of the SRM 987 standard solution of the wheel for each analytical session; the 2σ error is the absolute error value of the individual sample analysis (internal error) reported as x10[6].
[c]Nd isotopic ratios measured by TIMS (HSDP-2b samples) and MC-ICP-MS (HSDP-2c samples), normalized to the mean value of the La Jolla standard solution during the TIMS analytical session (for the HSDP-2b samples) or to the mean value of the Rennes Nd standard solution run during the analytical session with the MC-ICP-MS (for the HSDP-2c samples); the 2σ error is the absolute error value of the individual sample analysis (internal error) reported as x10[6].
[d]εNd values are calculated using the [143]Nd/[144]Nd CHUR value = 0.512638 [*Jacobsen and Wasserburg*, 1984].
[e]dup = full procedural duplicate analysis of the same sample.
[f]rep = replicate analysis of the same sample solution by MC-ICP-MS.
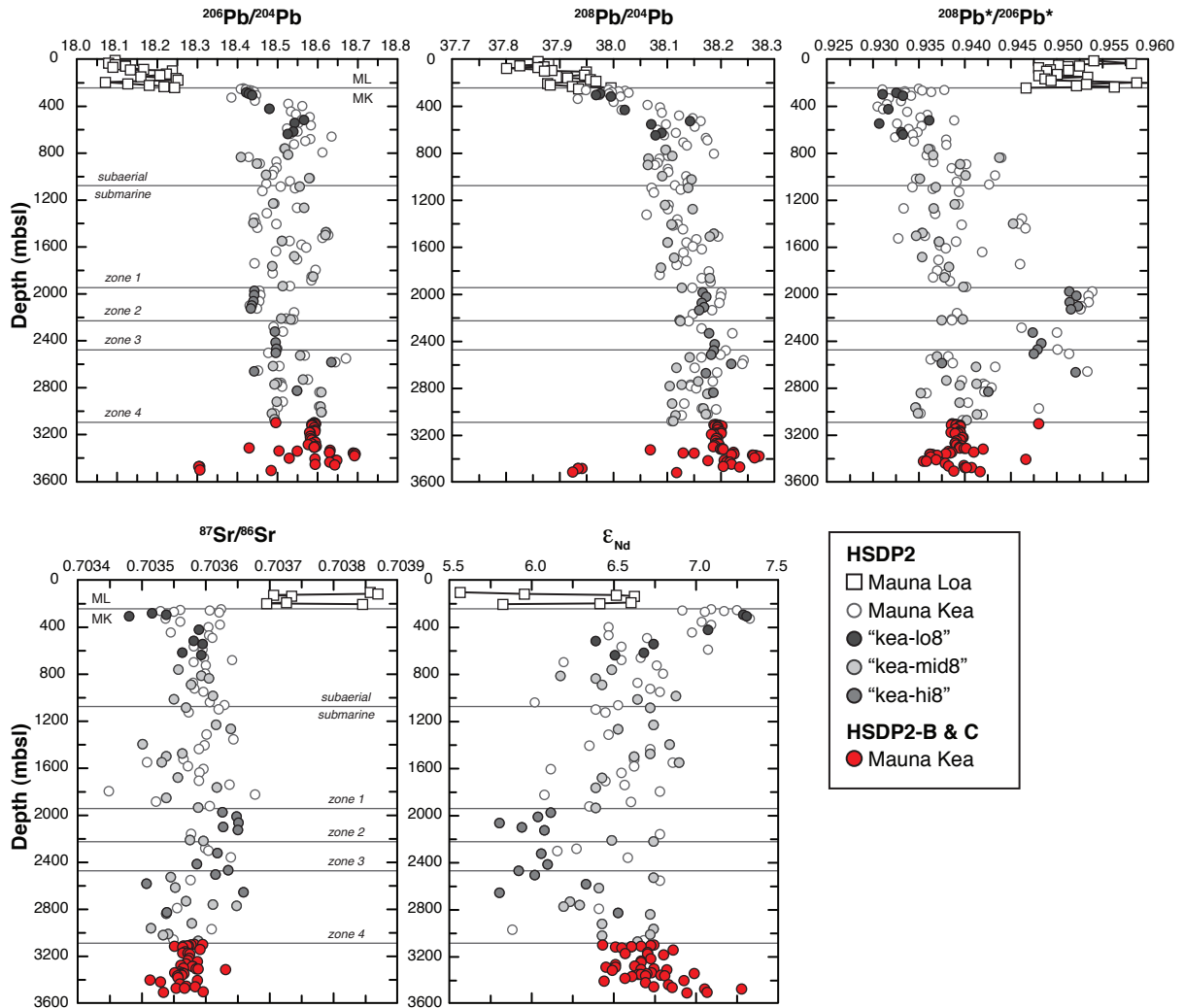
Figure 5.3. Pb, Sr, and Nd isotopic variations with depth (meters below sea level, mbsl) in the HSDP2 drill core. Red filed symbols at the bottom of the core indicate the samples analyzed in this study. Other HSDP2 data sources are as follows: Mauna Loa, *DePaolo et al.* [2001] and *Blichert-Toft et al.* [2003]; Mauna Kea, *Blichert-Toft et al*. [2003], *Eisele et al.* [2003] and *Bryce et al.* [2005]. Also indicated are the Mauna Loa/Mauna Kea and subaerial/submarine boundaries, as well as the four zones identified by *Stolper et al.* [2004]. All literature data were normalized to the same standard values, i.e., triple spike values of SRM 981 [*Abouchami et al.*, 2000], La Jolla $^{143}Nd/^{144}Nd = 0.511858$ and SRM 987 = 0.710248 [*Weis et al.*, 2006].

2005] and show a systematic progression of increasing $^{87}Sr/^{86}Sr$ and increasing e_{Nd} with depth (Figure 5.3). In this deeper section of the core, few samples have major and trace element compositions that trend towards Mauna Loa compositions (Table 5.1, Rhodes unpublished data). However, their Pb, Sr and Nd isotope compositions are distinct from those of Mauna Loa, especially their Nd isotopic compositions that are most similar to those of the late shield and post-shield groups found in the upper Mauna Kea sections of the drill core [e.g., *Bryce et al.*, 2005; *Hanano et al.*, 2010].

5.7.2. Isotope Correlations

The Sr, Nd and Pb isotopic compositions of the tholeiites from phases -B and -C of the HSDP2 drill core show some degree of correlation, consistent with the trends formed by other Hawaiian volcanoes. With respect to Sr-Nd isotopes, these older tholeiites lie within the compositional range of Mauna Kea, at the depleted end (low $^{87}Sr/^{86}Sr$, high $^{143}Nd/^{144}Nd$) of the array formed by the Hawaiian Islands (Figure 5.4). Compared to other Mauna Kea basalts, the $^{87}Sr/^{86}Sr$ and $^{143}Nd/^{144}Nd$ of HSDP2-B and -C basalts are displaced towards the lower and higher limits, respectively, of the isotopic ranges. In Sr-Pb and Nd-Pb isotope diagrams, these basalts extend from the compositional trend defined by other Mauna Kea and Kea-like shield basalts, towards slightly lower $^{87}Sr/^{86}Sr$ and higher $^{143}Nd/^{144}Nd$ values, most similar to the compositions of the late stage, post-shield lavas from Mauna Kea and Kohala [*Holcomb et al.*, 2000; *Eisele et al.*, 2003; *Bryce et al.*, 2005; *Hanano et al.*, 2010] (Figures 5.5 and 5.6).

The HSDP2-B and -C basalts form two distinct Pb isotope arrays that intersect at the radiogenic end (Figure 5.7), extending the range of $^{206}Pb/^{204}Pb$ and $^{208}Pb/^{204}Pb$ of Mauna Kea to significantly more radiogenic values, similar to those of "ancestral" Kilauea lavas [*Kimura et al.*, 2006]. One Pb isotope array falls within the main Pb isotopic compositional field for Mauna Kea, best represented by the "Kea-mid8" array defined by the younger HSDP2 samples [*Eisele et al.*, 2003]. The second array is defined by samples R6-2.15-3.0 and R184-1.15-2.1 (two massive intrusive units with low SiO_2 and Zr/Nb at depths of 3098.2 and
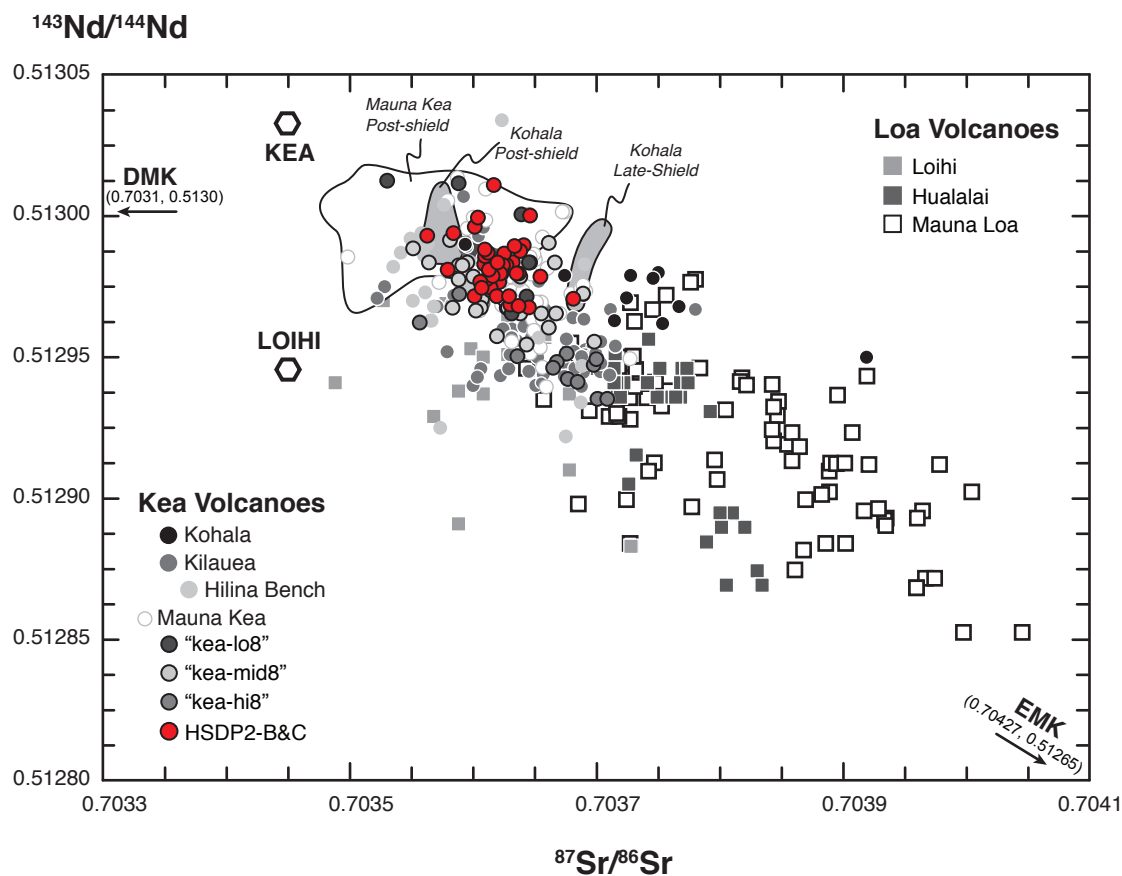
Figure 5.4. Diagram of $^{143}Nd/^{144}Nd$ versus $^{87}Sr/^{86}Sr$ for the HSDP2 Mauna Kea basalts compared to shield basalts from other volcanoes on the Big Island of Hawaii (Kohala, Hualalai, Mauna Loa, Kilauea, Loihi) and to the post-shield lavas of Mauna Kea and Kohala. The analytical uncertainty (2s error) is smaller than the symbol sizes. For reference, the "Kea", depleted Makapuu (DMK), and enriched Makapuu (EMK) end-members from *Tanaka et al.* [2002] and the "Loihi" end-member from *Tanaka et al.* [2008] are shown (open hexagons). Data sources are as follows: Mauna Kea, *Bryce et al.* [2005]; Kilauea, *Pietruszka and Garcia* [1999], *Abouchami et al.* [2005], *Marske et al.* [2007]; Hilina bench, *Chen et al.* [1996], *Kimura et al.* [2006]; Kohala, *Hofmann et al.* [1987], M. O. Garcia (unpublished data, 2001), and D. Weis (unpublished data, 2001); Hualalai, *Yamasaki et al.* [2009]; Mauna Loa, *DePaolo et al.* [2001] and D. Weis (in preparation, 2011); Loihi, *Garcia et al.* [1993]; Mauna Kea post-shield, *Bryce et al.* [2005]; *Hanano et al.* [2010]; Kohala post-shield, *Holcomb et al.* [2000]; *Hanano et al.* [2010]. Literature data were normalized to the same standard values as noted in Figure 5.3.

3400.9 metres, respectively), which plot together with other low-SiO_2 samples higher in the core within the "Kea-hi8" array [*Eisele et al.*, 2003]. Samples R210-3.3-3.95 and R219-5.55-6.2; 7.25-7.7, at the bottom of the core, extend the Pb isotopic compositions of Mauna Kea to significantly less radiogenic values. Although these samples have $^{208}Pb/^{204}Pb$ that are within the range of Mauna Loa values, their $^{206}Pb/^{204}Pb$ and $^{207}Pb/^{204}Pb$ (not shown) are higher, comparable to those for lavas from Kohala, Kilauea and post-shield stage of Mauna Kea (Figure 5.7).

5.8. Discussion

5.8.1. HSDP2: A Record of the Evolution of a Single Volcano or the Output of Different Volcanoes?

Hawaiian volcanoes evolve through several growth stages (pre-shield, shield, post-shield) marked by changes in composition and eruption rates as they are carried by the Pacific plate across the magma-production region of the Hawaiian mantle plume [e.g., *Chen and Frey*, 1983; *Clague and Dalrymple*, 1987; *Moore and Clague*, 1992]. Oceanic lithosphere is considered to not significantly influence the isotopic compositions of Hawaiian lavas [e.g., *Lassiter et al.*, 1996; *Fekiacova et al.*, 2007; *Marske et al.*, 2007; *Hanano et al.*, 2010]. The geochemical variations within the stratigraphic sequence of lavas derived from a single volcano can therefore be interpreted as reflecting the temporal geochemical variations within the magma source [e.g., *Lassiter et al.*, 1996; *Rhodes,* 1996; *Pietruska and Garcia*, 1999; *DePaolo et al.*, 2001; *Abouchami et al.*, 2005; *Bryce et al.*, 2005; *Marske et al.*, 2007, 2008]. As different volcanoes grow to form the Hawaiian Islands, their lavas overlap and inter-layer, with older volcanoes becoming partially covered by lavas from younger volcanoes [e.g., *Moore and Clague*, 1992; *DePaolo and Stolper*, 1996]. Mauna Kea is built on top of ~6 km thick Cretaceous oceanic crust plus pelagic and clastic sediments, and on the flank of the adjacent older Kohala volcano [e.g., *Moore and Clague*, 1992; *DePaolo and Stolper*, 1996].
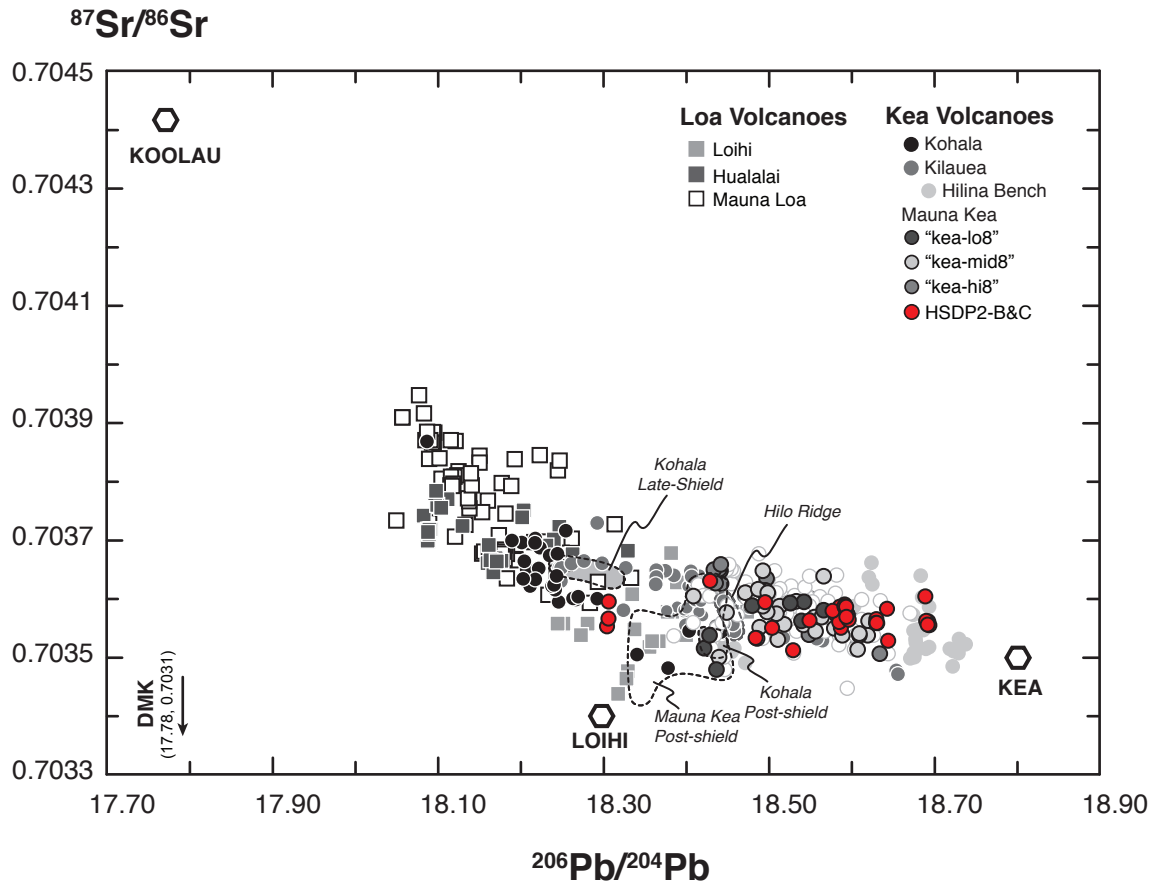
Figure 5.5. Diagram of $^{87}Sr/^{86}Sr$ versus $^{206}Pb/^{204}Pb$ for the HSDP2 Mauna Kea basalts compared to shield basalts from the other volcanoes on the Big Island of Hawaii (Kohala, Hualalai, Mauna Loa, Kilauea, Loihi) and to post-shield lavas of Mauna Kea and Kohala. Symbols are as in Figure 5.4. Data sources for Pb isotopes are as follows: Mauna Kea, *Blichert-Toft et al.* [2003], and *Eisele et al.* [2003]; Kilauea, *Pietruszka and Garcia* [1999], *Abouchami et al.* [2005], and *Marske et al.* [2007]; Hilina bench, *Chen et al.* [1996], *Abouchami et al.* [2005], and *Kimura et al.* [2006]; Kohala, *Abouchami et al.* [2005], M. O. Garcia (unpublished data, 2001), and D. Weis (unpublished data, 2001); Hualalai, *Yamasaki et al.* [2009]; Mauna Loa, *Blichert-Toft et al.* [2003] and D. Weis (in preparation, 2011); Loihi, *Abouchami et al.* [2005]; Mauna Kea post-shield, *Hanano et al.* [2010]; Kohala post-shield, *Holcomb et al.* [2000], and *Hanano et al*. [2010]. Symbols and standard normalization values are as noted in Figure 5.3.

It has been suggested that the lavas encountered in the deeper section of the HSDP2 core (characterized by low SiO_2, high $^{208}Pb*/^{206}Pb*$) may not represent the variable output of the Mauna Kea volcano, but instead that of Kohala [*Holcomb et al.*, 2000] or of another unknown volcano [e.g., *Stolper et al.*, 2004; *Blichert-Toft and Albarède*, 2009]. The isotopic similarities between basalts dredged along the Hilo Ridge below ~1100 mbsl and subaerial lavas from Kohala volcano (Pololu and Hawi volcanic rocks) suggest that the deeper section of the Hilo Ridge may be part of Kohala's southeast rift zone rather than belonging to Mauna Kea [*Holcomb et al.*, 2000]. Thus, older Kohala lavas should be encountered at the HSDP2 drill site location at ~3400 mbsl [e.g., *Stolper et al.*, 2004]. Based on the elemental and isotopic distinction between the HSDP2 samples shallower than 3098 mbsl and known Kohala samples, *Rhodes and Vollinger* [2004] and *Stolper et al.* [2004] argued against the presence of Kohala lavas within this section of HSDP2 core, although they did not dismiss the possibility of encountering Kohala lavas at deeper levels.

The last phase of drilling of the HSDP2 extended the core to ~3500 mbsl. Within the deeper part of the core stratigraphy, the abundance of type-4 basalts (low Zr/Nb and high SiO_2) increases down-section, whereas type-1 basalts are mostly absent in the last 170 m of the core (Table 5.1, Rhodes personal communication). Some of the basalts at the stratigraphic base of the core do show isotopic similarities to late shield (Pololu) and post-shield (Hawi) lavas from Kohala, as suggested by *Holcomb et al.* [2000], as well as to post-shield lavas of Mauna Kea [e.g., *Eisele et al.*, 2003; *Bryce et al.*, 2005; *Hanano et al.*, 2010] (Figures 5.4 to 5.7). To assume that these samples in question are derived from Kohala would imply that ~650 thousand years ago the volcano was reaching the end of its evolution. This is not supported by growth models for Kohala, which at this period of time should have been in its vigorous tholeiitic shield-building stage [*Moore and Clague*, 1992], nor it is supported by the age range of subaerially exposed Kohala post-shield lavas (~175–450 ka; *Clague and Dalrymple* [1987]; *Aciego et al.*, [2009]). Although little is known about the history and interactions between Hawaiian volcanoes [*Stolper et al.*, 2004], it is difficult to geometrically reconcile the existence of an unknown volcano older than Mauna Kea [e.g., *Baker et al.*, 2003]. The overall isotopic consistency of the basalts deeper in the core
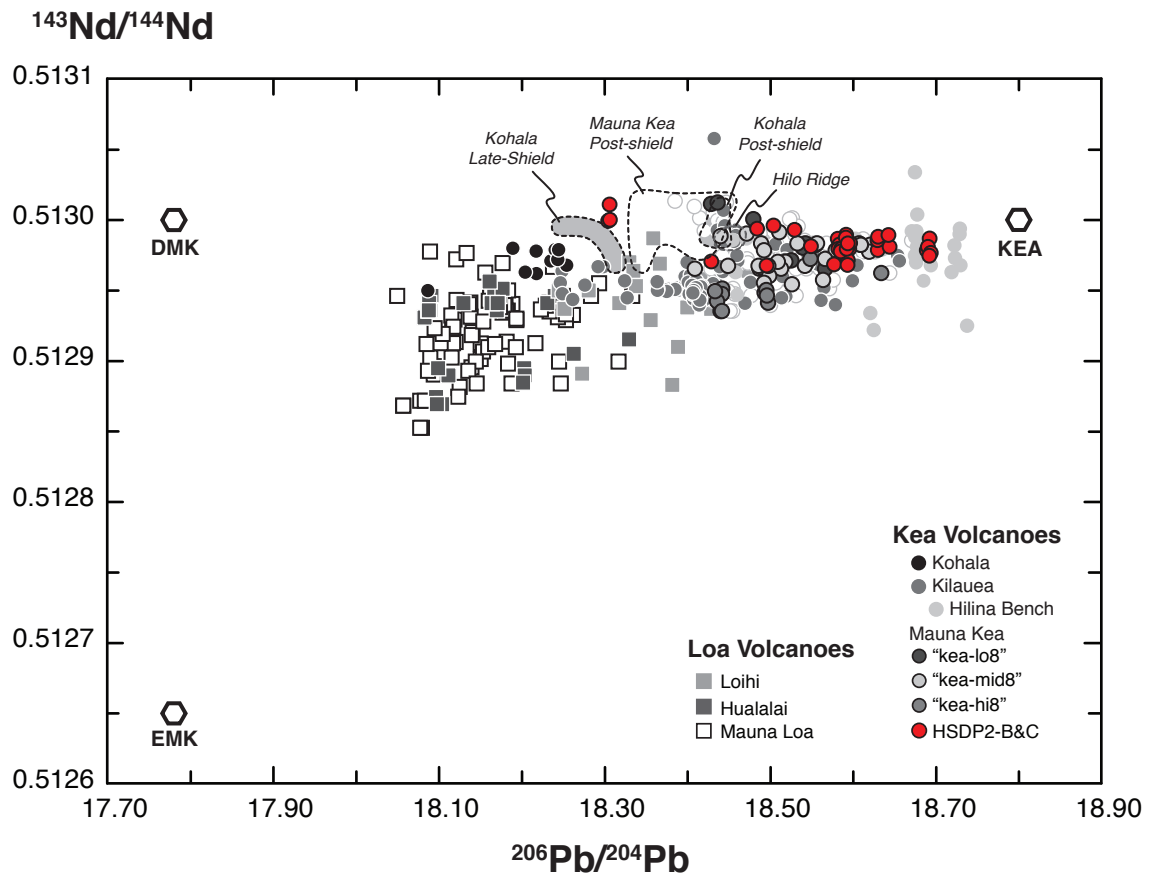
Figure 5.6. Diagram of $^{143}Nd/^{144}Nd$ versus $^{206}Pb/^{204}Pb$ for the HSDP2 Mauna Kea basalts compared to shield basalts from the other volcanoes on the Big Island of Hawaii (Kohala, Hualalai, Mauna Loa, Kilauea, Loihi) and to post-shield lavas of Mauna Kea and Kohala. Symbols, data sources and standard normalization values are as in previous figures.

stratigraphy with those from the preceding younger Mauna Kea lavas (Figures 5.4 to 5.7) attests to the continuity of the Mauna Kea section, and for the relative homogeneity of the Mauna Kea source throughout its evolution.

The ~3263.7 m long Mauna Kea section of the HSDP2 core is thus interpreted to represent a continuous record of the last ~650 kyr of the volcanic activity of the Mauna Kea volcano as it crossed ~60–80 km over the melting region of the Hawaiian mantle plume [e.g., *Stolper et al.*, 2009]. Assuming a model ~1.5 Myr lifetime for typical Hawaiian volcanoes [e.g., *Garcia et al.*, 2006], it is unlikely that the early growth history (i.e., pre-shield stage) of Mauna Kea was sampled by the deep HSDP2 core. The fact that the deeper section of the core is constituted solely of tholeiitic basalts supports this hypothesis. Nevertheless, the duration of individual volcanoes is likely to vary, depending on the proximity of the volcano track to the center of the hotspot's melting region, which influences the amount of magma supplied to each volcano [e.g., *DePaolo and Stolper*, 1996; *DePaolo et al.*, 2001; Baker et al., 2003]. According to the model of *DePaolo and Stolper* [1996], Mauna Kea is likely to have started to grow ~1.050 Myr ago. This would place the bottom of the HSDP2 core (>650 kyr) close to the transition between the pre-shield and shield growth stages.

The older basalts recovered from deeper in the stratigraphy of the core show greater isotopic variability compared to the preceding younger tholeiitic basalts, and are isotopically similar, especially in ^{206}Pb/^{204}Pb, ^{87}Sr/^{86}Sr and ^{143}Nd/^{144}Nd, to post-shield stage lavas of Mauna Kea (Figures 5.3 to 5.7). Together with the low Zr/Nb of these basalts, which are characteristic of Kilauea and Loihi [*Rhodes and Vollinger*, 2004], this suggests that the deeper samples of the HSDP2 core may represent the very early shield stage of Mauna Kea's growth history. At this time, the degrees of melting would have increased enough to continuously produce tholeiitic compositions, but the volcano capture zone was still close enough to the edge of the melting region of the plume to sample a similar compositional domain to that sampled by the post-shield lavas.
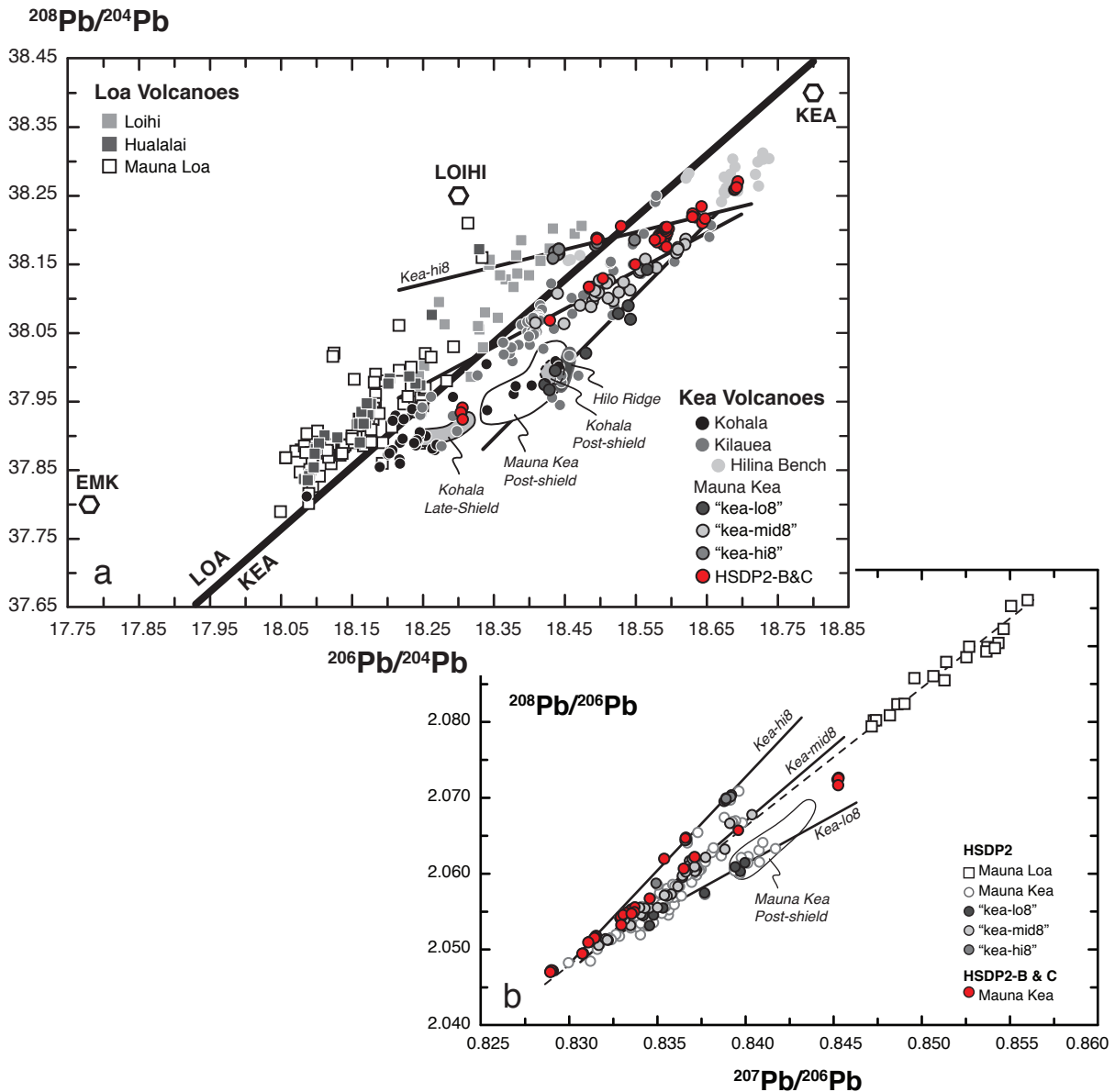
Figure 5.7. (a) $^{208}Pb/^{204}Pb$ versus $^{206}Pb/^{204}Pb$ and (b) $^{208}Pb/^{206}Pb$ versus $^{207}Pb/^{206}Pb$ diagrams for the HSDP2 Mauna Kea basalts compared to shield basalts from other volcanoes on the Big Island of Hawaii (Kohala, Hualalai, Mauna Loa, Kilauea, Loihi) and to the post-shield lavas of Mauna Kea and Kohala. The thick black line represents the Pb isotopic division for Loa and Kea trend volcanoes as defined by *Abouchami et al.* [2005]. The thin black lines represent the HSDP2 Pb isotopic arrays "Kea hi8", "Kea-mid8", and "Kea-lo8" defined by *Eisele et al.* [2003]. Symbols, data sources and standard normalization values are as in previous figures. The dashed line represents the linear regression though the "Kea-mid8" and Mauna Loa Pb isotopic compositions, indicating the involvement of Loa-like compositions, best defined by the EMK component in the Mauna Kea source region.

165

5.8.2. HSDP2 Isotope Variability and the Hawaiian Source Components

The isotopic heterogeneity among Hawaiian shield basalts has been interpreted as reflecting mixing between at least three isotopically distinct source components [e.g., *Staudigel et al.*, 1984; *Eiler et al.*, 1996; *Hauri et al.*, 1996]. These include: a relatively "depleted" component (with low $^{87}Sr/^{86}Sr$, $^3He/^4He$, $^{207}Pb/^{204}Pb$, $\delta^{18}O$, and high $^{206}Pb/^{204}Pb$, $^{208}Pb/^{204}Pb$, $^{143}Nd/^{144}Nd$, and $^{176}Hf/^{177}Hf$), best observed in basalts from Kilauea (especially in the Hilina bench) and Mauna Kea, and referred to as the "Kea" component; a "modestly depleted" component (with low $^{87}Sr/^{86}Sr$, high $^3He/^4He$, $^{143}Nd/^{144}Nd$, and $^{176}Hf/^{177}Hf$, and higher $^{208}Pb/^{204}Pb$) best expressed in basalts from Loihi, hence referred to as the "Loihi" component; and an "enriched" component (with high $^{87}Sr/^{86}Sr$, $^{207}Pb/^{204}Pb$, $\delta^{18}O$, and low $^{206}Pb/^{204}Pb$, $^{208}Pb/^{204}Pb$, $^{143}Nd/^{144}Nd$, and $^{176}Hf/^{177}Hf$) best recognized in basalts from Koolau and Lanai, and referred to as "Koolau" component [e.g., *Eiler et al.*, 1996]. Given the large isotopic variability among shield basalts from Koolau volcano, recent studies have proposed that two end-member compositions contribute to the Koolau component [e.g., *Tanaka et al.*, 2002; 2008; *Fekiacova et al.*, 2007]. The enriched Koolau end-member, which is best observed in the Makapuu stage lavas, is widely referred to as the "enriched Makapuu component" (EMK). However, two different isotopic compositions have been attributed to the depleted Koolau end-member. *Fekiacova et al.* [2007] considered the depleted Koolau end-member to be best represented by the Kahili stage lavas and referred to it as the "Kahili" component, whereas *Tanaka et al.* [2008] considered the depleted Koolau end-member to also include rejuvenated-stage lavas and termed it the "depleted Makapuu component" (DMK).

The isotopic variability observed at the scale of growth of a single volcano can be explained by similar mixing relations involving systematically different proportions of these components. Koolau (or enriched Makapuu) and Loihi components are interpreted to contribute to most of the Loa-like volcano variability, and Kea is considered the major component in Kea-like volcanoes [e.g., *Eiler et al.*, 1996; *Kimura et al.*, 2006; *Tanaka et al.*, 2008]. Based on the Pb isotope variations within the first 3100 m of the HSDP2 core, *Eisele et al.* [2003] recognized the necessity of four distinct components in the Mauna Kea source

to explain the geometry of the three "Kea" Pb arrays. The Pb isotope variability of the basalts recovered in the bottom 400 m of the core is consistent with this isotopic end-member scenario, involving a radiogenic Pb end-member, most similar to the "Kea" component, and three other distinct components of unradiogenic Pb isotopic compositions with distinct $^{208}Pb/^{204}Pb$, most similar to "Loihi", EMK, and DMK (Figure 5.7). Whereas "Kea" is a common component throughout the long-term evolution of Mauna Kea, "Loihi"-, EMK-, and DMK-like components were involved at different stages of the volcano's eruptive history and each contributed to the shorter-term isotopic variability of Mauna Kea as represented by the different "Kea-hi8", "-mid8", and "-lo8" arrays of *Eisele et al.* [2003], respectively (Figure 5.7). Some basalts in the deeper stratigraphic section of the core, characterized by low-SiO_2 contents, plot within the "Kea-hi8" array defined by a restricted group of basalts higher in the stratigraphic section of Mauna Kea [*Eisele et al.,* 2003]. This implies that the component responsible for producing low-SiO_2–high $^{208}Pb*/^{206}Pb*$ lavas was sampled early in Mauna Kea's history and not only for a short time period (~45 kyr, corresponding to a depth interval of ~900 m) of its evolution.

5.8.3. Chemical Structure of the Hawaiian Plume During the Growth of Mauna Kea

Hawaiian volcanoes younger than 5 Ma form two subparallel chains, termed Kea and Loa [*Dana*, 1849; *Jackson et al.*, 1972] that are systematically distinct chemically and isotopically [e.g., *Frey and Rhodes*, 1993; *Abouchami et al.*, 2005]. The geochemical differences between volcanoes along the two chains are interpreted to be related to the structure of the Hawaiian plume. Two main models of plume structure are invoked to explain the geochemical differences between Kea and Loa volcanoes: a concentrically zoned plume [e.g., *Hauri et al.*, 1996; *Lassiter et al.*, 1996; *DePaolo et al.*, 2001] and a bilaterally zoned plume [*Abouchami et al.*, 2005]. Both purely concentric and bilateral asymmetrical models are however unable to fully explain all the geochemical variability observed in Hawaiian basalts, and a diversity of variations of these structures incorporating vertical heterogeneities within the upwelling plume have been proposed, [e.g., *Frey and Rhodes*, 1993; *DePaolo et*

al., 2001; *Blichert-Toft et al.*, 2003; *Kurz et al.*, 2004; *Abouchami et al.*, 2005; *Huang and Frey*, 2005; *Marske et al.*, 2007; *Xu et al.*, 2007; *Blichert-Toft and Albarède*, 2009; *Hanano et al.*, 2010; *Farnetani and Hofmann*, 2010].

The similarity of the Sr and Nd isotopic compositions of basalts from the deeper section of the HSDP2 core to those of lavas erupted during the post-shield stage indicates that during both the early and late stages of Mauna Kea evolution the volcano sampled a compositionally similar domain within the melting region of the Hawaiian plume. This would be consistent with a concentrically zoned chemical structure of the Hawaiian plume [e.g., *Lassiter et al.*, 1996; *DePaolo et al.*, 2001; *Bryce et al.*, 2005]. However, the Pb isotopic compositions of the deeper basalts of the Mauna Kea HSDP2 core differ from the respective post-shield lavas, having higher $^{208}Pb/^{206}Pb$ (Figure 5.7). This indicates that the early shield stage sampled a domain of the plume characterized by higher Th/U than the post-shield stage lavas. In a comparative study of the geochemistry of post-shield and shield lavas from consecutive Loa and Kea volcano pairs, *Hanano et al.* [2010] showed that the post-shield lavas retain their Loa- and Kea-like Pb isotope signatures, which also does not support a concentrically zoned plume structure.

The isotopic similarity of the old Mauna Kea basalts from the HSDP2 core to pre-historic and to young Kilauea basalts [*Kimura et al.*, 2006; *Marske et al.*, 2007; 2008] supports the proposals that heterogeneities within the Hawaiian plume are sampled by melting regions of consecutive Kea volcanoes [*Abouchami et al.*, 2005; *Farnetani and Hofmann*, 2010]. Vertical heterogeneity appears to be an intrinsic feature of the Hawaiian plume and is superimposed on radial heterogeneity derived from the thermal structure of the plume [e.g., *Hauri et al.*, 1996]. The Sr and Nd isotopic compositions of Hawaiian basalts follow the concentric thermal structure of the Hawaiian plume as the potential temperature of the plume varies from the periphery to the core of the plume [e.g., *DePaolo et al.*, 2001; *Bryce et al.*, 2005]. As each volcano moves across the melting region of the plume the range of $^{87}Sr/^{86}Sr$ and $^{143}Nd/^{144}Nd$ compositions sampled increases and decreases, respectively, from the periphery to the centre of the plume. In contrast, the Pb isotopic compositions

sampled during the lifetime of Hawaiian volcanoes support an aspect of bilateralism in the distribution of compositional heterogeneities in the plume. These heterogeneities may be restricted to the "core zone" of the plume [*Bryce et al.*, 2005] or distributed through the entire plume radius [e.g., *Abouchami et al.*, 2005; *Farnetani and Hofmann*, 2010].

5.8.4. The Nature of the "Kea" Component and the Deep Pacific Mantle

The enriched nature of the Koolau component is considered to result from incorporation of ancient subducted oceanic crust and sediments into the Hawaiian plume [e.g., *Lassiter and Hauri*, 1998; *Blichert-Toft et al.*, 1999; *Tanaka et al.*, 2008], however the depleted nature of the "Kea" component continues to be a matter of debate. On the basis of Sr and Nd isotopic compositions, "Kea" was first interpreted to result from entrainment of depleted asthenospheric mantle [*Lassiter et al.*, 1996], but O, Os, and Pb isotopic studies precluded this hypothesis and instead support assimilation of Pacific lithosphere [*Eiler et al.*, 1996], or the presence of recycled oceanic lithosphere [*Lassiter and Hauri*, 1998] or "young HIMU" material (recycled oceanic crust younger than 1.5 Ga) in the Hawaiian plume source [*Thirlwall*, 1997; *Eisele et al.*, 2003]. Some of the basalts recovered in the bottom 400 m of the HSDP2 core, together with the pre-historical Kilauea basalts from the Hilina bench [*Kimura et al.*, 2006], have the most "depleted" Sr, Nd and Hf isotopic characteristics and the most radiogenic Pb compositions of all Hawaiian shield basalts. This suggests that during the earlier phase of shield building of a Kea trend volcano the "Kea" component is sampled in higher proportions compared to later periods of volcano growth. The compositions of these basalts erupted early in the growth history of a Kea trend volcano thus provide insight into the nature of the "Kea" component.

The correlation between high $^{143}Nd/^{144}Nd$, $^{208-7-6}Pb/^{204}Pb$, and low $^{87}Sr/^{86}Sr$ of "Kea" compositions reflects derivation from a source that developed high Sm/Nd and (U,Th)/Pb with lower Th/U and Rb/Sr over time. Such geochemical characteristics are normally attributed to a HIMU-like source, generated by recycling of ancient subduction-modified oceanic lithosphere [e.g., *Hofmann and White*, 1982; *Zindler and Hart*, 1986; *Chauvel et al.*,
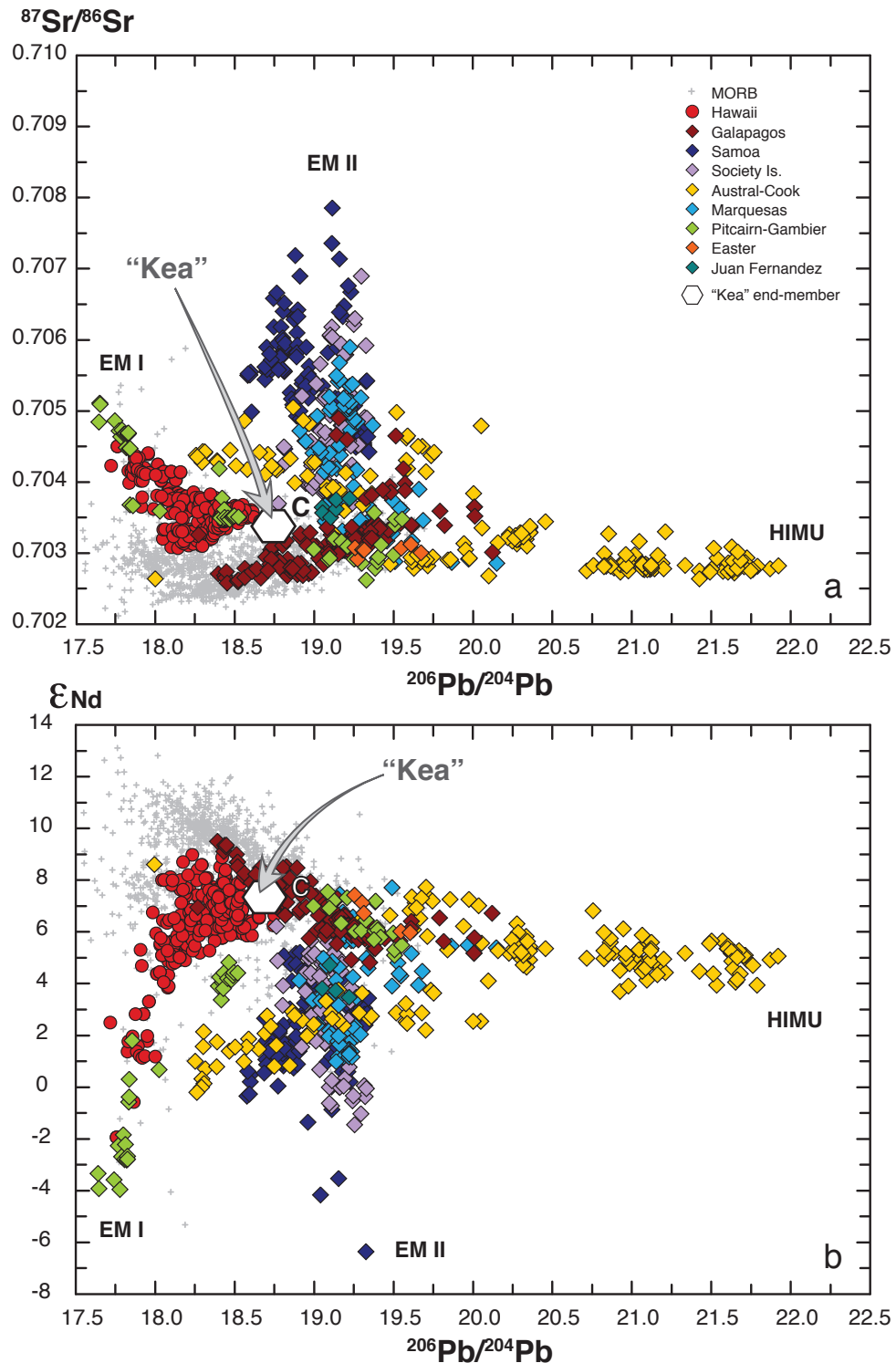
Figure 5.8. Comparison of the isotopic compositions of Hawaiian basalts and of the "Kea" component to those of other groups of Pacific Ocean island basalts. (a) $^{87}Sr/^{86}Sr$ versus $^{206}Pb/^{204}Pb$, and (b) $^{143}Nd/^{144}Nd$ versus $^{206}Pb/^{204}Pb$ diagrams. Data compiled from the GEOROC database (http://www.georoc.mpch-mainz.gwdg.de). End-members are from *Zindler and Hart* [1986] and *Hanan and Graham* [1996].

1992; *Stracke et al.*, 2005; *Willbold and Stracke*, 2006]. Compared to "Kea", HIMU-like compositions have much more radiogenic Pb isotopic signatures, which indicates that "Kea" must be derived from a source with significantly lower μ ($^{238}U/^{204}Pb$) values to produce $^{206}Pb/^{204}Pb$ ratios below 19.

Throughout the volcanic activity related to the Hawaiian mantle plume, the "Kea" component has been a prevalent composition. When comparing the Pb-Sr-Nd isotopic compositions of Hawaiian basalts to other Pacific Ocean island basalts, the "Kea" component occupies an intermediate position towards which general trends (from EM-1, EM-2 and HIMU) converge in binary diagrams (Figure 5.8). The isotopic characteristics of the Kea component are not very different from those of the common mantle component "C" [*Hanan and Graham*, 1996]. The Hawaiian plume is one of the most productive mantle plumes on Earth, having erupted ~$7x10^6$ km^3 of volcanic material over the formation of the Hawaiian-Emperor chain [*Vidal and Bonneville*, 2004] and Kea-like compositions have been erupted throughout its life [e.g., *Regelous et al.*, 2003; *Abouchami et al.*, 2005; *Tanaka et al.*, 2008]. This may imply that the Kea composition is itself a common and widespread composition within the Pacific mantle.

5.9. Conclusions

High-precision Sr, Nd, and Pb isotopic compositions of basalts from the bottom 400 m of the ~3500 m long HSDP2 drill core on Mauna Kea reveal compositional continuity with the overlying basalts and the presence of two distinct sample groups. Basalts from the top 210 m form the longest interval (~10 kyr) of limited variation within the sampled output record of Mauna Kea. This indicates the sampling of a more homogeneous domain within the magma source region of Mauna Kea during the time interval represented by those basalts. In contrast, basalts from the bottom 192 m show the largest range of variation in their Pb isotopic compositions. These older basalts extend the isotopic compositions of Mauna Kea to significantly more radiogenic values, similar to those of "ancestral" Kilauea lavas, and also to significantly less radiogenic values, similar to those of late shield and post-shield lavas

(<400 kyr) from Mauna Kea and Kohala. Based on their older ages (> 650 kyr) and compositional characteristics, these basalts likely erupted in the very early shield phase of Mauna Kea, rather than representing part of the output of Kohala or another unknown volcano. The Pb isotopic compositions of the HSDP2 basalts are consistent with the presence of four source components during the growth of Mauna Kea and include the "Kea", "Loihi", EMK, and DMK components. "Kea" is the prevailing component throughout the evolution of Mauna Kea, whereas the remaining three components appear to have been involved in different stages of volcano development and contribute to the short-term isotopic variability of Mauna Kea basalts. In Pb-Sr-Nd isotope binary diagrams, "Kea" occupies an intermediate position towards which the general trends formed by other Pacific Ocean island groups (from EM-1, EM-2 and HIMU) converge. This indicates that the "Kea" component is not only the common composition within the Hawaiian mantle plume, but also that it is a common composition within the deep Pacific mantle.

Chapter 6

Conclusions

6.1 Summary and Conclusions

For geochemists, oceanic basalts related to hotspot activity represent the best samples to access and characterize the composition of regions of the deep mantle, in contrast to mid-ocean ridge basalts that sample the relatively shallow asthenospheric mantle. The research reported in this dissertation focused on deciphering the nature and relative proportions of mantle source components involved in the formation of two major hotspot tracks on Earth, the Ninetyeast Ridge [*Luyendyk*, 1977; *Royer et al*., 1991] and Hawaii [*Dana*, 1849; *Jackson et al*., 1972]. These two hotspot tracks are associated with volcanic activity of the deep and long-lived Kerguelen and Hawaiian mantle plumes, respectively [e.g., *Morgan*, 1971; *Sleep*, 1990; *Weis et al*., 1991; *Montelli et al*., 2004, 2006; *Bryce et al*., 2005]. To ensure that the measured isotopic compositions (e.g., Pb-Sr-Nd-Hf) of ocean island basalts are indeed representative of their mantle sources, an analytical investigation of the efficiency of acid leaching in removing post-magmatic alteration phases and extraneous contaminants was first undertaken.

Scientific drilling (e.g. Deep Sea Drilling Project [DSDP], Ocean Drilling Program [ODP], Integrated Ocean Drilling Program [IODP] and International Continental Scientific Drilling Program [ICDP]) is an essential sampling method for recovering deep ocean basalt. Drilling provides a continuous sequence of samples that can be studied and interpreted in the context of shallow-level magmatic processes and deeper mantle evolution with time. As part of two major international research programs (IODP and ICDP), this project provided a detailed study of Pb, Hf, Sr and Nd isotope variations on key stratigraphically controlled samples from the Ninetyeast Ridge, the longest linear feature on Earth, and Hawaii. These results were then used to understand the chemical evolution of the Kerguelen and Hawaii hotspot systems and place constraints on the composition of distinct deep mantle domains beneath the Indian and Pacific Ocean basins, respectively.

6.1.1. Leaching Systematics of Ocean Island Basalts

The Pb and Sr isotopic compositions of oceanic basalts can be significantly modified by post-magmatic, low-temperature seawater alteration, hindering their use as geochemical tracers of mantle source compositions (Chapters 2 and 3). In contrast, the Nd and Hf isotopic compositions are not significantly affected by alteration. Additional disturbances to the isotopic compositions of basalts can be introduced by assimilation of external contaminants such as Fe-Mn oxides, deep-sea sediments, or loess, and by contamination during sample collection, crushing and grinding. To overcome such chemical disturbances and to obtain the most accurate and reproducible isotopic compositions on basalts required to decipher mantle source components, the samples must be subjected to acid-leaching treatment prior to isotopic analysis. The studies presented in Chapters 2 and 3 show that the elemental concentrations are greatly affected by acid leaching and thus are not reliable magmatic elemental signatures. In contrast, comparison of the isotopic differences between several unleached and acid-leached basalts of different ages, from the Hawaii and Kerguelen hotspots, indicate that reproducible high-precision isotopic compositions, representative of the magma source of oceanic basalts, can be achieved by adequate sample treatment, encompassing both thorough acid leaching and careful matrix elimination.

6.1.2. Identifying Mantle Components in Basalts from Major Hotspot Tracks on Earth

High-precision isotopic analysis of ODP Leg 121 basalts from the Ninetyeast Ridge and of basalts from the deeper stratigraphic section of the HSDP2 on Hawaii were obtained following a careful sample preparation and analysis using state-of-the-art analytical instruments such as the Nu Plasma MC-ICP-MS. These results have allowed for enhanced resolution of the source components involved in the Ninetyeast Ridge and in the Mauna Kea volcano.

The isotopic compositions of the Ninetyeast Ridge, a 5000 km-long linear aseismic ridge located in the Indian Ocean, are consistent with the involvement of at least three

distinct components intrinsic to the mantle source of the ridge (Chapter 4). Contrary to earlier studies [e.g., *Weis and Frey*, 1991], the new and more precise isotopic data reveal that the depleted Indian asthenospheric mantle does not take part in its genesis. The isotopic compositions of the Ninetyeast Ridge are intermediate to those of the volcanic products of both the Kerguelen and Amsterdam-St. Paul hotspots. Simple binary mixing between the two cannot account for the isotopic variability observed among the Ninetyeast Ridge basalts. This implies that the mantle sources of the ridge are compositionally more heterogeneous in time and space than previously assumed.

The ~3500 metre-long HSDP2 core represents the longest record of the magmatic output of a single volcano yet, covering >600 kyr of the evolution of Mauna Kea. Integration of the isotopic compositions of the older basalts deeper in the stratigraphy of the HSDP2 core obtained during this research (Chapter 5) with those of the younger basalts higher in the stratigraphic section of Mauna Kea confirms the presence of four source components during the growth of this Hawaiian volcano. The "Kea" component is the prevailing component throughout the evolution of Mauna Kea, whereas the remaining three components ("Loihi", Enriched Makapuu [EMK] and Depleted Makapuu [DMK]) were involved in different stages of volcano development and contributed to the short-term isotopic variability of Mauna Kea basalts.

6.1.3. Fingerprinting Deep Mantle Heterogeneities Beneath the Indian and the Pacific Ocean Basins

At the broader, regional scale, isotopic compositions of basalts from both the Ninetyeast Ridge and Hawaiian reflect sampling of a mantle source with geochemical characteristics that are intrinsic their respective mantle domains (Chapters 4 and 5). Within the Indian Ocean basin, the Ninetyeast Ridge, together with other Indian Ocean island basalts, has isotopic characteristics typical of the Dupal isotopic domain [*Hart*, 1984]. These characteristics are interpreted to result from mixing of a common mantle source of composition similar to "C" or "FOZO" [*Hanan and Graham*, 1996; *Stracke et al.*, 2005] and

an enriched mantle source component. In contrast to the early stages of evolution of the Kerguelen Plateau that show evidence for contamination by continental crust [e.g., *Weis et al.*, 2001; *Frey et al.*, 2000a, 2002a], the isotopic and trace element compositions of the Ninetyeast Ridge do not indicate incorporation of continental material at shallow depths. This implies that the enriched EM-1-like, Dupal compositions observed in the Ninetyeast Ridge basalts are inherited from its deep source. The compositions are best explained by a contribution of a mixture of pelagic sediments and lower continental crust recycled together with altered oceanic crust in their deep mantle source (Chapter 4). This is in agreement with models proposed for the generation of enriched mantle compositions [e.g., *Willbold and Stracke*, 2010] and argues for a deep-seated origin the Dupal isotopic domain [e.g., *Castillo*, 1988; *Weis et al.*, 1991].

Relatively "depleted" isotopic signatures inherent to the mantle plume source have been observed in a number of hotspot settings, including Galapagos, Iceland, Kerguelen, and Hawaii [e.g., *Blichert-Toft and White*, 2001; *Doucet et al.*, 2002; *Fitton et al.*, 2003; *Mukhopadyay et al.*, 2003; *Frey et al.*, 2005]. Throughout the volcanic activity related to the Hawaiian mantle plume (~7×10^6 km^3 of volcanic material over ~80 Myr; *Vidal and Bonneville* [2004]), the "Kea" component has been a prevalent composition. Within the Pacific Ocean basin, the relatively "depleted" isotopic compositions of the Hawaiian "Kea" component represent an end-member shared by other Pacific OIB groups (Chapter 5). The isotopic compositions of the "Kea" component are not very different from those of the common mantle component "C" [*Hanan and Graham*, 1996]. This may imply that the Kea composition is itself a common and widespread composition within the Pacific mantle.

6.2. Directions for Future Research

6.2.1. Broader Leaching Studies

The capabilities of analytical instrumentation continue to advance and the level of precision and accuracy required to make progress in our understanding of mantle geochemistry continues to improve. Careful sample preparation and chemical separation protocols are thus inevitable for reliable, accurate, and precise isotopic analyses and

elemental concentrations. The present study focused on a step-by-step characterization of how Pb, Sr, Nd, and Hf isotopes and elemental concentrations in oceanic basalts of tholeiitic to mildly alkalic compositions behave during acid leaching treatment and matrix elimination. To fully understand the effects of seawater alteration on other types of volcanic rocks in or near the ocean environment, it would be beneficial to undertake a similar study using samples of more alkalic compositions such as trachybasalts and basanites, as well as more evolved rocks such as trachytes and phonolites.

6.2.2. Additional Sampling on the Ninetyeast Ridge

The results reported in Chapter 4 provide new insight into the mantle source components of the Ninetyeast Ridge. However, the genetic relationship of the Kerguelen and Amsterdam-St. Paul hotspots and the timing of interaction between the two to form the Ninetyeast Ridge are still not clearly understood. Stratigraphically controlled samples from the Ninetyeast Ridge for geochronological and geochemical analyses are sparse and may not be fully representative of the compositions of the main phase of volcanism of the ridge. This is evidenced by the relatively shallow (< 200 m) basaltic basement penetrations at only seven sites during both DSDP and ODP drilling campaigns in the late 1980s.

After the IODP site survey in June-July of 2007, the sampling density along the Ninetyeast Ridge increased significantly. Dredging represents a good complement to drilling as it allows for sampling larger amounts of material and recovers a greater range of lithologies from a more diverse sampling region. Although this is a good technique for reconnaissance, it does not allow for stratigraphically-controlled geochemical studies, which are essential for characterizing the temporal geochemical variations that occur at the volcanic edifice scale and for constraining the compositional variability within the plume source region. Additional constraints to the Ninetyeast Ridge source variability would benefit from deepening of the existing drill holes (using the IODP Chikyu research vessel, which has deeper drilling capabilities), as well as from sampling at new drill sites of interest based on the preliminary geochemical results obtained on the dredged samples (Appendix B).

A better understanding of the relation between the Kerguelen and Amsterdam-St. Paul hotspots and the formation of the Ninetyeast Ridge would benefit from sampling the seamount chains between the southeastern end of the Ninetyeast Ridge and the Amsterdam-St. Paul Plateau and between the southeastern part Amsterdam-St. Paul Plateau and the northeastern part of the Kerguelen Plateau (Figure 1.3).

6.2.3. Drilling of a Loa Trend Volcano?

The temporal and spatial chemical variations of basalts erupted by Hawaiian volcanoes provide information about the physical and chemical structure of one of the most productive and long-lived mantle plumes on Earth [e.g., *Sleep*, 1990]. To test models for the temporal and spatial distribution of compositional heterogeneities within the Hawaiian plume conduit, recent studies, including the one presented in Chapter 5, have focused on the high-resolution of temporal chemical variations within a single volcano as observed in subaerial stratigraphic lava successions [e.g., *Pietruszka and Garcia*, 1999; *Marske et al*., 2007; 2008], deep drilling cores [e.g., HSDP on Mauna Kea, *DePaolo et al*., 2001; *Blichert-Toft et al*., 2003; *Bryce et al.*, 2005; SOH on Kilauea, *Quane et al*., 2000; KSDP on Koolau, *Huang and Frey*, 2005; *Salters et al*., 2006; *Fekiacova et al*., 2007], or submarine stratigraphic successions sampled by ROV [e.g., Mauna Loa SWRZ, Weis unpublished data, 2002] .

The geochemical differences between basalts from the Loa and Kea trend volcanoes are interpreted to reflect sampling of two different areas of the Hawaiian mantle plume [e.g., *Lassiter et al*., 1996; *Abouchami et al*., 2005; *Bryce et al*., 2005; Weis, 2010 in preparation]. The recovery of volcanic rocks up to a depth of ~3500 metres below sea level during the HSDP, which span most of Mauna Kea's life cycle, has allowed for the characterization and quantification of the geochemical evolution of a single Kea trend volcano as it moved across the melting source region and has provided important information about plume conduit dynamics [e.g., *Abouchami et al*., 2005; *Bryce et al*., 2005; *Farnetani and Hofmann*, 2010]. Additional knowledge regarding the Hawaiian plume structure would be gained by a similar deep drilling study on a Loa trend volcano. Although scientific drilling has been conducted in Koolau, which is a Loa trend volcano, the shallow penetration depth (~632 mbsl) allowed

only for characterization of the later portions of volcano evolution (late-shield, post-shield and rejuvenated stages). Koolau also has some of the most extreme isotopic compositions observed in Hawaii and is not representative of the main Loa compositions. The most suitable target volcano for scientific drilling and studying the temporal geochemical evolution of a Loa volcano, and subsequently of the Loa source region, would be Hualalai. This is the third youngest and third-most historically active volcano on the Island of Hawaii. Hualalai has gone through all the major growth stages of the life cycle of a Hawaiian volcano. Compared to Mauna Loa, its much smaller size (2,521 m high and 12,400 km^3) would allow for recovery of lavas representative of the entire output of a single volcano, especially from the very early pre-shield growth stage.

BIBLIOGRAPHY

Abouchami, W., and S. J. G. Galer (1998), The provinciality of Pb isotopes in Pacific Fe-Mn deposits, 8th Goldschmidt Conf., *Mineral. Mag.*, *62A*, 1–2, doi:10.1180/minmag.1998.62A.1.01.

Abouchami, W., S. J. G. Galer, and A. W. Hofmann (2000), High precision lead isotope systematics of lavas from the Hawaiian Scientific Drilling Project, *Chem. Geol., 169*, 187–209.

Abouchami, W., A. W. Hofmann, S. J. G. Galer, F. A. Frey, J. Eisele, and M. Feigenson (2005), Lead isotopes reveal bilateral asymmetry and vertical continuity in the Hawaiian mantle plume, *Nature, 434*, 851–856.

Aciego, S. M., F. Jourdan, D. J. DePaolo, B. M. Kennedy, P. R. Renne, and K. W. W. Sims (2010), Combined U-Th/He and $^{40}Ar/^{39}Ar$ geochronology of post-shield lavas from the Mauna Kea and Kohala volcanoes, Hawaii, *Geochim. Cosmochim. Acta*, *74*(5), 1620–1635.

Albarède, F. (1995), Introduction to geochemical modelling, Cambridge University Press, 545 p., ISBN: 978–0–52157804–2.

Albarède, F., S. L. Goldstein, and D. Dautel (1997a), The neodymium isotopic composition of manganese nodules from the Southern and Indian oceans, the global oceanic neodymium budget, and their bearing on deep ocean circulation, *Geochim. Cosmochim. Acta*, *61*(6), 1277–1291.

Albarède, F., B. Luais, G. Fitton, M. Semet, E. Kaminski, B. G. J. Upton, P. Bachelery, and J.-L. Cheminee (1997b), The geochemical regimes of Piton de la Fournaise volcano (Réunion) during the last 530 000 years, *J. Petrol., 38*, 171–201.

Albarède, F., P. Télouk, J. Blichert-Toft, M. Boyet, A. Agranier, and B. Nelson (2004), Precise and accurate isotopic measurements using multiple-collector ICPMS. *Geochim. Cosmochim. Acta, 68*, 2725–2744.

Albarède, F., A. Stracke, V. J. M. Salters, D. Weis, J. Blichert-Toft, P. Télouk, and A. Agranier (2005), Comment to ''Pb isotopic analysis of standards and samples using a ^{207}Pb-^{204}Pb double spike and thallium to correct for mass bias with a double-focusing MC-ICP-MS'' by Baker et al., *Chem. Geol., 217*, 171–174.

Baker, J., D. Peate, T. Waight, and C. Meysen (2004), Pb isotopic analysis of standards and samples using a ^{207}Pb-^{204}Pb double spike and thallium to correct for mass bias with a double-focusing MC-ICP-MS, *Chem. Geol., 211*, 275–303.

Baker, J., D. Peate, T. Waight, and M. Thirlwall (2005), Reply to the comment to ''Pb isotopic analysis of standards and samples using a ^{207}Pb-^{204}Pb double spike and thallium to correct for mass bias with a double-focusing MC-ICP-MS'' by Baker et al., *Chem. Geol., 217*, 175–179.

Baker, M., D.A., Stolper, E.M., Stolper, Y., Fialko (2003), Modelling the growth of Hawaiian volcanoes, *EOS Trans. AGU, 84*(46), Fall Meet. Suppl., Abstracts V11B03.

Barling, J., and S. L. Goldstein (1990), Extreme isotopic variations in Heard Island lavas and the nature of mantle reservoirs, *Nature, 348*, 59–62.

Barling, J., S. L. Goldstein, and I. A. Nicholls (1994), Geochemistry of Heard Island (Southern Indian Ocean): characterization of an enriched mantle component and implications for enrichment of the Sub-Indian Ocean mantle, *J. Petrol., 35*, 1017–1053.

Barling, J., and D. Weis (2008), Influence of non-spectral matrix effects on the accuracy of Pb isotope ratio measurement by MC-ICP-MS: implications for the external normalization method of instrumental mass bias correction, *J. Anal. At. Spectrom., 23*, 1017–1025, doi: 10.1039/b717418g.

Barry, T. L., P. D. Kempton, and A. D. Saunders (2002), Hf isotopes from the Ninetyeast Ridge. Goldschmidt Conference Abstracts. *Geochim. Cosmochim. Acta, 66*, 1–100.

Barry, T. L., P. D. Kempton, and A. D. Saunders (2003), Contribution from two mantle plumes to the Ninetyeast Ridge basalts, but did it form at a ridge? *EGS - AGU - EUG Joint Assembly*, Abstract #13048.

Bau, M., A. Koschinsky, P. Dulski, and J. R. Hein (1996), Comparison of the partitioning behaviours of yttrium, rare earth elements, and titanium between hydrogenetic marine ferromanganese crusts and seawater, *Geochim. Cosmochim. Acta, 60*(10), 1709–1725.

Belshaw, N. S., P. A. Freedman, R. K. O'Nions, M. Frank, and Y. Guo (1998), A new variable dispersion double-focusing plasma mass spectrometer with performance illustrated for Pb isotopes, *Int. J. Mass Spectrom., 181*, 51–58.

Blichert-Toft, J., C. Chauvel, and F. Albarède (1997), Separation of Hf and Lu for high-precision isotope analysis of rock samples by magnetic sector-multiple collector ICP-MS, *Contrib. Mineral. Petrol., 127*, 248–260.

Blichert-Toft, J., F. A. Frey, and F. Albarède (1999), Hf isotope evidence for pelagic sediments in the source of Hawaiian basalts, *Science, 285*(5429), 879–882.

Blichert‑Toft, J. and W. M. White (2001), Hf isotope geochemistry of the Galapagos Islands, *Geochem. Geophys. Geosyst.*, 2, 1043, doi:10.1029/2000GC000138.

Blichert-Toft, J., D. Weis, C. Maerschalk, A. Agranier, and F. Albarède (2003), Hawaiian hot spot dynamics as inferred from the Hf and Pb isotope evolution of Mauna Kea volcano, *Geochem. Geophys. Geosyst., 4* (2), 8704, doi:10.1029/2002GC000340.

Blichert-Toft, J., and F. Albarède (2009), Mixing of isotopic heterogeneities in the Mauna Kea plume conduit, *Earth Planet. Sci. Lett., 282*(1-4), 190–200.

Borisova, A. Y., B. V. Belyatsky, M. V. Portnyagin, and N. M. Sushchevskaya (2001), Petrogenesis of olivine-phyric basalts from the Aphanasey Nikitin Rise: evidence for contamination by cratonic lower continental crust, *J. Petrol., 42*, 277–319.

Bosch, D., J. Blichert-Toft, F. Moynier, B. K Nelson, P. Telouk, P. -Y. Gillot, and F. Albarède (2008), Pb, Hf and Nd isotope compositions of the two Réunion volcanoes (Indian Ocean): A tale of two small-scale mantle "blobs"?, *Earth Planet. Sci. Lett., 265*, 748–768.

Bryce, J. G., D. J. DePaolo, and J. C. Lassiter (2005), Geochemical structure of the Hawaiian plume: Sr, Nd, and Os isotopes in the 2.8 km HSDP-2 section of Mauna Kea volcano, *Geochem. Geophys. Geosyst., 6,* Q09G18, doi:10.1029/2004GC000809.

Campbell, I. H. (2005), Large Igneous Provinces and the Mantle Plume Hypothesis, *Elements, 1*(5), 265–269.

Campbell, I. H., and R. W. Griffiths (1990), Implications of mantle plume structure for the evolution of flood basalts, *Earth Planet. Sci. Lett., 99,* 79–93.

Campbell, I. H., and R. W. Griffiths (1991), On the dynamics of long-lived plume conduits in the convecting mantle, *Earth Planet. Sci. Lett., 103*, 214–227.

Castillo, P. (1988), The Dupal anomaly as a trace of the upwelling lower mantle, *Nature, 336*, 667–670.

Chauvel, C., A. W. Hofmann, and P. Vidal (1992), HIMU-EM: The French Polynesian connection, *Earth Planet. Sci. Lett., 110*, 99–119.

Chauvel, C., and J. Blichert-Toft (2001), A hafnium isotope and trace element perspective on melting of the depleted mantle, *Earth Planet. Sci. Lett., 190*, 137–151.

Chauvel, C., E. Lewin, M. Carpentier, N. T. Arndt, and J. -C. Marini (2008), Role of recycled oceanic basalt and sediment in generating the Hf-Nd mantle array, *Nature Geosciences, 1*, 64–67.

Chen, C.-Y., and F. A. Frey (1983), Origin of Hawaiian tholeiite and alkalic basalt, *Nature, 302*, 785–789.

Chen, C.Y., Frey, F.A., Rhodes, J.M. and Easton, R.M. (1996). Temporal geochemical evolution of Kilauea Volcano: comparison of Hilina and Puna Basalt. In: Basu, A. and Hart, S.R., Editors, 1996. Earth Processes: Reading the Isotopic Code *Am. Geophys. Monogr. 95*, pp. 161–181.

Chester, R. (2003), Marine Geochemistry (2nd ed.), *Blackwell Science Ltd*., 520p., ISBN: 1–4051–0172–5.

Class, C., S. L. Goldstein, S. J. G. Galer, and D. Weis (1993), Young formation age of a mantle plume source, *Nature, 362*, 715–721.

Class, C., S. L. Goldstein, and S. J. G. Galer (1996), Discussion of "Temporal evolution of the Kerguelen plume: geochemical evidence from ~38 to 82 Ma lavas forming the Ninetyeast Ridge" by F.A. Frey and D. Weis, *Contr. Mineral. Petrol.*, *124*(1), 98–103.

Clague, D. A., and G. B. Dalrymple (1987), The Hawaiian-Emperor Volcanic Chain Part 1: geologic evolution, *U.S. Geol. Surv. Prof. Pap.*, *1350*, 5–54.

Clague, D. A. (1987), Hawaiian xenolith populations, magma supply rates, and development of magma chambers, *Bull. Volc., 49*(4), 577–587.

Clift, P., and P. Vannucchi (2004), Controls on tectonic accretion versus erosion in subduction zones: Implications for the origin and recycling of the continental crust, *Rev. Geophys., 42*, RG2001, doi:10.1029/2003RG000127.

Coffin, M. F., and O. Eldholm (1994), Large igneous provinces: Crustal structure, dimensions, and external consequences, *Rev. Geophys., 32*, 1, doi:10.1029/93RG02508.

Coffin, M. F., et al. (2002), Kerguelen Hotspot Magma Output since 130 Ma, *J. Petrol.*, *43*(7), 1121–1137.

Coffin, M. F., et al. (2006), Large igneous provinces and scientific ocean drilling: Status quo and a look ahead, *Oceanography, 19*(4), 150–160.

Cohen, R. S., and R. K. O'Nions (1982), Identification of recycled continental material in the mantle from Sr, Nd and Pb isotope investigations, *Earth Planet. Sci. Lett.*, *61*, 73–84.

Cotten, J., et al. (1995), Origin of anomalous rare-earth element and yttrium enrichments in subaerially exposed basalts: Evidence from French Polynesia, *Chem. Geol.*, *119*(1–4), 115–138.

Courtillot, V. E., A. Davaille, J. Besse, and J. Stock (2003), Three distinct types of hotspots in the Earth's mantle, *Earth Planet. Sci. Lett.*, *205*(3-4), 295–308.

Dana, D.J. (1849), Geology, United States exploring expedition 1838-1842, vol. 10, C.Sherman, Philadelphia, PA.

David, K., M. Frank, R. K. O'Nions, N. S. Belshaw, and J. W. Arden (2001), The Hf isotope composition of global seawater and the evolution of Hf isotopes in the deep Pacific Ocean from Fe-Mn crusts, *Chem. Geol.*, *178*(1–4), 23.

Davies, G. F. (1988), Ocean bathymetry and mantle convection 1. Large-scale flow and hotspots. *J. Geophys. Res., 93*, 10,467-10,480. doi:10.1029/JB093iB09p10467.

Davies, G. F. (1999), *Dynamic Earth: Plates plumes and mantle convection*, Cambridge University Press, 472 p., ISBN: 13 978–0–521–59933–7.

DePaolo, D., and D. Weis (2007), Hotspot volcanoes and Large Igneous Provinces, In: Harms, U., C. Koeberl, and M. Zoback (eds.), *Continental Scientific Drilling: A Decade of Progress, and Challenges for the Future*, Berlin Heidelberg: Springer, 259–288.

DePaolo, D. J., and E. M. Stolper (1996), Models of Hawaiian volcano growth and plume structure: Implications of results from the Hawaii Scientific Drilling Project, *J. Geophys. Res.*, *101*(B5), 11643–11654.

DePaolo, D. J., J. G. Bryce, A. Dodson, D. L. Shuster, and B. M. Kennedy (2001), Isotopic evolution of Mauna Loa and the chemical structure of the Hawaiian plume, *Geochem. Geophys. Geosyst., 2*, 1-32, doi: 10.1029/2000gc000139.

Dixon, J. E. and D. A. Clague (2001), Volatiles in basaltic glasses from Loihi Seamount, Hawaii: evidence for a relatively dry plume component, *J. Petrol., 42* (3), 627–654.

Doucet, S., D. Weis, J. S. Scoates, K. Nicolaysen, F. A. Frey, and A. Giret (2002), The depleted mantle component in Kerguelen Archipelago basalts: Petrogenesis of the tholeiitic-transitional basalts from the Loranchet Peninsula, *J. Petrol.*, *43*(7), 1341–1366.

Doucet, S., D. Weis, J. S. Scoates, V. Debaille, and A. Giret (2004), Geochemical and Hf-Pb-Sr-Nd isotopic constraints on the origin of the Amsterdam-St. Paul (Indian Ocean) hotspot basalts, *Earth Planet. Sci. Lett., 218*, 179–195.

Doucet S., J. S. Scoates, D. Weis, and A. Giret (2005), Constraining the components of the Kerguelen mantle plume: A Hf-Pb-Sr-Nd isotopic study of picrites and high-MgO basalts from the Kerguelen Archipelago, *Geochem. Geophys. Geosyst.*, *6*, Q04007, doi:10.1029/2004GC000806.

Douglass, J., and J. G. Schilling (2000), Systematics of three-component, pseudo-binary mixing lines in 2D isotope ratio space representations and implications for mantle plume-ridge interaction, *Chem. Geol.*, *163*(1-4), 1–23.

Douglass, J., J.-G. Schilling, and D. Fontignie (1999), Plume-ridge interactions of the Discovery and Shona mantle plumes with the southern Mid-Atlantic Ridge (40º-55ºS), *J. Geophys. Res.*, *104*(B2), 2941–2962.

Duncan, R. A. (1978), Geochronology of basalts from the Ninetyeast Ridge and continental dispersion in the eastern Indian Ocean, *J. Volcanol. Geotherm. Res., 4*, 283–305.

Duncan, R.A. (1991), Age distribution of volcanism along aseismic ridges in the eastern Indian Ocean, *In* Weissel, J., J. Peirce, E. Taylor, J. Alt, et al. (eds.), *Proc. Ocean Drill. Program, Sci. Results, 121*: College Station, TX (Ocean Drill. Program), 507–517, doi:10.2973/odp.proc.sr.121.162.1991.

Duncan, R. A. and M. Storey (1992), The life cycle of Indian Ocean hotspots, In: Duncan, R. A., D. K. Rea, R. B. Kidd, U. von Rad, and J. K. Weissel (eds.), *Synthesis of Results from Scientific Drilling in the Indian Ocean. Geophysical Monograph*, *American Geophysical Union, 70*, 91–103.

Duncan, R. A. (2002), A time frame for construction of the Kerguelen Plateau and Broken Ridge, *J. Petrol.*, *43*(7), 1109–1119.

Dupré, B., and C.-J. Allègre (1980), Pb-Sr-Nd isotopic correlation and the chemistry of the north Atlantic mantle, *Nature*, *286*, 17–22.

Dupré, B., and C.-J. Allègre (1983), Pb-Sr isotope variation in Indian Ocean basalts and mixing phenomena, *Nature*, *303*, 142–146.

Eggins, S. M., J. D. Woodhead, L. P. J. Kinsley, G. E. Mortimer, P. Sylvester, M. T. McCulloch, J. M. Hergt and M. R. Handler (1997), A simple method for the precise determination of ≥ 40 trace elements in geological samples by ICPMS using enriched isotope internal standardization, *Chem. Geol.*, *134*, 311–326.

Eiler, J. M., J. W. Valley, and E. M. Stolper (1996), Oxygen isotope ratios in olivine from the Hawaii Scientific Drilling Project, *J. Geophys. Res.*, *101*(B5), 11807–11813. doi:10.1029/95JB03194.

Eisele, J., M. Sharma, S. J. G. Galer, J. Blichert-Toft, C. W. Devey and A. W. Hofmann (2002). The role of sediment recycling in EM-1 inferred from Os, Pb, Hf, Nd, Sr isotope and trace element systematics of the Pitcairn hotspot, *Earth Planet. Sci. Lett.*, *196*, 197–212.

Eisele, J., W. Abouchami, S. J. G. Galer, and A. W. Hofmann (2003), The 320 kyr Pb isotope evolution of Mauna Kea lavas recorded in the HSDP-2 drill core, *Geochem. Geophys. Geosyst.*, *4*(5), 8710, doi:10.1029/2002GC000339.

Ernst, R. E., K. L. Buchan, and I. H. Campbell (2005), Frontiers in large igneous province research, *Lithos, 79*, 271–297.

Escrig, S., F. Capmas, B. Dupré, and C. J. Allègre (2004), Osmium isotopic constraints on the nature of the DUPAL anomaly from Indian mid-ocean-ridge basalts, *Nature, 431*, 59–63.

Farnetani, C. G. (1997), Excess temperature of mantle plumes: The role of chemical stratification across D'', *Geophys. Res. Lett., 24*(13), 1583–1586. doi:10.1029/97GL01548.

Farnetani, C. G., and H. Samuel (2005), Beyond the thermal plume paradigm, *Geophys. Res. Lett., 32*, L07311, doi:10.1029/2005GL022360.

Farnetani, C. G., and A. W. Hofmann (2010), Dynamics and internal structure of the Hawaiian plume, *Earth Planet. Sci. Lett.*, *295*(1-2), 231–240.

Farnetani, C. G., B. Legras and P. J. Tackley (2002), Mixing and deformations in mantle plumes, *Earth Planet. Sci. Lett., 196*, 1–15.

Faure, G. (1986), Principles of Isotope Geology (2nd ed.), John Wiley & Sons, Inc. New York, 589p., ISBN: 0–471–86412–9.

Feigenson, M. D., L. L. Bolge, M. J. Carr, and C. T. Herzberg (2003), REE inverse modeling of HSDP2 basalts: Evidence for multiple sources in the Hawaiian plume, *Geochem. Geophys. Geosyst.*, *4*(2), 8706, doi:10.1029/2001GC000271.

Fekiacova, Z., W. Abouchami, S. J. G. Galer, M. O. Garcia, and A. W. Hofmann (2007), Origin and temporal evolution of Ko'olau Volcano, Hawaii: Inferences from isotope data on the Ko'olau Scientific Drilling Project (KSDP), the Honolulu Volcanics and ODP Site 843, *Earth Planet. Sci. Lett.*, *261*(1-2), 65–83.

Fitton, J. G., A. D. Saunders, P. D. Kempton, and B. S. Hardarson (2003), Does depleted mantle form an intrinsic part of the Iceland plume?, *Geochem. Geophys. Geosyst.*, 4, 1032, doi:10.1029/2002GC000424.

Frey, F. A., and C. M. Sung (1974), Geochemical results for basalts from Sites 253 and 254, *In* Luyendyk B. P. and T. A. Davies (eds.), *Initial Rep. Deep Sea Drill. Proj., 22*: Washington (US Govt. Printing Office), 567–572, doi:10.2973/dsdp.proc.26.123.1974.

Frey, F. A., and J. M. Rhodes (1993), Intershield geochemical differences among Hawaiian volcanoes: implications for source compositions, melting process and magma ascent paths, *Royal Soc. Lond.*, *342*, 121–136.

Frey, F. A., and D. Weis (1995), Temporal evolution of the Kerguelen plume: Geochemical evidence from 38 to 82 Ma lavas forming the Ninetyeast Ridge, *Contrib. Mineral. Petrol.*, *121*, 12–28.

Frey, F. A. and D. Weis (1996), Reply to the Class et al. discussion of "Temporal evolution of the Kerguelen plume: geochemical evidence from ~38 to 82 Ma lavas forming the Ninetyeast Ridge", *Contrib. Mineral. Petrol.*, *124*, 104–110.

Frey, F. A., W. S. Wise, M. O. Garcia, H. West, S.-T. Kwon, and A. Kennedy (1990), Evolution of Mauna Kea volcano, Hawaii: petrologic and geochemical constraints on postshield volcanism, *J. Geophys. Res.*, *95*, 1271-1300. doi:10.1029/JB095iB02p01271

Frey, F.A., W.B. Jones, H. Davies, and D. Weis (1991), Geochemical and petrologic data for basalts from Sites 756, 757, and 758: implications for the origin and evolution of the Ninetyeast Ridge, *In* Weissel, J., J. Peirce, E. Taylor, J. Alt, et al. (eds.), *Proc. Ocean Drill. Program, Sci. Results, 121*: College Station, TX (Ocean Drill. Program), 611–659. doi:10.2973/odp.proc.sr.121.163.1991.

Frey, F. A., M. O. Garcia, and M. F. Roden (1994), Geochemical characteristics of Koolau Volcano: Implications of intershield geochemical differences among Hawaiian volcanoes, *Geochim. Cosmochim. Acta*, *58*, 1441–1462.

Frey, F. A., et al. (2000a), Origin and evolution of a submarine large igneous province: the Kerguelen Plateau and Broken Ridge, southern Indian Ocean, *Earth Planet. Sci. Lett., 176*, 73–89.

Frey, F. A., D. Weis, H. J. Yang, K. Nicolaysen, H. Leyrit, and A. Giret (2000b), Temporal geochemical trends in Kerguelen Archipelago basalts: evidence for decreasing magma supply from the Kerguelen Plume, *Chem. Geol.*, *164*, 61–80.

Frey, F. A., D. Weis, A. Y. Borisova, and G. Xu (2002a), Involvement of continental crust in the formation of the Cretaceous Kerguelen Plateau: new perspectives from ODP Leg 120 sites, *J. Petrol.*, *43*(7), 1207–1239.

Frey, F. A., K. Nicolaysen, B. K. Kubit, D. Weis, and A. Giret (2002b). Flood basalt from Mont Tourmente in the central Kerguelen Archipelago: the change from transitional to alkalic basalt at ~25 Ma, *J. Petrol.*, *43*, 1367–1387.

Frey, F.A., Coffin, M.F., Wallace, P.J., and Weis, D. (2003). Leg 183 synthesis: Kerguelen Plateau–Broken Ridge—a large igneous province. *In* Frey, F.A., Coffin, M.F., Wallace, P.J., and Quilty, P.G. (Eds.), *Proc. ODP, Sci. Results,* 183: College Station, TX (Ocean Drilling Program), 1–48. doi:10.2973/odp.proc.sr.183.015.2003.

Galer, S. J. G (1999), Optimal double and triple spiking for high precision lead isotopic measurement, *Chem. Geol., 157*, 255–274.

Galer, S. J. G., and R. K. O'Nions (1985), Residence time of thorium, uranium and lead in the mantle with implications for mantle convection, *Nature*, *316*(6031), 778–782.

Galer, S. J. G., and W. Abouchami (1998), Practical application of lead triple spiking for correction of instrumental mass discrimination, *Mineral. Mag., 62A*, 491–492.

Gallet, S., B.-M. Jahn, and M. Torii (1996), Geochemical characterization of the Luochuan loess-paleosol sequence, China, and paleoclimatic implications, *Chem.Geol.*, *133*(1–4), 67–88.

Garcia, M. O., B. A. Jorgenson, J. J. Mahoney, E. Ito, and A. J. Irving (1993), An Evaluation of Temporal Geochemical Evolution of Loihi Summit Lavas: Results From Alvin Submersible Dives, *J. Geophys. Res.*, *98*(B1), 537–550.

Garcia, M. O., A. J. Pietruszka, J. M. Rhodes, and K. Swanson (2000), Magmatic processes during the prolonged Pu'u 'O'o eruption of Kilauea volcano, Hawaii, *J. Petrol.*, *41*, 967–990.

Garcia, M. O., J. Caplan-Auerbach, E. H. De Carlo, M. D. Kurz, and N. Becker (2006), Geology, geochemistry and earthquake history of Lo'ihi Seamount, Hawai'i's youngest volcano, *Chemie der Erde - Geochemistry*, *66*(2), 81–108.

Garcia, M. O., E. H. Haskins, E. M. Stolper, and M. Baker (2007), Stratigraphy of the Hawai'i Scientific Drilling Project core (HSDP2): Anatomy of a Hawaiian shield volcano, *Geochem. Geophys. Geosyst.*, *8,* Q02G20, doi:10.1029/2006gc001379.

Garcia, M, G. Ito, D. Weis, D. Geist, L. Swinnard, T. Bianco, A Flinders, B. Taylor, B. Appelgate, C. Blay, D. Hanano, I. Nobre Silva, T. Naumann, C. Maerschalk, K. Harpp, B. Christensen, L. Sciaroni, T. Tagami, and S. Yamasaki (2008), Widespread secondary volcanism near Northern Hawaiian Islands, *Eos Trans.*, *89 (52)*, 542–543.

Gast, P. W., G. R. Tilton, and C. Hedge (1964), Isotopic composition of lead and strontium from Ascension and Gough islands, *Science, 145* (3637), 1181–1185.

Gast, P. W. (1969), Isotopic composition of lead from St Helena and Ascencion Islands, *Earth Planet. Sci. Lett.*, *5* (5), 353–359.

Geldmacher, J., K. Hoernle, A. Klügel, P. van den Bogaard, and I. Bindeman (2008), Geochemistry of a new enriched mantle type locality in the northern hemisphere: Implications for the origin of the EM-I source, *Earth Planet. Sci. Lett.*, *265*, 167–182.

Goldstein, S. L., G. Soffer, C. H. Langmuir, K. A. Lehnert, D. W. Graham and P. J. Michael (2008), Origin of a "Southern Hemisphere" geochemical signature in the Arctic upper mantle, *Nature, 453*, 89–93.

Gonnermann, H. M., A. M. Jellinek, M. A. Richards, and M. Manga (2004), Modulation of mantle plumes and heat flow at the core mantle boundary by plate-scale flow: results from laboratory experiments, *Earth Planet. Sci. Lett.*, *226*, 53–67.

Graham, D. W., J. Blichert-Toft, C. J. Russo, K. H. Rubin, and F. Albarède (2006), Cryptic striations in the upper mantle revealed by hafnium isotopes in southeast Indian ridge basalts, *Nature, 440*, 199–202.

Greene, A. R., M. O. Garcia, D. Weis, G. Ito, M. Kuga, J. Robinson, and S. Yamasaki (2010), Low-productivity Hawaiian volcanism between Kaua'i and O'ahu, *Geochem. Geophys. Geosyst., 11*, Q0AC08, doi:10.1029/2010gc003233.

Griffiths, R. W., and I. H. Campbell (1990), Stirring and structure in mantle starting plumes, *Earth Planet. Sci. Lett.*, *99*(1-2), 66–78.

Hamelin, B., B. Dupré, and C. J. Allègre (1986), Pb-Sr-Nd isotopic data of Indian Ocean ridges: new evidence of large-scale mapping of mantle heterogeneities, *Earth Planet. Sci. Lett., 76*, 288–298.

Hanan, B. B., and D. W. Graham (1996), Lead and helium isotope evidence from oceanic basalts for a common deep source of mantle plumes, *Science, 272*, 991–995.

Hanan, B. B., J. Blichert-Toft, D. G. Pyle, and D. M. Christie (2004), Contrasting origins of the upper mantle revealed by hafnium and lead isotopes from the Southeast Indian Ridge, *Nature, 432*, 91–94.

Hanano, D., J. S. Scoates, and D. Weis (2009), Alteration mineralogy and the effect of acid-leaching on the Pb isotope systematics of ocean island basalts, *Am. Mineral.*, *94*, 17–26, doi:10.2138/am.2009.2845.

Hanano, D., D. Weis, J. S. Scoates, S. Aciego, and D. J. DePaolo (2010), Horizontal and vertical zoning of heterogeneities in the Hawaiian mantle plume from the geochemistry of consecutive postshield volcano pairs: Kohala-Mahukona and Mauna Kea-Hualalai, *Geochem. Geophys. Geosyst.*, *11*, Q01004, doi:10.1029/2009GC002782.

Hart, S. R. (1984), The DUPAL anomaly: A large scale isotopic mantle anomaly in the Southern Hemisphere, *Nature*, *309*, 753–757.

Hart, S. R. (1988), Heterogeneous mantle domains: signatures, genesis and mixing chronologies, *Earth Planet. Sci. Lett.*, *90*(3), 273–296.

Hart, S. R., A. J. Erlank, and E. J. D. Kable (1974), Sea floor basalt alteration: Some chemical and Sr isotopic effects, *Contrib. Mineral. Petrol.*, *44*(3), 219–230.

Hart, S. R., E. H. Hauri, L. A. Oschmann, and J. A. Whitehead (1992), Mantle plumes and entrainment: Isotopic Evidence, *Science, 256*, 517–520.

Hauff, F., K. Hoernle, and A. Schmidt (2003), Sr-Nd-Pb composition of Mesozoic Pacific oceanic crust (Site 1149 and 801, ODP Leg 185): Implications for alteration of ocean crust and the input into the Izu-Bonin-Mariana subduction system, *Geochem. Geophys. Geosyst.*, *4(8)*, 8913, doi:10.1029/2002GC000241.

Hauri, E. H., J. C. Lassister, and D. J. DePaolo (1996), Osmium isotope systematics of drilled lavas from Mauna Loa, Hawaii, *J. Geophys. Res.*, *101(B5)*, 11,793–711,806.

Hawkesworth, C. J., and M. A. Morrison (1978), A reduction in $^{87}Sr/^{86}Sr$ during basalt alteration, *Nature, 276*, 381–383.

Hekinian, R. (1974), Petrology of the Ninety East Ridge (Indian Ocean) compared to other aseismic ridges, *Contrib. Mineral. Petrol., 43*, 125–147.

Herzberg, C., et al. (2007), Temperatures in ambient mantle and plumes: Constraints from basalts, picrites, and komatiites, *Geochem. Geophys. Geosyst., 8*(Q02006). doi:10.1029/2006GC001390.

Hoernle, K, and H.-U. Schmincke (1993), The role of partial melting in the 15-Ma geochemical evolution of Gran Canaria: a blob model for the Canary hotspot, *J. Petrol., 34*, 599–626.

Hofmann, A. W. (1997), Mantle geochemistry: the message from oceanic volcanism, *Nature, 385*, 219–229.

Hofmann, A. W. (2003), Sampling mantle heterogeneity through oceanic basalts: isotopes and trace elements, in *Treatise on Geochemistry*, edited, pp. 61–101, Elsevier Ltd.

Hofmann, A. W., and W. M. White (1982), Mantle plumes from ancient oceanic crust, *Earth Planet. Sci. Lett., 57*(2), 421–436.

Hofmann, A. W., M. D. Feigenson, and I. Raczek (1987), Kohala revisited, *Contrib. Mineral. Petrol., 95*, 114–122.

Holcomb, R. T., B. K. Nelson, P. W. Reiners, and N. E. Sawyer (2000), Overlapping volcanoes: The origin of Hilo Ridge, Hawaii, *Geology, 28*(6), 547–550.

Huang, S., and F. A. Frey (2003), Trace element abundances of Mauna Kea basalt from phase 2 of the Hawaii Scientific Drilling Project: Petrogenetic implications of correlations with major element content and isotopic ratios, *Geochem. Geophys. Geosyst., 4*(6), 8711, doi:10.1029/2002GC000322.

Huang, S., and F. A. Frey (2005), Recycled oceanic crust in the Hawaiian Plume: Evidence from temporal geochemical variations within the Koolau shield, *Contrib. Mineral. Petrol.*, 149, 556–575, doi:10.1007/s00410-005-0664-9

Ingle, S., D. Weis, and F. A. Frey (2002), Indian continental crust recovered from Elan Bank, Kerguelen plateau (ODP Leg 183, Site 1137), *J. Petrol., 43*, 1241–1257.

Ingle, S., D. Weis, S. Doucet, and N. Mattielli, (2003), Hf isotope constraints on mantle sources and shallow-level contaminants during Kerguelen hot spot activity since ~120 Ma, *Geochem. Geophys. Geosyst., 4*, 1-28, doi:10.1029/2002gc000482.

Janney, P. E., A. P. Le Roex, and R. W. Carlson (2005), Hafnium isotope and trace element constraints on the nature of mantle heterogeneity beneath the Central Southwest Indian Ridge (13°E to 47°E), *J. Petrol., 46*(12), 2427–2464.

Jackson, E. D., E. A. Silver, and G. B. Dalrymple (1972), Hawaiian-Emperor Chain and its relation to Cenozoic circumpacific tectonics, *Geol. Soc. Amer. Bull., 83*(3), 601–618.

Jackson, M. G., S. R. Hart, A. A. P. Koppers, H. Staudigel, J. Konter, J. Blusztajn, M. Kurz, and J. A. Russell (2007), The return of subducted continental crust in Samoan lavas, *Nature, 448*, 684–687.

Jacobsen, S. B., and G. J. Wasserburg (1984), Sm-Nd isotopic evolution of chondrites and achondrites, II, *Earth Planet. Sci. Lett., 67*(2), 137–150.

Jellinek, A. M., H. M. Gonnermann, and M. A. Richards (2003), Plume capture by divergent plate motions: implications for the distribution of hotspots, geochemistry of mid-ocean ridge basalts, and estimates of the heat flux at the core-mantle boundary, *Earth Planet. Sci. Lett., 205*(3-4), 361–378.

Jellinek, A. M., and M. Manga (2004), Links between long-lived hot spots, mantle plumes, D", and plate tectonics, *Rev. Geophys., 42*(3), RG3002, doi: 10.1029/2003RG000144.

Jones, C. E., A. N. Halliday, D. K. Rea, and R. M. Owen (2000), Eolian inputs of lead to the North Pacific, *Geochim. Cosmochim. Acta, 64*(8), 1405–1416.

Kamenov, G. D., P. A. Mueller, and M. R. Perfit (2004), Optimization of mixed Pb-Tl solutions for high precision isotopic analyses by MC-ICP-MS, *J. Anal. At. Spectrom., 19*, 1262–1267.

Keller, R. A., M. R. Fisk, and W. M. White (2000), Isotopic evidence for Late Cretaceous plume-ridge interaction at the Hawaiian hotspot, *Nature, 405*(6787), 673–676.

Kellogg, L. H., B. H. Hager, and R. D. van der Hilst (1999), Compositional Stratification in the Deep Mantle, *Science, 283*, 1881–1884.

Kempton, P., J. Pearce, T. Barry, J. Fitton, C. Langmuir, and D. Christie (2002), Sr-Nd-Pb-Hf isotope results from ODP Leg 187: Evidence for mantle dynamics of the Australian-Antarctic discordance and origin of the Indian MORB source. *Geochem. Geophys. Geosyst., 3*(12), 1074, doi: 10.1029/2002GC000320.

Kennedy, M. J., O. A. Chadwick, P. M. Vitousek, L. A. Derry, and D. M. Hendricks (1998), Changing sources of base cations during ecosystem development, Hawaiian Islands, *Geology, 26*(11), 1015–1018.

Kerr, A. C., and J. Tarney (2005), Tectonic evolution of the Caribbean and northwestern South America: The case for accretion of two Late Cretaceous oceanic plateaus, *Geology, 33*(4), 269–272.

Kimura, J.-I., T. W. Sisson, N. Nakano, M. L. Coombs, and P. W. Lipman (2006), Isotope geochemistry of early Kilauea magmas from the submarine Hilina bench: The nature of the Hilina mantle component, *J. Volcan. Geotherm. Res., 151*(1-3), 51–72.

Klootwijk, C. T., J. S. Gee, J. W. Peirce, and G. M. Smith (1991), Constraints on the India-Asia convergence: paleomagnetic results from Ninetyeast Ridge, *In* Weissel, J., J. Peirce, E.

Taylor, J. Alt, et al. (eds.), *Proc. Ocean Drill. Program, Sci. Results, 121*: College Station, TX (Ocean Drill. Program), 777–882, doi:10.2973/odp.proc.sr.121.121.1991.

Krauskopf, K. B., and D. K. Bird (1995), Introduction to Geochemistry (3rd ed.), McGraw-Hill, Inc., 647p., ISBN: 0–07–035820–6.

Krishna, K. S., D. G. Rao, M. V. Ramana, , V. Subrahmanyam, K. V. L. N. S. Sarma, A. I. Pilipenko, V. S. Shcherbakov, and I. V. R. Murthy (1995), Tectonic model for the evolution of oceanic crust in the northeastern Indian Ocean from the Late Cretaceous to the early Tertiary, *J. Geophys. Res., 100*, 20,011–20,024.

Krishna, K., D. Rao, L. Raju, A. Chaubey, V. Shcherbakov, A. Pilipenko, and I. Murthy (1999), Paleocene on-spreading-axis hotspot volcanism along the Ninetyeast Ridge: An interaction between the Kerguelen hotspot and the Wharton spreading center, *J. Earth Syst. Sci., 108*, 255–267.

Krishna, K. S., Y. P. Neprochnov, D. G. Rao, and B. N. Grinko (2001), Crustal structure and tectonics of the Ninetyeast Ridge from seismic and gravity studies, *Tectonics, 20*, 416–433.

Krolikowska-Ciaglo, S., F. Hauff, and K. Hoernle (2005), Sr-Nd isotope systematics in 14-28 Ma low-temperature altered mid-ocean ridge basalt from the Australian Antarctic Discordance, Ocean Drilling Program Leg 187, *Geochem. Geophys. Geosyst.*, *6*(1), Q01001, doi: 10.1029/2004GC000802.

Kurz, M. D., J. Curtice, D. E. Lott, and A. Solow (2004), Rapid helium isotopic variability in Mauna Kea shield lavas from the Hawaiian Scientific Drilling Project, *Geochem. Geophys. Geosyst.*, *5*(4), 1–35.

Larson, R. L. (1991), Geological consequences of superplumes, *Geology, 19,* 963–966.

Lassiter, J. C., and E. H. Hauri (1998), Osmium-isotope variations in Hawaiian lavas: evidence for recycled oceanic lithosphere in the Hawaiian plume, *Earth Planet. Sci. Lett.*, *164*(3-4), 483–496.

Lassiter, J. C., D. J. DePaolo, and M. Tatsumoto (1996), Isotopic evolution of Mauna Kea Volcano: results from the initial phase of the Hawaii Scientific Drilling Project, *J. Geophys. Res.*, *101*(B5), 11,769–11,780.

Le Bas, M. J., R. W. Le Maitre, A. Streckeisen, and B. Zanettin (1986), A chemical classification of volcanic rocks based on the total alkali-silica diagram, *J. Petrol.*, *27*, 745–750.

Lenardic, A., and W. M. Kaula (1994), Self lubricated mantle convection: Two dimensional models, *Geophys. Res. Lett.*, *21*(16), 1707–1710.

Ling, H. F., et al. (1997), Evolution of Nd and Pb isotopes in Central Pacific seawater from ferromanganese crusts, *Earth Planet. Sci. Lett.*, *146*(1–2), 1–12.

Longerich, H. P., B. J. Fryer, and D. F. Strong (1987), Determination of lead isotope ratios by inductively coupled plasma-mass spectrometry ICP-MS, *Spectrochim. Acta*, *42B*, 39–48.

Ludden, J. N., and G. Thompson (1979), An evaluation of the behavior of the rare earth elements during weathering of sea-floor basalt, *Earth Planet. Sci. Lett., 43*, 85–92.

Ludden, J. N., G. Thompson, W. B. Bryan, and F. A. Frey (1980), The origin of lavas from the Ninetyeast Ridge, Eastern Indian Ocean: an evaluation of fractional crystallization models, *J. Geophys. Res., 85*, 4405–4420.

Luyendyk, B. P. (1977), Deep sea Drilling on the Ninetyeast Ridge: Synthesis and a tectonic model, in *Indian Ocean Geology and Biostratigraphy* edited by J. R. Heirtzler et al., pp. 165–187, AGU, Washington, D. C.

Macdonald, G. A. and T. Katsura (1964), Chemical composition of Hawaiian lavas, *J. Petrol.*, *5*, 82–133.

Mahoney, J. J. (1987), An isotopic survey of Pacific oceanic plateaus: Implications for their nature and origin, in Seamounts, Islands, and Atolls, *Geophys. Monogr. Ser.*, vol. 43, edited by B. H. Keating et al., pp. 207–220, AGU, Washington, D. C.

Mahoney, J. J., W. B. Jones, F. A. Frey, V. J. M. Salters, D. G. Pyle, and H. L. Davies (1995), Geochemical characteristics of Lavas from Broken Ridge, the Naturaliste Plateau and southernmost Kerguelen plateau - Cretaceous plateau volcanism in the Southeast Indian-Ocean, *Chem. Geol., 120*, 315–345.

Mahoney, J. J., W. M. White, B. G. J. Upton, C. R. Neal, and R. A. Scrutton (1996), Beyond EM-1: Lavas from Afanasy-Nikitin Rise and the Crozet Archipelago, Indian Ocean, *Geology, 24*, 615–618.

Mahoney, J. J., D. W. Graham, D. M. Christie, K. T. M. Johnson, L. S. Hall, and D. L. Vonderhaar (2002), Between a hotspot and a cold spot: Isotopic variation in the Southeast Indian Ridge asthenosphere, 86°E–118°E, *J. Petrol., 43*, 1155–1176.

Manhès, G., J. F. Minster, and C.-J. Allègre (1978), Comparative uranium-thorium-lead and rubidium-strontium study of the Saint Sèverin amphoterite: Consequences for early solar system chronology, *Earth Planet. Sci. Lett., 39*, 14–24.

Marske, J. P., A. J. Pietruszka, D. Weis, M. O. Garcia, and J. M. Rhodes (2007), Rapid passage of a small-scale mantle heterogeneity through the melting regions of Kilauea and Mauna Loa Volcanoes, *Earth Planet. Sci. Lett., 259*, 34–50.

Marske, J.P., M. O. Garcia, A. J.Pietruszka, J. M. Rhodes, and M. D. Norman (2008), Geochemical variations during Kilauea's Pu'u 'O'o eruption reveal a fine-scale mixture of mantle heterogeneities within the Hawaiian mantle plume. *J. Petrol., 49*, 1297–1318.

Mattieli, N., D. Weis, J. Blichert-Toft, and F. Albarède (2002), Hf isotope evidence for a Miocene change in the Kerguelen mantle plume composition, *J. Petrol., 43*, 1327–1339.

McDonough, W. F., and C. Chauvel (1991), Sample contamination explains the Pb isotopic composition of some Rurutu island and Sasha seamount basalts, *Earth Planet. Sci. Lett., 105*, 397–404.

McDonough, W. F., and S. Sun (1995), The composition of the Earth, *Chem. Geol., 120*(34), 223–253.

Meyzen, C. M., J. N. Ludden, E. Humler, B. Luais, M. J. Toplis, C. Mével, and M. Storey (2005), New insights into the origin and distribution of the DUPAL isotope anomaly in the Indian Ocean mantle from MORB of the Southwest Indian Ridge, *Geochem. Geophys. Geosyst., 6*, Q11K11, doi:10.1029/2005gc000979.

Montelli, R., G. Nolet, F. A. Dahlen, G. Masters, E. R. Engdahl, and S.-H. Hung (2004), Finite-frequency tomography reveals a variety of plumes in the mantle, *Science, 303*, 338–343.

Montelli, R., G. Nolet, F. A. Dahlen, and G. Masters (2006), A catalogue of deep mantle plumes: New results from finite-frequency tomography, *Geochem. Geophys. Geosyst., 7*, Q11007, doi:10.1029/2006gc001248.

Moore, J. G., and D. A. Clague (1992), Volcano growth and evolution of the island of Hawaii, *Geol. Soc. Amer. Bull., 104*, 1471–1484.

Morgan, W. J. (1971), Convection plumes in the lower mantle, *Nature, 230*, 42–43.

Morgan, W. J. (1972), Deep mantle convection plumes and plate motions, *A. A. P. G. Bulletin, 56*, 203–213.

Morgan, W. J. (1981), Hotspot tracks and the opening of the Atlantic and Indian oceans, In: Emiliani, C. (ed.) *The Sea (vol. 7)*. New-York: Wiley-Interscience, 443–487.

Mukhopadhyay, M., and M. B. R. Krishna (1995), Gravity anomalies and deep structure of the Ninetyeast Ridge north of the equator, eastern Indian Ocean – a hot spot trace model, *Mar. Geophys. Res., 17*, 201–216.

Müller, R. D., J.-Y Royer, and L. A. Lawver (1993), Revised plate motions relative to the hotspots from combined Atlantic and Indian Ocean hotspot tracks, *Geology, 21*, 275–278.

Müller, R. D., M. Sdrolias, C. Gaina and W. R. Roest (2008), Age, spreading rates, and spreading asymmetry of the world's ocean crust, *Geochem. Geophys. Geosyst., 9*, Q04006, doi:10.1029/2007gc001743.

Mutter, J. C., and S. C. Cande (1983), The early opening between Broken Ridge and Kerguelen Plateau, *Earth Planet. Sci. Lett., 65*, 369–376.

Munschy, M., J. Dyment, M. O. Boulanger, D. Boulanger, J. D. Tissot, R. Schlich, Y. Rotstein, and M. F. Coffin (1992), Breakup and seafloor spreading between the Kerguelen Plateau–Labuan Basin and the Broken Ridge–Diamantina zone, *In* Wise, S.W., Jr., R. Schlich, et al. (eds.), *Proc. Ocean Drill. Program, Sci. Results, 120*: College Station, TX (Ocean Drill. Program), 931–944, doi:10.2973.odp.proc.sr.120.123.1992.

Nakai, S., A. N. Halliday, and D. K. Rea (1993), Provenance of dust in the Pacific Ocean, *Earth Planet. Sci. Lett.*, *119*(1–2), 143–157.

Nauret, F., et al. (2006), Correlated trace element-Pb isotope enrichments in Indian MORB along 18-20ºS, Central Indian Ridge, *Earth and Planetary Science Letters*, *245*(1-2), 137–152.

Neal, C. R., J. J. Mahoney, and W. J. Chazey (2002), Mantle sources and the highly variable role of continental lithosphere in basalt petrogenesis of the Kerguelen Plateau and Broken Ridge LIP: Results from ODP Leg 183, *J. Petrol.*, *43*(7), 1177–1205.

Nicolaysen, K., F. A. Frey, K. V. Hodges, D. Weis, and A. Giret (2000), ^{40}Ar/^{39}Ar geochronology of flood basalts from the Kerguelen Archipelago, southern Indian Ocean: Implications for Cenozoic eruption rates of the Kerguelen plume, *Earth Planet. Sci. Lett., 174*, 313–328.

Nicolaysen, K., S. Bowring, F. Frey, D. Weis, S. Ingle, M. S. Pringle, and M. F. Coffin (2001), Provenance of Proterozoic garnet-biotite gneiss recovered from Elan Bank, Kerguelen Plateau, southern Indian Ocean, *Geology, 29*, 235–238.

Nicolaysen, K. P., F. A. Frey, J. J. Mahoney, K. T. M. Johnson, and D. W. Graham (2007), Influence of the Amsterdam/St. Paul hot spot along the Southeast Indian Ridge between 77° and 88°E: Correlations of Sr, Nd, Pb, and He isotopic variations with ridge segmentation, *Geochem. Geophys. Geosyst.*, *8*, Q09007, doi: 10.1029/2006gc001540.

Nobre Silva, I. G., D. Weis, J. Barling, and J. S. Scoates (2009), Leaching systematics and matrix elimination for the determination of high-precision Pb isotope compositions of ocean island basalts, *Geochem. Geophys. Geosyst., 10*, Q08012, doi:10.1029/2009GC002537.

Nobre Silva, I. G., D. Weis, and J. S. Scoates (2010), Effects of acid leaching on the Sr-Nd-Hf isotopic compositions of ocean island basalts, *Geochem. Geophys. Geosyst.*, *11*, Q09011, doi: 10.1029/2010gc003176.

Nougier, J., R. Ballestracci, and B. Blavoux (1982), Les manifestations post-volcaniques dans les îles Australes françaises (TAAF); zones fumerolliennes et sources thermo-minérales, *C. R. Acad. Sci. Paris, 295*, 389–392.

O'Neill, C., D. Müller, and B. Steinberger (2003), Geodynamic implications of moving Indian Ocean hotspots, *Earth Planet. Sci. Lett.*, *215*, 151–168.

O'Nions, R. K. and D. McKenzie (1993), Estimates of mantle thorium/uranium ratios from Th, U and Pb isotope abundances in basaltic melts, *Phil. Trans. R. Soc. A, 342*, 65–77.

Patchett, P. J. and M. Tatsumoto (1981), A routine high-precision method for Lu-Hf isotope geochemistry and chronology, *Contrib. Mineral. Petrol.*, *75*, 263–267.

Peirce, J., Weissel, J., et al., 1989. *Proc. ODP, Init. Repts.*, 121: College Station, TX (Ocean Drilling Program). doi:10.2973/odp.proc.ir.121.1989.

Piepgras, D. J., and G. J. Wasserburg (1980), Neodymium isotopic variations in seawater, *Earth Planet. Sci. Lett., 50*(1), 128–138.

Pietruszka, A. J., and M. O. Garcia (1999), A rapid fluctuation in the mantle sour and melting history of Kilauea Volcano inferred from the geochemistry of its historical summit lavas (1790-1982), *J. Petrol.*, *48*(8), 1321–1342.

Pietruszka, A. J., E. H. Hauri, and J. Blichert-Toft (2009), Crustal contamination of mantle-derived magmas within Piton de la Fournaise volcano, Réunion Island, *J. Petrol.*, *50*, 661–684.

Plank, T., K. A. Kelley, R. W. Murray, and L. Q. Stern (2007), Chemical composition of sediments subducting at the Izu-Bonin trench, *Geochem. Geophys. Geosyst.*, *8*, Q04I16, doi:10.1029/2006GC001444.

Porter, K. A., and W. M. White (2009), Deep mantle subduction flux, *Geochem. Geophys. Geosyst.*, *10*(12), Q12016. doi:10.1029/2009GC002656.

Putirka, K. (1999), Melting depths and mantle heterogeneity beneath Hawaii and the East Pacific Rise: Constraints from Na/Ti and rare earth element ratios, *J. Geophys. Res.*, *104*(B2), 2817–2829.

Quane, S. L., M. O. Garcia, H. Guillou, and T. P. Hulsebosch (2000), Magmatic history of the East Rift Zone of Kilauea Volcano, Hawaii based on drill core from SOH 1, *J. Volcanol. Geotherm. Res.*, 102(3–4), 319–338, doi:10.1016/S0377-0273(00)00194-3.

Regelous, M., A. W. Hofmann, W. Abouchami, and S. J. G. Galer (2003), Geochemistry of lavas from the Emperor Seamounts, and the geochemical evolution of Hawaiian magmatism from 85 to 42 Ma, *J. Petrol., 44*, 113–140.

Regelous, M., Y. Niu, W. Abouchami, and P. R. Castillo (2009), Shallow origin for South Atlantic Dupal Anomaly from lower continental crust: Geochemical evidence from the Mid-Atlantic Ridge at 26°S, *Lithos, 112*, 57–72.

Rehkämper, M., and A. W. Hofmann (1997), Recycled ocean crust and sediment in Indian Ocean MORB, *Earth Planet. Sci. Lett.*, *147*(1-4), 93–106.

Rehkämper, M., and A. N. Halliday (1998), Accuracy and long-term reproducibility of lead isotopic measurements by multiple-collector inductively coupled plasma mass spectrometry using an external method for correction of mass discrimination, *Int. J. Mass Spectrom.*, *181*, 123–33.

Rhodes, J. M. (1996), Geochemical stratigraphy of lava flows samples by the Hawaii Scientific Drilling Project, *J. Geophys. Res.*, *101*(B5), 11,729–11,746.

Rhodes, J. M., and M. J. Vollinger (2004), Composition of basaltic lavas sampled by phase-2 of the Hawaii Scientific Drilling Project: Geochemical stratigraphy and magma types, *Geochem. Geophys. Geosyst.*, *5*, Q03G13, doi:10.1029/2002GC000434.

Richards, M. A., R. A. Duncan, and V.E. Courtillot (1989), Flood basalts and Hot-spot tracks: plume heads and tails, *Science, 246*, 103–107.

Rickers, K., K. Mezger, and M. M. Raith (2001), Evolution of the Continental Crust in the Proterozoic Eastern Ghats Belt, India and new constraints for Rodinia reconstruction: implications from Sm-Nd, Rb-Sr and Pb-Pb isotopes, *Precambrian Res.*, *112*(3-4), 183–210.

Rosman, K.J.R., and P.D.P. Taylor (1997), Isotopic compositions of the elements, *Pure Appl. Chem.*, *70*(217–235).

Royer, J.-Y., and R. Schlich (1988), Southeast Indian Ridge between the Rodriguez triple junction and the Amsterdam and Saint-Paul Islands: detailed kinematics for the past 20 m.y, *J. Geophys. Res., 93*, 13,524–13,550.

Royer, J.-Y., J. W. Peirce, and J.K. Weissel (1991), Tectonic constraints on the hotspot formation of the Ninetyeast Ridge, *In* Weissel, J., J. Peirce, E. Taylor, J. Alt, et al. (eds.), *Proc. Ocean Drill. Program, Sci. Results*, *121*: College Station, TX (Ocean Drill. Program), 763–776, doi:10.2973/odp.proc.sr.121.122.1991.

Salters, V. J. M. and W. M. White (1998), Hf isotope constraints on mantle evolution, *Chem. Geol.*, 145, 447–460.

Salters, V., J. Blichert-Toft, Z. Fekiacova, A. Sachi-Kocher, and M. Bizimis (2006), Isotope and trace element evidence for depleted lithosphere in the source of enriched Ko'olau basalts, *Contrib. Mineral. Petrol.*, *151*(3), 297–312.

Saunders, A. D., M. Storey, I. L. Gibson, P. Leat, J. Hergt, and R. N. Thompson (1991), Chemical and isotopic constraints on the origin of basalts from Ninetyeast Ridge, Indian Ocean: results from DSDP Legs 22 and 26 and ODP Leg 121, *In* Weissel, J., J. Peirce, E. Taylor, J. Alt, et al. (eds.), *Proc. Ocean Drill. Program, Sci. Results, 121*: College Station, TX (Ocean Drill. Program), 559–590, doi:10.2973/odp.proc.sr.121.169.1991.

Saunders, A. D. (2005), Large igneous provinces: Origin and environmental consequences, *Elements, 1*, 259–263.

Scheirer, D. S., D. W. Forsyth, J. A. Conder, M. A. Eberle, S.-H. Hung, K. T. M. Johnson, and D. W. Graham (2000), Anomalous seafloor spreading of the Southeast Indian Ridge near the Amsterdam-St. Paul Plateau, *J. Geophys. Res., 105*, 8243–8262.

Schubert, G. and D. Sandwell (1989), Crustal volumes of the continents and of oceanic and continental submarine plateaus, *Earth Planet. Sci. Lett.*, *92*, 234–246.

Sharp, W. D., and P. R. Renne (2005), The $^{40}Ar/^{39}Ar$ dating of core recovered by the Hawaii Scientific Drilling Project (phase 2), Hilo, Hawaii, *Geochem. Geophy. Geosyst., 6*, Q04G17, doi:10.1029/2004GC000846.

Sharp, W. D., and D. Clague (2006), 50-Ma initiation if Hawaiian-Emperor bend records major change in Pacific plate motion, *Science, 313*, 1281–1284.

Shipboard Scientific Party (1989), Leg 121 background and objectives. *In* Peirce, J., J. Weissel, et al. (eds.), *Proc. Ocean Drill. Program, Initial Reports, 121*: College Station, TX (Ocean Drill. Program), 5–31, doi:10.2973/odp.proc.ir.121.101.1989.

Shipboard Scientific Party (2007), Cruise Report KNOX06RR – A site survey expedition to the Indian ocean, 1–82.

Sleep, N. H. (1990), Hotspots and mantle plumes: some phenomenology, *J. Geophys. Res., 95*, 6715–6736.

Sleep, N. H. (1992), Hotspots volcanism and mantle plumes, *Annual Rev. Earth Planet. Sci.*, *20*, 19–43.

Smith, M. P., et al. (2000), Fractionation of the REE during hydrothermal processes: constraints from the Bayan Obo Fe-REE-Nb deposit, Inner Mongolia, China, *Geochim. Cosmochim. Acta*, *64*(18), 3141–3160.

Stacey, F. D., and D. E. Loper (1983), The thermal boundary-layer interpretation of D" and its role as a plume source, *Phys. Earth Planet. Int., 33*, 45–55.

Stacey, F. D., and D. E. Loper (1984), Thermal histories of the core and mantle, *Phys. Earth Planet. Int., 36*, 99–115.

Staudigel, H. A., A. Zindler, S. R. Hart, T. Leslie, C.-Y. Chen, and D. Clague (1984), The isotope systematics of a juvenile intraplate volcano: Pb, Nd and Sr isotope ratios of basalts from Loihi Seamount, Hawaii, *Earth Planet. Sci. Lett.*, *69*, 13–29.

Staudigel, H., G. R. Davies, S. R. Hart, K. M. Marchant, and B. M. Smith (1995), Large scale isotopic Sr, Nd and O isotopic anatomy of altered oceanic crust: DSDP/ODP sites 417/418, *Earth Planet. Sci. Lett.*, *130*(1–4), 169–185.

Steinberger, B. (2000), Plumes in a convecting mantle: Models and observations for individual hotspots, *J. Geophys. Res., 105*, 11,127–11,152.

Stolper, E. M., D. J. DePaolo, and D. M. Thomas (1996), Introduction to special section: Hawaii Scientific Drilling Project, *J. Geophys. Res.*, *101*(B5), 11593–11598.

Stolper, E. M., S. Sherman, M. Garcia, M. Baker, and C. Seaman (2004), Glass in the submarine section of the HSDP2 drill core, Hilo, Hawaii, *Geochem. Geophys. Geosyst.*, *5*(7), Q07G15, doi:10.1029/2003GC000553.

Stolper, E.M., DePaolo, D.J., and D.M. Thomas (2009), Deep drilling into a mantle plume volcano: the Hawaii Scientific Drilling Project, *Scientific Drilling*, *7*, March 2009, doi: 10.2204/iodp.sd.7.02.2009.

Storey, M., A. D. Saunders, J. Tarney, I. L. Gibson, M. J. Norry, M. F. Thirlwall, P. Leat, R. N. Thompson, and M. A. Menzies (1989), Contamination of Indian Ocean asthenosphere by the Kerguelen-Heard mantle plume, *Nature, 338*, 574–576.

Storey, M., R. W. Kent, A. D. Saunders, V. J. M. Salters, J. Hergt, H. Whitechurch, J. H. Sevigny, M. F. Thirlwall, , P. Leat, N. C. Ghose, and M. Gifford (1992), Lower Cretaceous volcanic rocks on continental margins and their relationship to the Kerguelen Plateau. *In* Wise, S.W., Jr., R. Schlich, et al. (eds.), *Proc. Ocean Drill. Program, Sci. Results, 120*: College Station, TX (Ocean Drill. Program), 33–53, doi:10.2973.odp.proc.sr.120.118.1992.

Stracke, A., and E. Hegner (1998), Rifting-related volcanism in an oceanic post-collisional setting: the Tabar-Lihir-Tanga-Feni (TLTF) island chain, Papua New Guinea, *Lithos, 45*, 545–560.

Stracke, A., A. Zindler, V. J. M. Salters, D. McKenzie, J. Blichert-Toft, F. Albarède, and K. Grönvold (2003), Theistareykir revisited, *Geochem. Geophys. Geosyst.*, *4(2)*, 8507, doi:10.1029/2001GC000201.

Stracke, A., A. W. Hofmann, and S. R. Hart (2005), FOZO, HIMU, and the rest of the mantle zoo, *Geochem. Geophys. Geosyst.*, *6*(5), Q05007, doi: 10.1029/2004gc000824.

Subrahmanyam, C., R. Gireesh, S. Chand, K. A. K. Raju, and D. G. Rao (2008), Geophysical characteristics of the Ninetyeast Ridge-Andaman island arc/trench convergent zone, *Earth Planet. Sci. Lett.*, *266*(1-2), 29–45.

Sun, S. S. (1980), Lead isotopic studies of mid-ocean ridges, young volcanic rocks form ocean islands, and island arcs, *Phil. Trans. R. Soc. Lond, A297*, 409–445.

Sun, S.-S., and W. F. McDonough (1989), Chemical and isotopic systematics of oceanic basalts: Implications for mantle composition and processes, in *Magmatism in the Ocean Basins*, edited by A. D. Saunders and M. J. Norry, pp. 313–345, Blackwell, London.

Tanaka, R., E. Nakamura, and E. Takahashi (2002), Geochemical evolution of Koolau volcano, Hawaii, in Hawaiian Volcanoes: *Deep Underwater Perspectives, Geophys. Monogr. Ser.*, vol. 128, edited by E. Takahashi et al., pp. 311–332, AGU, Washington, D. C.

Tanaka, R., A. Makishima, and E. Nakamura (2008), Hawaiian double volcanic chain triggered by an episodic involvement of recycled material: Constraints from temporal Sr-Nd-Hf-Pb isotopic trend of the Loa-type volcanoes, *Earth Planet. Sci. Lett.*, *265*, 450–465.

Tarduno, J. A., et al. (2003), The Emperor Seamounts: Southward motion of the Hawaiian Hotspot Plume in Earth's mantle, *Science, 301*, 1064–1069.

Tatsumoto, M. (1966), Genetic relations of oceanic basalts as indicated by lead isotopes, *Science*, *153* (3740), 1094–1101.

Tatsumoto, M. (1978), Isotopic composition of lead in oceanic basalt and its implication to mantle evolution, *Earth Planet. Sci. Lett., 38*, 63–87.

Thirlwall, M. F. (1997), Pb isotopic and elemental evidence for OIB derivation from young HIMU mantle, *Chemical Geology*, *139*(1-4), 51–74.

Thirlwall, M. F. (2000), Inter-laboratory and other errors in Pb isotope analyses investigated using a ^{207}Pb–^{204}Pb double spike, *Chem. Geol., 163*, 299–322.

Thirlwall, M. F. (2002), Multicollector ICP-MS analysis of Pb isotopes using a ^{207}Pb-^{204}Pb double spike demonstrates up to 400 ppm/amu systematic errors in Tl-normalization, *Chem. Geol.*, *184*, 255–279.

Thomas, D. M., F. L. Paillet, and M. E. Conrad (1996), Hydrogeology of the Hawaii scientific drilling project borehole KP-1 2. Groundwater geochemistry and regional flow patterns, *J. Geophys. Res.*, *101*(B5), 11,683–11,694.

Thompson, G., W. B. Bryan, F. A. Frey, and C. M. Sung (1974), Petrology and geochemistry of basalts and related Rocks from Sites 214, 215, 217, DSDP Leg 22, Indian Ocean, *In* von der Borch, C. C., J. G. Sclater, et al. (eds.), *Initial Rep. Deep Sea Drill. Proj., 22*: Washington (US Govt. Printing Office), 459–468, doi:10.2973/dsdp.proc.22.119.197.

Thompson, P. M. E., P. M. Kempton, and A. C. Kerr (2008), Evaluation of the effects of alteration and leaching on Sm-Nd and Lu-Hf systematics in submarine mafic rocks, *Lithos*, *104*(1–4), 164–176.

Verdier, O. (1989), Champs géothermiques et zéolitisation des îles Kerguelen: Implications géologiques (Terres Australes et Antarctiques françaises, Océan Indien Austral), Ph.D. dissertation, 271 pp., Univ. Paris.

Verma, S. P. (1992), Seawater alteration effects on REE, K, Rb, Cs, Sr, U, Th, Pb and Sr–Nd–Pb isotope systematics of Mid-Ocean Ridge Basalt, *Geochem. J., 26*, 159–177.

Vervoort, J. D., and J. Blichert-Toft (1999), Evolution of the depleted mantle: Hf isotope evidence from juvenile rocks through time, *Geochim. Cosmochim. Acta, 63*, 533–556.

Vidal, V., and A. Bonneville (2004), Variations of the Hawaiian hot spot activity revealed by variations in the magma production rate, *J. Geophys. Res.*, *109*. doi:10.1029/2003JB002559.

Vlastélic, I., W. Abouchami, S. J. G. Galer, and A. W. Hofmann (2001), Geographic control on Pb isotope distribution and sources in Indian Ocean Fe-Mn deposits, *Geochim. Cosmochim. Acta*, *65*(23), 4303–4319.

Vlastélic, I., A. Peltier, and T. Staudacher (2007), Short-term (1998-2006) fluctuations of Pb isotopes at Piton de la Fournaise volcano (Reunion Island): Origins and constraints on the size and shape of the magma reservoir, *Chem. Geol.*, *244*, 202–220.

Vlastélic, I., C. Deniel, C. Bosq, P. Tèlouk, P. Boivin, P. Bachélery, V. Famin, and T. Staudacher (2009), Pb isotope geochemistry of Piton de la Fournaise historical lavas, *J. Volcanol. Geotherm. Res., 184*, 63–78.

Walder, A. J., and N. Furuta (1993), High precision lead isotope ratio measurement by inductively coupled plasma multiple collector mass spectrometry, *Anal. Sci.*, *9*, 675–680.

Wang, Y., and L. Wen (2004), Mapping the geometry and geographic distribution of a very low velocity province at the base of the Earth's mantle, *J. Geophys. Res., 109*, B10305. doi:10.1029/2003JB002674.

Wanless V. D., M. O. Garcia, F. A. Trusdell, J. M. Rhodes, M. D. Norman, D. Weis, D. J. Fornari, M. D. Kurz, and H. Guillou (2006), Submarine radial vents on Mauna Loa Volcano, Hawaii, *Geochem. Geophys. Geosyst.*, *7*, Q05001, doi:10.1029/2005GC001086.

Wasserburg, G. J. and D. J. DePaolo (1979), Models of earth structure inferred from neodymium and strontium isotopic abundances, *Proc. Nat. Acad. Sci. U. S. A., 76*, 3594–3598.

Weaver, B. L. (1991), The origin of ocean island basalt end-member compositions: trace element and isotopic constraints, *Earth Planet. Sci. Lett*., *104*, 381–397.

Weis, D. (1992), Role of the Kerguelen Plume in the geochemical evolution of the Indian Ocean, *Habilitation thesis*, Université Libre de Bruxelles.

Weis, D., and F. A. Frey, (1991), Isotope geochemistry of Ninetyeast Ridge basement basalts: Sr, Nd, and Pb evidence for involvement of the Kerguelen hot spot, *In* Weissel, J., J. Peirce, E. Taylor, J. Alt, et al. (eds.), *Proc. Ocean Drill. Program, Sci. Results, 121*: College Station, TX (Ocean Drill. Program), 591–610, doi:10.2973/odp.proc.sr.121.170.1991.

Weis, D., and A. Giret (1994), Kerguelen plutonic complexes: Sr, Nd, Pb isotopic study and inferences about their sources, ages and geodynamic setting, *Bull. Soc. Géol. France, 166 (Special Issue: Géologie et géophysique des Kerguelen)*, 47–59.

Weis, D., and F. A. Frey (2002), Submarine basalts of the Northern Kerguelen Plateau: interaction between the Kerguelen Plume and the Southeast Indian Ridge revealed at ODP site 1140, *J. Petrol., 43*(7), 1287–1309.

Weis, D., F. A. Frey, A. Saunders, and I. Gibson (1991), Ninetyeast Ridge (Indian Ocean): A 5000 km record of a Dupal mantle plume, *Geology, 19*, 99–102.

Weis, D., F. A. Frey, A. Giret, and J.-M. Cantagrel (1998), Geochemical characteristics of the youngest volcano (Mount Ross) in the Kerguelen Archipelago: inferences for magma flux, lithosphere assimilation and composition of the Kerguelen plume, *J. Petrol., 39*, 973–994.

Weis, D., W. M. White, F. A. Frey, R. A. Duncan, M. R. Fisk, J. Dehn, J. Ludden, A. Saunders, and M. Storey (1992), The influence of mantle plumes in generation of Indian oceanic crust, *Synthesis of Results from Scientific Drilling in the Indian Ocean*, American Geophysical Union, 57–89.

Weis, D., S. Ingle, D. Damasceno, F. A. Frey, K. Nicolaysen, J. Barling and Leg 183 Shipboard Scientific Party (2001), Origin of continental components in Indian Ocean basalts: Evidence from Elan Bank (Kerguelen Plateau, ODP Leg 183, Site 1137), *Geology, 29*, 147-150.

Weis, D., F. A. Frey, R. Schlich, M. Schaming, R. Montigny, D. Damasceno, N. Mattielli, K. E. Nicolaysen, and J. S. Scoates (2002), Trace of the Kerguelen mantle plume: Evidence from seamounts between the Kerguelen Archipelago and Heard Island, Indian Ocean, *Geochem. Geophys. Geosyst., 3*(6), 1-27. doi:10.1029/2001GC000251.

Weis, D., B. Kieffer, C. Maerschalk, W. Pretorius, and J. Barling (2005), High-precision Pb-Sr-Nd-Hf isotopic characterization of USGS BHVO-1 and BHVO-2 reference materials, *Geochem. Geophys. Geosyst., 6*, Q02002, doi:10.1029/2004GC000852.

Weis, D., et al. (2006), High-precision isotopic characterization of USGS reference materials by TIMS and MC-ICP-MS, *Geochem. Geophys. Geosyst., 7*, Q08006, doi:10.1029/2006GC001283.

Weis, D., B. Kieffer, D. Hanano, I. Nobre Silva, J. Barling, W. Pretorius, C. Maerschalk, and N. Mattielli (2007), Hf isotope compositions of U.S. Geological Survey reference materials, *Geochem. Geophys. Geosyst., 8*, Q06006, doi:10.1029/2006GC001473.

Wen, L. (2006), A compositional anomaly at the Earth's core-mantle boundary as an anchor to the relatively slowly moving surface hotspots and as source to the DUPAL anomaly, *Earth Planet. Sci. Lett., 246*, 138–148.

White, R. S., and D. P. McKenzie (1989), Volcanism at Rifts, *Scientific American, July*, 62-71.

White, R. S., and D. P. McKenzie (1995), Mantle plumes and flood basalts, *J. Geophys. Res., 100*, 17,543–17,585.

White, W. M. (1985), Sources of oceanic basalts: Radiogenic isotopic evidence, *Geology*, *13*, 115–118.

White, W. M. (2010), Oceanic Island Basalts and Mantle Plumes: The Geochemical Perspective, *Ann. Rev. Earth Plan. Sci.*, *38*(1), 133–160.

White, W. M., and A. W. Hofmann (1982), Sr and Nd isotope geochemistry of oceanic basalts and mantle evolution, *Nature*, *296*, 821–825.

White, W. M., F. Albarède, and P. Télouk (2000), High-precision analysis of Pb isotope ratios by multi-collector ICP-MS, *Chem. Geol., 167*, 257–270.

Whitford D. J., and R.A. Duncan (1978), Origin of the Ninetyeast Ridge: trace element and Sr isotope evidence, *Annual Report of the Director Department of Terrestrial Magnetism*, Carnegie Inst. Washington, 77, 606–613.

Whitford D. J., and R.A. Duncan (1979), Origin of the Ninetyeast Ridge: Sr isotope and trace element evidence, In Zartman (Ed.) *Short papers of the fourth International Conference, Geochronology, Cosmochronology, Isotope geology*. Open-file Rep. U.S.G.S., 78-701, 451–453.

Wilson, J. T. (1963), A possible origin of the Hawaiian Islands, *Can. J. Physics, 41*, 863-871.

Willbold, M., and A. Stracke (2006), Trace element composition of mantle end-members: Implications for recycling of oceanic and upper and lower continental crust. *Geochem. Geophys. Geosyst., 7*, Q04004, doi:10.1029/2005gc001005.

Willbold, M., and A. Stracke (2010), Formation of enriched mantle components by recycling of upper and lower continental crust. *Chem. Geol.*, 276, 188–197.

Wolfe E. W. and J. Morris (1996), Geological map of the island of Hawaii. *Miscellaneous Investigations Series*, USGS, 1–18.

Woodhead, J. D. (2002), A simple method for obtaining highly accurate Pb-isotope data by MC-ICP-MS, *J. Anal. At. Spectrom.*, *17*, 1381–1385.

Woodhead, J. D., and J. M. Hergt (2000), Pb-isotope analysis of USGS reference materials, *Geostand. Newsl.*, *24*(1), 33–38.

Xu, G., F. A. Frey, D. Weis, J. S. Scoates, and A. Giret (2007), Flood basalts from Mt. Capitole in the central Kerguelen Archipelago: Insights into the growth of the archipelago and source components contributing to plume-related volcanism, *Geochem. Geophys. Geosyst., 8*, Q06007, doi:10.1029/2007GC001608.

Yamasaki, S., T. Kani, B. B. Hanan, and T. Tagami (2009), Isotopic geochemistry of Hualalai shield-stage tholeiitic basalts from submarine North Kona region, Hawaii, *J. Volcanol. Geotherm. Res,*, *185*(3), 223–230.

Yang, H.-J., F. A. Frey, D. Weis, A. Giret, D. Pyle, and G. Michon (1998), Petrogenesis of the flood basalts forming the northern Kerguelen Archipelago: Implications for the Kerguelen plume, *J. Petrol.*, *39*(4), 711–748.

Zindler, A., and S. R. Hart (1986), Chemical Geodynamics, *Ann. Rev. Earth Plan. Sci.*, *14*, 493–571.

Zindler, A., E. Jagoutz, and S. Goldstein (1982), Nd, Sr and Pb isotopic systematics in a three-component mantle: a new perspective, *Nature*, *298*(5874), 519–523.

Appendix A

HSDP2–B and –C
Analytical Precision and Accuracy

Assessment of the precision and accuracy of the HSDP2–B and –C isotopic dataset was discussed in section 5.5. Precision was assessed by the external reproducibility of replicate analyses of freshly prepared Pb, Sr and Nd standard solutions analyzed during the measurement sessions (see section 5.5) and that of several sets of complete procedural duplicates as well as replicate analyses of the same sample solution (Tables 5.3 and 5.4). Accuracy was evaluated by analysis of rock reference material solutions of known isotopic composition, such as BHVO-2 and Kil-93 [*Weis et al.*, 2005; 2006].

The HSDP2–B and –C Pb and Nd isotopic results have also been compared to the values of *Blichert-Toft and Albarède* [2009] for the same samples (Figures A1 to A3). For accurate and direct comparison between the two datasets, the data from *Blichert-Toft and Albarède* [2009] was renormalized to the same accepted values of the NBS 981 and Rennes standard solutions used in this study [*Abouchami et al.*, 2000; *Weis et al.*, 2006]. The agreement between the two datasets is excellent for $^{206}Pb/^{204}Pb$ and for $^{208}Pb/^{204}Pb$, for which the linear correlations are ~0.97. For $^{207}Pb/^{204}Pb$ and $^{143}Nd/^{144}Nd$, the agreement is not as close. Our values of $^{207}Pb/^{204}Pb$ and $^{143}Nd/^{144}Nd$ are systematically higher and lower, respectively, compared to those of *Blichert-Toft and Albarède* [2009]. Even so, the $^{143}Nd/^{144}Nd$ of both research groups are within error of each other (Figures A1 and A3). Our Nd isotopic compositions were obtained during two analytical sessions, one on the TIMS and the other on the MC-ICP-MC, and are in good agreement with each other. The Pb, Nd, and Sr isotopic compositions of BHVO-2 acquired during this study are also in good agreement with the literature values for this reference material [*Weis et al.*, 2005; 2006]. Given our careful sample treatment protocol prior to analysis, we have therefore no explanation for the differences between the two datasets.
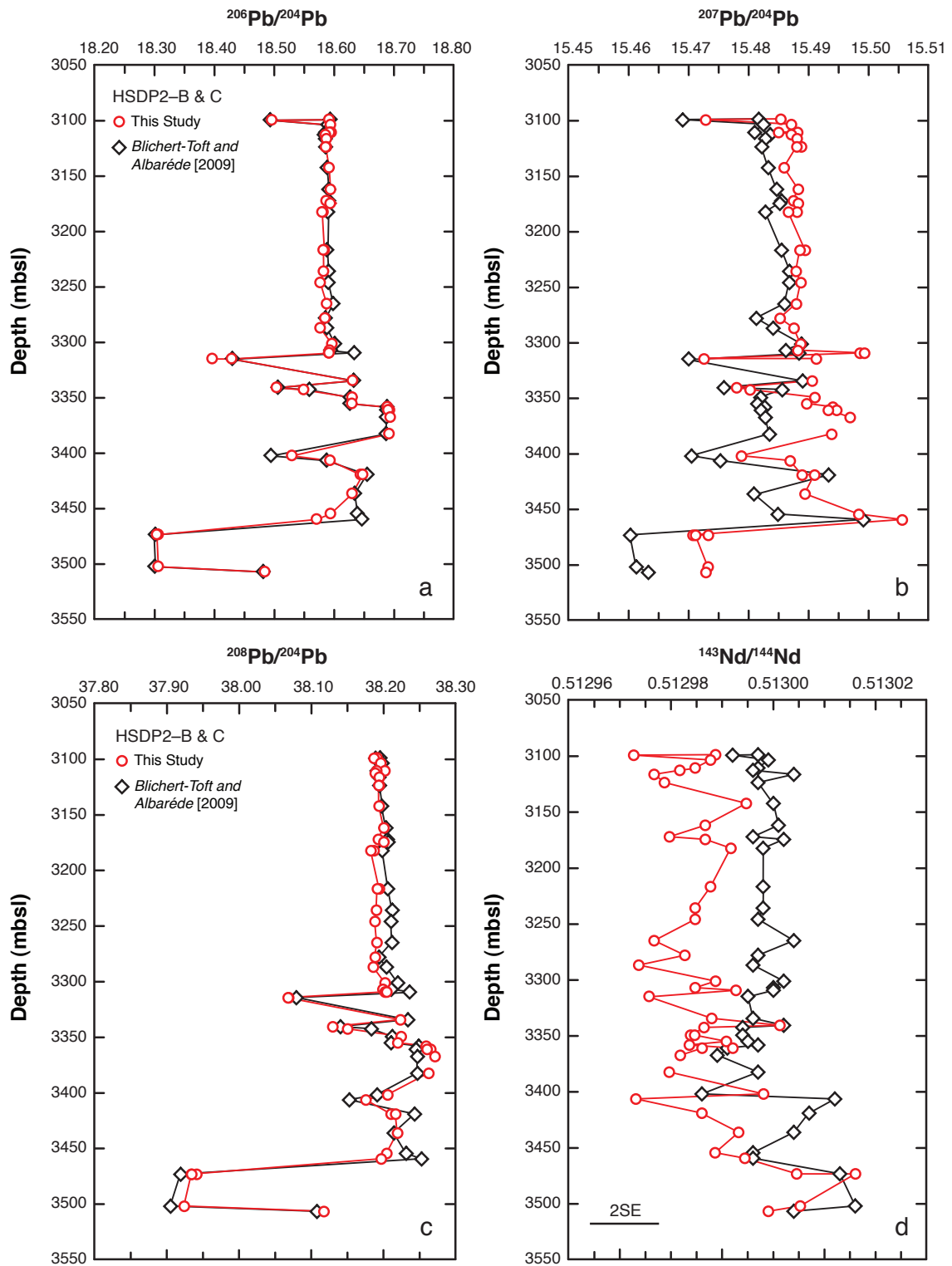
Figure A1. Down-hole comparison of the Pb and Nd isotopic compositions determined in this study and by *Blichert-Toft and Albarède* [2009] for the same set of samples recovered during the HSDP2-B and -C. Analytical uncertainty (2SE) is smaller than the symbol size except for ^{143}Nd/^{144}Nd, where it is repersented by the error bar.
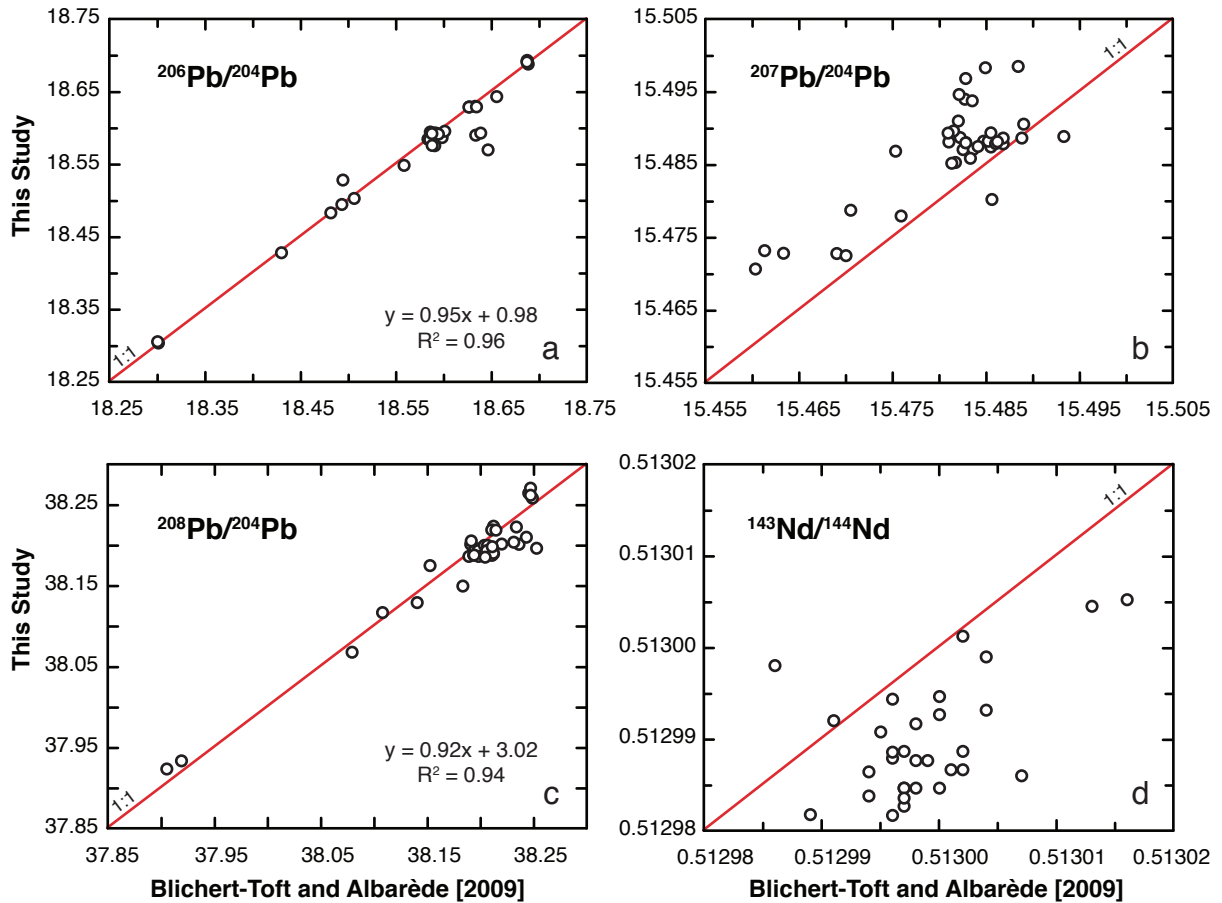
Figure A2. Binary diagrams comparing the Pb and Nd isotopic compositions determined in this study and by *Blichert-Toft and Albarède* [2009] for samples recovered during the HSDP2-B and -C. Slopes of unity are shown for reference.
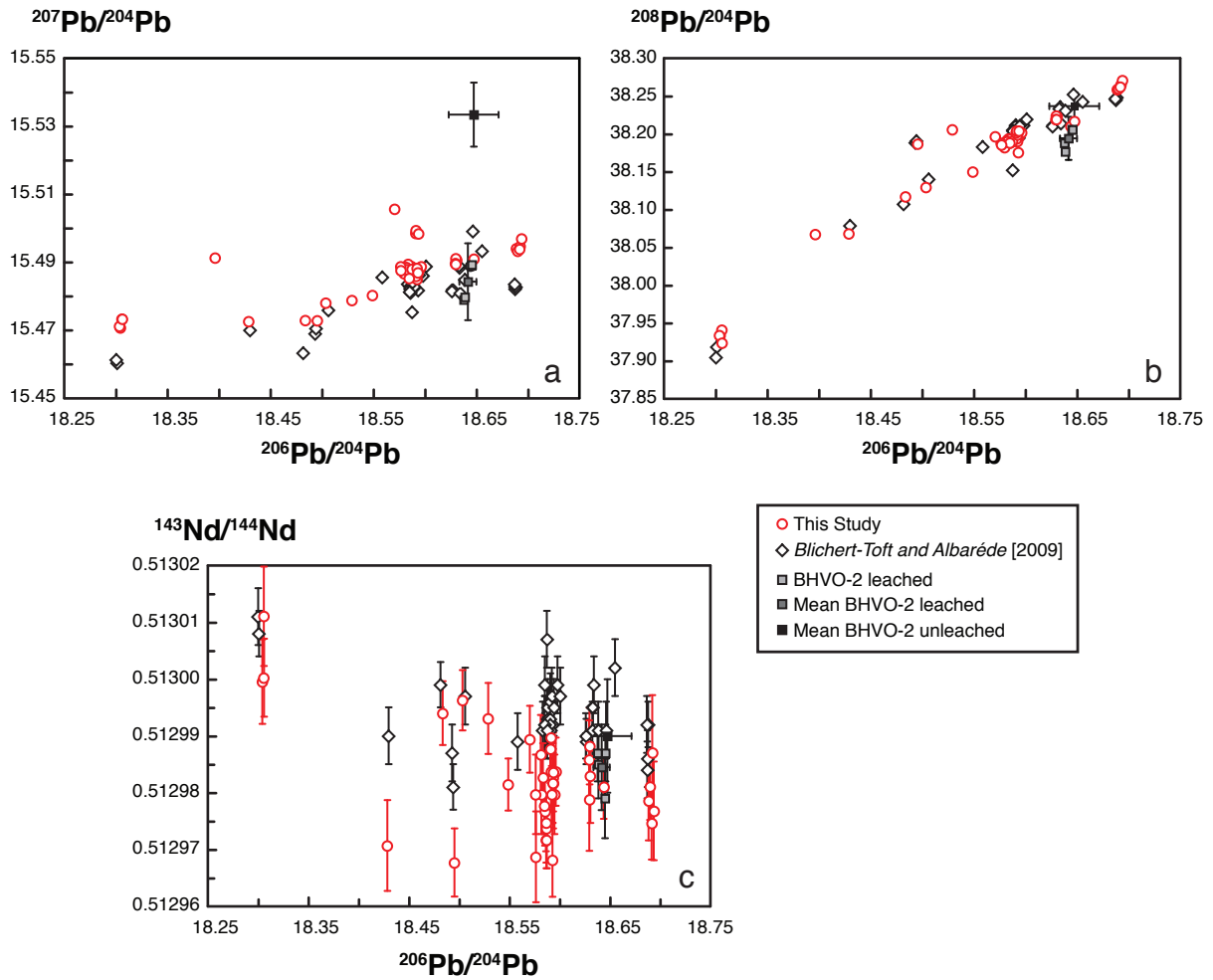
Figure A3. Pb-Pb and Nd-Pb isotope diagrams comparing the isotopic compositions determined in this study and those by *Blichert-Toft and Albarède* [2009]. For reference, the compositions of USGS reference material BHVO-2 analyzed by *Weis et al.* [2005, 2006] and in this study are also shown.

APPENDIX B

Ninetyeast Ridge
Supplementary Dredge Samples

The Ninetyeast Ridge, the longest linear feature on Earth (~5000 km), corresponds to ~44 Myr of evolution of the Indian Ocean basin related to the Kerguelen mantle plume. Almost two decades after its basement was successfully drilled during ODP Leg 121, the Ninetyeast Ridge was the scientific destination of a National Science Foundation-funded cruise during the summer of 2007. One of the scientific objectives of this research cruise was to dredge several sites along the ridge to recover suitable igneous basement rocks for geochemical and geochronological analyses, and use these new data to re-examine and test the models proposed for the magmatic origin of the ridge. Basaltic basement was recovered in 23 of the total 33 dredges that spanned ~3000 km of the Ninetyeast Ridge. High-precision isotopic compositions by MC-ICP-MS (Pb, Hf, and Nd) and TIMS (Sr) were obtained on basalts from 10 of the dredges, selected to sample most of the ridge length. The 32 basalts were chosen based on their lowest alteration degree (lowest LOI), high Mg#, and variable trace element ratios (e.g., Zr/Nb, Y/Nb, La/Sm). The dredged samples analyzed to date yield wider within-site isotopic variability compared to high-precision analyses of the previously drilled samples reported in Chapter 4. The isotopic compositions of the dredge samples are consistent with contributions from the Kerguelen, Amsterdam and St. Paul mantle plumes to the origin of the Ninetyeast Ridge basalts. Additionally, the dredge samples now extend the isotopic range of the Ninetyeast Ridge to Indian MORB compositions, as samples collected in dredges located at basal scarps along the edge of the ridge and the seafloor (e.g., dredges 3, 4, 16 and 33) fall in all isotope systems along mixing lines between the enriched St. Paul and Kerguelen mantle plumes with depleted Indian MORB. Further isotopic results on the remaining dredge samples will allow us to better constrain the mixing relationship of the Kerguelen, Amsterdam and St. Paul mantle plumes with Indian MORB, as well as improve our understanding of the magmatic and tectonic history of the Indian Ocean basin.

Table B1. Ninetyeast Ridge KNOX06 Dredge Summary[a]

Dredge	Date	Location	Depth (mbsl)	Total recovery (kg)	Total basalt recovery (kg)	Basalt Alteration Degree	Rock Groups
1	20-Jun-07	Cone SE of ODP Site 758	2950 - 2587	~2	~2	-	Calcite fragments
2	23-Jun-07	Between ODP Site 758 and DSDP Site 216	3035 - 2390	44.8	~22	medium to high (>50%)	13 kg of flowtop breccia in vesicular basalt 7 kg of aphanitic, massive basalt 2 kg of plagioclase-microphyric, massive basalt 18 kg of volcaniclastic claystone to sandstone 3 kg of chert 1 kg of calcium carbonate cobbles
3	26-Jun-07	Tall seamount E of DSDP Site 216	4377 - 3814	~82	~82	<50%	Aphanitic, massive, aphyric to sparsely-phyric basalt. Phenocrysts of plagioclase and clinopyroxene are present in the sparsely-phyric samples.
4	26-Jun-07	SE slope of DSDP Site 216	4478 - 3850	399	~155	40 to 90%	144 kg of aphyric to sparsely-phyric basalt (3 subgroups: massive- 72 kg, vesicular- 62 kg, and pillow rims- 10 kg) 11 kg of palagonite (altered glass) breccias 0.30 kg of altered pumice 0.15 kg of phosphoritic carbonate 182 kg of bulk sample, not examined in detail but most likely all basalt
5	27-Jun-07	Between DSDP Site 216 and proposed Site NER	2782 - 2418	~14	~14	30 to 50% 1 is ~85%	5.9 kg, 0.25 kg of aphanitic,vesicular, aphyric basalts 0.35 kg aphanitic, massive, aphyric basalt 7.6 kg fine to medium-grained, massive, aphyric basalt
6	28-Jun-07	Steep scarp face south of Drill Site 216	4525 - 3454	572	~566	~40%	200 kg of aphanitic to fine-grained, aphyric basalt 160 kg of aphanitic to fine-grained, plagioclase-phyric basalt 66 kg of aphanitic, clinopyroxene-plagioclase-phyric basalt 14 kg of fine-grained, clinopyroxene-phyric basalt 0.15 kg of basalt breccia Also- 126 kg of bulk sample, not examined in detail but likely all basalt
7	28-Jun-07	South of DSDP Site 216	3807 - 3016	77	65	~40 to 70%	50 kg of aphanitic to fine-grained, aphyric basalt 8 kg of fine-grained, possible ultramafic (olivine-phyric?) basalt 2 kg of very fine-grained, sparsely plagioclase-phyric basalt 5 kg of assorted basalt cobbles 5 kg of assorted manganese-encrusted cobbles 6 kg of phosphoritic conglomerate 1 kg of volcaniclastic/carbonate cobbles
8	29-Jun-07	scarp at proposed Site NER1	2967 - 2467	75	0	-	calcium carbonate boulders and cobbles
9	3-Jul-07	Northernmost seamount of proposed Site NER 2 dredging NW-SE along side of seamount	3017 - 2812	0.5	0	-	0.3 kg carbonaceous conglomerate 0.2 kg manganese crust on top of a thin layer of carbonaceous conglomerate
10	4-Jul-07	Northernmost seamount of NER 2, dredge track is of a degree SE of dredge track #9	2951 - 2622	0	0	-	-
11	4-Jul-07	Steep scarp at proposed Site NER 2	3988 - 3578	~17	~17	~60 to 70%	16.6 kg of aphanitic to fine-grained basalt. Both vesicular and massive basalt were recovered. ~ 1/3 of the basalt recovered is plagioclase phyric while the rest is aphyric. 0.4 kg of volcaniclastic breccia 0.02 kg of volcanic tuff
12	7-Jul-07	W of proposed Site NER 2	4133 - 3542	29.3	0	-	3 calcium carbonate boulders (4 kg, 5 kg, and 15 kg) Assorted calcium carbonate cobbles (4.8 kg) 1 carbonate crust (0.2 kg) 1 volcanic tuff (0.3 kg)
13	7-Jul-07	S scarp of proposed Site NER 2, along NER 3 seis line 1	3655 - 2949	41	~29	<40%	14 kg of aphanitic to medium-grained, aphyric basalt 8 kg of fine to medium-grained, olivine-phyric basalt 6 kg of fine to medium-grained, plagioclase-phyric basalt 1 kg of assorted basalt cobbles 11 kg of calcareous/volcaniclastic cobbles 0.5 kg of volcaniclastic sandstone 0.3 kg of volcanic tuff Also- 2 Mantle Xenoliths: 1 fine-grained, massive, aphyric garnet pyroxenite (0.1 kg) 1 garnet peridotite (0.3 kg)

[a]Adapted from *Shipboard Sciencitif Party* [2007], Cruise Report.

Table B1. Continued

Dredge	Date	Location	Depth (mbsl)	Total recovery (kg)	Total basalt recovery (kg)	Basalt Alteration Degree	Rock Groups
14	8-Jul-07	N scarp of porposed Site NER 3, 1 mile east of NE seismic line 1	3655 - 2911	204	143	20 to 60%	83 kg of very fine to medium-grained, aphyric basalt 21 kg of fine-grained, plagioclase-phyric basalt 12 kg of aphanitic to fine-grained, clinopyroxene-phyric basalt 1 kg of fine-grained, clinopyroxene-plagioclase-phyric basalt 1 kg of fine-grained, olivine-phyric basalt 25 kg of assorted basalt cobbles 44 kg of calcium carbonate cobbles and boulders 8 kg of volcaniclastic breccia 4 kg of volcaniclastic conglomerate 4 kg of volcaniclastic tuff 1 kg of volcaniclastic claystone
15	8-Jul-07	S scarp of porposed Site NER 3	4053 - 3438	~122	~115	20 to 50%	115 kg of aphanitic to fine-grained, aphyric basalt 0.5 kg of hyaloclastic breccia 5 kg of pink (iron-rich?) phosphorite cobbles 1 kg of chert 0.1 kg of pumice cobbles 0.1 kg of volcanic tuff cobbles 0.5 kg of calcium carbonate cobbles
16	9-Jul-07	W scarp of seamount north of DSDP Site 214	3957 - 3443	145	~110	>80%	80 kg of aphanitic to fine-grained, aphyric basalt 9 kg of very fine to fine-grained, olivine-phyric basalt 6 kg of aphanitic to fine-grained, plagioclase-phyric basalt 15 kg of assorted basalt cobbles 14 kg of marl (volcaniclastic and calcium carbonate) cobbles and boulders 10 kg of calcium carbonate cobbles and boulders 8 kg of chert 3 kg of phosphorite cobbles
17	14-Jul-07	E basal scarp of DSDP Site 214	4947 - 4435	30	~28	25 to 70%	20 kg of aphanitic to fine-grained, aphyric basalt 4 kg of very fine-grained, plagioclase-phyric basalt 3 kg of serpentinized or chloritized basalt 1 kg of fine-grained, olivine-phyric basalt 1 kg of basalt breccia 0.5 kg of chert
18	15-Jul-07	North-facing scarp on the E side of seamount south DSDP Site 214	3334 - 2999	10	~4	>90%	4 kg of highly-altered basalt 5 kg of volcaniclastic sandstone 0.5 kg of chert 0.25 kg of siltstone
19	15-Jul-07	North-facing scarp on the E side of seamount south DSDP Site 214	2899 - 2291	~40	0	-	35 kg of calcium carbonate cobbles and boulders 2 kg of chert 1 kg of volcaniclastic claystone to sandstone 1 kg of phosphate-chalk cobbles 0.5 kg of marl (volcaniclastic and calcium carbonate) cobbles
20	16-Jul-07	Northwest scarp of N-S trending seamount cluster minutes W of main NER	3859 - 3236	0.4	0	-	0.40 kg of botryoidal manganese crusts
21	16-Jul-07	about 10 miles S of the location of Dredge 20	3974 - 2749	0	0	-	-
22	18-Jul-07	SW scarp of seamount on W edge of Ninetyeast R at same latitude as Osbourne Knoll	2728 - 2157	55	~54	15 to 60%	46 kg of aphanitic to fine-grained, massive to vesicular, aphyric basalt 8 kg of aphanitic to very fine-grained, massive, plagioclase-phyric basalt 0.5 kg of volcaniclastic claystone to sandstone 0.5 kg of botryoidal manganese crusts
23	18-Jul-07	NW scarp of tall seamount between NER and Osb Knoll	2868 - 1883	~22	0	-	22 kg of calcium carbonate boulders and cobbles

[a]Adapted from *Shipboard Sciencitif Party* [2007], Cruise Report.

Dredge	Date	Location	Depth (mbsl)	Total recovery (kg)	Total basalt recovery (kg)	Basalt Alteration Degree	Rock Groups
24	19-Jul-07	East-facing scarp E of ODP Site 757	4100 - 2864	192	~130	10 to 70% some >90%	75 kg of aphanitic to medium-grained, massive, aphyric basalt 29 kg of very fine to fine-grained, massive, plagioclase-phyric basalt 10 kg of very fine-grained, massive, clinopyroxene-phyric basalt 8 kg of very fine-grained, massive, olivine-clinopyroxene-phyric basalt 8 kg of basalt breccia 37 kg chert 25 kg of calcium carbonate boulders and cobbles 0.1 kg of volcaniclastic sandstone
25	19-Jul-07	East-facing scarp NE of ODP Site 757	4718 - 3222	62	~35	~30% some >90%	26 kg very fine-grained to medium-grained, massive, aphyric basalt 9 kg very fine-grained to medium-grained, massive to vesicular, plagioclase-phyric basalt 26 kg basalt/palagonite breccia 1 kg volcaniclastic sandstone
26	20-Jul-07	SE corner of E scarp of ODP Site 757 seamount	4939 - 4124	47	~40	40 to 80%	20 kg of aphanitic, massive, olivine-phyric basalt 20 kg of aphanitic to very fine-grained, olivine-microphyric, plagioclase-phyric basalt 7 kg of basalt/palagonite breccia
27	21-Jul-07	E scarp of proposed Site NER 4	4642 - 3770	85	~81	20 to 65%	50 kg of aphanitic to very fine-grained, massive to vesicular, olivine-microphyric to olivine (note: both pillow fragments and flow interiors) 22 kg of aphanitic to medium-grained, massive to vesicular, aphyric basalt (note: both pillow fragments and flow interiors) 9 kg of assorted basalt cobbles 3 kg of assorted basalt breccia cobbles 1 kg of basalt/palagonite breccia
28	21-Jul-07	E upper scarp of porposed Site NER 4, 20 miles southwest of Dredge 27	4116 - 3024	135	~132	20 to 40%	56 kg of aphanitic to medium-grained, massive, aphyric basalt 32 kg of aphanitic to fine-grained, massive, clinopyroxene-phyric basalt 6 kg of fine-grained, massive, plagioclase-clinopyroxene-phyric basalt 5 kg of fine-grained to medium-grained, massive, olivine-phyric basalt 1 kg of very fine-grained, massive, plagioclase-phyric basalt 32 kg of assorted basalt cobbles 2 kg of basalt-phosphorite breccia 1 kg of volcaniclastic sandstone/ tuff
29	23-Jul-07	North-facing scarp, graben E of summit of propo... Site NER 4. 40 miles west of Dredge 27.	2208 - 1718	127	~0.1	~20%	0.1 kg of aphanitic, massive, sparsely feldspar-phyric, evolved? volcanic rock 70 kg of volcaniclastic sandstone / tuff boulders and cobbles 55 kg of phosphorite boulders and cobbles 2 kg of phosphorite breccia 0.3 kg calcium carbonate cobbles
30	24-Jul-07	W scarp of NER	3734 - 2460	82	~68	25 to 70% some ~90%	45 kg of aphanitic, massive to vesicular plagioclase-phyric basalt 14 kg of aphanitic, massive to vesicular, aphyric basalt 4 kg of aphanitic, massive, clinopyroxene-phyric basalt 1 kg of aphanitic, massive, plagioclase-pyroxene phyric basalt 4 kg of assorted basalt cobbles 8 kg of palagonite breccia 3.5 kg of basalt breccia 1 kg of assorted phosphorite-chalk cobbles 1 kg of volcaniclastic sandstone/tuff cobbles 0.5 kg of basalt-phosphorite breccia cobbles
31	24-Jul-07	SW-facing scarp on NW corner of DSDP Site 253 edifice	3597 - 2496	101	~7	20 to 40%	6 kg of aphanitic to medium-grained, massive to vesicular aphyric basalt 0.3 kg of fine-grained, massive, plagioclase-phyric basalt 0.5 g of fine-grained to medium-grained, massive, olivine-phyric basalt 0.5 kg of fine-grained, massive, plagioclase-olivine-phyric basalt 81 kg of volcaniclastic conglomerate boulders and cobbles 4 kg of phosphorite cobbles 4 kg of volcaniclastic/biogenic conglomerate boulders and cobbles 2.5 kg of volcaniclastic sandstone/tuff boulders and cobbles 2 kg of carbonate/volcanic claystone cobbles

[a]Adapted from *Shipboard Sciencitif Party* [2007], Cruise Report.

Table B1. Continued

Dredge	Date	Location	Depth (mbsl)	Total recovery (kg)	Total basalt recovery (kg)	Basalt Alteration Degree	Rock Groups
32	28-Jul-07	SW-facing scarp of graben SE of DSDP Site 253	3588 -2140	133	~122	20 to 60%	61 kg of very fine-grained to medium-grained, massive to vesicular, plagioclase-phyric basa 41 kg of aphanitic to fine-grained, massive to vesicular, aphyric basalt 9 kg of aphanitic to very fine-grained, massive to vesicular, olivine-phyric basalt 2 kg of aphanitic, massive, clinopyroxene-phyric basalt 1 kg of aphanitic, massive, olivine-clinopyroxene-phyric basalt 8 kg of assorted basalt cobbles 8 kg of hyaloclastic / basalt breccia cobbles and boulders 3 kg of volcaniclastic sandstone / tuff cobbles and boulders
33	29-Jul-07	E-facing scarp of N-S ridge to the E of DSDP Site edifice	4752 - 3475	196	~37	30 to 60% some >80%	13 kg of aphanitic, massive, olivine-plagioclase-phyric basalt 10 kg of aphanitic to very fine-grained, massive, olivine-phyric basalt 7 kg of aphanitic to medium-grained, massive, aphyric basalt 0.5 kg of aphanitic, massive, clinopyroxene-phyric basalt 0.5 kg of aphanitic, massive, plagioclase-phyric basalt 6 kg of assorted basalt cobbles 132 kg of basalt breccia boulders and cobbles 14 kg of volcaniclastic sandstone / tuff boulders and cobbles 11 kg of hyaloclastic / basalt boulders and cobbles 2 kg of assorted manganese crusts

[a]Adapted from *Shipboard Sciencitif Party* [2007], Cruise Report.

Table B2. Major Element and Trace Element Abundances of NER Whole Rock Basalts Collected During the KNOX06 Cruise[a]

Sample	NER 2-9	NER 2-15	NER 3-21	NER 3-26	NER 4-1	NER 4-5	NER 4-8	NER 5-4	NER 6-36	NER 6-41	NER 7-7	NER 7-20	NER 7-70
Unnormalized Major Element Oxides (by XRF in Wt%)													
SiO_2	49.45	46.66	50.44	50.29	50.27	48.55	49.37	48.37	50.03	49.77	49.62	49.09	49.71
TiO_2	2.23	1.56	1.08	1.17	1.12	1.49	1.13	1.63	1.29	1.45	2.57	1.70	1.45
Al_2O_3	13.88	14.81	15.81	15.24	14.62	15.53	15.90	16.93	14.70	14.52	14.84	14.68	14.89
Fe_2O_3*	14.00	16.15	11.27	12.18	13.74	11.86	14.27	12.60	12.94	13.96	16.20	12.57	11.41
MnO	0.28	0.12	0.19	0.19	0.22	0.16	0.20	0.19	0.21	0.21	0.21	0.12	0.17
MgO	6.41	10.16	6.08	5.77	5.71	5.05	4.61	8.03	7.46	6.98	5.34	8.27	7.09
CaO	11.22	7.32	11.83	11.74	11.26	12.08	11.34	9.80	9.78	10.49	7.63	9.95	12.07
Na_2O	2.49	2.53	2.31	2.37	2.32	2.70	2.39	2.15	2.14	2.18	2.81	2.54	2.40
K_2O	0.25	0.98	0.63	0.51	0.70	0.98	0.75	0.93	1.85	0.24	1.26	0.51	0.42
P_2O_5	0.18	0.09	0.24	0.42	0.12	1.48	0.17	0.21	0.17	0.14	0.30	0.15	0.13
Total	100.4	100.4	99.88	99.88	100.1	99.88	100.1	100.8	100.6	100.0	100.8	99.58	99.74
LOI	0.66	6.01	1.54	1.09	0.31	2.98	0.45	–	–	–	–	–	–
Total Alkalis	2.74	3.51	2.94	2.88	3.02	3.68	3.14	3.08	3.98	2.42	4.08	3.05	2.83
Trace Elements (by ICP-MS in ppm)													
Sc	48.3	49.2	52.0	55.9	54.5	45.2	57.7	–	–	–	–	–	–
Rb	4.39	5.31	9.30	7.49	9.53	15.4	10.1	–	–	–	–	–	–
Sr	144	105	117	97.5	80.4	190	96.5	–	–	–	–	–	–
Y	35.4	26.4	30.1	32.7	28.4	31.4	33.0	–	–	–	–	–	–
Zr	112	71.2	59.2	58.9	57.9	92.4	53.9	–	–	–	–	–	–
Nb	11.6	4.85	6.99	4.60	3.39	10.9	2.71	–	–	–	–	–	–
Ba	42.6	24.2	22.6	13.0	29.9	58.0	23.5	–	–	–	–	–	–
La	7.63	3.68	6.52	3.96	3.13	10.1	2.60	–	–	–	–	–	–
Ce	18.8	10.4	11.4	8.98	7.76	19.2	6.81	–	–	–	–	–	–
Pr	2.84	1.78	1.82	1.43	1.31	2.73	1.20	–	–	–	–	–	–
Nd	13.4	9.18	8.91	7.28	6.71	12.2	6.92	–	–	–	–	–	–
Sm	3.97	2.99	2.58	2.48	2.27	3.26	2.54	–	–	–	–	–	–
Eu	1.40	0.97	0.95	0.90	0.91	1.11	0.93	–	–	–	–	–	–
Gd	4.23	2.75	2.86	2.99	2.87	3.75	3.52	–	–	–	–	–	–
Tb	0.83	0.65	0.60	0.66	0.65	0.67	0.70	–	–	–	–	–	–
Dy	5.56	4.40	4.29	4.68	4.67	4.40	4.96	–	–	–	–	–	–
Ho	1.17	0.94	0.95	1.08	1.06	0.98	1.11	–	–	–	–	–	–
Er	3.40	2.51	2.81	3.13	3.04	2.86	3.23	–	–	–	–	–	–
Tm	0.53	0.39	0.45	0.50	0.48	0.46	0.54	–	–	–	–	–	–
Yb	3.21	2.25	2.72	3.02	2.97	2.75	3.18	–	–	–	–	–	–
Lu	0.51	0.34	0.44	0.49	0.45	0.43	0.49	–	–	–	–	–	–
Hf	3.09	2.02	1.68	1.77	1.77	2.36	1.64	–	–	–	–	–	–
Ta	0.85	0.39	0.47	0.36	0.28	0.71	0.22	–	–	–	–	–	–
Pb	0.82	0.58	0.68	0.44	0.62	1.09	0.54	–	–	–	–	–	–
Th	0.92	0.36	0.61	0.41	0.38	0.96	0.17	–	–	–	–	–	–
U	0.20	0.07	0.56	0.59	0.53	0.86	0.65	–	–	–	–	–	–

[a]Geochemical data courtesy of F.A.Frey (MIT, unpublished data, 2010)

Table B2. Continued

Sample	NER 11-4	NER 13-20	NER 14-2	NER 14-58	NER 15-51 i	NER 16-14	NER 16-19	NER 16-31 core	NER 16-45	NER 16-46	NER 27-37	NER 27-69	NER 27-100
Unnormalized Major Element Oxides (by XRF in Wt%)													
SiO_2	49.49	49.93	50.42	51.07	50.05	50.58	49.85	50.51	49.07	51.18	50.04	48.99	49.95
TiO_2	1.67	1.43	1.42	1.36	1.77	2.87	1.96	1.92	2.65	3.05	2.45	2.13	2.27
Al_2O_3	17.29	14.89	15.24	16.33	14.72	16.15	14.78	14.96	15.24	15.98	16.87	17.09	15.94
Fe_2O_3*	14.75	11.70	10.90	9.48	13.63	11.72	12.53	11.14	14.81	11.76	9.84	10.69	9.88
MnO	0.18	0.16	0.11	0.11	0.19	0.11	0.18	0.17	0.15	0.11	0.14	0.14	0.13
MgO	3.22	8.01	8.36	8.50	5.48	4.28	5.76	6.16	4.53	3.54	4.49	5.84	7.60
CaO	9.03	10.01	10.23	7.22	10.99	8.27	11.53	11.66	9.14	8.77	10.57	11.16	8.87
Na_2O	2.79	2.61	2.46	2.37	2.44	3.32	2.50	2.73	3.29	3.48	3.31	2.74	3.10
K_2O	1.44	1.26	0.85	3.23	0.86	1.59	0.72	0.76	1.08	1.60	2.11	0.98	1.83
P_2O_5	0.45	0.20	0.13	0.21	0.22	0.65	0.20	0.17	0.33	0.61	0.51	0.43	0.38
Total	100.3	100.2	100.1	99.88	100.4	99.54	100.0	100.2	100.3	100.1	100.3	100.2	99.95
LOI	3.21	3.77	4.20	4.42	1.91	3.27	1.44	2.17	3.02	2.47	2.86	4.84	4.15
Total Alkalis	4.23	3.87	3.31	5.60	3.30	4.91	3.22	3.49	4.37	5.08	5.42	3.72	4.93
Trace Elements (by ICP-MS in ppm)													
Sc	43.4	47.4	33.5	30.1	–	41.2	31.7	51.9	–	26.2	16.4	25.3	20.2
Rb	22.2	111.4	8.9	36.3	–	30.6	6.8	12.1	–	8.2	22.2	11.2	26.4
Sr	207	137	121	126	–	186	142	172	–	170	359	353	313
Y	41.0	28.3	19.7	18.4	–	44.5	31.9	34.2	–	54.5	23.0	23.7	20.5
Zr	104	82.8	72.0	75.6	–	221	109	115	–	195	189	167	188
Nb	10.3	4.74	4.79	8.74	–	23.1	7.51	7.55	–	20.6	35.3	30.9	37.5
Ba	88.0	36.7	30.4	367.6	–	192	47.3	62.1	–	162	250	185	229
La	14.5	5.44	4.20	9.66	–	19.6	6.75	6.85	–	22.3	21.5	17.0	20.2
Ce	24.0	12.6	11.5	19.4	–	45.4	17.4	17.4	–	44.1	42.7	36.3	42.1
Pr	3.73	1.99	1.79	2.99	–	6.04	2.77	2.69	–	6.34	5.57	4.52	5.10
Nd	16.7	10.1	9.08	13.1	–	26.1	13.4	13.2	–	27.9	22.4	19.4	21.2
Sm	4.17	3.07	2.77	3.09	–	6.23	3.95	3.84	–	6.20	4.33	4.11	4.36
Eu	1.39	1.10	0.94	1.05	–	1.94	1.37	1.41	–	1.94	1.48	1.33	1.44
Gd	4.55	3.48	3.18	3.38	–	6.71	4.52	4.57	–	7.18	4.35	4.07	4.33
Tb	0.82	0.66	0.62	0.57	–	1.16	0.84	0.85	–	1.31	0.70	0.67	0.65
Dy	5.26	4.20	3.70	3.22	–	7.23	5.32	5.33	–	8.10	3.88	3.96	3.63
Ho	1.21	0.92	0.75	0.66	–	1.52	1.13	1.11	–	1.78	0.79	0.82	0.74
Er	3.51	2.57	2.24	1.79	–	4.25	3.14	3.19	–	5.36	2.23	2.20	2.06
Tm	0.54	0.40	0.33	0.29	–	0.68	0.52	0.50	–	0.90	0.35	0.35	0.31
Yb	3.20	2.30	1.82	1.60	–	3.92	2.84	2.95	–	5.22	2.04	2.05	1.79
Lu	0.50	0.34	0.28	0.25	–	0.57	0.43	0.42	–	0.81	0.31	0.31	0.27
Hf	2.71	2.08	2.08	2.12	–	5.36	3.12	2.88	–	5.14	4.68	4.06	4.67
Ta	0.66	0.38	0.40	0.66	–	1.53	0.57	0.55	–	1.44	2.92	2.39	2.89
Pb	1.47	0.33	0.45	2.80	–	1.15	0.68	0.61	–	1.45	2.03	1.39	1.40
Th	1.44	0.48	0.51	1.19	–	2.51	0.79	0.72	–	2.31	2.60	2.14	2.57
U	0.41	0.21	0.38	0.42	–	1.41	0.34	0.99	–	1.91	0.72	0.46	0.79

[a]Geochemical data courtesy of F.A.Frey (MIT, unpublished data, 2010)

Table B2. Continued

Sample	NER 27-108	NER 32-38	NER 32-45	NER 33-9	NER 33-42	BHVO-2 (n=11)	% SD/AVE
Unnormalized Major Element Oxides (by XRF in Wt%)							
SiO_2	48.99	49.15	48.85	48.34	50.36	–	–
TiO_2	2.08	1.70	3.04	2.75	1.01	–	–
Al_2O_3	16.80	14.58	16.92	15.23	16.48	–	–
Fe_2O_3*	10.45	12.88	11.02	14.70	8.73	–	–
MnO	0.14	0.21	0.20	0.18	0.14	–	–
MgO	5.10	7.40	3.41	4.91	8.39	–	–
CaO	11.11	10.12	8.59	9.89	11.92	–	–
Na_2O	2.87	3.27	3.33	2.69	2.09	–	–
K_2O	1.66	0.81	3.13	0.66	0.58	–	–
P_2O_5	0.71	0.14	1.18	0.39	0.17	–	–
Total	99.91	100.3	99.67	99.74	99.87	–	–
LOI	2.80	3.57	4.09	2.03	2.35	–	–
Total Alkalis	4.53	4.08	6.46	3.35	2.67	–	–
Trace Elements (by ICP-MS in ppm)							
Sc	25.4	33.1	17.7	38.5	32.3	29.8	14.0%
Rb	17.6	10.4	58.7	14.9	7.98	8.44	22.6%
Sr	330	202	827	116	200	389	5.0%
Y	24.0	20.4	46.3	62.9	20.6	27.7	5.3%
Zr	159	59	437	161	72.2	173	6.0%
Nb	29.6	5.55	84.6	16.0	15.2	18.8	4.7%
Ba	202	29	593	61	142	128	5.1%
La	18.3	3.75	64.7	10.3	9.88	14.7	6.1%
Ce	35.9	9.99	124	24.1	20.5	36.7	5.1%
Pr	4.64	1.55	14.7	3.75	2.58	5.33	4.3%
Nd	19.0	8.13	56.3	17.8	11.2	24.1	4.3%
Sm	4.16	2.68	10.8	6.03	2.51	6.04	4.9%
Eu	1.36	0.91	3.37	1.89	0.89	2.00	3.9%
Gd	4.17	3.10	9.73	6.86	2.87	5.73	6.7%
Tb	0.69	0.69	1.45	1.51	0.52	0.92	4.3%
Dy	4.01	4.30	7.78	10.1	3.31	5.10	4.2%
Ho	0.88	0.92	1.47	2.27	0.74	0.97	4.1%
Er	2.32	2.62	3.76	6.58	2.08	2.45	3.8%
Tm	0.38	0.41	0.56	1.09	0.33	0.36	2.1%
Yb	2.04	2.28	3.25	6.14	1.86	1.99	3.2%
Lu	0.34	0.37	0.43	0.94	0.29	0.27	3.5%
Hf	4.11	2.25	9.46	4.97	1.85	4.39	3.3%
Ta	2.36	0.54	4.60	1.11	1.01	1.24	3.8%
Pb	1.56	0.56	6.18	1.38	1.01	1.38	6.0%
Th	2.12	0.56	8.93	1.39	1.62	1.19	2.8%
U	0.64	0.48	2.61	0.30	0.41	0.40	3.8%

[a]Geochemical data courtesy of F.A.Frey (MIT, unpublished data, 2010)

Table B3. Pb Isotopic Compositions by MC-ICP-MS From a Subset of Ninetyeast Ridge Basalts Collectected During the KNOX06 Cruise

Sample	$^{206}Pb/^{206}Pb^a$	2SE	$^{207}Pb/^{204}Pb^a$	2SE	$^{208}Pb/^{204}Pb^a$	2SE	$^{208}Pb/^{206}Pb$	$^{208}Pb*/^{206}Pb*^b$	$^{207}Pb/^{206}Pb$	$^{207}Pb*/^{206}Pb*^c$
NER 2-9	18.4772	0.0015	15.5536	0.0012	38.8828	0.0039	2.104	1.026	0.842	0.574
NER 2-15	17.9450	0.0030	15.5278	0.0038	38.3294	0.0127	2.136	1.025	0.865	0.606
NER 3-21	18.5607	0.0043	15.5617	0.0040	38.6526	0.0051	2.082	0.992	0.838	0.569
NER 3-26	18.4011	0.0015	15.6162	0.0017	38.2084	0.0054	2.076	0.960	0.849	0.585
NER 4-1	18.2471	0.0016	15.5483	0.0015	38.4007	0.0040	2.104	0.998	0.852	0.588
NER 4-5	18.3808	0.0023	15.5664	0.0018	38.7641	0.0050	2.109	1.024	0.847	0.581
NER 4-8	18.1951	0.0020	15.5693	0.0022	38.1750	0.0068	2.098	0.979	0.856	0.594
NER 5-4	17.7681	0.0007	15.5632	0.0008	38.3094	0.0022	2.156	1.044	0.876	0.623
NER 6-36	18.4144	0.0015	15.5582	0.0014	38.6446	0.0039	2.099	1.007	0.845	0.578
NER 6-36 dup.[d]	18.4122	0.0032	15.5609	0.0040	38.6485	0.0135	2.099	1.007	0.845	0.579
NER 6-41	18.1869	0.0023	15.5402	0.0027	38.6060	0.0090	2.123	1.028	0.854	0.591
NER 7-7	18.9520	0.0016	15.5947	0.0018	39.4915	0.0056	2.084	1.038	0.823	0.550
NER 7-20	18.6318	0.0011	15.5697	0.0010	39.0822	0.0031	2.098	1.030	0.836	0.566
NER 7-70	18.4979	0.0025	15.5623	0.0029	38.8585	0.0078	2.101	1.021	0.841	0.573
NER 11-4	18.9786	0.0040	15.6134	0.0018	39.8727	0.0138	2.101	1.075	0.823	0.550
NER 13-20	18.4153	0.0014	15.5539	0.0012	38.5846	0.0036	2.095	1.000	0.845	0.578
NER 13-20 dup.	18.4185	0.0019	15.5538	0.0020	38.5847	0.0055	2.095	1.000	0.844	0.577
NER 14-2	18.5444	0.0013	15.5590	0.0014	38.6624	0.0042	2.085	0.995	0.839	0.570
NER 14-58	18.7964	0.0020	15.5942	0.0027	39.2340	0.0092	2.087	1.028	0.830	0.559
NER 15-51 i	18.9145	0.0032	15.5859	0.0034	39.1225	0.0100	2.068	1.004	0.824	0.551
NER 16-14	18.7933	0.0017	15.6252	0.0016	38.8294	0.0049	2.066	0.986	0.831	0.562
NER 16-31 core	18.4997	0.0011	15.5497	0.0012	38.5471	0.0032	2.084	0.987	0.841	0.572
NER 16-19	18.3548	0.0017	15.5441	0.0020	38.5007	0.0067	2.098	0.998	0.847	0.580
NER 16-45	19.4321	0.0018	15.5990	0.0021	38.9094	0.0064	2.002	0.932	0.803	0.524
NER 16-46	19.4152	0.0014	15.6497	0.0016	39.5845	0.0054	2.039	1.000	0.806	0.530
NER 27-37	18.4476	0.0012	15.5705	0.0012	38.8603	0.0036	2.107	1.027	0.844	0.577
NER 27-37 dup.	18.4466	0.0013	15.5699	0.0011	38.8582	0.0035	2.107	1.027	0.844	0.577
NER 27-69	18.3748	0.0026	15.5668	0.0032	38.8523	0.0104	2.114	1.034	0.847	0.582
NER 27-100	18.4597	0.0013	15.5733	0.0016	38.8753	0.0049	2.106	1.027	0.844	0.577
NER 27-108	18.4366	0.0013	15.5690	0.0013	38.9102	0.0038	2.110	1.033	0.844	0.578
NER 32-38	18.7179	0.0020	15.5617	0.0019	38.9019	0.0045	2.078	1.002	0.831	0.560
NER 32-45	19.1605	0.0016	15.6148	0.0014	39.4635	0.0046	2.060	1.014	0.815	0.540
NER 33-9	18.2442	0.0011	15.5242	0.0012	38.6203	0.0036	2.117	1.023	0.851	0.585
NER 33-9 dup.	18.2423	0.0024	15.5242	0.0030	38.6161	0.0096	2.117	1.023	0.851	0.585
NER 33-42	18.5540	0.0016	15.6187	0.0018	39.1381	0.0062	2.109	1.045	0.842	0.576
Reference Materials										
BHVO-2	18.6411	0.0018	15.4900	0.0021	38.1916	0.0068				
Koolau	17.8470	0.0016	15.4382	0.0022	37.7476	0.0072				

[a] Pb isotopic compositions are reported relative to the SRM 981 Pb standard solution TS-TIMS reference values of *Abouchami et al.* [2000]; 2SE is the absolute error value of the individual sample analysis (internal error).
[b] $^{208}Pb*/^{206}Pb*$ defined as $(^{208}Pb/^{204}Pb_{sample} - 29.475)/(^{206}Pb/^{204}Pb_{sample} - 9.306)$ by *Galer and O'Nions.* [1985].
[c] $^{207}Pb*/^{206}Pb*$ defined as $(^{207}Pb/^{204}Pb_{sample} - 10.293)/(^{206}Pb/^{204}Pb_{sample} - 9.306)$ by *Galer and O'Nions* [1985].
[d] dup. = full procedural duplicate analysis of the same starting sample powder.

Table B4. Sr, Nd, and Hf Isotopic Compositions by TIMS and MC-ICP-MS From a Subset of Ninetyeast Ridge Basalts Collectected During the KNOX06 Cruise

Sample	$^{87}Sr/^{86}Sr^a$	2SE	$^{143}Nd/^{144}Nd^b$	2SE	$\varepsilon_{Nd}{}^d$	$^{176}Hf/^{177}Hf^c$	2SE	$\varepsilon_{Hf}{}^d$
NER 2-9	0.704572	9	0.512805	8	3.3	0.282993	4	7.8
NER 2-15	0.704701	8	0.512845	7	4.0	0.283028	6	9.1
NER 3-21	0.704430	10	0.512879	6	4.7	0.283111	12	12
NER 3-26	0.704540	7	0.512912	6	5.3	0.283110	9	12
NER 4-1	0.704874	8	0.512846	7	4.1	0.283107	9	12
NER 4-5	0.705233	8	0.512695	10	1.1	0.282937	11	5.8
NER 4-8	0.704704	9	0.512900	7	5.1	0.283149	7	13
NER 5-4	0.705654	8	0.512588	6	-1.0	0.282755	4	-0.62
NER 6-36	0.705333	9	0.512708	8	1.4	0.282984	6	7.5
NER 6-36 dup.[e]	0.705318	7	0.512695	8	1.1	0.282967	5	6.9
NER 6-41	0.704722	9	0.512756	7	2.3	0.282970	7	7.0
NER 7-7	0.704855	9	0.512753	7	2.2	0.282935	6	5.8
NER 7-20	0.704653	9	0.512791	8	3.0	0.282968	6	6.9
NER 7-70	0.704666	7	0.512792	6	3.0	0.283013	5	8.5
NER 11-4	0.705340	7	0.512714	6	1.5	0.282937	15	5.8
NER 13-20	0.704677	9	0.512877	6	4.7	0.283086	13	11.1
NER 13-20 dup.	0.704645	8	0.512869	6	4.5	0.283078	6	10.8
NER 14-2	0.704505	8	0.512858	8	4.3	0.283097	3	11.5
NER 14-58	0.706144	6	0.512668	9	0.59	0.282913	4	5.0
NER 15-51 i	0.704237	8	0.512873	9	4.6	0.283106	4	11.8
NER 16-14	0.704963	9	0.512724	8	1.7	0.282974	5	7.2
NER 16-31 core	0.704317	8	0.512871	5	4.5	0.283106	11	11.8
NER 16-19	0.704333	9	0.512859	7	4.3	0.283083	5	11.0
NER 16-45	0.704764	7	0.512793	8	3.0	0.283075	4	10.7
NER 16-46	0.705016	8	0.512721	8	1.6	0.282980	4	7.3
NER 16-46 rep.[f]						0.282980	3	7.3
NER 27-37	0.704697	8	0.512745	6	2.1	0.282831	4	2.1
NER 27-37 dup.	0.704679	7	0.512738	8	2.0	0.282832	5	2.1
NER 27-69	0.704557	8	0.512761	6	2.4	0.282845	6	2.6
NER 27-100	0.704672	9	0.512749	7	2.2	0.282829	5	2.0
NER 27-108	0.704604	9	0.512744	6	2.1	0.282849	7	2.7
NER 32-38	0.704582	10	0.512888	8	4.9	0.283059	7	10.2
NER 32-45	0.703622	7	0.512859	7	4.3	0.282958	4	6.6
NER 33-9	0.703650	7	0.512978	5	6.6	0.283168	5	14.0
NER 33-9 dup.	0.703653	8	0.512976	5	6.6	0.283185	20	14.6
NER 33-42	0.705037	8	0.512688	6	0.98	0.283004	6	8.2

Reference Materials

BHVO-2	0.703473	9	0.512990	8		0.283098	7	
Koolau	0.704102	9	0.512757	11		0.282950	3	

[a]Sr isotopic compositions are reported relative to $^{87}Sr/^{86}Sr = 0.710248$ for the NBS-987 standard solution, based on the mean of the barrel; 2SE is the absolute error value of the individual sample analysis (internal error) and reported as x106.
[b]Nd isotopic compositions are reported relative to $^{143}Nd/^{144}Nd = 0.511973$ of the Rennes standard solution, based on the mean of analyses of the day; 2SE is the absolute error value of the individual sample analysis (internal error) and reported as x10⁶.
[c]Hf isotopic ratio compositions are reported relative to $^{176}Hf/^{177}Hf = 0.282160$ of the JMC475 standard solution, based on the mean of analyses of the day; 2SE is the absolute error value of the individual sample analysis (internal error) and reported as x10⁶.
[d]ε_{Nd} and ε_{Hf} are calculated using present day $^{143}Nd/^{144}Nd$ and $^{176}Hf/^{177}Hf$ values for CHUR = 0.512638 and 0.282772, respectively.
[e]dup. = full procedural duplicate analysis of the same starting sample powder.
[f]rep. = replicate analysis of the same sample solution on the MC-ICP-MS.
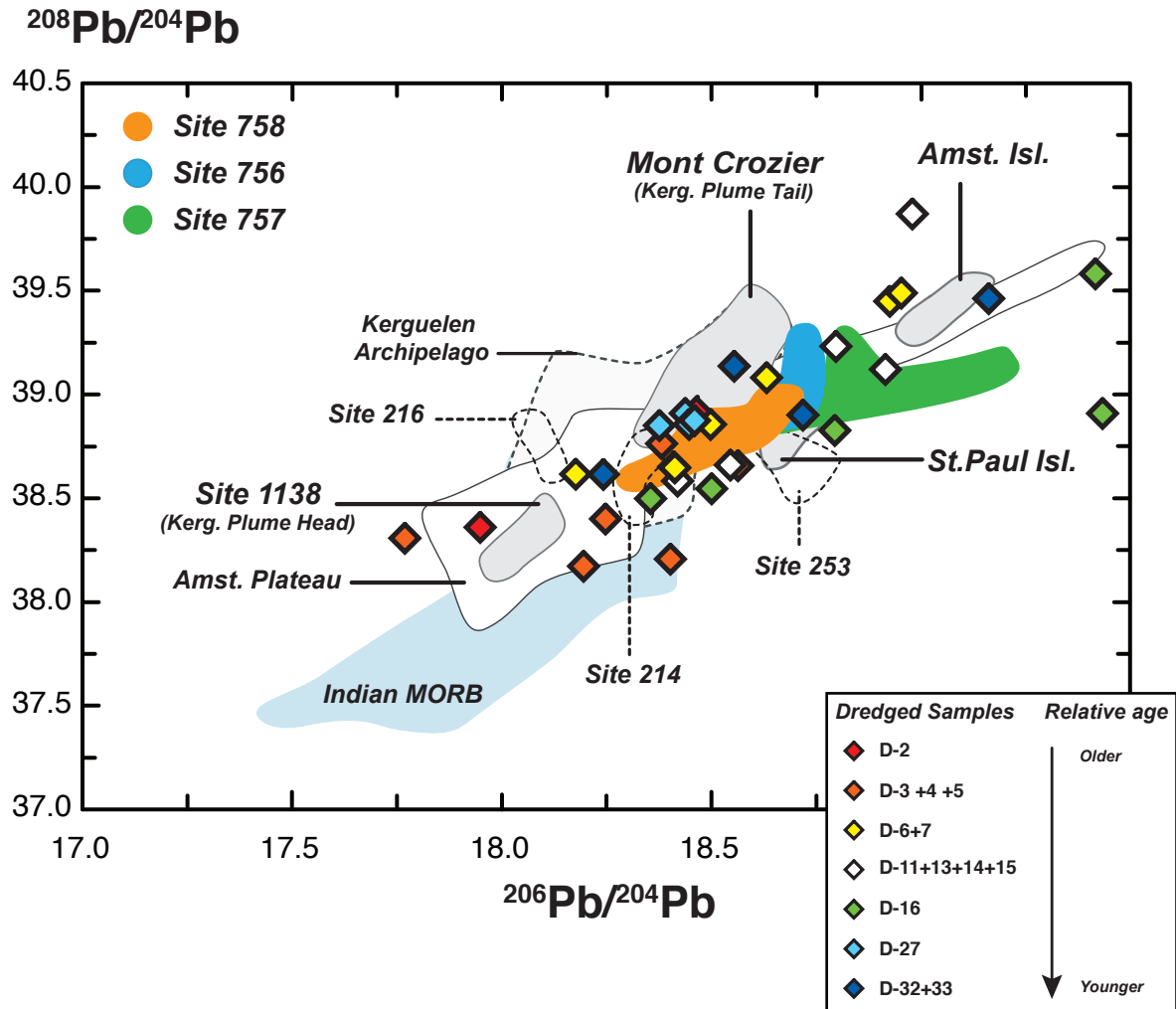
Figure B1. Diagram of measured $^{208}Pb/^{204}Pb$ versus $^{206}Pb/^{204}Pb$ for the Ninetyeast Ridge KNOX06RR dredged samples compared to other Ninetyeast Ridge basalts recovered by drilling and to other Indian Ocean basalts. Data sources are as follows: Indian MORB: *Chauvel and Blichert-Toft* [2001]; *Mahoney et al.* [2002]; *Nicolaysen et al.* [2007]; *Rehkämper and Hofmann* [1997]; *Mahoney et al.* [1992]; *Janney et al.* [2005]; *Meyzen et al.* [2005]; Amsterdam Plateau: *Nicolaysen et al.* [2007]; Amsterdam and St. Paul islands: *Doucet et al.* [2004]; Kerguelen Archipelago: *Weis et al.* [1998]; *Frey et al.*, 2002b]; *Doucet et al.* [2005]; *Xu et al.* [2007]; Mont Crozier (D. Weis unpublished data, 2001); ODP Site 1138 on the South and Central Kerguelen Plateaus:*Neal et al* [2002]; *Ingle et al.* [2003]; DSDP Sites 214, 216, and 253: *Frey and Weis* [1995].

Figure B2. Diagram of measured (a) $^{143}Nd/^{144}Nd$ and (b) $^{176}Hf/^{177}Hf$ versus $^{206}Pb/^{204}Pb$ for the Ninetyeast Ridge KNOX06RR dredged samples compared to other Ninetyeast Ridge basalts recovered by drilling and to other Indian Ocean basalts. Data sources are as follows: Indian MORB: *Chauvel and Blichert-Toft* [2001]; *Mahoney et al.* [2002]; *Nicolaysen et al.* [2007]; *Rehkämper and Hofmann* [1997]; *Mahoney et al.* [1992]; *Janney et al.* [2005]; *Meyzen et al.* [2005]; Amsterdam Plateau: *Nicolaysen et al.* [2007]; Amsterdam and St. Paul islands: *Doucet et al.* [2004]; Kerguelen Archipelago: *Weis et al.* [1998]; *Frey et al.*, 2002b]; *Doucet et al.* [2005]; *Xu et al.* [2007]; Mont Crozier (D. Weis unpublished data, 2001); ODP Site 1138 on the South and Central Kerguelen Plateaus: *Neal et al* [2002]; *Ingle et al.* [2003]; DSDP Sites 214, 216, and 253: *Frey and Weis* [1995].

Figure B3. Diagram of measured (a) ^{143}Nd/^{144}Nd versus ^{87}Sr/^{86}Sr and (b) ε_{Hf} versus ε_{Nd} for the Ninetyeast Ridge KNOX06RR dredged samples compared to other Ninetyeast Ridge basalts recovered by drilling and to other Indian Ocean basalts. Data sources are as follows: Indian MORB: *Chauvel and Blichert-Toft* [2001]; *Mahoney et al.* [2002]; *Nicolaysen et al.* [2007]; *Rehkämper and Hofmann* [1997]; *Mahoney et al.* [1992]; J*anney et al.* [2005]; *Meyzen et al.* [2005]; Amsterdam Plateau: *Nicolaysen et al.* [2007]; Amsterdam and St. Paul islands: *Doucet et al.* [2004]; Kerguelen Archipelago: *Weis et al.* [1998]; *Frey et al.*, 2002b]; *Doucet et al.* [2005]; *Xu et al.* [2007]; Mont Crozier (D. Weis unpublished data, 2001); ODP Site 1138 on the South and Central Kerguelen Plateaus:*Neal et al* [2002]; *Ingle et al.* [2003]; DSDP Sites 214, 216, and 253: *Frey and Weis* [1995]. OIB array

Appendix C

Scientific Communications During the PhD

C1. Peer-Reviewed Publications

Nobre Silva, I. G., D. Weis, and J. S. Scoates (2010), Effects of acid leaching on the Sr-Nd-Hf isotopic compositions of ocean island basalts, *Geochem. Geophys. Geosyst.*, *11*, Q09011, doi:10.1029/2010GC003176.

Nobre Silva, I. G., D. Weis, J. Barling, and J. S. Scoates (2009), Leaching systematics and matrix elimination for the determination of high-precision Pb isotope compositions of ocean island basalts, *Geochem. Geophys. Geosyst.*, *10*, Q08012, doi:10.1029/2009GC002537.

Garcia, M, G. Ito, D. Weis, D. Geist, L. Swinnard, T. Bianco, A Flinders, B. Taylor, B. Appelgate, C. Blay, D. Hanano, **I. Nobre Silva**, T. Naumann, C. Maerschalk, K. Harpp, B. Christensen, L. Sciaroni, T. Tagami, and S. Yamasaki (2008), Widespread secondary volcanism near Northern Hawaiian Islands, *Eos Trans.*, *89 (52)*, 542-543.

Weis, D., B. Kieffer, D. Hanano, **I. Nobre Silva**, J. Barling, W. Pretorius, C. Maerschalk, and N. Mattielli (2007), Hf isotope compositions of U.S. Geological Survey reference materials, *Geochem. Geophys. Geosyst.*, *8*, Q06006, doi:10.1029/2006GC001473.

C2. Communications at Scientific Meetings

C2.1. Oral Presentations

Nobre Silva, I.G., D. Weis, J.S. Scoates, and F.A. Frey (2008b), Ninetyeast Ridge, KNOX06RR: High-Precision Isotopic Compositions From New Dredge Samples. *Eos Trans. AGU, 89(53)*, Fall Meet. Suppl., Abstract T54B-05.

Nobre Silva, I.G., D. Weis, and J.S. Scoates (2005), Reproducibility of Pb Isotopic Compositions of Ocean Island Basalts: From Leaching to Analysis. Hawaii Scientific Drilling Project Workshop, University of California, Berkley, December 4, 2005.

C2.2. Poster Presentations

Nobre Silva, I.G., D. Weis, and J.S. Scoates (2009), The Effects of Acid Leaching on the Sr-Nd-Hf Isotopic Compositions of Ocean Island Basalts. *Eos Trans. AGU, 90(52)*, Fall Meet. Suppl., Abstract V31D-1990.

M. Pringle, E. Mervine, F. Frey, **I. Nobre Silva**, and D. Weis, H. Owens, E. Gauntlett (2008), Geochemistry and Geochronology of the Ninetyeast Ridge, Indian Ocean: New Constraints on Paleotectonics and Hotspot Dynamics. *Geochim. Cosmochim. Acta 72*, p. A762.

Nobre Silva, I. G., D. Weis, and J.S. Scoates (2008a), High-Precision Isotopic Compositions of Basalts from the Last Phase of the Hawai'i Scientific Drilling Project. *Geochim. Cosmochim. Acta 72,* p. A687.

Nobre Silva, I. G., D. Weis, L. Swinnard, and J.S. Scoates (2007), Ninetyeast Ridge, Indian Ocean: Constraining its Origin and Relation with the Kerguelen, Amsterdam and St. Paul Hotspots. *Geochim. Cosmochim. Acta 71*, p. A721.

J. Barling, **I.G. Nobre Silva**, and D. Weis (2007), The Effect of Sample Matrix on the Precision and Accuracy of Radiogenic Isotope Ratio Measurements by MC-ICP-MS. *Geochim. Cosmochim. Acta 71*, A61.

Nobre Silva, I., D. Weis, and J.S. Scoates (2006c), High-Precision Pb Isotopic Compositions of Basalts from Phase 2B of the Hawaiian Scientific Drilling Project. *Eos Trans. AGU, 87 (52),* Fall Meet. Suppl., Abstract V13B-0672.

Nobre Silva, I., L. Swinnard, and D. Weis (2006b), New Insights on the Origin of the Ninetyeast Ridge and its Connection to the Kerguelen Hot Spot. *Geochim. Cosmochim. Acta*, 70, 18, A448.

Nobre Silva, I., D. Weis, and J.S. Scoates (2006a), The Effects of Leaching on the Pb Isotopic Compositions of Ocean Island Basalts. *CAC-MAC* Program with Abstracts, v.31, p.110.

Nobre Silva, I., D. Weis, and J.S. Scoates (2005), Reproducibility of Pb Isotopic Compositions of Ocean Island Basalts: From Leaching to Analysis. *Eos Trans. AGU, 86 (52),* Fall Meet. Suppl., Abstract V41D-1482.

Weis, D., **I. Nobre Silva**, B. Kieffer, J. Barling, W. Pretorius, and C. Maerschalk (2005), Hf Isotope Geochemistry of USGS Reference Materials and Various Labware: Insight into Potential Contaminant Sources. *Eos Trans. AGU, 86 (52),* Fall Meet. Suppl., Abstract V41D-1477.